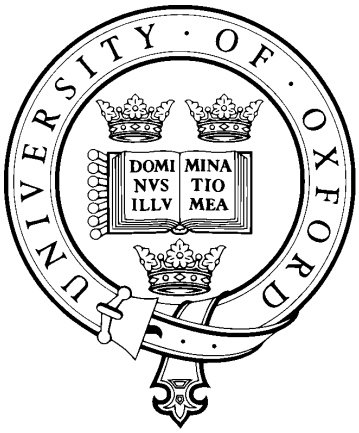
Characterisation of 2-oxoglutarate- and Fe(II)-dependent oxygenases targeting the protein synthesis apparatus

Tianshu Feng

Supervised by
Dr. Mathew Coleman
Prof. Sir Peter Ratcliffe

A thesis submitted for the degree of Doctor of Philosophy



Wolfson College
University of Oxford
Trinity 2014

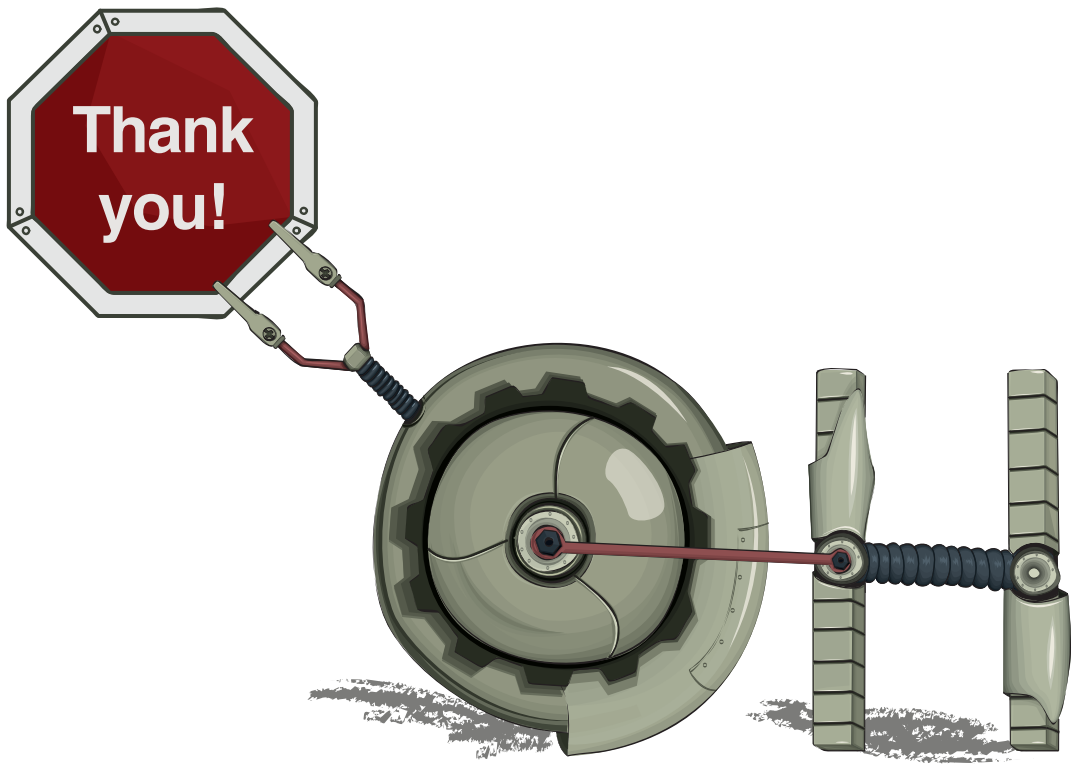
Acknowledgements

First and foremost, I would like to thank Peter and Chris for providing me with the opportunity to join the Ratcliffe lab. I would like to thank Peter for his patience and guidance through the years, and his sage advice and vision that I've only begun to understand. I would like to acknowledge Chris for his ever so important presence in the lab. Same goes for Zuzana, whose efforts are vital to the maintenance of order in the lab. I am grateful to Catherine for her constant encouragements and sympathy, especially during the final few months. My time in the Ratcliffe lab was made particularly enjoyable by my desk 'neighbours' Rachelle and Phebee. I am grateful to Rachelle for the delightful conversations and the guilt-free 3pm cakes, and to Phebee for her invaluable friendship. I would like to thank Phebee, Yamin, Tzu-Lan, Min, Xijin and others for the best Chinese New Year I've had since I was child, it truly brought back a lot of good memories. I have gained much from Norma's encouragements and positivity, and her scandalous though often inconspicuous sense of humour has always been entertaining. I would like to thank Matt for always being so helpful and friendly, and for paving the way for the study of protein hydroxylations. I thank Adam and Melroy, for making me feel at home when I first arrived at Oxford and the Ratcliffe lab, even if my real home was far away. I would like to acknowledge all members of the Ratcliffe lab, who have been incredibly helpful and friendly during this challenging journey. Good science is rarely accomplished alone; I am incredibly grateful to everyone who participated in the NO66 and JMJD4 projects: Adam, Sarah, Pooja, Jake, Roman, Nikola, Benedikt, Rok, Ben, Wei, Luke and many others that I did not mention. Their efforts were instrumental to the projects' success. Most importantly, I would like to extend my greatest gratitude to Mat, without whom this thesis would not have been possible. I have learned a great deal from him during the past four years, and I am forever grateful for having such a responsible and supportive supervisor.

I would like to thank my friends, both old and new - for making the good times better, and the bad times that much more bearable. I am grateful for having my friends around the globe and my troupe ladies, who have been fantastically wonderful and supportive. I would also like to thank Wolfson college for providing a sense of community and allowing me to meet such interesting people.

Words cannot express my gratitude for my soul mate Alistair, to whom I owe everything.

I would like to thank my parents, for instilling me with the spirit of hard work and optimism, and for believing in me always. I will never be able to repay the extent of their unspoken though unconditional love. Lastly, I would like to dedicate this thesis to my grandparents and family in China. It was their efforts that shaped me into the person I am today.



Characterisation of 2-oxoglutarate- and Fe(II)-dependent oxygenases targeting the protein synthesis apparatus

Tianshu Feng
Thesis submitted for the degree of Doctor of Philosophy in Clinical Medicine
Wolfson College
Trinity 2014

Abstract

Members of the 2-oxoglutarate (2OG)- and Fe(II)-dependent oxygenase (2OG oxygenase) superfamily catalyse a wide range of oxidative reactions in biology. 2OG oxygenases require Fe(II) and atmospheric oxygen for their activity, and couple substrate oxidation with the decarboxylation of 2OG into succinate and carbon dioxide. There are more than sixty known 2OG oxygenases in the human genome; they modify small molecules, nucleic acids and proteins implicated in diverse biological processes.

Importantly, the seemingly disparate functions of 2OG oxygenases often converge to regulate gene expression. 2OG oxygenases have been shown to affect epigenetic reprogramming, chromatin remodelling, transcription factor activity and mRNA splicing. Emerging evidence indicates that 2OG oxygenases are also involved in the translational control of gene expression. Oxygenases TYW5, ALKBH8, ALKBH5 and FTO were found to catalyse modifications of tRNA and mRNA. The work in this thesis extends these observations by demonstrating that 2OG oxygenase-catalysed protein hydroxylations also play an important role in protein synthesis. The catalytic activities of two oxygenases belonging to the JmjC-only family, NO66 and JMJD4, are described. NO66 catalyses the histidinyl hydroxylation of 60S ribosomal subunit protein L8. NO66 is part of a conserved group of ribosomal protein hydroxylases that can be traced back to prokaryotes. JMJD4 is a lysyl hydroxylase of eRF1, the eukaryotic release factor responsible for translation termination. The hydroxylation of eRF1 takes place on a conserved NIKS motif important for release factor activity, and promotes efficient translational termination. JMJD4 is further implicated in cell growth and cancer, though the link between its activity and tumourigenesis remains to be determined. These results highlight the potential of 2OG oxygenases as regulators of protein synthesis, and further extends the scope of 2OG oxygenase function. The small molecule inhibition of 2OG oxygenases presents a novel therapeutic possibility targeting translational control in cancer and other diseases.

Declaration

I hereby declare that this thesis is entirely my own work, with the exception of the following:

Experiments shown in Figure 2.2 were carried out by Dr. Wei Ge (Chemistry Research Laboratory, University of Oxford; currently unaffiliated).

Experiments shown in Figure 2.4 were carried out by Dr. Phebee Yi-Liu (Centre for Cell and Molecular Physiology, University of Oxford; currently unaffiliated).

Experiments shown in Figures 4.4 and 4.5 were carried out by Dr. Atsushi Yamamoto (Centre for Cell and Molecular Physiology, University of Oxford).

Experiments shown in Figure 4.10 were carried out by Dr. Elizaveta Sokolova (Engelhardt Institute of Molecular Biology, the Russian Academy of Sciences).

Contributions by others elsewhere in this thesis have been acknowledged within the text of this work. All copyright materials were licensed.

Contents

		Page
Chapter 1	**Literature review**	**1**
1.1	2OG- and Fe(II)-dependent oxygenases in biology	1
1.1.1	Structure and catalytic mechanism	2
1.1.2	Classification and substrate specificity	5
1.2	Oxidative demethylation by 2OG oxygenases	8
1.2.1	Histone and histone tail methylation	8
1.2.2	Discovery and classification of histone demethylases	9
1.3	2OG oxygenases-catalysed protein hydroxylation	10
1.3.1	Hydroxylation of collagens	10
1.3.2	Hydroxylation of EGF-like domains	17
1.3.3	Hydroxylation of hypoxia-inducible factor (HIF)	18
1.3.4	Ankryin repeat domain (ARD) hydroxylation by FIH	24
1.4	Post-translational modifications catalysed by the JmjC-only enzymes	26
1.4.1	Members of the JmjC-only enzyme family	26
1.5	Aim and scope of this thesis	34
Chapter 2	**NO66 is a ribosomal histidinyl hydroxylase**	**37**
2.1	Introduction	37
2.2	Results	39
2.2.1	Mass spectrometry techniques	39
2.2.2	Identification of the NO66 substrate RPL8	40
2.2.3	Purification and characterisation of endogenous RPL8	45
2.2.4	Generation of an inducible NO66 knockdown system	52
2.2.5	Endogenous RPL8 hydroxylation is dependent on NO66	58
2.2.6	Hydroxylation of RPL8 is conserved	66
2.2.7	NO66 activity is dependent on oxygen availability	68
2.2.8	Biological consequence of NO66 enzymatic activity	70
2.3	Discussion	73
Chapter 3	**JMJD4 catalyses lysyl hydroxylation of eRF1**	**83**
3.1	Introduction	83
3.2	Results	85
3.2.1	Identification of a JMJD4 candidate substrate	85
3.2.2	Overexpressed JMJD4 promotes eRF1 hydroxylation	87
3.2.3	Recombinant JMJD4 hydroxylates eRF1 *in vitro*	91
3.2.4	Endogenous eRF1 is hydroxylated at K63	97
3.2.5	Hydroxylation of eRF1 is ubiquitious and conserved	101
3.2.6	Endogenous eRF1 hydroxylation requires JMJD4 enzyme activity	105
3.2.7	JMJD4 activity is dependent on oxygen and 2OG	108
3.2.8	eRF1 hydroxylation is not affected by fumarate accumulation	114
3.2.9	eRF1 hydroxylation is saturated in non-Hodgkin lymphoma	118

3.3 Discussion . . . 118
Chapter 4 Role of eRF1 hydroxylation in translational termination 124
4.1 Introduction . . . 124
4.2 Results . . . 128
4.2.1 Synthetic reporter for measuring stop codon readthrough . . . 128
4.2.2 Loss of JMJD4 activity promotes stop codon readthrough . . . 128
4.2.3 K63 hydroxylation optimises eRF1 activity *in vitro* . . . 135
4.2.4 JMJD4 inhibition mediates readthrough at premature termination codons 141
4.2.5 Depletion of JMJD4 promotes readthrough at endogenous termination sequence contexts . . . 143
4.2.6 Knockdown of JMJD4 and eRF1 alters cellular polysome profile . . . 147
4.2.7 JMJD4 is required for cell proliferation . . . 149
4.3 Discussion . . . 155
Chapter 5 Discussions, conclusions and future work 161
5.1 Introduction . . . 161
5.2 Post-translational modifications of the ribosome . . . 162
5.3 Post-translational modifications in translational termination . . . 163
5.4 Physiological significance of NO66- and JMJD4-catalysed post-translational hydroxylations . . . 164
5.5 Final conclusions . . . 167
Chapter 6 Materials and Methods 168
6.1 Reagents . . . 168
6.1.1 Solutions . . . 168
6.2 Bacterial techniques . . . 170
6.2.1 Solutions and reagents . . . 170
6.2.2 Bacterial culture . . . 170
6.2.3 Transformation . . . 171
6.2.4 Plasmid DNA purification . . . 171
6.3 Nucleic acid techniques . . . 172
6.3.1 Polymerase chain reaction (PCR) . . . 172
6.3.2 Agarose gel electrophoresis . . . 172
6.3.3 DNA purification from agarose gel and PCR reactions . . . 172
6.3.4 Restriction enzyme digestion . . . 172
6.3.5 Ligation . . . 173
6.3.6 Site-directed mutagenesis (SDM) . . . 173
6.3.7 DNA sequencing . . . 173
6.3.8 Genotype PCR . . . 174
6.3.9 RNA extraction . . . 174
6.3.10 cDNA synthesis . . . 175
6.3.11 Real-time quantitative PCR (RT-qPCR) . . . 175
6.3.12 End point reverse transcription PCR (RT-PCR) . . . 176
6.4 Mammalian cell culture techniques . . . 177
6.4.1 Cell culture . . . 177
6.4.2 Hypoxia and DMOG treatments in cell culture . . . 177
6.4.3 Plasmid transfection . . . 177
6.4.4 siRNA transfection . . . 178
6.4.5 Generation of stable cell lines . . . 179
6.4.6 Cell proliferation assays . . . 180
6.4.7 Synthetic lethality screening . . . 181
6.4.8 Readthrough reporter assay . . . 181

6.4.9 Immunofluorescence . . . 182
6.4.10 Microscopy imaging . . . 182
6.4.11 Preparation of cell lysates . . . 183
6.4.12 Polysome profile analysis . . . 183
6.5 Protein techniques . . . 184
6.5.1 Relative protein quantitation . . . 184
6.5.2 Sodium dodecyl sulfate polyacrylamide gel electrophoresis (SDS-PAGE) 185
6.5.3 Immunoblotting . . . 185
6.6 Proteomic techniques . . . 186
6.6.1 SILAC (Stable Isotopic Labelling of Amino acids in Cell culture) . . . 186
6.6.2 Immunoprecipitation . . . 187
6.6.3 Methanol-chloroform precipitation . . . 188
6.6.4 Purification of ribosomal proteins . . . 189
6.6.5 In-gel protein digestion . . . 190
6.6.6 In-solution protein digestion . . . 191
6.6.7 Mass Spectrometry analysis using Thermos LTQ Orbitrap Velos . . . 191
6.7 Other techniques . . . 192
6.7.1 *In vitro* hydroxylation assays . . . 192
6.7.1.1 Statistical analyses . . . 193
6.8 Plasmids and oligonucleotide primers . . . 194
6.8.1 oligonucleotides primers used for construction of plasmids . . . 194
6.8.1.1 Plasmids for expression in mammalian cells . . . 194
Bibliography . . . 196

List of Figures

Page

Chapter 1 Literature review

1.1 Double-stranded β-helix fold in 2OG oxygenases . . . 3
1.2 Postulated catalytic mechanism of 2OG oxygenases . . . 4
1.3 Phylogenetic tree of the 2OG oxygenase superfamily in humans . . . 6
1.4 The regulation of hypoxia signalling . . . 20
1.5 Sequence alignment of enzymes from the JmjC-only family . . . 33

Chapter 2 NO66 is a ribosomal histidinyl hydroxylase

2.1 Schematic of MS/MS . . . 41
2.2 Recombinant NO66 hydroxylates 60S ribosomal protein L8 (RPL8) peptide NPVEHPFGGGNHQHIGKPST . . . 44
2.3 NO66 interacts with RPL8 in cells . . . 46
2.4 HPLC purification of RPL8 from endogenous ribosomes . . . 47
2.5 Endogenous RPL8 in HeLa cells is hydroxylated at H216 . . . 49
2.6 Representative LC-MS chromatograms of RPL8 tryptic peptide$_{201\text{-}226}$ . . . 50
2.7 Endogenous RPL8 in HeLa cells is hydroxylated at H216 . . . 51
2.8 Schematic of the pTRIBz inducible lentiviral shRNA vector . . . 53
2.9 Characterisation of RFP expression in stable cell lines expressing inducible shRNA against NO66 . . . 54
2.10 Characterisation of NO66 protein level in stable cell lines expressing inducible shRNA against NO66 . . . 55
2.11 Time course of doxycycline-induced shRNA expression and NO66 knockdown in HeLa cells . . . 56
2.12 Time course of doxycycline-induced inducible shRNA expression and NO66 knockdown in A549 cells . . . 57
2.13 RPL8 H216 hydroxylation is reduced upon NO66 knockdown . . . 59
2.14 RPL8 H216 hydroxylation is not affected by suppression of MINA53 expression 60
2.15 Ablation of MINA53 expression does not alter RPL8 H216 hydroxylation . . . 62
2.16 Genotypic and biochemical validation of NO66 knockout MEFs . . . 63
2.17 RPL8 is not hydroxylated in the absence of NO66 . . . 64
2.18 Ectopic expression of NO66 partially rescues RPL8 H216 hydroxylation in HEK293T cells . . . 65
2.19 RPL8 H216 hydroxylation is conserved in mice and *D. melanogaster* . . . 67
2.20 RPL8 H216 hydroxylation is reduced under hypoxia . . . 69
2.21 Polysome profile analysis of wild-type and NO66 reconstituted HEK293T cells 71
2.22 Suppression of NO66 in HeLa and A549 cells does not alter cell proliferation . 74
2.23 Ablation of NO66 expression does not alter MEF growth . . . 75
2.24 Proliferation of HEK293T cells is not affected by NO66 expression . . . 76
2.25 NO66 knockdown does not affect cellular sensitivity to antibiotics . . . 77

2.26 The position of RPL8 H216 in the ribosome 81

Chapter 3 JMJD4 catalyses lysyl hydroxylation of eRF1

3.1 Conservation of JMJD4 in eukaryotes 84
3.2 JMJD4 interacts with eRF1 in cells 88
3.3 JMJD4 and eRF1 co-localise in cells 89
3.4 Overexpressed JMJD4 hydroxylates eRF1 at K63 90
3.5 Recombinant JMJD4 modifies eRF1 at K63 *in vitro* 92
3.6 MS/MS sequencing of recombinant eRF1 peptide$_{51\text{-}63}$ 93
3.7 MS/MS sequencing of recombinant K63R eRF1 peptide$_{51\text{-}63}$ 94
3.8 MS/MS sequencing of recombinant K63A eRF1 peptide$_{51\text{-}65}$ 95
3.9 JMJD4 is a 2OG- and Fe(II)-dependent oxygenase 96
3.10 Purification and mass spectrometry characterisation of endogenous eRF1 . . . 98
3.11 MS/MS sequencing of endogenous eRF1 digested with trypsin 99
3.12 MS/MS sequencing of endogenous eRF1 digested with Arg-C 100
3.13 eRF1 K63 hydroxylation is widespread in tissue culture cell lines 102
3.14 eRF1 K63 hydroxylation is ubiquitious and conserved 103
3.15 eRF1 K63 hydroxylation is conserved in zebrafish 104
3.16 Hydroxylation of endogenous eRF1 is dependent on JMJD4 activity in A549 cells 106
3.17 Hydroxylation of endogenous eRF1 is dependent on JMJD4 activity in HeLa cells 107
3.18 eRF1 hydroxylation in HeLa cells is dependent on oxygen 109
3.19 eRF1 hydroxylation in HeLa cells is dependent on 2OG 111
3.20 Hydroxylation of eRF1 in U2OS cells is dependent on oxygen and 2OG 112
3.21 Hydroxylation of eRF1 in Hep3B cells is dependent on oxygen and 2OG . . . 113
3.22 K63 hydroxylation of eRF1 is not inhibited by fumarate accumulation 115
3.23 eRF1 hydroxylation is mildly reduced in kidney of FH KO mouse 117
3.24 eRF1 K63 hydroxylation is not affected by the tumour microenvironment . . 119

Chapter 4 Role of eRF1 hydroxylation in translational termination

4.1 Structure and conservation of eRF1 NIKS motif 126
4.2 Schematic of the proposed role of JMJD4-catalysed eRF1 K63 hydroxylation in translational termination 127
4.3 Schematic of the p2luc dual-luciferase reporter system 129
4.4 Suppression of JMJD4 induces stop codon readthrough 131
4.5 JMJD4 activity promotes translational termination efficiency 133
4.6 JMJD4 specifically affects translational termination 134
4.7 End point RT-PCR analysis of p2luc reporter mRNA integrity 136
4.8 Quantitative RT-PCR analysis of p2luc reporter mRNA integrity 137
4.9 Hydroxylation of recombinant eRF1 by recombinant JMJD4 *in vitro* 139
4.10 K63 hydroxylation promotes eRF1 translational termination efficiency *in vitro* 140
4.11 JMJD4 suppression mediates readthrough at CFTR and DMD premature termination codons in synthetic reporters 142
4.12 JMJD4 suppression mediates readthrough at APC premature termination codons in synthetic reporters 144
4.13 Knockdown of JMJD4 induces readthrough at selected endogenous termination sequences 146
4.14 Depletion of JMJD4 alters polysome profile of HeLa cells 148
4.15 JMJD4 knockdown in HeLa cells inhibits proliferation 150
4.16 JMJD4 expression is required for the proliferation of U2OS cells 151

4.17 Depletion of JMJD4 inhibits Hep3B cell proliferation 152
4.18 JMJD4 is important for U87 cell proliferation 153
4.19 *Jmjd4* gene amplification in cancer 154

Chapter 5 Discussions, conclusions and future work
5.1 The interaction between 2OG oxygenase activity and the physiological environment 166

List of Tables

Page

Chapter 1 Literature review

1.1 Small molecule and nucleic acid hydroxylases and their substrate specificities. 7
1.2 JmjC domain containing histone demethylases and their substrate specificities 11
1.3 2OG-dependent protein hydroxylases and their substrate specificities 12
1.4 JmjC-only hydroxylases and their substrate specificities 27

Chapter 2 NO66 is a ribosomal histidinyl hydroxylase

2.1 List of NO66 interacting proteins 43

Chapter 3 JMJD4 catalyses lysyl hydroxylation of eRF1

3.1 List of JMJD4 proteomic interactors 86

Chapter 6 Materials and Methods

6.1 Oligonucleotide primers used for genotype PCR of NO66 WT and KO MEFs 174
6.2 Oligonucleotide primers used for RT-qPCR 176
6.3 siRNA duplexes 179
6.4 Antibodies for immunoblotting 187
6.5 Oligonucleotide primers used for cloning 194
6.6 Oligonucleotide primers used for cloning of p2luc readthrough reporters . . . 194

Chapter 1

Literature review

1.1 2OG- and Fe(II)-dependent oxygenases in biology

2-oxoglutarate (2OG)- and Fe(II)- dependent oxygenases, or 2OG oxygenases, are a large superfamily of enzymes that catalyse a wide range of oxidation reactions. They rely on molecular oxygen for substrate oxidation, and require Fe(II) and 2OG for their catalytic activity. Identified in 1967, collagen prolyl hydroxylases were the first examples of 2OG oxygenases (Hutton Jr et al., 1967). It is now known that members of the 2OG oxgenase superfamily are functionally diverse enzymes involved in a vast array of biological processes.

Phylogenetic analyses indicate that there are more than sixty known 2OG oxygenases in the human genome, with even more found in other species (Johansson et al., 2014). In plants and micoorganisms, 2OG oxygenases are capable of catalysing reactions including desaturation, oxidative cyclisation, halogenation, epimerisation and most commonly hydroxylation (Clifton et al., 2006; Aik et al., 2012). In animals however, hydroxylation is the only identified reaction to date. Despite this limitation, 2OG oxygenase-catalysed hydroxylation is a highly versatile modification that occurs on a wide range of substrates including proteins, nucleic acids and small molecules.

1.1.1 Structure and catalytic mechanism

The 2OG oxygenases belong to the cupin superfamily, a functionally diverse superfamily of proteins characterised by their presence of a conserved double-stranded β-helix (DSBH) fold or 'jelly-roll' motif (McDonough et al., 2010; Dunwell et al., 2001). The DSBH fold in a subclass of 2OG oxygenases is also referred to as the Jumonji C (JmjC) domain, based on their conservation in the Jumonji family of transcription factors (Clissold and Ponting, 2001; Balciunas and Ronne, 2000). The core of the 2OG oxygenase DSBH fold consists of eight β-strands forming two anti-parallel β-sheets. The overall structure is shaped like a 'barrel', with the active site positioned at the more open end of the barrel (Figure 1.1). A 'facial triad' of amino acids belonging to the conserved HXD/E...H motif orchestrates iron coordination, with water and 2OG occupying the remaining iron coordination sites (Koehntop et al., 2005; Figure 1.2A). The 5-carboxylate group of 2OG usually binds to semi-conserved amino acids of the barrel interior by hydrogen bonding and electrostatic interactions.

Binding of 2OG to the DSBH core precedes that of the prime substrate, following which molecular oxygen reacts with the quaternary complex of enzyme-Fe(II)-2OG-substrate (Aik et al., 2012). Binding of molecular oxygen displaces the water molecule at the Fe(II) coordination site (Figure 1.2B). Upon activation by Fe(II), molecular oxygen attacks the C2 position of 2OG. This results in the oxidative decarboxylation of 2OG into succinate and carbon dioxide, generating a highly reactive Fe(IV)-oxo intermediate (Price et al., 2003; Hoffart et al., 2006; Figure 1.2C). The Fe(IV)-oxo intermediate proceeds to extract a hydrogen from the prime substrate, which creates a substrate-centred radical (Figure 1.2D). This is followed by hydroxylation of the prime substrate and regeneration of the Fe(II) catalytic core (Figure 1.2D and E). In certain cases, presence of ascorbate as a reducing agent stimulates 2OG oxygenase activity.

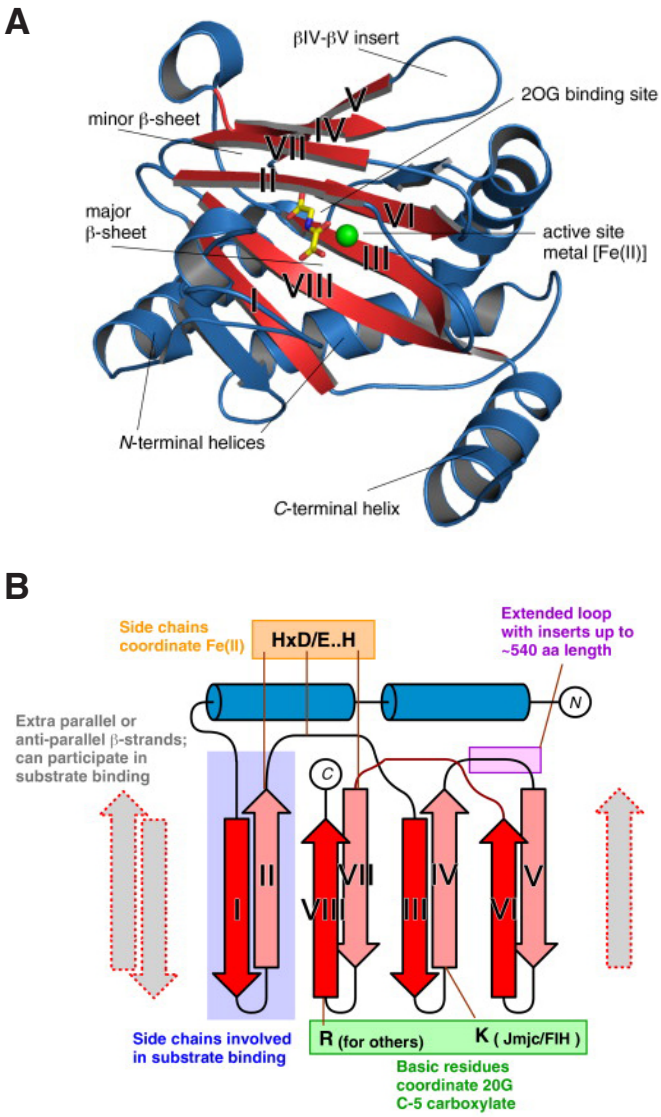


Figure 1.1: Double-stranded β-helix fold in 2OG oxygenases. A) Crystal structure of PHD2 active site bound to iron (green) and the non-reactive 2OG analogue N-oxalylglycine (NOG; yellow). β-strands are highlighted in red, and the surrounding α-helices are in blue. **B)** Two-dimensional topology diagram depicting the general structure of 2OG oxygenase DSBH fold. Figure adapted from McDonough et al. (2010).

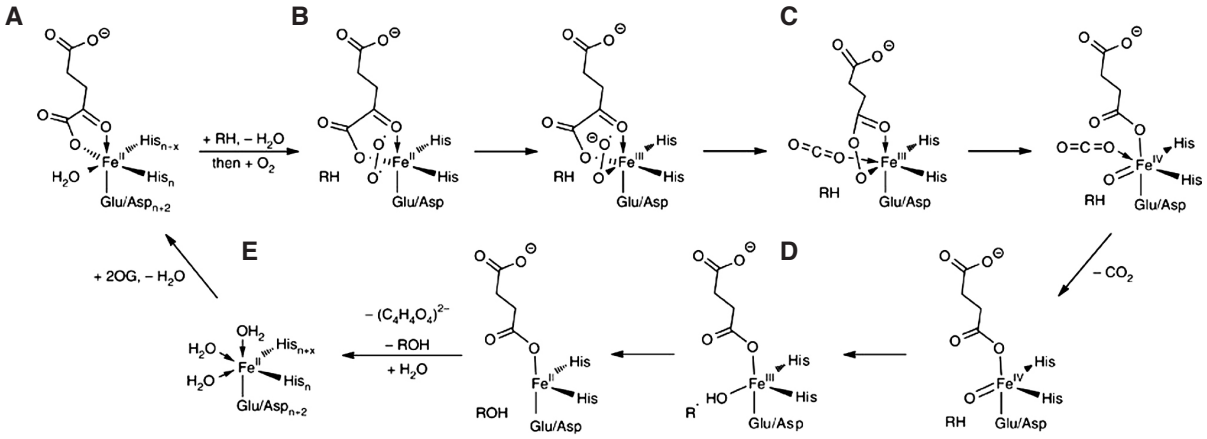


Figure 1.2: Postulated catalytic mechanism of 2OG oxygenases. **A)** Fe(II) is coordinated by two histidine residues, one aspartate/glutamate residue, 2OG and H_2O. **B)** Molecular oxygen reacts with the enzyme-substrate-cofactor complex. **C)** 2OG undergoes oxidative decarboxylation, which generates a Fe(IV)-oxo intermediate enabling hydroxylation of the substrate **(D)**. **E)** The Fe(II) catalytic centre is regenerated. Figure adapted from Tarhonskaya et al. (2014).

1.1.2 Classification and substrate specificity

2OG oxygenases can be separated into distinctive subfamilies based on their domain architecture and sequence homology (Figure 1.3). Members of the same subfamily often share similar substrate specificities. The 2OG oxygenases that modify small molecules and nucleic acids and their respective substrate specificities are shown in Table 1.1. Of the 2OG oxygenases that modify small molecules, trimethyllysine dioxygenase (TMLH) and gamma-butyrobetaine dioxygenase (BBOX) hydroxylate precursors of the L-carnitine biosynthetic pathway (Hulse et al., 1978; Lindstedt and Lindstedt, 1970). Phytanoyl-CoA dioxygenase (PHYH) catalyses the first step in the alpha oxidation of a branched-chain fatty acid, phytanic acid. Inactivation of PHYH is associated with Refsum disease, a recessive neurological disorder that arises from abnormal phytanic acid accumulation (Mihalik et al., 1997; Jansen et al., 1997).

Alkylated DNA repair protein alkB homologue (ALKBH), ten-eleven translocation methylcytosine dioxygenase (TET), and fat mass and obesity-associated protein (FTO) enzymes are nucleic acid modifying 2OG oxygenases. AlkB is a highly conserved 2OG oxygenase in *Escherichia coli* that removes methylation adducts in DNA using a hydroxylation mechanism (Falnes et al., 2002; Duncan et al., 2002). It has eight human homologues, termed ALKBH1-8. ALKBH2 and ALKBH3 demethylate and repair 1-methyladenine and 3-methylcytosine lesions in DNA (Duncan et al., 2002; Aas et al., 2003). Other homologues are found to have varying enzymatic activities targeting both DNA and RNA (Westbye et al., 2008; Fu et al., 2010; van den Born et al., 2011; Li et al., 2013). TET1-3 enzymes convert 5-methylcytosine, a prevalent epigenetic modification in DNA, into 5-hydroxymethylcytosine (Tahiliani et al., 2009; Ito et al., 2010). They can also further oxidise the substrate to form 5-formylcytosine and 5-carboxylcytosine (Ito et al., 2011; He et al., 2011). The expression of TET1 is critical for embryonic stem (ES) cell maintenance (Ito et al., 2010). Furthermore, the inactivation or downregulation of TET catalytic activity is related to cancer (Ko et al., 2010; Yang et al., 2012; Huang and Rao, 2014). The gene encoding FTO is as-

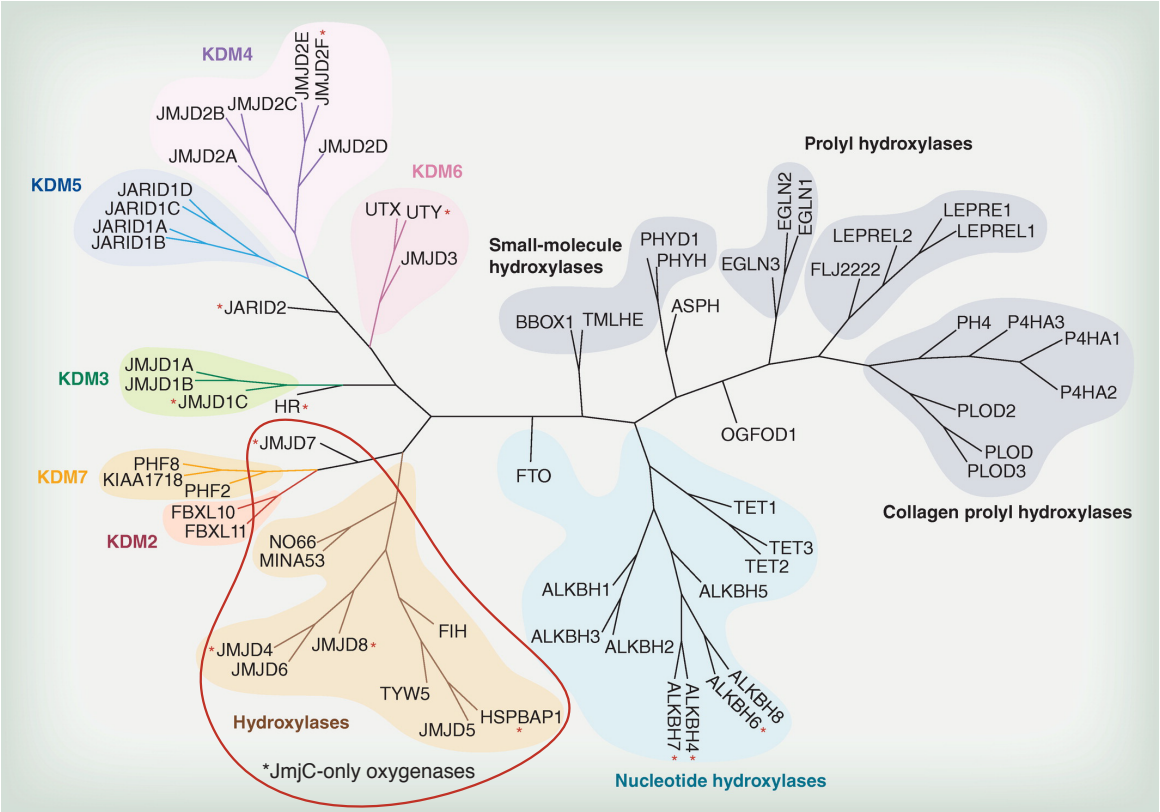


Figure 1.3: Phylogenetic tree of the 2OG oxygenase superfamily in humans. 2OG oxygenases are grouped into subfamilies based on their sequence conservation. Different subfamilies are highlighted as shown. The JmjC-only enzyme family, which is of interest to this thesis, is circled in red. Figure adapted from Johansson et al. (2014).

Small molecule hydroxylases			
Name	Alternative name(s)	Substrate(s)	References
TMLH	TMLD/TMLHE	ε-N-trimethyllysine	Hulse et al, 1978
BBOX	γ-BBH	γ-butyrobetaine	Lindstedt and Lindstedt, 1970
PHYH	PAHX	Phytanoyl-CoA	Mihalik et al, 1997; Jansen et al, 1997
PHYD1	PHYHD1	Unknown	Zhang et al, 2011
Nucleic acid hydroxylases			
Name	Alternative name(s)	Substrate(s)	References
ALKBH1	ABH1	3-methylcytosine	Westbye et al, 2008
ALKBH2	ABH2	1-methyladenosine; 3-methylcytosine	Duncan et al, 2002; Aas et al, 2003
ALKBH3	ABH3/DEPC1	1-methyladenosine; 3-methylcytosine	Duncan et al, 2002; Aas et al, 2003
ALKBH4	ABH4	Actin (lysine demethylation)	Li et al, 2013
ALKBH5	ABH5/OFOXD1	N(6)-methyladenosine	Zheng et al, 2013
ALKBH6	ABH6	Unknown	
ALKBH7	ABH7/SPATA11	Unknown	
ALKBH8	ABH8	5-carboxymethyluridine; 5-methoxycarbonylmethyluridine	Fu et al, 2010
FTO		3-methylthymine/uracil; N(6)-methyladenosine	Gerken et al, 2007; Jia et al, 2008; Jia et al, 2011
TET1	CXXC6/LCX	5-methylcytosine; 5-hydroxymethylcytosine	Tahiliani et al, 2009; Ito et al, 2011; He et al, 2011
TET2		5-methylcytosine; 5-hydroxymethylcytosine	Tahiliani et al, 2009; Ito et al, 2011; He et al, 2011
TET3		5-methylcytosine; 5-hydroxymethylcytosine	Tahiliani et al, 2009; Ito et al, 2011; He et al, 2011
TYW5		Wybutosine ($tRNA^{phe}$)	Noma et al, 2010

Table 1.1: Small molecule and nucleic acid hydroxylases and their substrate specificities. 2OG oxygenases that catalyse modifications of small molecules and nucleic acids, or homologous to nucleic acid hydroxylases, are outlined in this table with their respective substrate specificities.

sociated with obesity, though the exact mechanism is unknown (Frayling et al., 2007; Dina et al., 2007; Fischer et al., 2009). *In vitro* assays show that FTO demethylates 3-methylthymine and N6-methyladenosine in DNA and RNA, respectively (Gerken et al., 2007; Jia et al., 2011).

In addition to the small molecule and nucleic acid hydroxylases outlined above, other 2OG oxygenases are known to catalyse the post-translational modifications of proteins. These include enzymes that directly hydroxylate proteins, or catalyse oxidative demethylation reactions. Discoveries over the last decade have shown that these enzymes play important roles in epigenetic regulation, protein stability, hypoxia signalling and gene expression. Moreover, increasing evidence suggest that the full extent of protein hydroxylation in biology is not yet appreciated. As such, this thesis focuses on the biochemical and functional elucidation of novel protein hydroxylases, with particular emphasis placed on a subfamily of 2OG oxygenases termed the JmjC-only family. Current knowledge about relevant protein hydroxylases and demethylases are summarised in detail below.

1.2 Oxidative demethylation by 2OG oxygenases

1.2.1 Histone and histone tail methylation

DNA in living cells is organised into chromatin, which is made up of fundamental units called nucleosomes. Each nucleosome is formed by 147 base pairs of DNA wrapped around an octamer of four pairs of histone proteins (H2A, H2B, H3 and H4; Kornberg and Lorch, 1999). Histones are globular in structure, though they have an unstructured N-terminal tail that undergoes an array of post-translational modifications. These modifications include acetylation, ubiquitination, sumoylation, phosphorylation and methylation (Martin and Zhang, 2005).

Histone methylation plays important roles in diverse biological processes such as transcriptional regulation, epigenetic inheritance, chromatin structure and cell differen-

tiation (Martin and Zhang, 2005). Methylation most frequently occurs on either lysine or arginine residues in histone proteins H3 and H4. Methyl groups are able to replace all three hydrogen atoms on the ϵ-amino group of the lysine side chain, resulting in mono-, di- or trimethylation. Similarly, arginine can be mono- or dimethylated in an asymmetric or symmetric manner. Depending on the context and position, histone methylation can have either transcriptionally activating or repressive functions. For example, methylations of H3K4, H3K26, H3K79 are typically associated with transcriptional activation, whereas the H3K9, H3K27 and H4K20 methylations correlate with transcriptional repression (Klose et al., 2006a). The degree of methylation (mono-, di- or tri-) also has important functional consequences. Downstream effects of histone methylation are largely mediated by effector proteins that recognise and interact with specific modifications on the histone tail (Zhang and Reinberg, 2001).

1.2.2 Discovery and classification of histone demethylases

It was unclear whether histone methylations are reversible until the discovery of peptidylarginine deiminase type IV (PADI4). PADI4 converts monomethylated arginine in histones into citrulline, and is therefore not a true demethylase (Wang et al., 2004; Cuthbert et al., 2004). Lysine-specific demethylase 1 (LSD1), on the other hand, was the earliest identified true histone demethylase (Shi et al., 2004). LSD1 belongs to a family of amine oxidases that requires flavin as a co-factor (Shi et al., 2004; Metzger et al., 2005).

Soon after the discovery of LSD1, another family of histone demethylases was uncovered. They are characterised by the presence of a JmJC domain, and catalyse demethylation of histones *via* a hydroxylation mechanism. These JmjC-containing proteins are classical 2OG oxygenases that require Fe(II), molecular oxygen and 2OG for their enzymatic function. Mechanistically, JmjC histone demethylases hydroxylate the carbon atom of the Nϵ-methyl group of interest. This produces an unstable hemiaminal intermediate, resulting in spontaneous release of the hydroxylated methyl

group as formaldehyde (Ng et al., 2007). Its catalytic mechanism allows JmjC histone demethylases to remove mono-, di- and trimethylations, whereas LSD enzymes can only demethylate mono- and dimethylated products (Shi et al., 2004; Johansson et al., 2014).

JmJC histone demethylases can be grouped into distinctive subfamilies based on their sequence conservation and domain organisation. Together these enzymes modify a large variety of histone substrates, which are summarised in Table 1.2. Almost all histone substrates reported to date are methylated lysine residues. In addition to histones, several JmjC demethylases also target non-histone substrates. Notably, KDM2A has been shown to demethylate the p65 subunit of NF-κB at specific lysine residues, and thereby inhibit NF-κB binding to its target genes (Lu et al., 2009a, 2010). Furthermore, the JMJD2 family of enzymes were found to demethylate peptides from non-histone proteins *in vitro* (Ponnaluri et al., 2009). The enzymatic activity of JmjC demethylases has important and diverse functions in biology, which unfortunately is outside of the scope of this literature review. However, it is suffice to say that histone demethylases are important transcriptional regulators that make up a large proportion of the 2OG oxygenases superfamily. A separate class of enzymes that catalyses protein hydroxylation are summarised in Table 1.3 and discussed below.

1.3 2OG oxygenases-catalysed protein hydroxylation

1.3.1 Hydroxylation of collagens

Collagen structure and classification Collagen is an important family of structural proteins found in the extra cellular matrix (ECM). Collagen is characterised by the presence of triple helical domains, which are made up of three polypeptide strands called α-chains. α-chains themselves are left-handed helices, which supercoil around each other to form a right-handed rope-like bundle (Pauling and Corey, 1951). Glycine is found at every third position of the α chain in a Gly-X-Y repeat sequence. The

Histone demethylases			
Name	Alternative name(s)	Substrate(s)	References
FBXL10	KDM2B/JHDM1B/FBL10	H3K36me1/me2, H3K4me3	Tsukada et al, 2006; Frescas et al, 2007
FBXL11	KDM2A/JHDM1A/FBL7	H3K36me2	Tsukada et al, 2006
JMJD1A	KDM3A/JHDM2A/JMJD1	H3K9me1/me2	Yamane et al, 2006; Brauchle et al, 2013
JMJD1B	KDM3B/JHDM2B	H3K9me1/me2	Yamane et al, 2006; Brauchle et al, 2013
JMJD1C	JHDM2C	H3K9me1/me2	Kim et al, 2010
HR		H3K9me1/me2	Liu et al, 2014
JMJD2A	KDM4A/JHDM3A/JMJD2	H3K9me2/me3, H3K36me2/me3, H1.4K26me2/me3	Whetstine et al, 2006; Klose et al, 2006; Cloos et al, 2006; Trojer et al, 2009
JMJD2B	KDM4B/JHDM3B	H3K9me2/me3, H3K36me2/me3, H1.4K26me2/me3	Whetstine et al, 2006; Fodor et al, 2006; Cloos et al, 2006; Trojer et al, 2009
JMJD2C	KDM4C/JHDM3C/GASC1	H3K9me2/me3, H3K36me2/me3, H1.4K26me2/me3	Whetstine et al, 2006; Cloos et al, 2006; Trojer et al, 2009
JMJD2D	KDM4D/JHDM3D	H3K9me2/me3, H1.4K26me2/me3	Whetstine et al, 2006; Trojer et al, 2009
JMJD2E	KDM4E	H3K9me3/2/1	Hillringhaus et al, 2011
JMJD2F		Unknown	
JARID1A	KDM5A/RBP2	H3K4me2/me3	Klose et al, 2007; Christensen et al, 2007; Iwase et al, 2007
JARID1B	KDM5B/PLU1	H3K4me2/me3	Christensen et al, 2007; Iwase et al, 2007; Yamane et al, 2007; Seward et al, 2007
JARID1C	KDM5C/SMCX	H3K4me2/me3	Christensen et al, 2007; Iwase et al, 2007; Tahiliani et al, 2007
JARID1D	KDM5D/SMCY	H3K4me2/me3	Lee et al, 2007; Iwase et al, 2007
JARID2		Unknown	
UTX	KDM6A	H3K27me2/me3	Lan et al, 2007; Agger et al, 2007; Hong et al, 2007
UTY	KDM6C	Unknown	
JMJD3	KDM6B	H3K27me2/me3	De Santa et al, 2007; Lan et al, 2007; Agger et al, 2007; Hong et al, 2007
PHF2	JHDM1E	H4K20me1, H3K9me1/me2, H3K36me2	Wen et al, 2010
PHF8	JHDM1F	H4K20me1, H3K9me1/me2, H3K36me2	Qi et al, 2010; Zhu et al, 2010; Loenarz et al, 2010; Feng et al, 2010
KIAA1718	JHDM1D/KDM7/KDM7A	H3K9me1/me2, H3K27me1/me2	Tsukada et al, 2010; Huang et al, 2010

Table 1.2: JmjC domain containing histone demethylases and their substrate specificities. JmjC histone demethylases and their known substrate specificities are listed as shown.

Protein hydroxylases			
Name	Alternative name(s)	Substrate(s)	References
CP4H1-3	P4H1-3	Collagens; collagen domain containing proteins; elastin; Argonaute 2; prion protein	Ebert and Prockop, 1962; Peterkofsky and Udenfriend, 1963; Prockop and Juva, 1965; Uitto et al, 1976; Helaakoski et al, 1995; Annunen et al, 1997; Gill et al, 2000; Kukkola et al, 2003; Qi et al, 2008
P3H1-3	LEPRE1; LEPREL1-2	Collagens; collagen domain containing proteins	Ogle et al, 1962; Tryggvason et al, 1979; Vranka et al, 2004; Tiainen et al, 2008
PLOD1-3	LH1-3	Collagens; collagen domain containing proteins	Hausmann et al, 1967; Hautala et al, 1992; Valtavaara et al, 1997; Passoja et al, 1998; Valtavaara et al, 1998
ASPH	BAH	EGF-like domain containing proteins	Stenflo et al, 1989; Gronke et al, 1989
PHD1-3	EGLN1-3	HIFα	Bruick and McKnight, 2001; Epstein et al, 2001
OGFOD1	TPA1	RPS23	Katz et al, 2014; Loenarz et al, 2014; Singleton et al, 2014

Table 1.3: 2OG-dependent protein hydroxylases and their substrate specificities. 2OG oxygenases that are known to catalyse protein hydroxylations, and their substrates are listed as shown.

presence of glycine is essential, since triple helix is formed in such a way that glycine residues are packed along the central axis. Other amino acids cannot fit into the tightly packed helical structure. X and Y can be any amino acid, though proline and 4-hydroxyproline are commonly found at the X and Y positions, respectively. The unique structure of proline helps to establish the shape and rigidity of the collagen triple helix.

Collagen proteins are highly abundant, making up approximately one-third of total protein mass in humans. There are at least 29 members within the collagen superfamily, which can be classified based on their function and supramolecular structure (Söderhäll et al., 2007; Shoulders and Raines, 2009). Other proteins contain similar triple helical domains but are not classified as collagens. Collagen types I, II, III, V, XI, XXIV and XXVII are fibril-forming collagens. They assemble into thick fibers consisting of aggregates of quarter-staggered triple helices. These collagen fibrils are found in dermis, bones, tendons and other connective tissues. Collagen types IX, XII, XIV, XVI, XIX, XX, XXI, XXII and XXVI cannot form fibrils themselves but instead associate with surfaces of other fibrils. They are called fibril-associated collagens with interrupted triple helices (FACIT collagens). Collagen type IV is a network-forming collagen that forms sheet-like structures in the basement membrane. Type VIII and X collagens are found in Descemet's membrane of the cornea and cartilage, respectivly. Though they are also considered to be network-forming collagens, collagen types VIII and X are structurally distinct from collagen type IV, since they assemble into hexagonal lattices instead of sheet-like networks (Prockop, 1995). Type VII collagen form anchoring fibrils in the basement membrane, whereas type VI collagen make up beaded filaments that interweave between other collagen fibrils. Collagen types XIII and XVII are transmembrane proteins (Gelse et al., 2003).

Collagen biosynthesis and assembly occurs in the endoplasmic reticulum, where the collagen precursors undergo extensive post-translational modifications prior to assembly and export. Three hydroxylation modifications are found on collagens: prolyl 4-hydroxylation, prolyl 3-hydroxylation and lysyl hydroxylation, with the first being

most abundant. All three modifications play important roles in collagen function (Berg and Prockop, 1973).

Collagen prolyl-4 hydroxylation First isolated in 1902 by Fischer, 4-hydroxyproline is abundant in collagen triple helices and proteins containing collagenous domains. 4-hydroxyproline occurs at the Y position of the Gly-X-Y triple helical motif, and stabilises the triple helix by influencing prolyl cis-trans isomerisation through stereoelectronic effects. As such, 4-hydroxyproline is indispensible for collagen stability and function. Early isotopic study showed that dietary hydroxyproline was minimally incorporated into proteins, therefore hydroxyproline in collagen were most likely derived from proline oxidation (Stetten, 1949). Enzymatic fractions containing collagen prolyl hydroxlase activity were later isolated from chick embryos and other animal tissues (Ebert and Prockop, 1962; Peterkofsky and Udenfriend, 1963; Prockop and Juva, 1965). Further studies of these collagen hydroxylases showed that it requires Fe(II), 2OG and ascorbate as co-factors, making collagen prolyl-4 hydroxylase (C4PH) the earliest identified 2OG oxygenase (Hutton Jr et al., 1966).

C4PH exists as an $\alpha_2\beta_2$ tetramer. The invariant β subunit is a protein disulfide isomerase (PDI; Pihlajaniemi et al., 1987). The catalytic α subunit has three isoforms - α(I), α(II), and α(III) (Helaakoski et al., 1995; Annunen et al., 1997; Kukkola et al., 2003). The type I $\alpha(\mathrm{I})_2\beta_2$ tetramer is dominant in most cell lines and tissues, though type II $\alpha(\mathrm{II})_2\beta_2$ tetramer is the major isoenzyme of chondrocytes and capiliary endothelial cells (Annunen et al., 1998). Co-expression studies argue against the existence of a mixed $\alpha(\mathrm{I})\alpha(\mathrm{II})\beta_2$ tetramer (Annunen et al., 1997). Little is known about the type III $\alpha(\mathrm{III})2\beta_2$ tetramer, except that its mRNA is widely expressed in tissues at a low level (Kukkola et al., 2003).

In addition to collagen, C4PH also hydroxylates collagenous domains in other proteins. Its substrate includes acetylcholinesterase, C1q of the complement pathway, collectins, macrophage receptors and more (Gorres and Raines, 2010). Proteins that lack collagenous domains may also be C4PH substrates. One such example is Arg-

onaute 2, a key component of the RNA-induced silencing complex (RISC; Rand et al., 2005). RISC mediates sequence-specific cleavage of mRNA induced upon the incorporation of miRNA or siRNA into the complex (Rand et al., 2005). Argonaute 2 interacts with C4PH *in vivo*, and mass spectrometry shows that Argonaute 2 is hydroxylated at Pro700 (Qi et al., 2008). Suppression of C4PH affects Argonaute 2 stability and impairs the RNA interference response (Qi et al., 2008). The diversity of C4PH substrates reflects the importance of the enzyme in a number of biological pathways.

Collagen Prolyl-3 hydroxylation 3-hydroxyproline is found at the X position of the Gly-X-Y motif (Ogle et al., 1962). In comparison to 4-hydroxyproline, 3-hydroxyproline is relatively rare. The extent of modification is largely collagen type-dependent, with collagen IV having the largest number of 3-hydroxyprolines. However, the exact function of 3-hydroxyproline remains unclear. Prolyl-3 hydroxylation in fibrillar collagens is suggested to be involved in supramolecular assembly, though experimental evidence testing this claim is conflicting at best (Pokidysheva et al., 2013). There are three enzymes in the collagen prolyl-3 hydroxylase (P3H) family: P3H1-3. Of the three, P3H1 and P3H2 are relatively well studied.

Isolated only 25 years after its initial identification (Tryggvason et al., 1979; Vranka et al., 2004), P3H1 hydroxylates Pro986 on the α-chains of collagens I and II (Morello et al., 2006). Hydroxylation of other prolyl residues by P3H1 has also been reported (Baldridge et al., 2010; Pokidysheva et al., 2013). P3H1 co-purifies with cartilage-associated protein (CRTRAP) and peptidylprolyl isomerase B (PPIB) of the rough endoplasmic reticulum (Vranka et al., 2004). Formation of this ternary complex is important for P3H1 activity *in vivo*. In fact, loss-of-function of either CRTRAP or P3H1 would result in the absence of Pro986 α(I) hydroxylation (Morello et al., 2006; Cabral et al., 2007). P3H1 null mice are presented with connective tissue abnormalities indicative of collagen dysfunction (Vranka et al., 2010). Similarly, CRTRAP null mice also exhibit severe connective tissue and bone defects (Morello et al., 2006; Baldridge et al., 2010). Consistent with these observations, human mutations in all three members of

the P3H1 complex are associated with recessive osteogenesis imperfecta (OI) (Morello et al., 2006; Baldridge et al., 2008; Cabral et al., 2007; van Dijk et al., 2009). These clinical studies highlight the importance of P3H1-mediated collage hydroxylation in normal bone development. Curiously however, OI patients with PPIB mutations retain normal levels of 3-hydroxyproline, which suggests the potential existence of an alternative disease mechanism (van Dijk et al., 2009; Barnes et al., 2010).

P3H1 is expressed in tissues rich in fibrillar collagens (Vranka et al., 2004), whereas P3H2 is mostly found in tissues rich in basement membranes (Tiainen et al., 2008). As such, P3H2 likely hydroxylates collagen IV of the basement membrane, which contains a large number of 3-hydroxyprolines. This is supported by *in vitro* studies showing that recombinant P3H2 selectively hydroxylates peptides derived from collagen IV (Tiainen et al., 2008). However, P3H2 also hydroxylates several prolyl residues in fibrillar forming collagens (Fernandes et al., 2011). Genetic knockout of P3H2 is embryonic lethal and reportedly affects collagen-induced platelet aggregation (Pokidysheva et al., 2014). Furthermore, a single mutation of P3H2 is clinically associated with high-grade myopia (Mordechai et al., 2011). These genetic studies suggest that P3H2-mediated collagen hydroxylation has important functions that are yet to be identified.

Collagen lysyl-5 hydroxylation Similar to prolyl-3 hydroxylation, the degree of lysyl-5 hydroxylation varies significantly depending on the physiological context. 5-hydroxylysine can be found at the Y position of the Gly-X-Y triple helical motif, and also in the non-helical regions of collagen proteins. Non-helical lysyl hydroxylation is important for collagen supramolecular assembly. The side chain of lysine or hydroxylysine can convert into aldehyde, which reacts with the amino side chain of another lysine residue to form a covalent bond. These cross-links typically occur between two collagen proteins. Though the formation of similar cross-links are possible with unmodified lysines, covalent bonds formed by hydroxylysines are much more stable. 5-hydroxylysine residues in the triple helix, on the other hand, undergo glycosylation modifications such as galactosylation and glucosylation (Yamauchi and Sricholpech,

2012). The biological function of glycosylated hydroxylysine remains unclear, though excessive glycosylation is linked to OI (Cabral et al., 2007).

Collagen lysyl hydroxylase (LH) exists as an α_2 homodimer. There are three known isoforms, termed LH1-3 or PLOD1-3 (Hautala et al., 1992; Valtavaara et al., 1997; Passoja et al., 1998; Valtavaara et al., 1998). *In vitro* peptide studies show that all three LH hydroxylate lysine residues in the triple helical domain, though LH2 is the only isoenzyme that acts on the non-helical telopeptidyl sequence (Takaluoma et al., 2007). LH1 and LH2, however, are more evolutionarily related to each other than LH3 (Ruotsalainen et al., 1999). Interestingly, LH3 alone possesses glycosyltransferase activity in addition to its LH activity (Heikkinen et al., 2000; Wang et al., 2002).

LH gene mutations have important clinical implications. Loss-of-function of the LH1 gene is associated with Ehlers-Danlos syndrome type VI, a recessive connective tissue disorder characterised by kyphoscoliosis, hypermobile joints, hyperelastic skin and fragile tissues (Yeowell and Walker, 2000). Mutations of the LH2 gene, in comparison, cause a recessive OI-like condition called Bruck syndrome (van der Slot et al., 2003; Ha-Vinh et al., 2004; Puig-Hervás et al., 2012). LH3 is reportedly inactivated in a rare connective tissue disease (Salo et al., 2008). Additionally, loss of LH3 is embryonic lethal for mice and causes severe defects in basement membrane formation (Ruotsalainen et al., 2006). All in all, these studies show that LH isoforms play important yet distinctive roles in collagen biology.

1.3.2 Hydroxylation of EGF-like domains

The identification of hydroxylated aspartyl and asparaginyl residues in epidermal growth factor (EGF)-like domains indicated that post-translational hydroxylations are found in proteins other than collagens and collagen-like domain containing proteins (Drakenberg et al., 1983; McMullen et al., 1983). EGF is a 53 amino acid polypeptide containing three disulfide bonds, formed by cleavage from a larger EGF precursor (Stenflo et al., 1987). Domains homologous to the EGF precursor are evolutionarily conserved, and

found mostly in extracellular and membrane proteins (Stenflo et al., 2000). Hydroxylations of asparagine and asparate residues have been identified in the EGF-like domains of vitamin K-dependent proteins, clotting factors, complement proteins, thrombomodulin and low density lipoprotein receptor (Drakenberg et al., 1983; McMullen et al., 1983; Przysiecki et al., 1987; Stenflo et al., 1988).

EGF-like domain hydroxylations are catalysed by a 2OG oxygenase called asparaginyl/ aspartyl-β hydroxylase (ASPH or BAH) (Stenflo et al., 1989; Gronke et al., 1989). The biochemical function of EGF-like domain hydroxylation is unclear. The consensus site of Asp/Asn β-hydroxylation is related to Ca^{2+} binding, though the presence of Asp/Asn hydroxylation did not significantly affect Ca^{2+} binding affinity (Sunnerhagen et al., 1993; Stenflo et al., 2000).

ASPH is overexpressed in various types of cancer, including hepatocellular carcinoma and cholangiocarcinoma, medulloblastoma and neuroblastoma (Lavaissiere et al., 1996; Sepe et al., 2002; Cantarini et al., 2006). ASPH is linked to malignant cell transformations with increased cell growth and motility (Ince et al., 2000; Sepe et al., 2002; Monte et al., 2006). However, the loss of ASPH activity has been associated with increased tumourigenesis in a colorectal cancer mouse model (Dinchuk et al., 2002). The role of ASPH in cancer is perhaps linked to the Notch signalling pathway (Cantarini et al., 2006). ASPH deficiency in mice causes multiple developmental defects including craniofacial malformation, syndactyly and defective palate formation, similar to mice with Notch ligand mutations (Dinchuk et al., 2002; Sidow et al., 1997). While Notch contains EGF-like domains, direct hydroxylation by ASPH has not been demonstrated (Dinchuk et al., 2002).

1.3.3 Hydroxylation of hypoxia-inducible factor (HIF)

In addition to the collagen and EGF-like domain hydroxylases, a group of 2OG oxygenases exists to orchestrate mammalian oxygen homeostasis. 2OG oxygenases require oxygen as an obligate cosubstrate, which makes them ideal sensors of environmental

oxygen tension. Four oxygenases hydroxylate the transcription factor hypoxia-inducible factor (HIF) to modulate its activity and stability in an oxygen-dependent fashion. HIF is the central transcription factor regulating the adaptive responses to conditions of low oxygen tension. Prolyl hydroxylation of HIF targets the transcription factor for proteolytic degradation, whereas asparaginyl hydroxylation of HIF affects its recruitment of transcriptional co-activator CBP/p300 (Figure 1.4). Both regulatory mechanisms will be discussed in detail below.

The hypoxia-sensing pathway The story of HIF began with the discovery of a transcriptional enhancer 3' to the erythropoietin (EPO) gene which controls oxygen-sensitive EPO production (Pugh et al., 1991; Semenza et al., 1991). Subsequent analyses revealed that similar oxygen-sensing mechanisms are omnipresent in the mammalian system (Wang and Semenza, 1993; Maxwell et al., 1993). Isolation of the enhancer binding complex identified HIF, a heterodimeric transcription factor consisting of α and β subunits (Semenza and Wang, 1992; Wang et al., 1995). HIFα/β recognises a core binding motif (A/GCGTG) in hypoxia response elements (HREs), and mediates the transcription of hundreds of target genes (Schofield and Ratcliffe, 2004). Both subunits are basic helix-loop-helix (bHLH) proteins containing per-ARNT-Sim (PAS) domains (Wang et al., 1995). HIFβ is constitutively expressed and has multiple dimerisation partners involved in diverse transcriptional responses. HIFα, on the other hand, is only stable and functional under conditions of hypoxia.

There are three known HIF α-subunit isoforms: HIF1α, HIF2α and HIF3α (Wang et al., 1995; Ema et al., 1997; Tian et al., 1997; Gu et al., 1998). Unlike the other isoforms, HIF3α lacks transactivation activity (Gu et al., 1998). Instead, a splice variant of HIF3α (termed inhibitory PAS; IPAS) suppresses HIF-mediated gene expression in a dominant negative manner (Hara et al., 2001; Makino et al., 2001, 2002). Expression of IPAS is hypoxia-inducible, which is indicative of a negative feedback mechanism (Makino et al., 2007). HIF1α and HIF2α are similar in transcriptional activity though disparate in their downstream effects (for review see Ratcliffe, 2007; Loboda et al.,

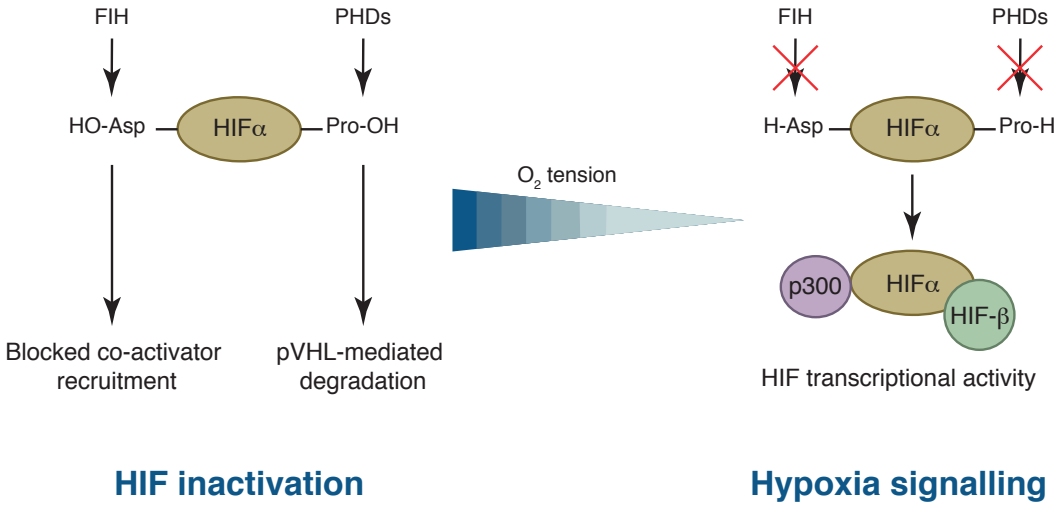


Figure 1.4: The regulation of hypoxia signalling. Under conditions of normoxia, HIFα is hydroxylated at prolyl residues (in N- and C-terminal oxygen dependent degradation domains) by the PHD enzymes. pVHL recognises and targets prolyl hydroxylated HIFα for proteosomal degradation. HIFα is also hydroxylated at an asparaginyl residue by FIH, which blocks p300 co-activator recruitment and HIF transcriptional activity. The activities of PHDs and FIH are inhibited by hypoxia, under which unhydroxylated HIFα forms a transcriptionally active complex and mediates hypoxia signalling.

2012). Together they control a complex network of cellular and systemic adaptive response to hypoxia. There are hundreds of identified HIF target genes involved in pathways such as energy metabolism, growth, angiogenesis, erythropoiesis and many more (Schofield and Ratcliffe, 2004). Moreover, since the cancer cell microenvironment is typically poorly oxygenated, the dysregulation of HIF presents a key oncogenic step in cancer progression (Semenza, 2010). As such, understanding of the hypoxia reponse pathway is of significant biological and therapeutic interest.

HIF prolyl hydroxylases The dominant form of HIF regulation is the oxygen-dependent proteolytic degradation of HIFα. Under normal oxygen tension, a family of prolyl hydroxylase domain-containing proteins (PHDs) hydroxylates HIF α-subunit at conserved proline residues (Bruick and McKnight, 2001; Epstein et al., 2001). Hydroxylation can occur on either Pro402 or Pro564 in two separate oxygen-dependent degradation domains (N-terminal ODDD and C-terminal ODDD; abbreviated NODD and CODD) of HIFα. E3 ligase von Hippel-Lindau tumour suppressor protein (pVHL) recognises hydroxylated HIFα (Ivan et al., 2001; Jaakkola et al., 2001), and targets HIFα for ubiquitination followed by proteosomal degradation (Ohh et al., 2000; Cockman et al., 2000). Low oxygen tension inhibits the catalytic activity of PHDs, which protects HIFα from proteosomal degradation, since unhydroxylated HIFα is not recognised by pVHL. Stabilised HIFα dimerises with HIFβ and translocates into the nucleus, where it mediates transcription of its target genes (Schofield and Ratcliffe, 2004).

Three HIF prolyl hydroxylases are found in humans: PHD1-3 (Epstein et al., 2001). PHD2 is the most abundant therefore dominant isoenzyme in most cell lines and tissues (Berra et al., 2003). However, PHD1 and PHD3 may play more important roles in a subset of physiological environments (Lieb et al., 2002). PHD1 is the only HIF hydroxylase found in testis. PHD3 is highly expressed in the heart, brain and skeletal muscles (Appelhoff et al., 2004). All three PHD isoenzymes are found in the kidney. In addition, expression of PHD isoenzymes may be induced differentially under specific physiological circumstances. For example, PHD3 is significantly induced under hypoxia

where it is proposed to dampen the HIF response, whilst PHD2 expression is only modestly affected and PHD1 is not induced (Appelhoff et al., 2004).

PHD2 knockout in mice causes embryonic lethality, consistent with its role as the primary HIF hydroxylase. In contrast, loss of PHD1 or PHD3 does not affect mouse viability (Takeda et al., 2006). PHD1 deficiency promotes anaerobic metabolism in skeletal muscles and induces HIF-2α mediated hypoxia tolerance (Aragonés et al., 2008). PHD3 deficiency is associated with abnormal neuronal development, consistent with its high expression in the brain (Bishop et al., 2008). Moreover, double knockout of PHD1 and PHD3 in mice causes moderate polycythemia, stemming from HIF2α accumulation in the liver (Takeda et al., 2008). Interestingly, conditional inactivation of PHD2 in mice also leads to polycythemia, though in this case it is related to HIF1α accumulation in kidney and liver (Takeda et al., 2008; Minamishima et al., 2008). This suggests that PHD2 preferentially regulates HIF1α, whilst the other PHD isoforms predominately affect HIF2α and may share functional redundancy. Collectively, these mouse studies highlight the differential roles of PHD isoforms and the importance of HIF signalling regulation in normal physiology.

An important question remains as to whether the ability of PHD enzymes to act as oxygen sensors is biochemically unique among 2OG oxygenases. The Km values of PHD for oxygen range from 65 to 240 µM depending on the assay condition, which is similar to other members of the superfamily (Hirsilä et al., 2003; Koivunen et al., 2006; Ehrismann et al., 2007). Intriguingly however, the PHD enzyme complex is unusually stable and reacts exceptionally slowly with oxygen *in vitro* (Flashman et al., 2010b). This observation differs significantly from other 2OG oxygenases and may contribute to the oxygen sensing ability of PHD enzymes.

In addition to oxygen, the requirement of Fe(II) and 2OG for PHD catalysis may provide an interface for additional regulation of HIF hydroxylation. Ascorbate is not essential for PHD activity, though it can act as a reducing agent and help to maintain the ferrous state of iron. Physiological concentration of ascorbate enhances PHD activity in normoxia, and increases the rate and extent of HIF hydroxylation *in vitro* (Knowles

et al., 2003; Flashman et al., 2010a). Therefore, ascorbate should be able to modulate HIF expression, at least in pathophysiological situations such as cancer (Kuiper et al., 2010). Furthermore, some metabolites have the ability to directly inhibit 2OG oxygenases. For instance, Krebs' cycle intermediates fumarate and succinate compete with 2OG for PHD binding and inhibit HIF hydroxylation (Pan et al., 2007; Koivunen et al., 2007). Consistent with *in vitro* experiments, HIF stabilisation is observed under *in vivo* conditions of fumarate hydratase (FH) inactivation and consequent fumarate accumulation (O'Flaherty et al., 2010). The above examples suggest that cross-talk between redox and metabolic pathways could serve to modulate the HIF signalling pathway by affecting PHD catalysis.

Factor-inhibiting HIF (FIH) A second HIF hydroxylase works synergistically with PHD enzymes to modulate HIF activity. FIH, or factor-inhibiting HIF, was initially identified as a transcriptional repressor of HIF (Mahon et al., 2001). It was later shown that FIH hydroxylates HIFα at Asp803 of the C-terminal transactivation domain (CAD; Lando et al., 2002a; Hewitson et al., 2002). Hydroxylation of the asparagine residue sterically blocks the interaction between HIF and its transcriptional co-activators p300/CBP (Lando et al., 2002b). In hypoxia, diminished asparaginyl hydroxylation enables HIF to recruit its co-activators, allowing for complete activation of HIF transcription factor activity.

FIH functions as a homodimer and is part of the 2OG oxygenase superfamily (Dann et al., 2002). *In vitro* measurements of the oxygen Km values for FIH are conflicting, with reports ranging from 90 to 240µM (Koivunen et al., 2004; Ehrismann et al., 2007). Regardless, FIH is thought to be less sensitive to hypoxia than PHD enzymes, at least in a large subset of cells (Koivunen et al., 2004; Stolze et al., 2004; Bracken et al., 2006; Tian et al., 2011). Comparison of HIFα hydroxylation sites by immunoblotting showed that Asn803 hydroxylation is more resistant to hypoxia than the prolyl hydroxylation (Tian et al., 2011). In addition, both RNA interference and overexpression of FIH altered HIF target gene expression at severe hypoxia, at which point PHD2

is no longer active (Stolze et al., 2004). Therefore, HIF α-subunits that escape from proteosomal degradation in moderate hypoxia are still subjected to regulation by FIH. Since subsets of HIF target genes respond differentially to FIH inhibition, asparaginyl hydroxylation may serve to fine-tune HIF transcriptional output under varying levels of oxygen (Dayan et al., 2006). Furthermore, FIH is reported to be more sensitive to inhibition by peroxide than PHD enzymes, which provides an additional platform for FIH to modulate hypoxia signalling under conditions of oxidative stress (Masson et al., 2012).

Rather unexpectedly, genetic knockout of FIH in mice does not elicit the classical HIF response pathway. Instead, FIH null mice display increased metabolism, hyperventilation and resistance to weight gain from high fat diets (Zhang et al., 2010). The relationship between HIF asparaginyl hydroxylation and the observed mice phenotype is unclear. However, it does raise the possibility that FIH has additional functions outside of the HIF signalling pathway.

1.3.4 Ankryin repeat domain (ARD) hydroxylation by FIH

In addition to HIF, FIH also hydroxylates proteins bearing ankryin repeat domains (ARD; Cockman et al., 2006). ARD contains variable number repeats of a 33-residue motif named ankyrin repeat (AR); each AR forms a helix-loop-helix structure where two anti-parallel α-helices are linked by a β-hairpin. These ARs do not mediate enzymatic activity. Instead, they stack together to form an interface for protein-protein interaction (Li et al., 2006). ARD is one of the most ubiquitous motifs in nature. It is found in a diverse range of proteins belonging to pathways including cell cycle, differentiation, cell adhesion, transcription regulation and more (Li et al., 2006).

FIH-catalysed hydroxylation is widespread in ARD proteins, with substrates including NFκB proteins, Notch receptors, MYPT1, tankyrase, cytoskeletal ankryin family, ASPP2 and likely many more (Cockman et al., 2006; Coleman et al., 2007; Webb et al., 2009; Cockman et al., 2009; Yang et al., 2011b; Janke et al., 2013). Each substrate often

has multiple hydroxylation sites. Many of the reported hydroxylation sites have been validated by mass spectrometry. Though FIH was believed to be just an asparaginyl hydroxylase, recent evidence suggests that FIH also hydroxylates histidine and aspartate residues of ARD (Yang et al., 2011a,b). This makes FIH highly promiscuous both in its substrate specificity and amino acid selectivity.

Despite the widespread occurrence of FIH-mediated ARD hydroxylation, its physiological significance remains unclear. RNA interference against FIH, which directly suppresses ARD hydroxylation, failed to exert any effects on Notch or NF-κB signalling (Cockman et al., 2006; Coleman et al., 2007). However, a separate study suggested that FIH inhibits Notch signalling and promotes myogenic differentiation (Zheng et al., 2008). Whether the observed effects are due to loss of hydroxylation or mutation of the asparagine residues is under debate.

The diverse range of ARD substrates argues against a global 'switch-like' function for the modifications. It is possible that FIH-mediated hydroxylation serves to stabilise ARD conformation. Asparaginyl hydroxylation forms a hydrogen bond with an aspartate residue, and increases the thermal stability of the ARD fold in solution (Kelly et al., 2009). However, ARD hydroxylation is often incomplete, and suppression of FIH expression does not affect the stability of ARD proteins in cells (Cockman et al., 2009; Janke et al., 2013). Interestingly, more stable ARDs are less efficiently hydroxylated by FIH, since unfolding of the ARD is required for FIH binding (Cockman et al., 2009; Hardy et al., 2009).

Alternatively, ARD proteins are proposed to fine-tune HIF signalling by competing for FIH binding. FIH has a much higher binding affinity for ARD relative to HIFα (Coleman et al., 2007). In support of this hypothesis, co-expression of an ARD substrate with HIF1α diminishes HIF asparaginyl hydroxylation and promotes HIF-CAD activity (Coleman et al., 2007; Zheng et al., 2008; Webb et al., 2009). ARD proteins may sequester FIH activity under chronic hypoxia, which would provide an extra layer of complexity in the HIF signalling pathway (Cockman et al., 2009)

1.4 Post-translational modifications catalysed by the JmjC-only enzymes

FIH belongs to a group of 2OG oxygenases termed the JmjC-only family. As the name suggests, proteins in this group have few distinguishable domains other than the JmjC catalytic domain. Members of the JmjC-only enzyme family include FIH, Myc-induced nuclear antigen with a molecular mass of 53 kDa (MINA53), nucleolar protein 66 (NO66), Jumonji domain containing proteins 4-8 (JMJD4-8), and heat shock protein beta-1 associated protein 1 (HSPBAP1; Figure 1.3). Although FIH is well studied, the biochemical activities of several other JmjC-only enzymes are relatively poorly characterised. The substrate specificities of JmJC-only enymes are summarised in Table 1.4. A few reports have implicated these enzymes in histone demethylation. However, overwhelming evidence suggest that they are likely protein hydroxylases, consistent with their lack of chromatin binding domains. The functional characterisation of JmjC-only 2OG oxygenases is an area of active interest.

1.4.1 Members of the JmjC-only enzyme family

MINA53 and NO66 MINA53 was first identified as a Myc-inducible protein important for cancer cell proliferation (Tsuneoka et al., 2002). It was later shown that MINA53 localises to the nucleus, and may play a role in ribosome biogenesis by interacting with preribosomal particles (Eilbracht et al., 2005). Interesingly, the expression of MINA53 is associated with increased rRNA (Lu et al., 2009b). MINA53 is proposed to modulate gene transcription *via* its demethylation of H3K9me3 (Lu et al., 2009b; Chen et al., 2013). However, another group was unable to show any MINA53 demethylase activity against histones (Ge et al., 2012).

RNA interference of MINA53 was reported to inhibit growth of a large number of cancer cell lines (Tsuneoka et al., 2002, 2004; Teye et al., 2004; Zhang et al., 2005). Moreover, MINA53 is overexpressed in cancerous tissues relative to normal tissues, and

Jumonji domain-containing hydroxylases (JmjC-only enzymes)				
Name	Alternative name(s)	Demethylation substrate(s)	Hydroxylation substrate(s)	References
FIH	HIF1AN	Unknown	HIFα; ARD-domain containing proteins	Lando et al, 2002a; Hewitson et al, 2002; Cockman et al, 2006; Coleman et al, 2007; Webb et al, 2009; Cockman et al, 2009; Yang et al, 2011b; Janke et al, 2013
MINA53	NO52/MDIG	H3K9me3*	RPL27A	Lu et al, 2009; Ge et al, 2012; Chen et al, 2013
NO66		H3K4me3*; HeK36me3*	RPL8	Sinha et al, 2010; Brien et al, 2012; Ge et al, 2012
JMJD4		Unknown	eRF1	Feng et al, 2014
JMJD5	KDM8	H3K26me1/2*	Unknown	Hsia et al, 2010; Ishimura et al, 2012
JMJD6	PTDSR/PSR	H3R2me2*; H4R3me1/2*; 7SK snRNA	U2AF65; LUC7L2; H2A/H2B; H3/H4	Chang et al, 2007; Webby et al, 2009; Mantri et al, 2011; Unoki et al, 2013; Liu et al, 2013
JMJD7		Unknown	Unknown	
JMJD8		Unknown	Unknown	
HSPBAP1		Unknown	Unknown	

Table 1.4: JmjC-only hydroxylases and their substrate specificities. Members of JmjC-only oxygenase family and their substrates are listed as shown. Several JmjC-only enzymes have been implicated in histone demethylation, though they are most likely to be protein hydroxylases. The two enzymes highlighted in red, NO66 and JMJD4, are central to the work in this thesis. * indicate substrates that are contested due to conflicting results in the published literature.

high level of MINA53 expression is correlated with poor patient prognosis. This has been observed in many tumour types including esophageal squamous cell carcinoma, adenocarcinoma, neuroblastoma, renal cell carcinoma, non-small cell lung carcinoma and cholangiocarcinoma (Tsuneoka et al., 2004; Teye et al., 2004; Fukahori et al., 2007; Ishizaki et al., 2007; Lu et al., 2009b; Tan et al., 2012; Chen et al., 2013). The expression of MINA53 mRNA is induced in alveolar macrophages isolated from the lungs of coal miners, and is linked to the development mineral dust-induced lung cancer (Zhang et al., 2005; Lu et al., 2009b). However, other studies reported that MINA53 overexpression is associated with favourable prognosis in early stages of lung cancer (Komiya et al., 2010). The conflicting observations might be explained by MINA53 playing a positive role in cell growth but a negative role in cancer cell invasion and motility (Komiya et al., 2010; Yu et al., 2014).

MINA53 also regulates immunity. It transcriptionally inhibits Il-4 expression, which decreases the likelihood of naïve CD4+ T cells differentiating into T helper 2 cells (Th2) cells (Okamoto et al., 2009). MINA53 expression is also induced during T helper 17 (Th17) differentiation. It suppresses the expression of T regulatory (Treg) transcription factor Foxp3, and consequently tips the Treg/Th17 balance towards Th17 differentiation (Yosef et al., 2013). Though MINA53 appears to be important in T cell differentiation, its exact mechanism is unclear. Future work should focus on deciphering the link between MINA53 enzymatic activity and its roles in immunity and oncogenesis.

NO66 is closely related to MINA53, sharing 39% sequence homology overall and 57% homology within the catalytic domain (Eilbracht et al., 2004, 2005). Like MINA53, NO66 is also found in the nucleolus (Eilbracht et al., 2004). NO66 is implicated in cancer cell growth, particularly in non-small cell lung carcinoma (Suzuki et al., 2007). Its *Caenorhabditis elegans* ortholog, JMJC-1, protects against osmotic, oxidative, heat shock and ethanol stresses by activating a set of stress responsive genes (Kirienko and Fay, 2010). NO66 reportedly demethylates histones, since *in vitro* reaction of recombinant NO66 with bulk histones reduced H3K4me3 and H3K36me3 methylation status (Sinha et al., 2010). Similar to MINA53 however, the histone demethylase ac-

tivity of NO66 was not observed by another group (Ge et al., 2012). Regardless of its catalytic mechanism, NO66 interacts with transcription factor Osterix (Osx) and represses Osx activity (Sinha et al., 2010). NO66 occupancy at Osx-target promoters is inversely correlated with that of Osx, and inhibits osteoblast differentiation through transcriptional repression of Osx-target genes (Sinha et al., 2010, 2014). In differentiating mouse ES cells, PHF19 of the polycomb repressive complex PRC2 associates with NO66 at the chromatin. This results in H3K36me3 demethylation, PRC2-mediated H3K27 trimethylation and transcriptional repression (Brien et al., 2012). Similar to MINA53, the relationship between NO66 catalytic activity and its phenotypic outcomes require further elucidation.

JMJD5 JMJD5 was originally predicted to be a histone demethylase, since both overexpression and knockdown of JMJD5 correlate with changes in H3K36 dimethylation (Hsia et al., 2010; Ishimura et al., 2012). Subsequent biochemical and cellular experiments failed to observe any JMJD5 demethylase activity against histones (Del Rizzo et al., 2012; Youn et al., 2012). This is consistent with structural and phylogenetic analyses showing that JMJD5 is more similar to protein hydroxylases FIH and other JMJC-only enzymes rather than JmjC histone demethylases (Del Rizzo et al., 2012). Interestingly however, an overexpression proteomic study identified JMJD5 to interact with the chromatin in complex with an uncharacterised protein named RCCD1 (Marcon et al., 2014). Either the presence of RCCD1 or the N-terminal truncation of JMJD5 is required for the JmjC enzyme to demethylate H3K36me3 peptides *in vitro* (Hsia et al., 2010; Marcon et al., 2014). This suggests that JMJD5 could indeed possess true histone demethylase activity, though additional experiments are required to directly demonstrate histone demethylation by JMJD5 in cells.

JMJD5 is involved in a diverse range of cellular processes. It is important for maintaining normal circadian rhythm in both *Arabidopsis thaliana* and mammalian cells (Jones et al., 2010). JMJD5 null mice are embryonic lethal at day 10.5 (Ishimura et al., 2012; Oh and Janknecht, 2012). Suppression of JMJD5 also affects prolifer-

ation of cultured cancer cells, and results in cell cycle arrest in addition to loss of pluripotency in human ES cells (hESCs; (Hsia et al., 2010; Zhu et al., 2014). The effect of JMJD5 on growth and development is partially mediated by p21, possible *via* induction of p53 expression (Ishimura et al., 2012; Oh and Janknecht, 2012; Zhu et al., 2014). In hypoxia, JMJD5 interacts directly with pyruvate kinase isoform M2 (PKM2) and is important for PKM2 nuclear translocation (Wang et al., 2014a). Furthermore, JMJD5 inhibits osteoclast differentiation by post-translational destabilisation of osteoclastogenesis transcription factor NFATc1 (Youn et al., 2012). Though JMJD5 is claimed to hydroxylate NFATc1 (Youn et al., 2012), biochemical characterisation by mass spectrometry is required to validate this hypothesis.

JMJD6 JMJD6 was originally identified as the phosphatidyl serine receptor (PSR). Phospholipid phosphatidyl serine appears uniquely on surfaces of apoptotic cells. PSR was thought to express on phagocyte cell surfaces, recognise phosphatidyl serine and target apoptotic cells for clearance (Williamson and Schlegel, 2004). However, the identity of PSR has been brought into question after it was discovered to be a 2OG oxygenase that localises to the nucleus (Cikala et al., 2004; Hahn et al., 2010). PSR, or JMJD6, was later shown to demethylate arginine residues in histones (Chang et al., 2007). However, subsequent studies have failed to make similar observations, which brought the biochemical activity of JMJD6 into question (Webby et al., 2009; Hahn et al., 2010; Hong et al., 2010; Boeckel et al., 2011; Han et al., 2012). Proteomic studies show that JMJD6 interacts with proteins related to RNA processing, many of which are proteins containing Arg-Ser-rich (RS) domains (Webby et al., 2009; Heim et al., 2014). Moreover, JMJD6 catalyses C5 lysyl hydroxylation of the RS domain in splicing factor U2 small nuclear ribonucleoprotein auxiliary factor 65-kilodalton subunit (U2AF65; Webby et al., 2009). In addition to RS domain proteins, JMJD6 also catalyses 5-lysyl hydroxylation of histones, as confirmed by amino acid analysis and mass spectrometry (Chang et al., 2007; Webby et al., 2009; Han et al., 2012; Unoki et al., 2013). It was recently shown that Brd4 recruits JMJD6 to distal transcriptional enhancer sites, where

JMJD6 was suggested to mediate transcriptional pause release through the demethylation of H4R3 and 7SK snRNA cap (Liu et al., 2013). However, additional biochemical characterisations are required to confirm its demethylase activity, since the study was mostly limited to *in vitro* assays measured using immunoblotting (Liu et al., 2013). It is also possible that JMJD6 is able to regulate gene expression *via* the hydroxylation rather than demethylation of histones (Chang et al., 2007; Webby et al., 2009; Han et al., 2012; Unoki et al., 2013).

In addition to gene transcription, JMJD6 may be involved in mRNA splicing and other RNA processing events (Webby et al., 2009; Heim et al., 2014). Suppression of JMJD6 expression affected mRNA splicing of both reporters and endogenous targets (Webby et al., 2009; Boeckel et al., 2011; Barman-Aksözen et al., 2013; Heim et al., 2014). One such endogenous gene is the VEGF-receptor 1 (Flt1). Loss of JMJD6 alters splicing of the Flt1 pre-mRNA and promotes production of a soluble Flt-1 variant, which inhibits angiogenesis by binding to VEGF and placental growth factor (PIGF; Boeckel et al., 2011. RNA interference of JMJD6 also increases aberrant splicing product of ferrochelatase, which interestingly mimics conditions of iron deficiency (Barman-Aksözen et al., 2013). Though yet to be demonstrated, it is likely that the involvement of JMJD6 in mRNA splicing could be a direct consequence of its catalytic activity towards RNA processing proteins. However, JMJD6 binds to single stranded RNA *in vitro* and co-localizes with nascent RNA in cells, which may suggest alternative JMJD6 functions (Hong et al., 2010; Heim et al., 2014).

The loss of JMJD6 in mice causes neonatal lethality. The absence of JMJD6 results in defective development of multiple organs including heart, kidney, intestine, liver and lungs (Böse et al., 2004; Schneider et al., 2004). JMJD6 is also important for normal erythroid differentiation, as JMJD6 null mice display severe anemia and thymus atrophy (Kunisaki et al., 2004). Furthermore, JMJD6 is overexpressed in lung adenocarcinoma and its expression is associated with poor patient prognosis (Zhang et al., 2013). It would be of significant interest to understand the mechanistic link between the physiological phenotype, cellular function, and catalytic activity of JMJD6.

Other JmJC-only enzymes JMJD4 is a poorly studied protein sharing the highest sequence homology with JMJD6. The gene encoding JMJD7 is located upstream of cytosolic phospholipase A2, group IVB (PLA2G4B) on chromosome 15 (Ghosh et al., 2006). Most tissues express a fusion product encoding PLA2G4B and the N-terminus of JMJD7 with a part of its JmjC domain (Ghosh et al., 2006). Regardless, the function of JMJD7 is unknown. JMJD8 is linked to cancer metastasis though its biochemical activity is unclear. RNA interference of JMJD8 significantly reduced the invasive properties of SCC23 cells, a squamous cell carcinoma cell line (Ding et al., 2013). HSPBAP1 was initially identified in a yeast two-hybrid assay as an interactor of heat shock protein 27 (Hsp27; Liu et al., 2000). Overexpression of HSPBAP1 in cells inhibits Hsp27-mediated protective response against heat shock (Liu et al., 2000). The rat ortholog of HSPBAP1 is highly expressed in kidney and testis, whereas human HSPBAP1 is mostly found in thymus and pancreas (Liu et al., 2000; Jiang et al., 2001). HSPBAP1 is not expressed in the brain, except in the anterior temporal neocortex of intractable epilepsy (IE) patients (Jiang et al., 2001; Xi et al., 2007). However, the biochemical function of HSPBAP1 is yet to be determined.

Summary The JmjC-only family encompasses an interesting group of 2OG oxygenases involved in biological pathways ranging from oxygen sensing to heat shock response. Though some of these enzymes were thought to be histone demethylases, mass spectrometry studies had assigned most JmjC-only enzymes as protein hydroxylases. Though several members of the JmjC-only family have unknown biochemical functions, bioinformatic analyses suggest that they retain the conserved Fe(II) and 2OG binding residues required for catalysis (Figure 1.5). Biochemical characterisation of these enzymes, such as the work presented in this thesis, will help to better understand the role of JmjC-only hydroxylases in biology.

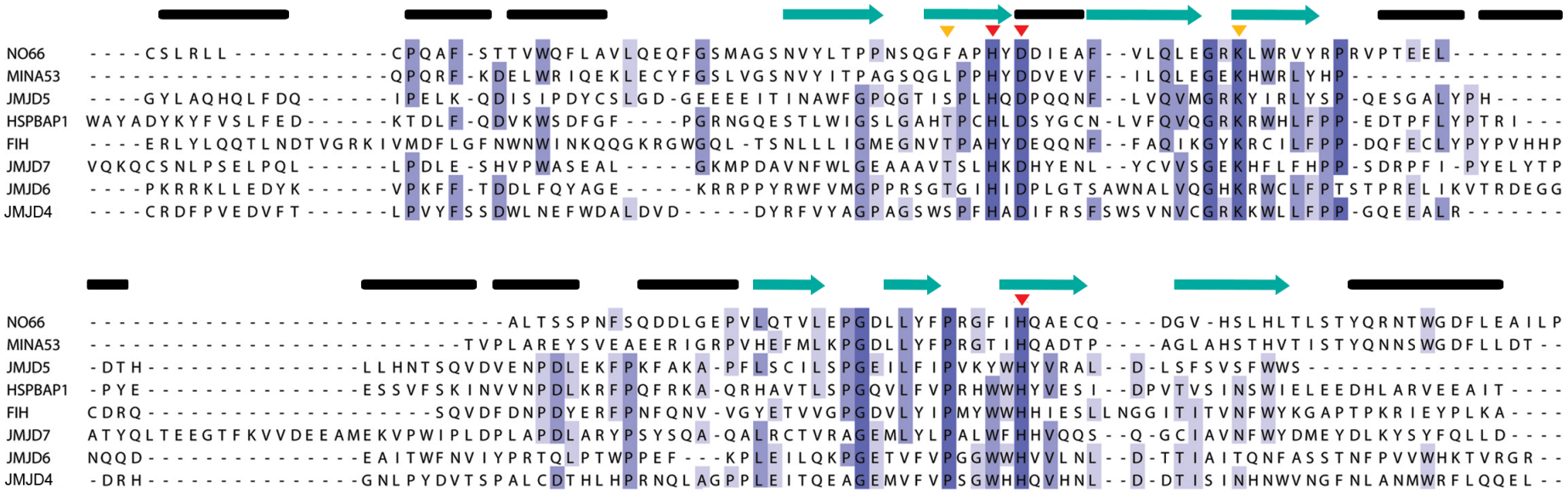


Figure 1.5: Sequence alignment of enzymes from the JmjC-only family. Amino acid alignment of JmjC domains from members of the JmjC-only enzyme family. The secondary structure of JMJD6 is labelled above the sequences, with cylinders and arrows indicating α-helices and β-strands, respectively. The triangles denote Fe(II) (red) and 2OG (yellow) binding residues. Figure adapted from Feng et al. (2014).

1.5 Aim and scope of this thesis

Despite the apparent diversity of 2OG oxygenases, a unifying theme emerges from their overarching importance in the regulation of gene expression. DNA modifications catalysed by the TET enzymes allow epigenetic reprogramming of gene expression (Tahiliani et al., 2009; Ito et al., 2010; Ko et al., 2010; Yang et al., 2012). At the level of the chromatin, JmjC domain-containing histone demethylases mediates both transcriptionally activating and repressive effects (Klose et al., 2006a; Johansson et al., 2014). In the case of the hypoxia response pathway, the stability of transcription factor HIF is directly modulated by 2OG oxygenase-catalysed hydroxylations (Schofield and Ratcliffe, 2004; Ratcliffe, 2013). JMJD6 catalyses 5-lysyl hydroxylation of mRNA splicing factor U2AF65, and affects mRNA splicing (Webby et al., 2009; Boeckel et al., 2011; Barman-Aksözen et al., 2013; Heim et al., 2014).

Emerging evidence indicates that 2OG oxygenases are also involved in the translational control of gene expression. For example, the 2OG oxygenase OGFOD1 is distantly related to HIF prolyl hydroxylases, and catalyses the prolyl hydroxylation of 40S ribosomal protein S23 (RPS23). Interestingly, RPS23 is doubly hydroxylated in yeast and algae, but is only singly hydroxylated in higher eukaryotes (Katz et al., 2014; Loenarz et al., 2014; Singleton et al., 2014). In both instances however, OGFOD1 hydroxylase activity modulates translational fidelity and stop codon decoding (Loenarz et al., 2014; Singleton et al., 2014). At least in yeast, its effect on stop codon decoding is context-dependent (Loenarz et al., 2014). Moreover, the loss of OGFOD1 activity is related to growth and translational arrest in both *Drosophila melanogaster* and mammalian systems (Katz et al., 2014; Singleton et al., 2014).

On the other hand, ALKBH8, a human homologue of *E. coli* DNA repair enzyme AlkB, possesses both hydroxylase and methyltransferase activities towards tRNA (Fu et al., 2010; van den Born et al., 2011). ALKBH8 modifies tRNA at the wobble position to generate 5-methoxycarbonylmethyluridine (Fu et al., 2010; van den Born et al., 2011). Both ALKBH5 and FTO demethylate N6-methyladenosine, one of the

most prevalent nucleotide modifications in mRNA and long noncoding RNA (Jia et al., 2011; Zheng et al., 2013). N6-methyladenosine is recognised by specific RNA-binding proteins that modulate RNA stability, and mediates widespread gene regulation (Wang et al., 2013, 2014b). Loss of ALKBH5 is associated with defective spermatogenesis in mice (Zheng et al., 2013). The FTO gene is linked to diabetes and obesity in humans, though the actual mechanism is not well understood (Frayling et al., 2007; Dina et al., 2007; Fischer et al., 2009). Furthermore, the JmJC-domain containing enzyme TYW5 hydroxylates the modified RNA base wybutosine to generate hydroxywybutosine in $tRNA_{phe}$ (Noma et al., 2010).

Taken together, these findings demonstrate that protein synthesis is a major new target of 2OG oxygenases. While 2OG oxygenases have been shown to modify nucleic acids involved in mRNA translation, little is known about the role of 2OG oxygenase-catalysed protein modifications in the protein synthesis pathway. As such, there is a distinctive possibility that additional 2OG oxygenases targeting the protein synthesis machinery are yet to be discovered.

This thesis aims to identify novel 2OG oxygenases involved in the regulation of gene expression. Several JmjC-only oxygenases retain conserved residues for cofactor binding, though their catalytic activities remain to be characterised. Given the studies to date implicating the JmjC-only proteins in both normal physiological function and disease pathogenesis, we sought to elucidate the activities of these putative 2OG oxygenases.

The work presented in this thesis describes two JmjC-only enzymes, NO66 and JMJD4. Chapter 2 is concerned with the biochemical characterisation of NO66. A proteomic pull-down of NO66 and its interacting proteins was performed in search for candidate NO66 substrates. A ribosomal protein, RPL8, was identified to be hydroxylated by NO66 at H216. Hydroxylation of RPL8 by NO66 was analysed in detail by mass spectrometry. Similar biochemical characterisation was performed for JMJD4 and presented in chapter 3. JMJD4 was found to hydroxylate the eukaryotic release factor, eRF1 at K63. eRF1 plays an important role in translational termination by recognis-

ing the stop codon at the ribosomal A site and mediating peptidyl release. Chapter 4 describes the effect of JMJD4-catalysed K63 hydroxylation on eRF1 translational termination activity, and its potential link to cell biology and disease.

Results are discussed individually in each chapter, but summarised and concluded in chapter 5. Materials and experimental procedures are outlined in chapter 6.

Chapter 2

NO66 is a ribosomal histidinyl hydroxylase

2.1 Introduction

NO66 was initially isolated from the nucleolus of *Xenopus laevis* oocytes (Eilbracht et al., 2004). Comparison across multiple mammalian cell lines revealed that the localisation of NO66 is strongly nucleolar. At least in *Xenopus*, NO66 is enriched in the granular component of the nucleolus (Eilbracht et al., 2004). The granular component is a major region in the nucleolus where the final steps of ribosome processing and assembly take place prior to export (Boisvert et al., 2007). Consistent with its localisation, NO66 co-fractionates with precursors of the large ribosomal subunit, suggesting a possible role in ribosome biogenesis (Eilbracht et al., 2004).

NO66 was identified in a separate study as Myc-associated protein with JmJC domain (MAPJD; Suzuki et al., 2007). NO66, or MAPJD, was overexpressed in non-small cell lung carcinoma (NSCLC) compared to normal lung tissues (Suzuki et al., 2007). Knockdown of NO66 by siRNA inhibited the proliferation of NSCLC cells, whereas overexpression of NO66 promoted cell proliferation (Suzuki et al., 2007). NO66 was therefore postulated to regulate cancer cell growth, possibly by modulating gene expression in conjunction with Myc (Suzuki et al., 2007). The *C. elegans* NO66 orthologue,

JMJC-1, has also been implicated in transcriptional control. JMJC-1 was proposed to act downstream of zinc finger protein SLR-2 to regulate transcription of genes belonging to a stress response network (Kirienko and Fay, 2010).

In addition to cell growth and stress responses, NO66 has been shown to regulate osteoblast differentiation. A proteomic screen found NO66 to be an interactor of Osx, a transcription factor important for osteoblastogenesis and bone development (Sinha et al., 2010). Co-expression of NO66 with Osx inhibited the transcriptional activation of an Osx-specific reporter. Furthermore, suppression of NO66 expression by shRNA accelerated the rate of osteoblastogenesis and increased expression of Osx target genes in preosteoblast cells (Sinha et al., 2010). The repressive effect of NO66 on Osx target genes was proposed to be caused by histone demethylation, since the addition of recombinant NO66 to bulk histones reduced trimethylations of H3K4 and H3K36. Additionally, overexpression of NO66 in COS7 cells was associated with decreased levels of H3K4me3 and H3K36me3 (Sinha et al., 2010). Interestingly, NO66 also interacts with PHF19, a component of Polycomb repressive complex 2 (PRC2; Brien et al., 2012). PRC2 transcriptionally represses gene expression by altering chromatin structure, most likely by catalysing H3K27 trimethylation (Bracken and Helin, 2009). The activity of PRC2 is important for stem cell fate and differentiation. Recruitment of NO66 to PRC2 was postulated to enable H3K36me3 demethylation (Brien et al., 2012). However, despite reports of histone demethylation by NO66, it failed to demethylate any histone peptides *in vitro* (Ge et al., 2012).

Conflicting results on NO66 histone demethylase activity inferred that NO66 might possess alternative catalytic functions. Among members of the JmjC-only family, NO66 is most similar to MINA53. MINA53 has also been described as a histone demethylase, though similar to NO66 it did not exhibit any demethylase activity against histone peptides *in vitro* (Lu et al., 2009b; Ge et al., 2012). Proteomic and peptide studies have additionally shown that MINA53 hydroxylates the 60s ribosomal protein L27A (RPL27A) at a histidine residue (Ge et al., 2012). Given the sequence homology between MINA53 and NO66, it is thus conceivable that NO66 also possesses protein

hydroxylase activity.

The work in this chapter describes the biochemical characterisation of NO66 catalytic activity. A proteomic screen was performed using HEK293T cells overexpressing tagged NO66, and RPL8 was identified as a candidate NO66 substrate. It was shown using inducible NO66 cell lines that RPL8 is endogenously hydroxylated at H216, and this modification is dependent on NO66 protein expression. Mass spectrometry characterisation of MINA53 knockdown and knockout cells demonstrated that NO66, but not MINA53, is responsible for RPL8 H216 hydroxylation. Finally, the biological consequences of NO66-catalysed RPL8 hydroxylation were explored.

2.2 Results

2.2.1 Mass spectrometry techniques

Employed extensively in this thesis, mass spectrometry (MS) is a powerful analytical technique that measures the mass to charge (m/z) ratios of charged molecules. It first converts the molecules in a sample into ions, and then separates the ions based on their respective m/z ratios. The m/z value of an ion is then used to infer its mass. Depending on the technique, MS can be used to determine the composition and relative abundance of certain compounds. When applied to proteins, MS becomes an important tool for studying both protein-protein interaction and post-translational modifications.

The mass spectrometer consists of three components: an ionisation source, a mass analyser and a detector. Ionisation of the sample takes place within the ionisation source. Methods of ionisation differ depending on the type of sample and mass spectrometer, and usually involve the addition or removal of protons and/or electrons. These ions are resolved in the mass analyser based on their m/z ratio, which is determined by their trajectories in an electric and/or magnetic field in vacuum. Multiple types of mass analysers exist and may vary in accuracy and resolution. Finally, ions that pass through the mass analyser are recorded by the detector and presented as a

mass spectrum.

One of the mass spectrometry technique of interest to this thesis is tandem mass spectrometry (MS/MS), which is used for amino acid sequencing of peptides and positional assignment of post-translational modifications. In MS/MS, multiple steps of MS are separated with a fragmentation step in between. Briefly, peptides are first analysed by simple MS. Ions of the same m/z values are further fragmented in a collision chamber, usually by collision with gas. The produced ion fragments are subjected to a second MS step (Figure 2.1A). Since peptides typically fragment at amide bonds, differences in m/z ratios between overlapping ion fragments are used to deduce the amino acid sequence of the original peptide. Figures 2.1B and C provide the schematic and explanation of a sample MS/MS spectrum. Ions that fragment from the N-terminal of the peptide are termed the b-ion series, whereas ions that fragment from the C-terminal of the peptide are termed the y-ion series. The mass spectrum in Figure 2.1 depicts the b-ion series, where the m/z difference between each ion fragment provides information regarding the missing amino acid. Moreover, post-translational modification of an amino acid will impart a m/z shift in all ion fragments containing the modified residue, which allows assignment of the post-translational modification with certainty.

In the context of complex peptide or protein mixtures, capillary liquid chromatography (LC) may be added as an extra step before MS. LC enables physical separation of the sample, which enhances MS detection and allows for analysis of more complicated mixtures. Moreover, LC can also be coupled with MS/MS, which allows sequencing of individual peptides from a complex proteomic sample. Both liquid chromatography-mass spectrometry (LC-MS) and MS/MS techniques have been used extensively in this work to characterise 2OG oxygenase-catalysed post-translational modifications.

2.2.2 Identification of the NO66 substrate RPL8

In order to identify putative NO66 substrates, a proteomic pull-down was performed using HEK293T cells overexpressing haemagglutinin (HA)-tagged NO66. Lysates from

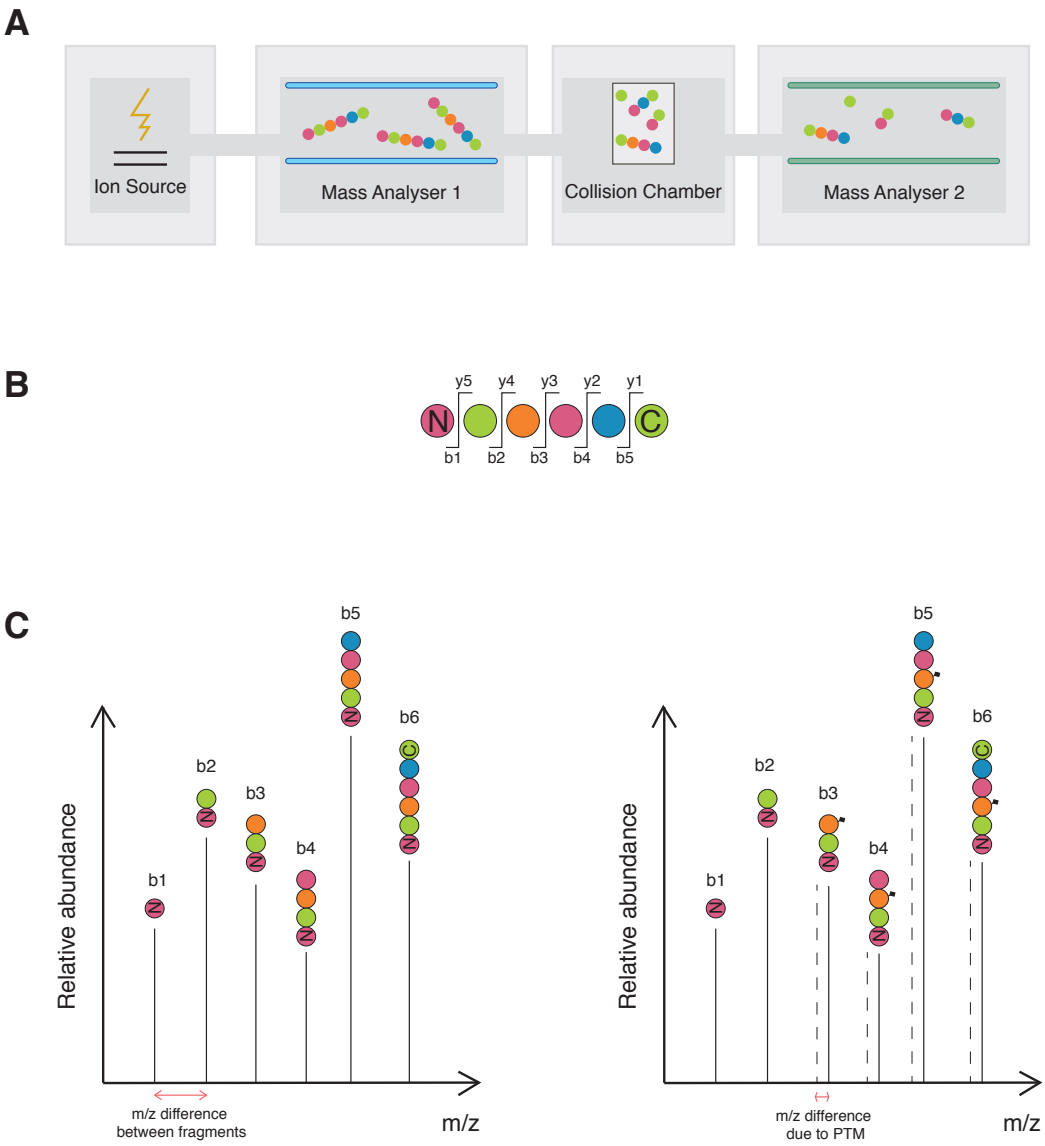


Figure 2.1: Schematic of MS/MS. A) In MS/MS, peptides are passed through the first mass analyser, fragmented in the collision chamber, and the resultant fragment ions are analysed in the second mass analyser. **B)** Fragmentation from the N-terminus of a peptide produces the b-ion series, whereas fragmentation from the C-terminus forms the y-ion series. **C)** The left panel shows MS/MS spectrum of b-ion series fragments of a peptide. The m/z difference between adjacent fragments helps to define the amino acid sequence of the peptide. The right panel shows MS/MS spectrum of b-ion series fragments from a modified peptide. Dashed lines denote m/z values of unmodified ion fragments. Instead of the predicted m/z values, ion fragments containing the modified amino acid exhibit an additional m/z shift consistent with the modification. This allows assignment of the amino acid position of the post-translational modification.

HA-NO66 or control cells were immunopurified with anti-HA agarose beads, prior to elution and trypsinolysis for liquid chromatography-tandem mass spectrometry (LC-MS/MS) analysis. NO66 interacting proteins were identified using the Mascot search engine (http://www.matrixscience.com). Mascot is a software that uses probability-based algorithms to identify proteins from MS/MS sequencing data, by comparing against a protein sequence database. In Mascot, each identified protein is given a score based on the number of different peptide sequences found, and the probability of each peptide sequence being a correct match to the database. Therefore, the Mascot protein score is an approximate correlate to the relative abundance of different proteins in the immunopurified sample.

The most abundant NO66 interacting proteins were shortlisted based on their sequence coverage and protein score derived from the Mascot search engine (Table 2.1). Most of the interactors were nucleolar or ribosomal proteins (Table 2.1), consistent with the nuclear localisation of NO66 (Eilbracht et al., 2004). However, several proteomic hits were localised elsewhere in the cell and were probably not true NO66 interactors. This was likely due to sample contamination, or non-physiological interactions with NO66 under conditions of overexpression. To screen for candidate NO66 substrates, a simple *in vitro* tile-based peptide assay was performed (Performed by Dr. Wei Ge; Ge et al., 2012). For each NO66 interactor listed in Table 2.1, a series of overlapping peptides covering the entire protein sequence were synthesised and tested for hydroxylation by NO66. The peptides were incubated at 37°C in assay buffer containing Fe(II), 2OG and ascorbate, in the presence or absence of recombinant NO66. The samples were analysed by matrix assisted laser desorption/ionisation-time of flight mass spectrometry (MALDI-TOF MS). In brief, peptides were suspended in a large amount of matrix, which was crystallised prior to ionisation. The m/z ratio of ionised peptides were determined by TOF-MS, by measuring the amount of time it takes for ions to pass through the mass analyser.

Upon reaction with NO66, a peptide sequence from RPL8 exhibited a +16 m/z shift, consistent with hydroxylation (Figure 2.2A). Mass shift of the RPL8 peptide was

Description	Localisation	Protein Score	Peptides Detected	Peptide Score
C1qBP	Mitochondrial/Membrane/ Nuclear/Nucleolus/Cytoplasmic	211	MSGGWELELNGTEAK EVSFQSTGESEWK AFVDFLSDEIK	517 480 451
40S ribosomal protein S3	Cytoplasmic/Nuclear/Nucleolar	166	ELAEDGYSGVEVR TEIIILATR GCEVVVSGK FVADGIFK	504 446 416 399
60S ribosomal protein L7	Cytoplasmic/Nuclear/Nucleolar	141	IALTDNALIAR EVPAVPETLK QIFNGTFVK	482 465 460
60S ribosomal protein L13	Cytoplasmic/Nuclear/Nucleolar	93	STESLQANVQR TIGISVDPR GFSLEELR LILFPR	446 376 372 275
40S ribosomal protein S4, X isoform	Cytoplasmic/Nuclear/Nucleolar	92	HPGSFDVVHVKDANGNSFATR DANGNSFATR LSNIFVIGK IGVITNR	794 408 384 287
60S ribosomal protein L8	Cytoplasmic/Nuclear/Nucleolar	72	AVVGVVAGGGR VGLIAAR NCWPR GAGSVFR	1039 609 292 260
PAF350/400	Nuclear	55	HRKENMAATNWK KIVLQVFHSLLK VIYEGLTNYEK	527 505 492
Delangin	Nuclear	55	NEHGIK VIKILR	264 308
Rotatin	Membrane/Cytoskeletal	55	VLAGLIR RVAANALMSLLAVSR	308 544
eIF-2B	Cytoplasmic	55	VLKIIR	308
Gemin-4	Nucleolar/Cytoplasmic	55	VLAGILR	308

Table 2.1: List of NO66 interacting proteins. HEK293T cells were made to stably express either HA-tagged NO66 or empty vector (EV) control and subjected to anti-HA immunoprecipitation. Control and HA-NO66 immunoprecipitates were subjected to in-solution trypsinolysis prior to proteomic analysis by MS. This table shows NO66 interactors that are short-listed based on their Mascot-derived protein scores and absence from the control pull-down. This shortlist was derived from a single proteomics experiment and was used for *in vitro* peptide screening. RPL8 was later confirmed to be hydroxylated by NO66, and is highlighted in red. A list of NO66 interacting proteins is provided in the supplementary CD.

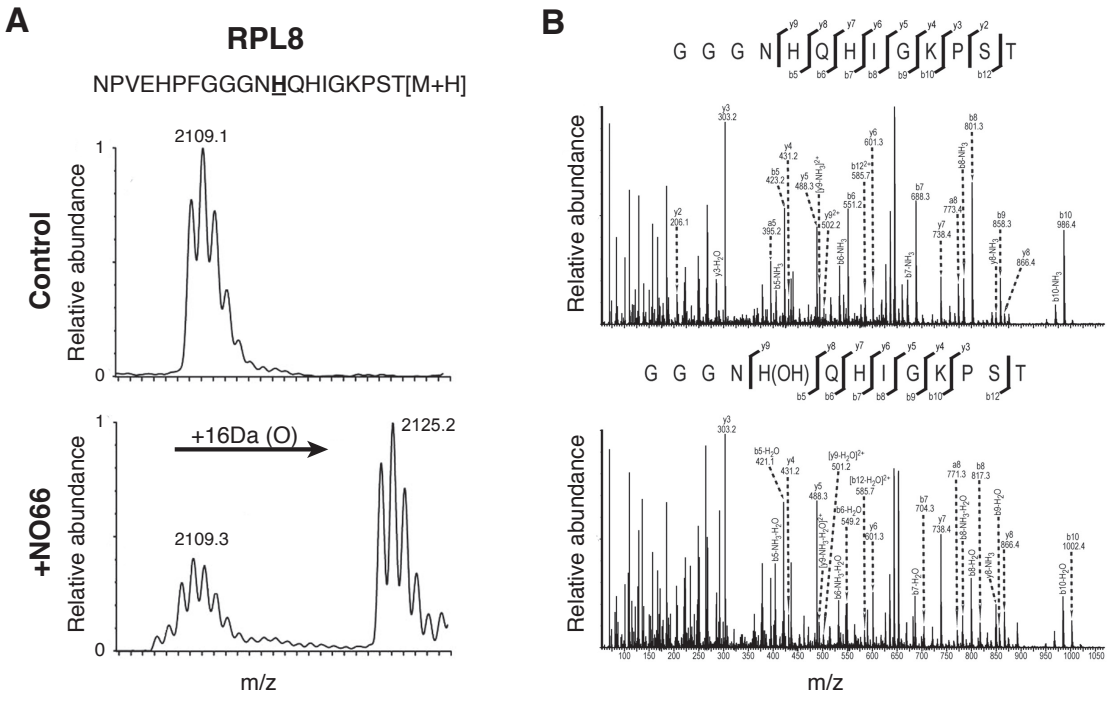


Figure 2.2: Recombinant NO66 hydroxylates RPL8 peptide NPVEHPFGGGNHQHIGKPST. Reaction mixtures containing the RPL8 peptide and necessary co-factors were incubated in the presence or absence of NO66. The reaction was allowed to proceed for 30 minutes at 37°C, before it was quenched with 1% formic acid and analysed by MALDI-MS. **A)** A mass shift of +16 Da was observed when comparing peptides incubated in the absence (top panel: [M+H]; *m/z* 2109) or presence (bottom panel: [M+H]; *m/z* 2125) of NO66. The mass shift is consistent with addition of an oxygen atom. **B)** MS/MS spectra of hydroxylated and unhydroxylated RPL8 peptides. In comparison to the MS/MS spectra of the unhydroxylated peptide (top panel), a +16 mass shift was observed for ion fragments derived from the hydroxylated peptide (bottom panel) that contain a specific histidine residue. The position of this histidine corresponds to H216 in human RPL8. Experiments performed by Dr. Wei Ge (Ge et al., 2012).

validated by MS/MS sequencing. Figure 2.2B shows MS/MS spectra of the hydroxylated and unhydroxylated peptides. For the modified peptide, a +16 mass shift was observed in ion fragments containing a specific histidine residue. The position of the histidine residue corresponded to H216 in the human RPL8 protein sequence. Results from the *in vitro* experiments suggest that RPL8 H216 is a candidate hydroxylation site for NO66 catalytic activity, though further characterisation is required to verify the modification in endogenous RPL8.

The interaction between RPL8 and NO66 was validated by repeating the proteomic pull-down from control and HA-NO66 HEK293T cells, and immunoblotting for the presence of RPL8. Consistent with the proteomic results, RPL8 was found in the HA-NO66, but not control immunoprecipitate sample (Figure 2.3). This confirms that NO66 and RPL8 interact in cells, at least in the setting of NO66 overexpression.

2.2.3 Purification and characterisation of endogenous RPL8

Next, we sought to determine whether RPL8 H216 hydroxylation occurs endogenously. To isolate enogenous RPL8, we purified whole ribosomes from HeLa cells by sucrose gradient ultracentrifugation. Crude cell lysates were centrifuged through a 32% sucrose cushion to pellet the ribosomes, after which ribosomal proteins were precipitated using ice-cold acetone prior to resuspension and HPLC.

Reverse phase HPLC involves a column coated with hydrophobic alkyl side chains termed the 'stationary phase'. An aqueous solvent, or 'mobile phase' is passed through the column, which consists of a mixture of hydrophilic and hydrophobic solvents that change in ratio over time. When the mobile phase is highly polar, most proteins that pass through the column remain attached to the nonpolar stationary phase. As the concentration of nonpolar solvent increases in the mobile phase, proteins progressively elute from the column in the order of increasing hydrophobicity. The eluted HPLC fractions were collected and dot blotted to identify RPL8 (Figure 2.4 i and ii). HPLC elutant containing RPL8 was resolved by sodium dodecyl sulfate polyacrylamide gel

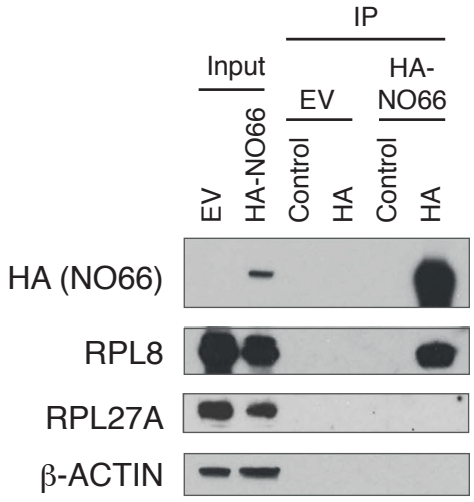


Figure 2.3: NO66 interacts with RPL8 in cells. HEK293T cells stably expressing either HA-tagged NO66 or empty vector control were lysed and immunoprecipitated with anti-HA or control (anti-V5) resin. The immunoprecipitates were washed, eluted, and then immunoblotted for NO66 (HA), RPL8, RPL27A and β-ACTIN. RPL8, but not RPL27A interacted specifically with HA-NO66. Input denotes cell extract prior to pull-down.

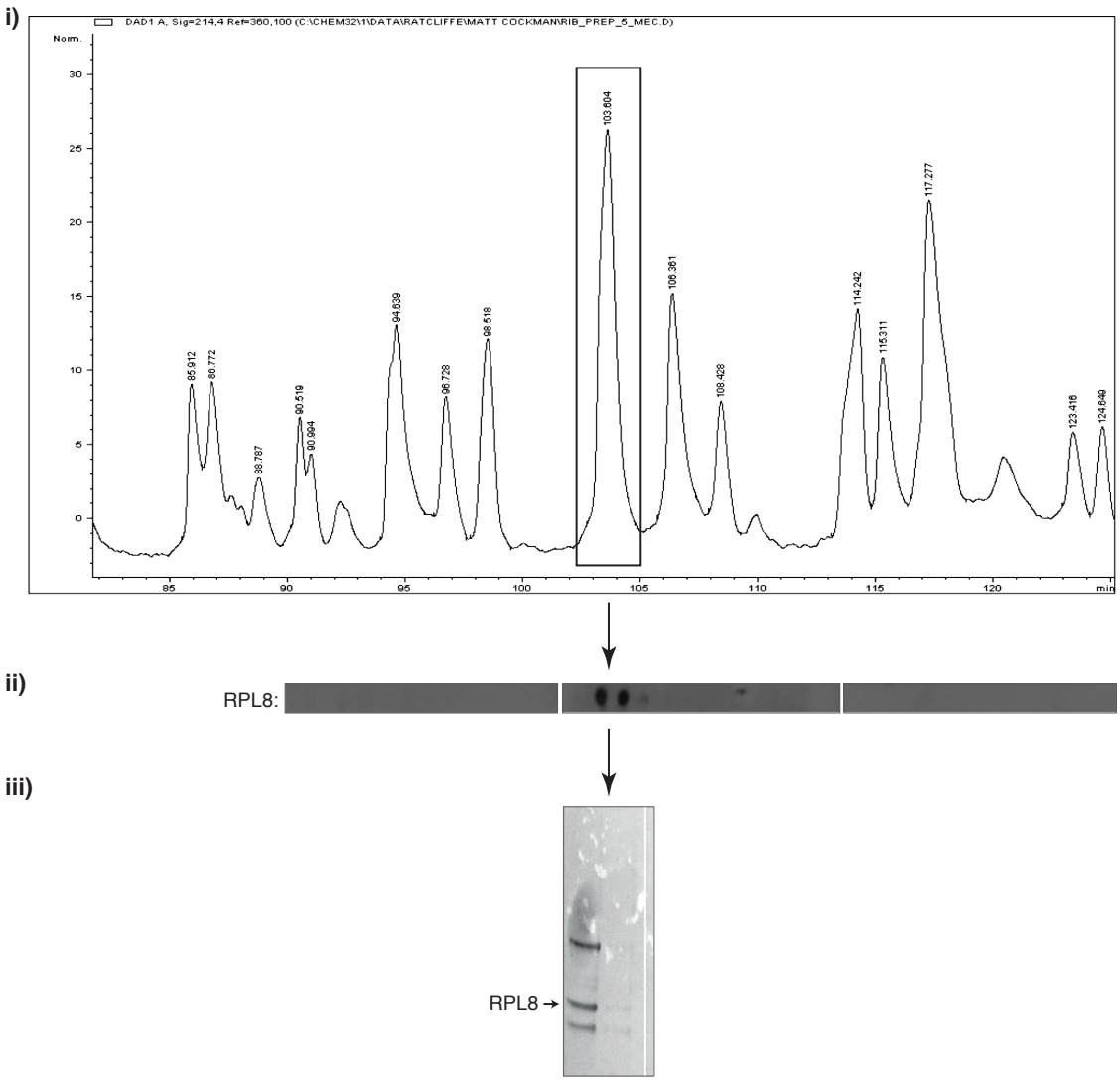
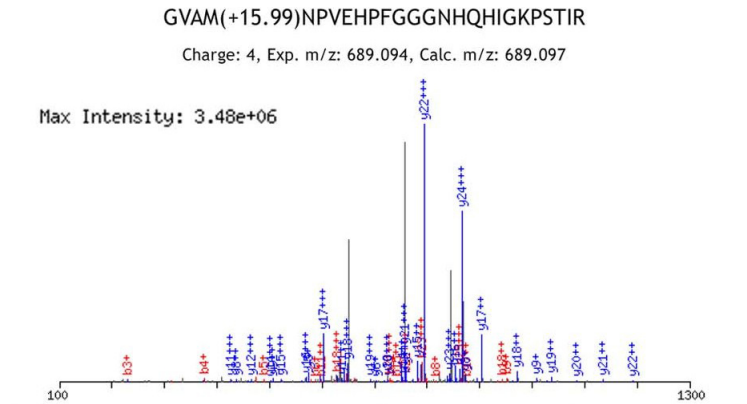


Figure 2.4: HPLC purification of RPL8 from endogenous ribosomes. Ribosomal proteins isolated by sucrose cushion centrifugation were loaded onto a high-performance liquid chromatography (HPLC) column and separated using a 10-43% acetonitrile gradient. The HPLC chromatogram (i) shows protein absorbance measured at 214nm. Corresponding elutants were collected at 1-minute intervals and dot-blotted for RPL8, which was identified to elute at approximately 103 minutes (ii). The HPLC fraction containing RPL8 was resolved by SDS-PAGE and stained using coomassie blue (iii). The protein bands were excised and digested in-gel with trypsin prior to MS identification. The middle band contained RPL8, whereas the remaining bands were identified to be other co-eluting ribosomal proteins (data not shown). Figure by Dr. Phebee Yi-Liu.

electrophoresis (SDS-PAGE) and stained with coomassie blue (Figure 2.4 iii). The gel band corresponding to RPL8 was excised, trypsinised then analysed by LC-MS/MS, which couples liquid chromatography with MS/MS sequencing (Figure 2.5).

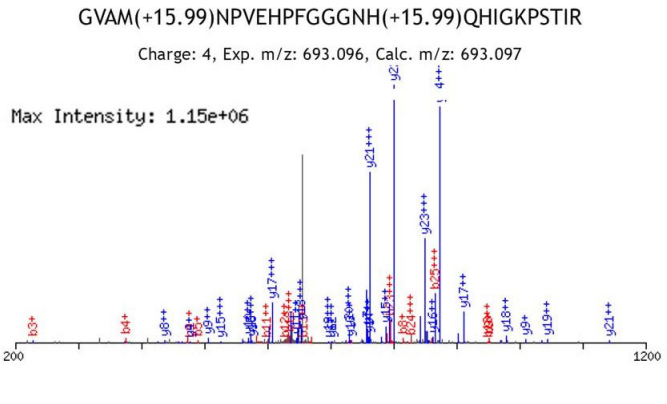
According to MS/MS sequencing, the tryptic digest of RPL8 produced a peptide fragment of sequence GVAMNPVEHPFGGGN<u>H</u>QHIGKPSTIR (human RPL8 residues 201-226) that contained the histidine of interest. A subset of these peptides exhibited a mass shift consistent with hydroxylation. Figure 2.5 shows MS/MS spectra of hydroxylated and unhydroxylated RPL8 tryptic peptides. Compared to the unhydroxylated peptide, the hydroxylated peptide fragments exhibited a +8 m/z shift in the y++ (doubly charged) ion series beginning from y11, consistent with the hydroxylation of H216. Both peptides also contained methionine oxidation, an experimental artefact that resulted from MS sample preparation.

The RPL8 tryptic peptide has three possible mass states: unoxidised, singly oxidised (at methionine or histidine), or doubly oxidised (at both methionine and histidine). Figure 2.6 (i) shows a representative total ion chromatogram, which can be used to extract the elution profile of ions with a specific m/z ratio (Figure 2.6 ii to iv). The extracted ion chromatograms (EICs) corresponding to RPL8 peptides in varying states of oxidation are also depicted in the same figure. Note that even though peptides containing either methionine or histidine oxidation have the same m/z values, methionine-oxidised peptides eluted several minutes earlier than the other peptide species due to its increased polarity (Figure 2.6 iii). For ease of understanding, the EICs of unoxidised and oxidised RPL8 peptides were simplified and overlaid as shown in Figure 2.7. All LC-MS results will be presented in the simplified format here after in this thesis. The presence of distinctive elution peaks allows for estimation of the level of H216 hydroxylation, by measuring the relative peak heights of histidine oxidised and unoxidised RPL8 peptides. LC-MS quantitation revealed that endogenous RPL8 from HeLa cells is almost completely hydroxylated at H216 (Figure 2.7).



		b+	b++	b+++	y+	y++	y+++		
G	1	58.03	29.52	20.01				26	G
V	2	157.10	79.05	53.04	2696.35	1348.68	899.45	25	V
A	3	228.13	114.57	76.72	2597.28	1299.14	866.43	24	A
M	4	375.17	188.09	125.73	2526.24	1263.62	842.75	23	M
N	5	489.21	245.11	163.74	2379.21	1190.11	793.74	22	N
P	6	586.27	293.64	196.09	2265.16	1133.09	755.73	21	P
V	7	685.33	343.17	229.12	2168.11	1084.56	723.38	20	V
E	8	814.38	407.69	272.13	2069.04	1035.02	690.35	19	E
H	9	951.44	476.22	317.82	1940.00	970.50	647.34	18	H
P	10	1048.49	524.75	350.17	1802.94	901.97	601.65	17	P
F	11	1195.56	598.28	399.19	1705.89	853.45	569.30	16	F
G	12	1252.58	626.79	418.20	1558.82	779.91	520.28	15	G
G	13	1309.60	655.30	437.20	1501.80	751.40	501.27	14	G
G	14	1366.62	683.81	456.21	1444.78	722.89	482.26	13	G
N	15	1480.66	740.84	494.23	1387.76	694.38	463.26	12	N
H	16	1617.72	809.36	539.91	1273.71	637.36	425.24	11	H
Q	17	1745.78	873.39	582.60	1136.65	568.83	379.56	10	Q
H	18	1882.84	941.92	628.28	1008.59	504.80	336.87	9	H
I	19	1995.92	998.47	665.98	871.54	436.27	291.18	8	I
G	20	2052.95	1026.98	684.99	758.45	379.73	253.49	7	G
K	21	2181.04	1091.02	727.69	701.43	351.22	234.48	6	K
P	22	2278.09	1139.55	760.04	573.34	287.17	191.78	5	P
S	23	2365.13	1183.07	789.05	476.28	238.65	159.43	4	S
T	24	2466.17	1233.59	822.73	389.25	195.13	130.42	3	T
I	25	2579.26	1290.13	860.42	288.20	144.61	96.74	2	I
R	26				175.12	88.06	59.04	1	R

Rpl8
H216



		b+	b++	b+++	y+	y++	y+++		
G	1	58.03	29.52	20.01				26	G
V	2	157.10	79.05	53.04	2712.34	1356.67	904.79	25	V
A	3	228.13	114.57	76.72	2613.27	1307.14	871.76	24	A
M	4	375.17	188.09	125.73	2542.24	1271.62	848.08	23	M
N	5	489.21	245.11	163.74	2395.20	1198.10	799.07	22	N
P	6	586.27	293.64	196.09	2281.16	1141.08	761.06	21	P
V	7	685.33	343.17	229.12	2184.11	1092.56	728.71	20	V
E	8	814.38	407.69	272.13	2085.04	1043.02	695.68	19	E
H	9	951.44	476.22	317.82	1955.99	978.50	652.67	18	H
P	10	1048.49	524.75	350.17	1818.94	909.97	606.98	17	P
F	11	1195.56	598.28	399.19	1721.88	861.45	574.63	16	F
G	12	1252.58	626.79	418.20	1574.81	787.91	525.61	15	G
G	13	1309.60	655.30	437.20	1517.79	759.40	506.60	14	G
G	14	1366.62	683.81	456.21	1460.77	730.89	487.60	13	G
N	15	1480.66	740.84	494.23	1403.75	702.38	468.59	12	N
H	16	1633.72	817.36	545.24	1289.71	645.36	430.57	11	H
Q	17	1761.78	881.39	587.93	1136.65	568.83	379.56	10	Q
H	18	1898.84	949.92	633.62	1008.59	504.80	336.87	9	H
I	19	2011.92	1006.46	671.31	871.54	436.27	291.18	8	I
G	20	2068.94	1034.97	690.32	758.45	379.73	253.49	7	G
K	21	2197.04	1099.02	733.02	701.43	351.22	234.48	6	K
P	22	2294.09	1147.55	765.37	573.34	287.17	191.78	5	P
S	23	2381.12	1191.06	794.38	476.28	238.65	159.43	4	S
T	24	2482.17	1241.59	828.06	389.25	195.13	130.42	3	T
I	25	2595.25	1298.13	865.76	288.20	144.61	96.74	2	I
R	26				175.12	88.06	59.04	1	R

+16Da $[M+H]^{2+}$

Figure 2.5: Endogenous RPL8 in HeLa cells is hydroxylated at H216. Endogenous RPL8 purified from HeLa cells was trypsinised prior to MS/MS sequencing. Left panel shows MS/MS spectra of the unmodified RPL8 tryptic peptide$_{201\text{-}226}$. The table below lists the predicted ion fragments and their m/z values, as well as the MS/MS coverage. Relative to the unmodified peptide, the MS/MS spectra of the hydroxylated RPL8 peptide$_{201\text{-}226}$ (right panel) exhibited a +8 m/z shift in the y++ (doubly charged) ion series beginning from y11, consistent with the addition of an oxygen on H216. Both peptides contained artefactual methionine oxidation as a consequence of the MS procedure.

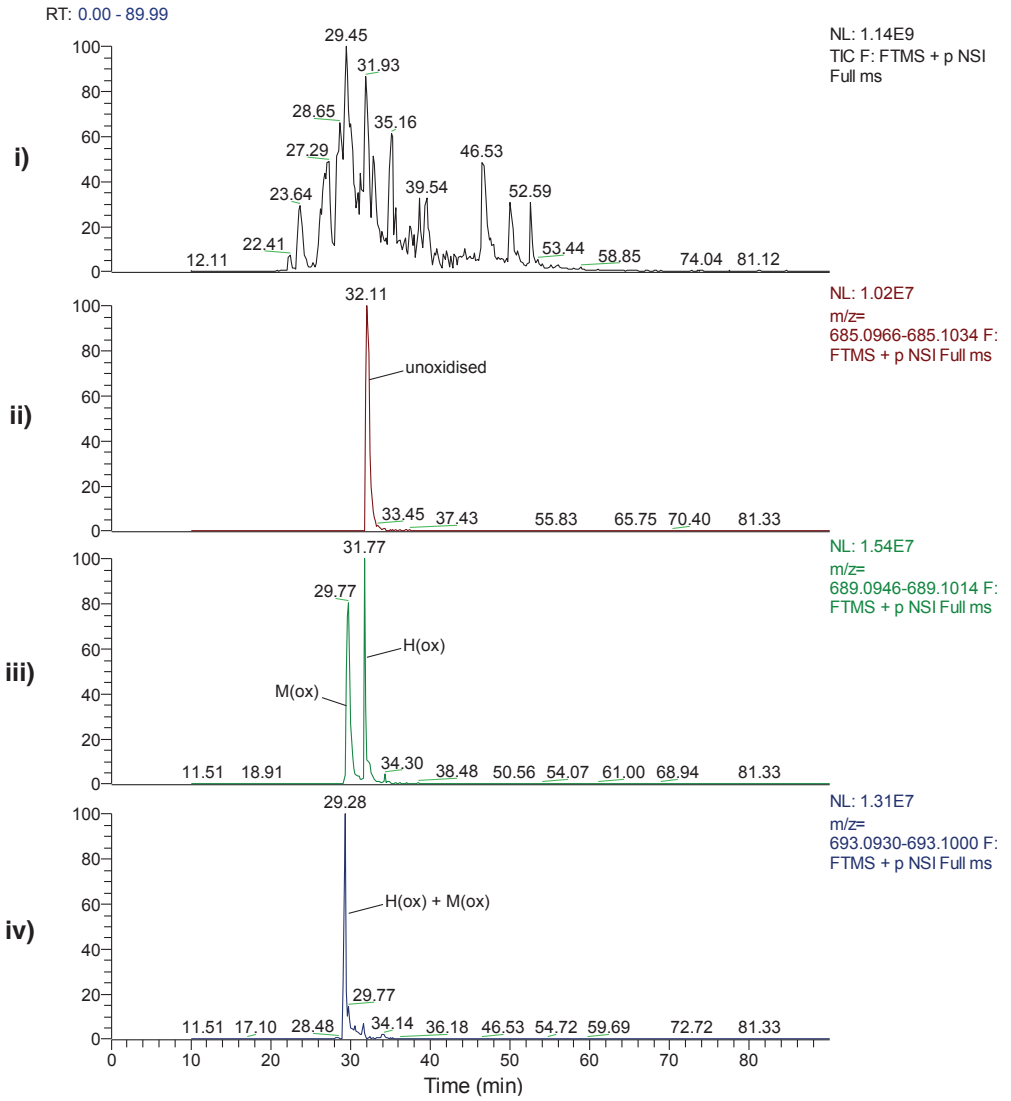


Figure 2.6: Representative LC-MS chromatograms of RPL8 tryptic peptide$_{201\text{-}226}$. RPL8 was purified from HeLa cells, digested with trypsin and analysed by LC-MS/MS. Panel i) shows the representative total LC-MS chromatogram of all the peptides eluted during the MS run. Chromatograms of peptide ions with specific m/z values were extracted from the total chromatogram. Panel ii) shows the EIC of unoxidised RPL8 tryptic peptide$_{201\text{-}226}$ ($[M+H]^{4+}$: m/z 685.100). Additionally, MS/MS sequencing revealed that oxidation may occur on both histidine (H216) and methionine residues of the peptide of interest. Panels iii) and iv) display EICs of m/z values corresponding to singly ($[M+H]^{4+}$: m/z 689.098) and doubly oxidised ($[M+H]^{4+}$: m/z 693.096) RPL8 peptides$_{201\text{-}226}$. Note that two types of singly oxidised species exist: methionine oxidised and histidine hydroxylated. However, the two peptide species elute at different times due to differences in polarity.

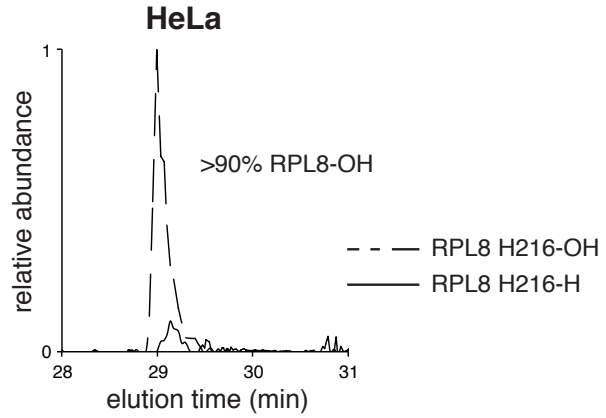


Figure 2.7: Endogenous RPL8 in HeLa cells is hydroxylated at H216. Trypsinised RPL8 was analysed by LC-MS. Representative EIC traces show tryptic peptide containing H216 in both hydroxylated and unhydroxylated states ($[M+H]^{4+}$; H216-H m/z 685.100; H216-OH m/z 689.098). Relative quantitation based on peak height showed that RPL8 is more than 90% hydroxylated at position H216.

2.2.4 Generation of an inducible NO66 knockdown system

The data obtained so far have shown that endogenous RPL8 is hydroxylated at H216. However, it is unclear whether the RPL8 modification is dependent on NO66 expression. To characterise the relationship between NO66 expression and RPL8 hydroxylation, HeLa and A549 cells were made to stably express doxycycline-inducible short hairpin RNA (shRNA) constructs targeting NO66. Given previous reports associating MINA53 and NO66 with cell growth, an inducible system was utilised to negate any potential selection pressures against cells with constitutive NO66 knockdown (Suzuki et al., 2007). shRNA against control or NO66 sequences were designed by Dr. Atsushi Yamamoto and cloned into the 'pTRIBz' vector. pTRIBz was modified from the commercially available pTRIPz lentiviral vector (Open Biosystems), and contains a blasticidin S rather than puromycin resistance cassette (Figure 2.8). The pTRIBz vector features a tetracycline-inducible promoter that drives the expression of the shRNA and a red fluorescent protein (RFP) reporter (Figure 2.8). The addition of doxycycline enables expression of the shRNA, which can be visually tracked by the RFP reporter. As shown by figures 2.9, stable expressions of the pTRIBz shRNA vectors achieved heterogeneous levels of RFP expression in HeLa and A549 cells, though the knockdown of NO66 was relatively efficient as evidenced by the immunoblots (Figure 2.10).

To better understand the dynamics of the pTRIBz inducible shRNA system, a doxycycline time course was performed. As expected, RFP expression increased with the duration of doxycycline treatment. At 72 hours post-treatment, the amount of RFP expression reaches an appreciable level and plateaus thereafter (Figures 2.11 and 2.12). However, the expression of NO66 persisted at the protein level until 120 hours after the initial addition of doxycycline (Figures 2.11 and 2.12). Therefore, a certain amount of delay occurs between the induction of shRNA expression and NO66 knockdown at the protein level. Nonetheless, results from the time course confirmed that reasonable levels of NO66 knockdown are achieved using the pTRIBz inducible shRNA system.

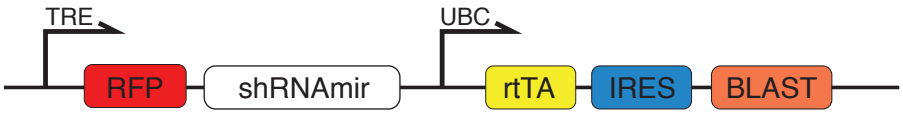


Figure 2.8: Schematic of the pTRIBz inducible lentiviral shRNA vector. pTRIBz is a Tet-on vector that induces shRNA expression in the presence of doxycycline. The tetracycline response element (TRE) drives the expression of the shRNA sequence, and the RFP reporter helps to visualise plasmid expression. Activation of the TRE requires binding of reverse tetracycline-controlled transactivator (rtTA), which is constitutively expressed though only functional under doxycycline. In addition to rtTA, stable expression of a blasticidin S resistance cassette ('BLAST') allows for generation of stable cell lines.

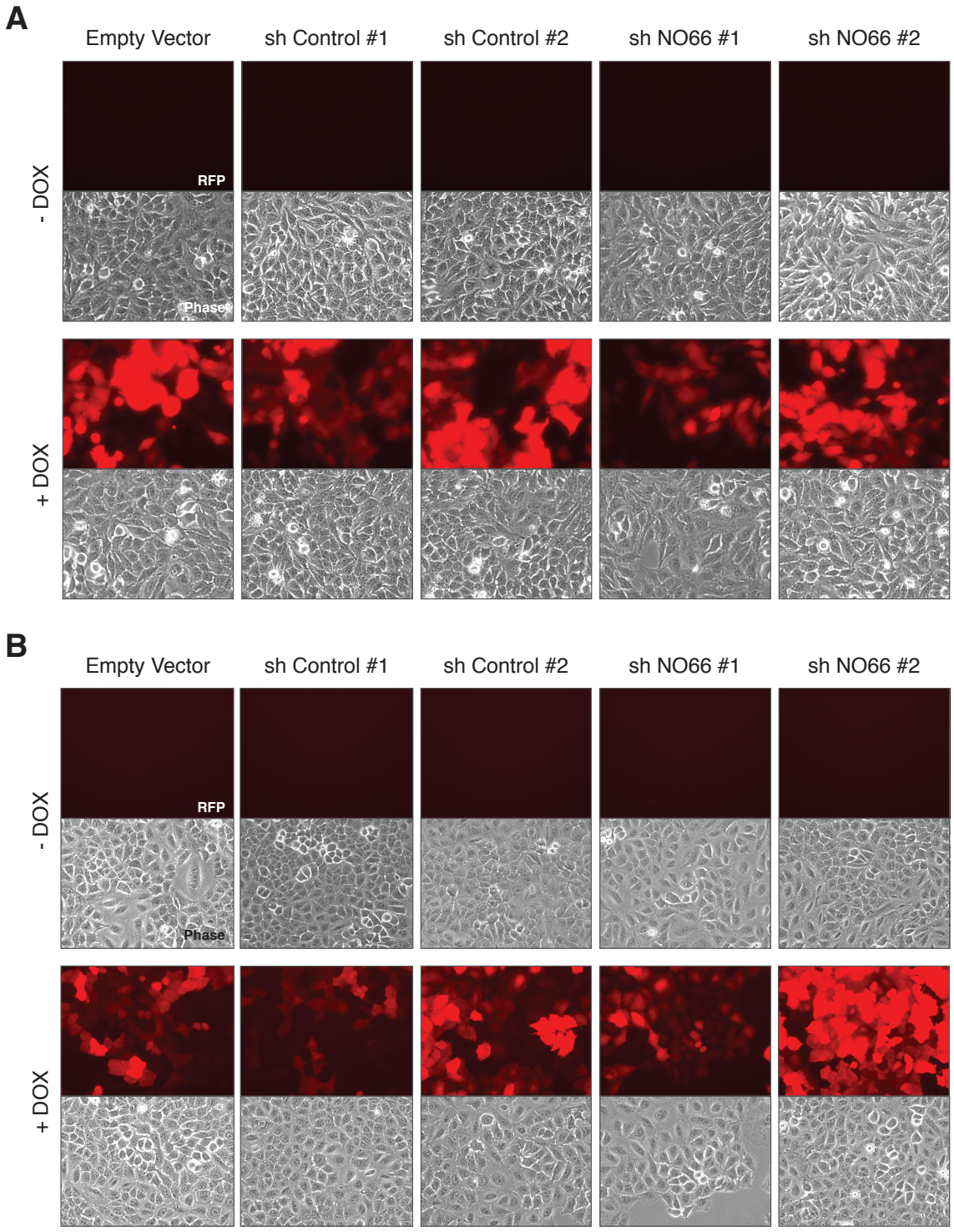


Figure 2.9: Characterisation of RFP expression in stable cell lines expressing inducible shRNA against NO66. HeLa and A549 cells were made to express pTRIBz inducible shRNA constructs against either negative control sequences or NO66. To rule out any off-target effects and optimise knockdown efficiency, two distinctive sequences were designed for both negative control and NO66. After antibiotic selection, the stable cell lines were treated with doxycycline for 120 hours prior to microscopy imaging and immunoblotting. RFP expression was induced under doxycycline treatment for both HeLa **(A)** and A549 **(B)** stable cell lines. Microscopy images show that RFP was not homogenously expressed across the cell populations.

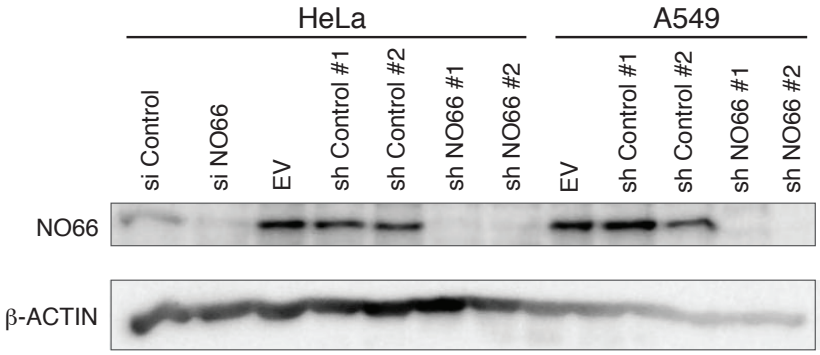


Figure 2.10: Characterisation of NO66 protein level in stable cell lines expressing inducible shRNA against NO66. HeLa and A549 cells were made to stably express pTRIBz inducible shRNA constructs against either negative control sequences or NO66. The cells were treated with doxycycline for 120 hours prior to microscopy imaging and immunoblotting. Immunoblots show the suppression of NO66 expression by both NO66 shRNA sequences relative to control shRNA. Lysates were prepared from HeLa cells transfected with siRNA against either NO66 or a negative control sequence, and immunoblotted in parallel to control for antibody specificity. Immunoblot of β-ACTIN shows uneven band levels as a result of inadequate chemiluminescent substrate coverage. Due to human oversight and technical limitations, a better quality immunoblot was not obtained.

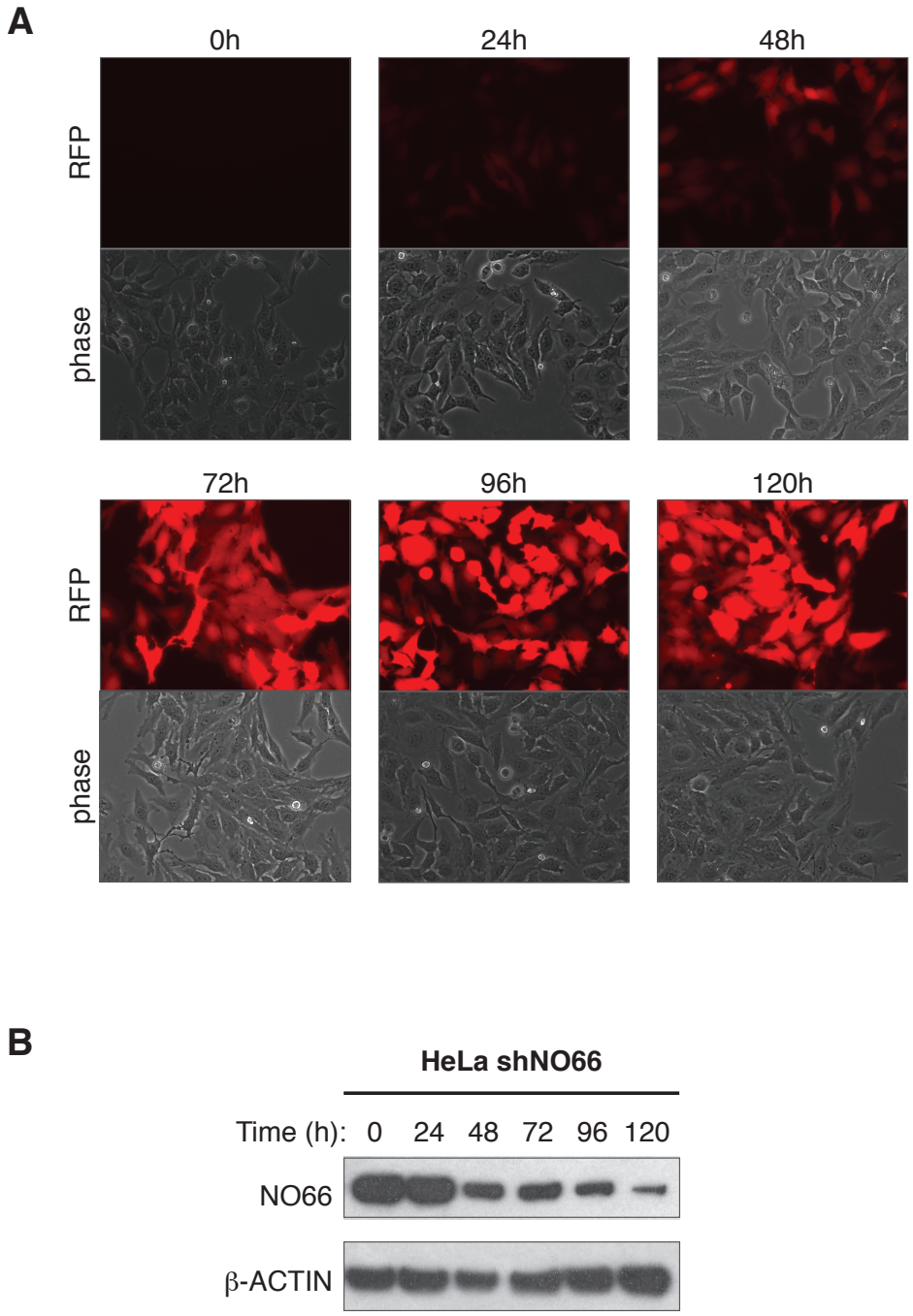


Figure 2.11: Time course of doxycycline-induced shRNA expression and NO66 knockdown in HeLa cells. HeLa cells stably expressing inducible shRNA construct against NO66 were treated with doxycycline for 120 hours. Microscopy images and cell lysates were collected at 24-hour intervals for 120 hours to monitor RFP expression and NO66 knockdown. **A)** Time course of RFP expression. **B)** Immunoblot showing the rate of NO66 knockdown.

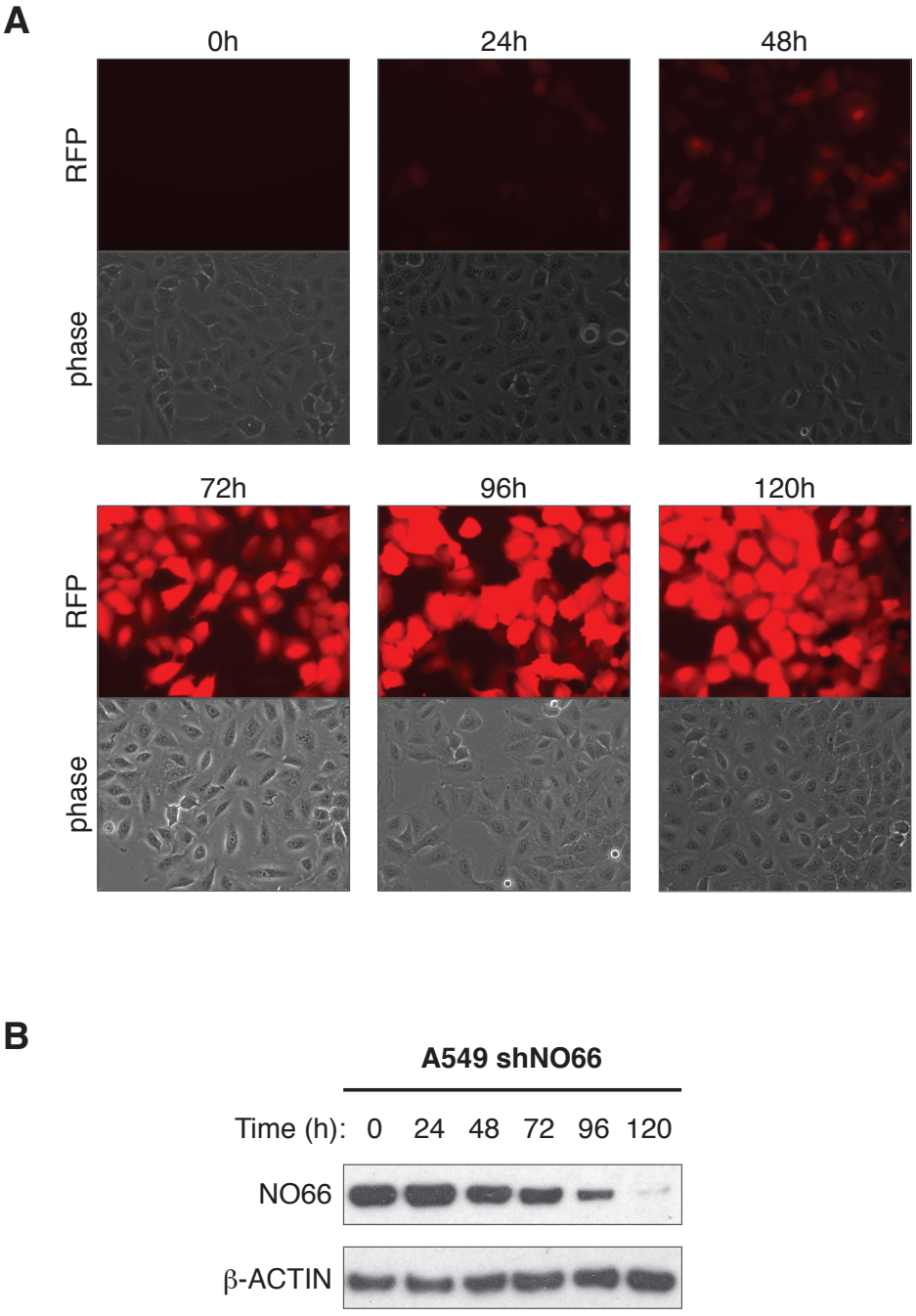


Figure 2.12: Time course of doxycycline-induced inducible shRNA expression and NO66 knockdown in A549 cells. A549 cells stably expressing inducible shRNA construct against NO66 were treated with doxycycline. Microscopy images and protein extracts were collected at 24-hour intervals for 120 hours to monitor RFP expression and NO66 knockdown. **A)** Time course of RFP expression. **B)** Immunoblot showing the rate of NO66 knockdown.

2.2.5 Endogenous RPL8 hydroxylation is dependent on NO66

The time course experiments suggested that more than 120 hours of doxycycline treatment was required to achieve significant suppression of NO66 protein expression (Figures 2.11 and 2.12). Given the long half-life of ribosomes (Hirsch and Hiatt, 1966), it may take considerably longer to detect any measurable changes in RPL8 H216 hydroxylation. Therefore, to examine the role of NO66 in RPL8 hydroxylation, inducible shRNA cell lines were treated with doxycycline for 12 days, after which RPL8 was purified and digested with trypsin for MS analysis. NO66 knockdown was confirmed by immunoblotting in parallel with ribosomal purifications (Figure 2.13A). Figure 2.13B shows representative EICs of RPL8 tryptic peptides from HeLa and A549 inducible shRNA cells. The extent of hydroxylation was quantified by measuring the relative peak heights of hydroxylated and unhydroxylated RPL8 peptides. RPL8 H216 hydroxylation was approximately 51% in HeLa cells after NO66 knockdown, and was near complete in control cells. Similarly, RPL8 hydroxylation was reduced to approximately 68% in A549 cells upon NO66 knockdown.

RPL8 hydroxylation in NO66 shRNA cells remained relatively high, despite prolonged doxycycline induction and relatively efficient NO66 knockdown. Moreover, an extended doxycycline treatment of 20 days did not further decrease RPL8 H216 hydroxylation (data not shown). It is possible that NO66 shares functional redundancy with its highly related homologue MINA53. To determine whether MINA53 contributes to RPL8 hydroxylation, RPL8 was purified from A549 cells stably expressing shRNA targeting MINA53 (gift from Dr. Adam Zayer). Immunoblots of the cell extracts showed efficient MINA53 suppression by shRNA (Figure 2.14A). Furthermore, hydroxylation of the known MINA53 substrate RPL27A was essentially absent in MINA53 shRNA cells (Ge et al., 2012). RPL8 was purified from control and MINA53 shRNA cells to measure the level of H216 hydroxylation by LC-MS. EICs show that RPL8 H216 was almost fully hydroxylated under both control and MINA53 knockdown conditions, indicating that MINA53 does not hydroxylate RPL8 at H216 (Figure 2.14B).

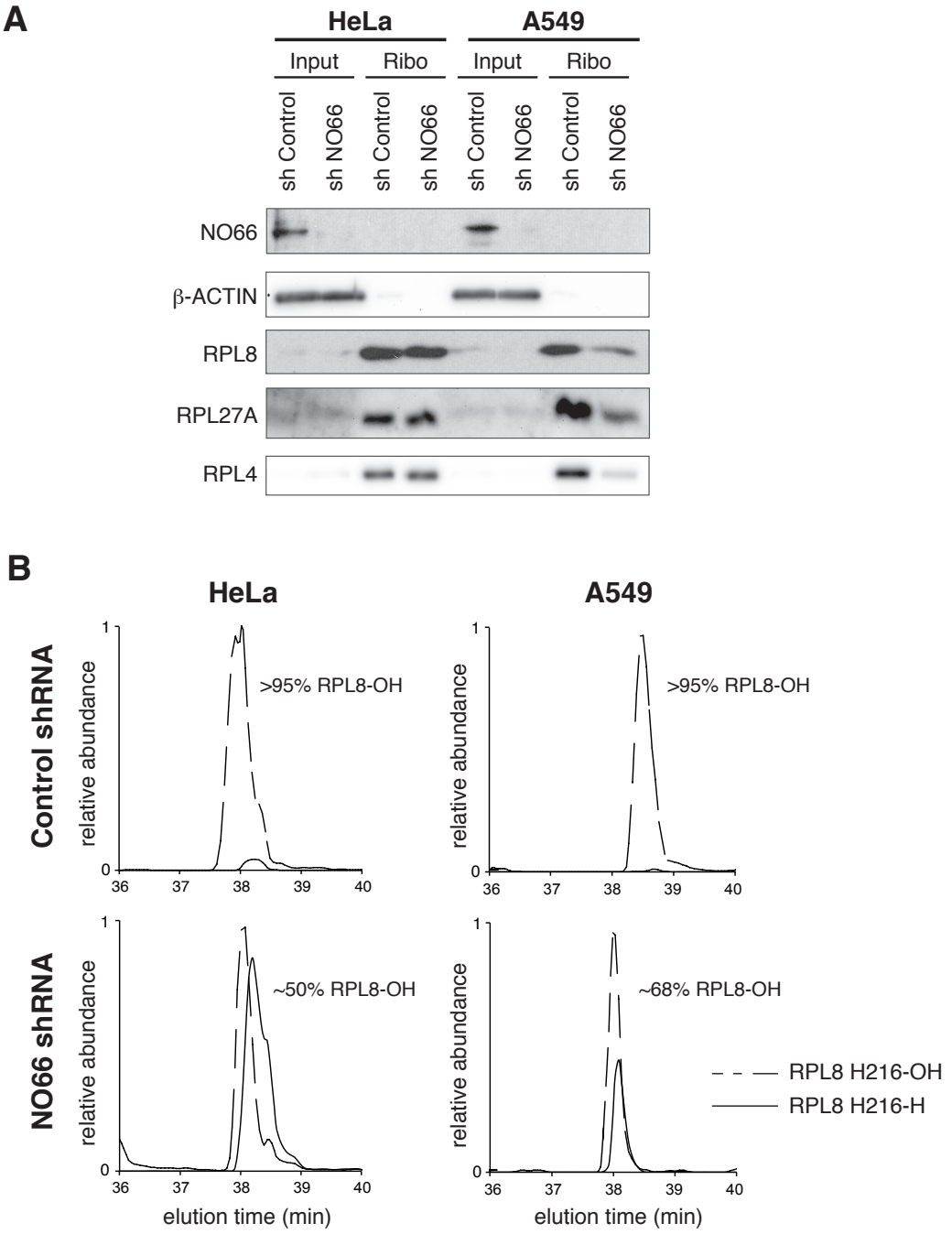


Figure 2.13: RPL8 H216 hydroxylation is reduced upon NO66 knockdown. Cells stably expressing control or NO66 shRNAs were treated with doxycycline for 12 days prior to RPL8 purification for MS analysis. **A)** Immunoblots showing the level of NO66 expression in knockdown and control cell lines after doxycycline treatment. 'Input' denotes whole cell extracts, whereas 'ribo' denotes whole ribosomes purified by sucrose cushion centrifugation. As expected, immunoblots of RPL8, RPL27A and RPL4 show enrichment following ribosomal purification. RPL8 was isolated in parallel to assess the level of H216 hydroxylation by LC-MS. **B)** EICs of hydroxylated and unhydroxylated RPL8 tryptic peptides$_{201\text{-}226}$ were quantified by measuring peak height. RPL8 H216 was fully hydroxylated in HeLa and A549 control cells, but was reduced under conditions of NO66 knockdown. The levels of RPL8 H216 hydroxylation were 50% and 68% in HeLa and A549 NO66 knockdown cells, respectively.

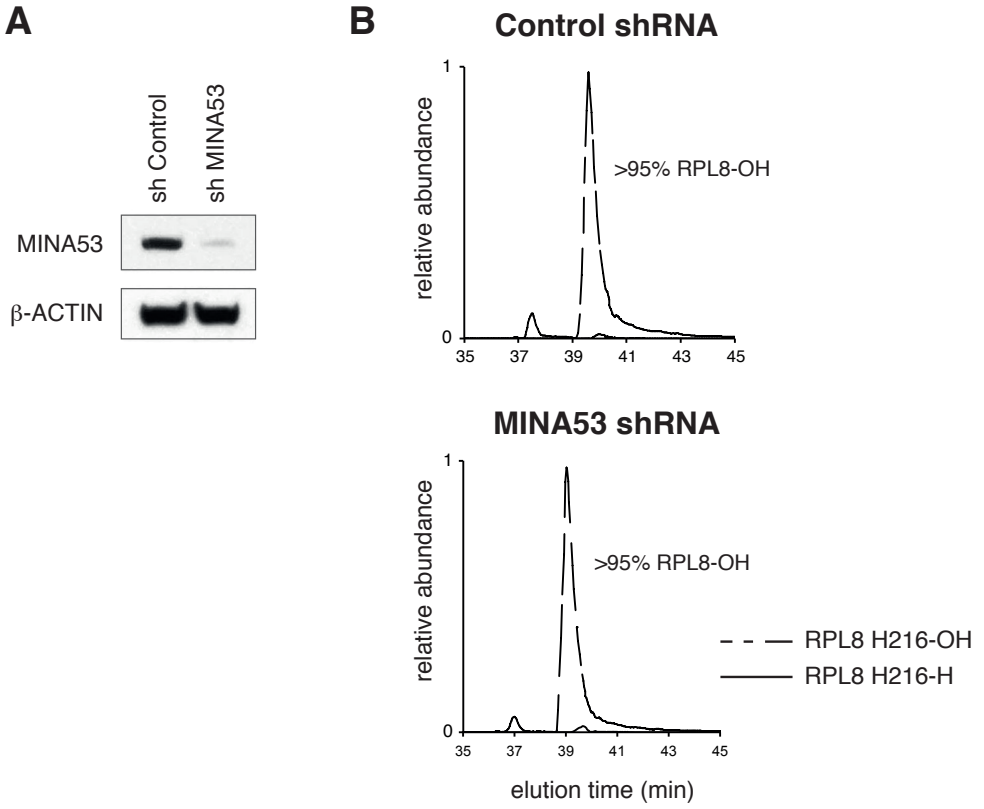


Figure 2.14: RPL8 H216 hydroxylation is not affected by suppression of MINA53 expression. A) Immunoblots show MINA53 protein level in A549 cells stably expressing control or MINA53 shRNA. In comparison to the control shRNA, shRNA against MINA53 effectively inhibited MINA53 expression at the protein level. RPL8 was purified from these cells to assess H216 hydroxylation by LC-MS **B)** EICs of RPL8 tryptic peptides$_{201\text{-}226}$ containing H216, purified from control and MINA53 knockdown cells. In both cell lines, quantitation by LC-MS indicate that RPL8 H216 hydroxylation is near complete. Generation of the cell lines and immunoblots by Dr. Adam Zayer.

In addition to MINA53 shRNA cells, a knockout model was tested to ensure that MINA53 activity does not contribute to RPL8 hydroxylation. The mouse embryonic fibroblasts (MEFs) were generated from MINA53 knockout (KO) and wild-type (WT) mice embryos, and transformed with the oncogene K-RAS (Malumbres and Barbacid, 2003). The hydroxylation of MINA53 substrate RPL27A was ablated in KO MEFs, but was restored by the re-expression of WT but not H179A MINA53 (Dr. Adam Zayer, unpublished data). H179 is a predicted Fe(II) binding residue in MINA53, and its mutation is proposed to ablate MINA53 activity. However, neither the absence or complementation of MINA53 enzymatic activity affected RPL8 H216 hydroxylation (Figure 2.15). Therefore, the results from MINA53 knockdown and knockout cell lines suggest that there is no functional redundancy between NO66 and MINA53 with regards to RPL8 hydroxylation. As such, persistant RPL8 hydroxylation in NO66 knockdown cells is likely due to residual enzyme activity.

To address the issue of insufficient NO66 knockdown, MEFs were isolated from NO66 WT or genetic KO mice embryos (gift from Dr. Benoit de Crombrugghe, MD Anderson Cancer Center, University of Texas). Due to the lack of an antibody that recognises mouse NO66, the genetic status of the MEFs were validated by polymerase chain reaction (PCR). Primers were designed against the 5'-loxp and 3'-loxp sites, such that PCR products of DNA extracted from NO66 KO MEFs will have different molecular weights from that of the WT MEFs (Figure 2.16). Results of the genotype PCR validated the genetic status of the NO66 KO MEFs. Next, RPL8 was analysed by MS to assess the level of H216 hydroxylation under complete absence of NO66 activity. EICs reveal that RPL8 hydroxylation was near complete in WT MEFs, but was essentially abrogated in NO66 KO MEFs (Figure 2.17). This is in accordance with the hypothesis that RPL8 is a substrate of and specific to NO66.

Concurrent with experimental validations of NO66 KO MEFs, HEK293T cells were surprisingly found to lack NO66 expression. This differs from other cell lines including HeLa, A549 and U2OS cells (Figure 2.18A). Consistent with the absence of NO66 protein expression, both LC-MS and MS/MS results indicate that endogenous RPL8 is not

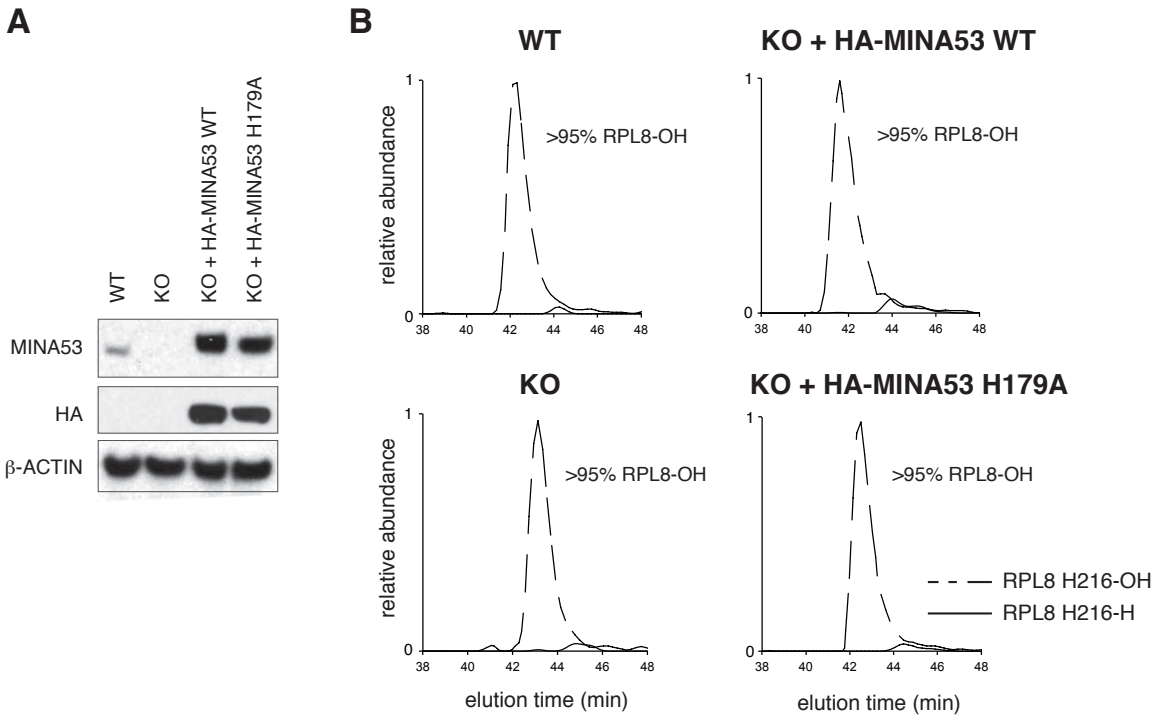


Figure 2.15: Ablation of MINA53 expression does not alter RPL8 H216 hydroxylation. A) Immunoblots show the level of MINA53 expression in MINA53 WT and KO, in addition to KO MEFs reconstituted with HA-tagged WT or H179A MINA53. H179 is a predicted Fe(II) binding residue of the MINA53 active site, and its mutation abolishes MINA53 enzymatic activity. As expected, MINA53 protein expression was absent in KO MEFs, but was restored in reconstituted KO MEFs. **B)** RPL8 was purified from MINA53 MEF cell lines for LC-MS analysis. EICs show that almost all of the RPL8 tryptic peptides$_{201\text{-}226}$ are hydroxylated at H216, which suggest that MINA53 is not involved in RPL8 hydroxylation. Generation of the cell lines and immunoblots by Dr. Adam Zayer.

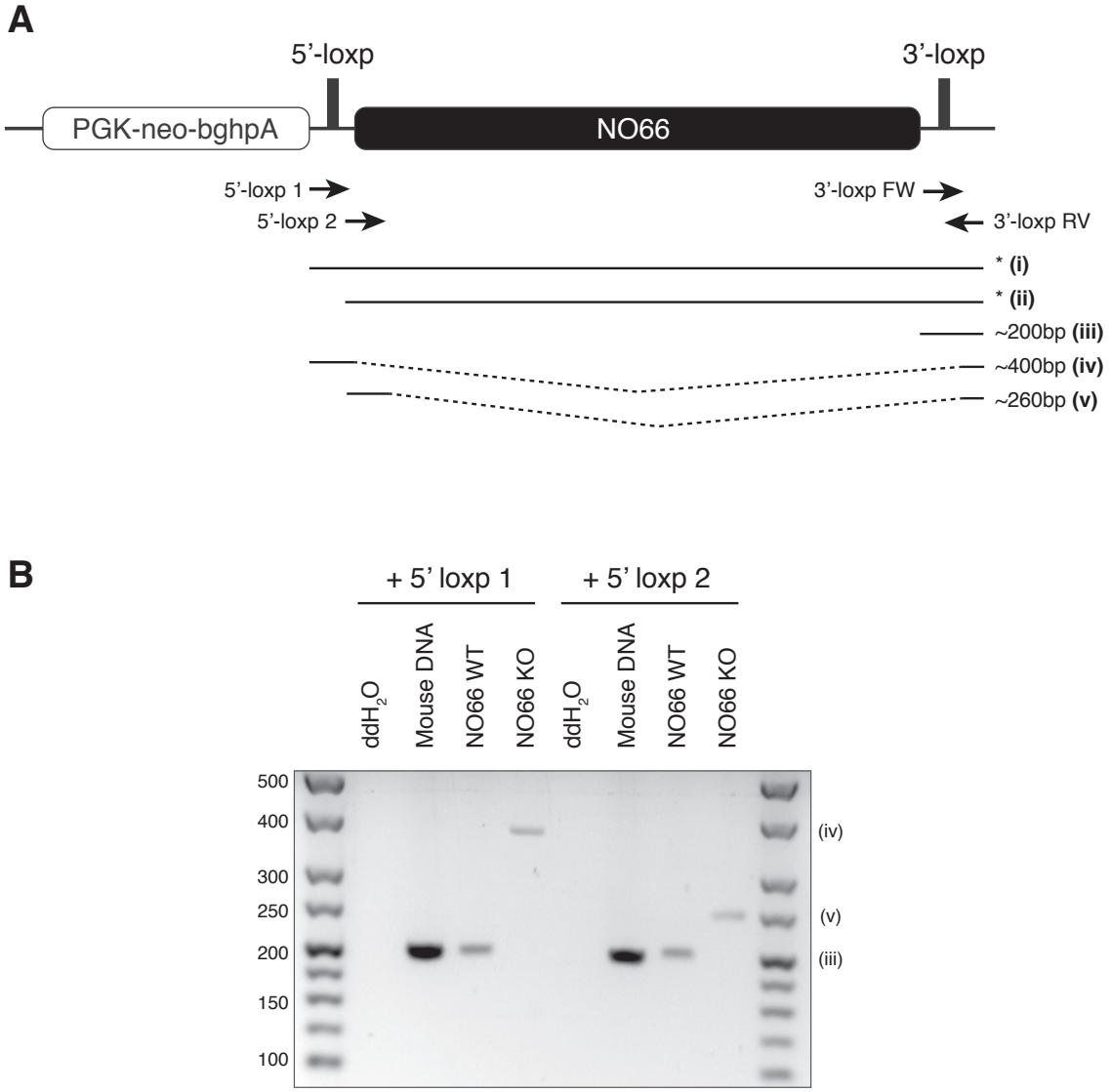


Figure 2.16: Genotypic and biochemical validation of NO66 knockout MEFs. A) Schematic of primer design. A pair of forward and reverse primers was designed against the 3'loxp site (3'-loxp FW and RV), and two forward primers were designed against the 5'loxp site (5'-loxp 1 and 2). In a PCR reaction containing 3'-loxp FW, 3'-loxp RV and a 5'loxp primer, there are two possible products. In MEFs derived from NO66 flox/flox mice, 5'loxp and 3'loxp-RV primers would generate a product too large to be amplified by the PCR reaction (i and ii). 3'loxp-FW and -RV primers would produce a 200bp DNA fragment (iii). After Cre recombinantion however, 5'loxp and 3'loxp-RV primers would produce a small DNA fragment amplifiable by PCR (iv and v), whereas the annealing site for 3'loxp-FW is no longer present. The 200bp product (iii) would also be absent. **B)** Genotyping PCR of DNA extracted from NO66 WT and KO MEFs. As expected, product (iii) was absent for NO66 KO MEFs, but was observed in NO66 flox/flox MEFs ('WT'). Control mouse DNA was extracted from FIH flox/flox mice, which also expectedly produces a 200bp PCR fragment.

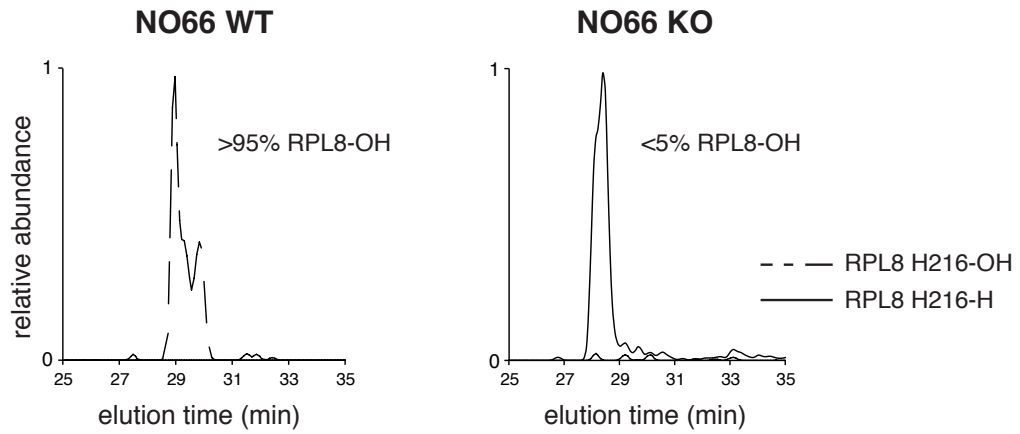


Figure 2.17: RPL8 is not hydroxylated in the absence of NO66. Endogenous RPL8 was purified from NO66 WT or KO MEFs using sucrose cushion centrifugation, prior to analysis by LC-MS. EICs of tryptic RPL8 peptides$_{201\text{-}226}$ show that H216 hydroxylation was near complete in NO66 WT cells, but was absent in NO66 KO MEFs.

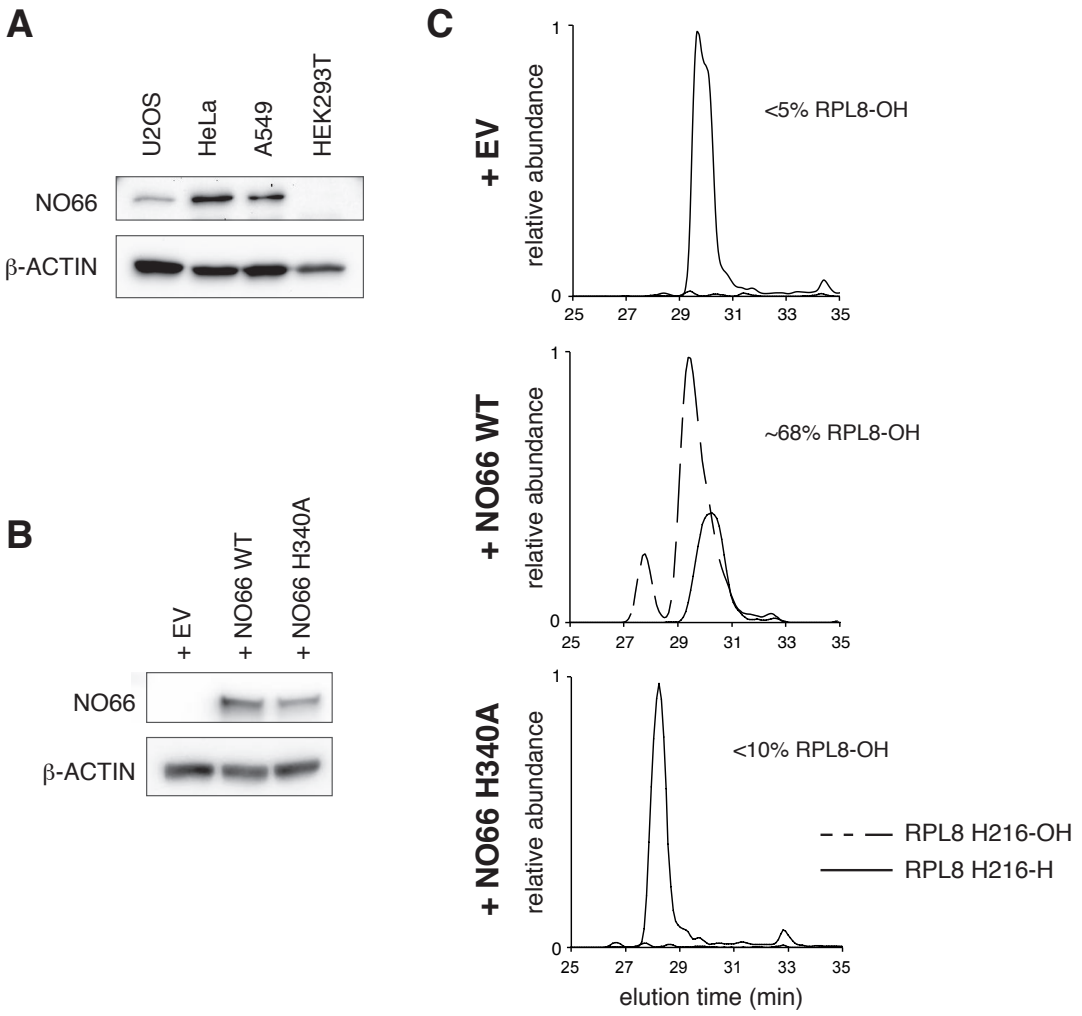
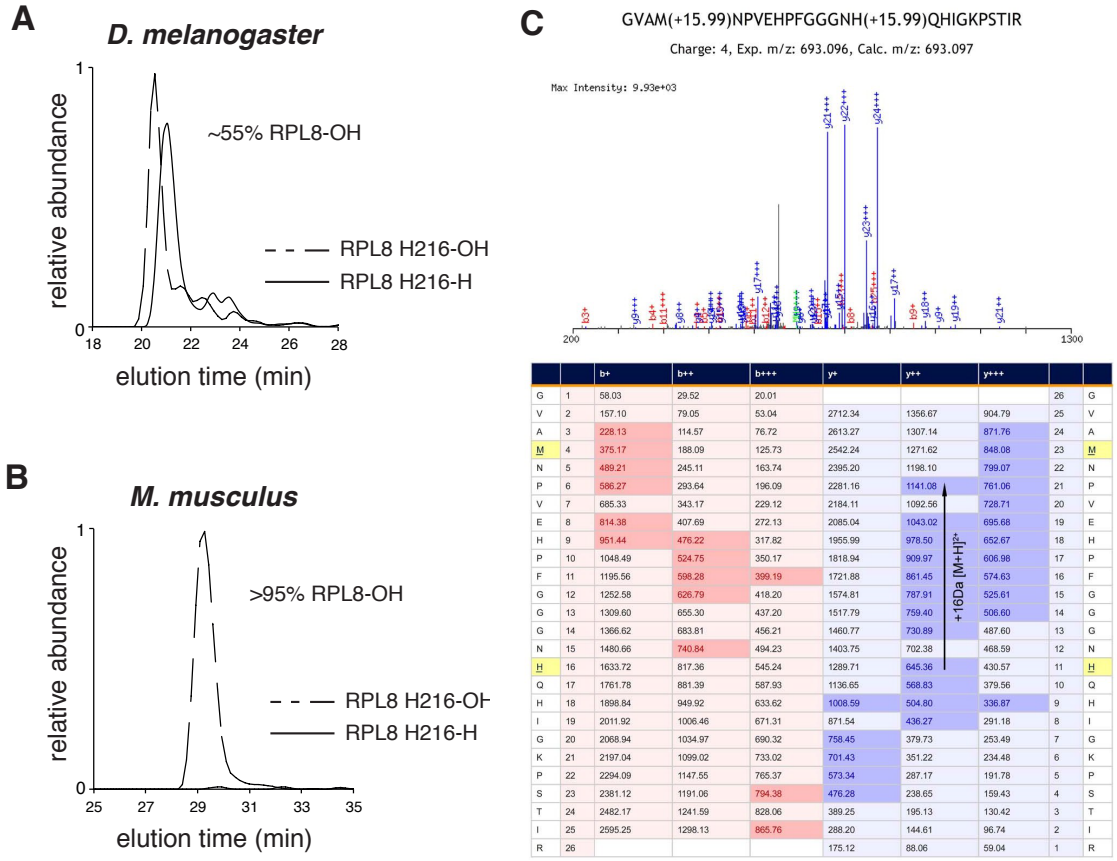


Figure 2.18: Ectopic expression of NO66 partially rescues RPL8 H216 hydroxylation in HEK293T cells. A) Immunoblot comparing NO66 protein levels in U2OS, A549, HeLa and HEK293T cell lines. NO66 protein expression was not detected in the whole cell lysate of HEK293T cells. Since HEK293Ts are a natural NO66-null cell model, they were made to stably overexpress WT or enzyme-dead H340A NO66. **B)** Expression of ectopic NO66 was confirmed by immunoblotting. **C)** HET293T overexpression cells were harvested for RPL8 purification followed by LC-MS analysis. Consistent with the lack of NO66 protein expression, RPL8 purified from HEK293T cells expressing EV control was not hydroxylated. Expression of WT but not enzyme-dead NO66 restored RPL8 H216 hydroxylation to approximately 68%.

hydroxylated in HEK293T cells (Figure 2.18C; data not shown). Since HEK293Ts are a natural NO66-null cell model, they were made to re-express WT or mutant H340A NO66 constructs. H340 is a predicted Fe(II) binding site within the NO66 JmjC domain, its mutation is predicted to inactivate NO66 hydroxylase activity. The expression of ectopic NO66 was validated by immunoblotting (Figure 2.18B). To study the effect of NO66 reconstitution on RPL8 hydroxylation, RPL8 was purified from HEK293T cells for tryptic digest followed by MS analysis. As shown in Figure 2.18C, reconstitution of wild type, but not H340A NO66 partially restored RPL8 H216 hydroxylation. The incompleteness of RPL8 hydroxylation was most likely due to insufficient NO66 re-expression in a subset of the stable cell line population. The results indicate that the hydroxylation of H216 in RPL8 is dependent on NO66 enzymatic activity, thus demonstrating that RPL8 is a true substrate of NO66. In summary, the results from NO66 shRNA knockdown cell lines, genetic knockout MEFs and HEK293T cells indicate that NO66 is both necessary and sufficient for the hydroxylation of RPL8 at H216.

2.2.6 Hydroxylation of RPL8 is conserved

The presence of RPL8 hydroxylation in MEFs suggested that NO66 activity may be conserved in species other than humans. Even though NO66 is absent in prokaryotes, it is structurally related to a prokaryotic ribosomal hydroxylase named YcFD (Ge et al., 2012; Chowdhury et al., 2014). On the other hand, NO66 orthologues are present in *Caenorhabditis elegans* and *Drosophila melanogaster*. To assess whether RPL8 H216 hydroxylation is conserved, RPL8 was purified from mouse liver and *D. melanogaster* SL2 cells. LC-MS quantitation revealed that RPL8 H216 was almost completely hydroxylated in mouse liver, and approximately 55% hydroxylated in *D. melanogaster* SL2 cells (Figure 2.19). Therefore, NO66 enzymatic activity towards RPL8 is evolutionarily conserved. The reason why RPL8 hydroxylation is reduced in *D. melanogaster* compared to all other cell types and species tested is unclear.



		b+	b++	b+++	y+	y++	y+++		
G	1	58.03	29.52	20.01				26	G
V	2	157.10	79.05	53.04	2712.34	1356.67	904.79	25	V
A	3	228.13	114.57	76.72	2613.27	1307.14	871.76	24	A
M	4	375.17	188.09	125.73	2542.24	1271.62	848.08	23	M
N	5	489.21	245.11	163.74	2395.20	1198.10	799.07	22	N
P	6	586.27	293.64	196.09	2281.16	1141.08	761.06	21	P
V	7	685.33	343.17	229.12	2184.11	1092.56	728.71	20	V
E	8	814.38	407.69	272.13	2085.04	1043.02	695.68	19	E
H	9	951.44	476.22	317.82	1955.99	978.50	652.67	18	H
P	10	1048.49	524.75	350.17	1818.94	909.97	606.98	17	P
F	11	1195.56	598.28	399.19	1721.88	861.45	574.63	16	F
G	12	1252.58	626.79	418.20	1574.81	787.91	525.61	15	G
G	13	1309.60	655.30	437.20	1517.79	759.40	506.60	14	G
G	14	1366.62	683.81	456.21	1460.77	730.89	487.60	13	G
N	15	1480.66	740.84	494.23	1403.75	702.38	468.59	12	N
H	16	1633.72	817.36	545.24	1289.71	645.36	430.57	11	H
Q	17	1761.78	881.39	587.93	1136.65	568.83	379.56	10	Q
H	18	1898.84	949.92	633.62	1008.59	504.80	336.87	9	H
I	19	2011.92	1006.46	671.31	871.54	436.27	291.18	8	I
G	20	2068.94	1034.97	690.32	758.45	379.73	253.49	7	G
K	21	2197.04	1099.02	733.02	701.43	351.22	234.48	6	K
P	22	2294.09	1147.55	765.37	573.34	287.17	191.78	5	P
S	23	2381.12	1191.06	794.38	476.28	238.65	159.43	4	S
T	24	2482.17	1241.59	828.06	389.25	195.13	130.42	3	T
I	25	2595.25	1298.13	865.76	288.20	144.61	96.74	2	I
R	26				175.12	88.06	59.04	1	R

Figure 2.19: RPL8 H216 hydroxylation is conserved in mice and *D. melanogaster*. EICs show hydroxylated and unhydroxylated tryptic RPL8 peptides$_{201\text{-}226}$ from **A)** *D. melanogaster* SL2 cells and **B)** mouse liver. LC-MS quantation showed that RPL8 H216 was almost fully hydroxylated in mice, but was only 55% hydroxylated in *D. melanogaster* SL2 cells. **C)** Representative MS/MS spectra of the hydroxylated RPL8 peptide$_{201\text{-}226}$ purified from mouse liver. A +16 m/z shift was observed in ion fragments containing H216, indicative of hydroxylation.

2.2.7 NO66 activity is dependent on oxygen availability

Hydroxylases PHDs and FIH act as cellular oxygen sensors by hydroxylating HIF, thereby modulating its activity in an oxygen-dependent manner. Since 2OG oxygenases share the same co-factor requirements, NO66 could theoretically also act as an oxygen sensor that hydroxylates RPL8 H216 in an oxygen-dependent manner. To characterise the effect of hypoxia on RPL8 hydroxylation, HeLa cells were placed in hypoxia incubators programmed at 1% and 0.1% oxygen for 24 hours. During the treatment, cell culture medium was replaced with Stable Isotopic Labelling by Amino acids in Culture (SILAC) medium containing a heavy isotopic variant of arginine. Proteins synthesised during the SILAC treatment will incorporate the heavy variant of arginine, since normal arginine is unavailable. The mass difference between normal and heavy amino acids will enable differentiation of proteins synthesised during the hypoxia treatment from the pre-existing pool by mass spectrometry.

The SILAC approach improved assay sensitivity, which was limited by short duration of the hypoxia treatment and long half-life of the ribosome. HeLa cells cultured under hypoxia were harvested for RPL8 purification and LC-MS/MS analysis. Figure 2.20 shows EICs of SILAC-labelled RPL8 tryptic peptides, from which H216 hydroxylation was quantified to be approximately 67% and 24% under 1% and 0.1% oxygen, respectively. Concurrent with reduction in RPL8 hydroxylation under hypoxia, NO66 protein level was moderately decreased (Figure 2.20). Changes in NO66 expression may provide an alternative explanation for the reduction of RPL8 hydroxylation, rather than the direct inhibition of NO66 activity by hypoxia. However, RPL8 H216 hydroxylation was relatively high under conditions of substantial NO66 knockdown (Figure 2.13), which suggests that a small decrease in NO66 protein level alone is insufficient to produce changes in RPL8 hydroxylation as seen under 0.1% oxygen. Therefore, we conclude that NO66 enzymatic activity is susceptible to inhibition by oxygen deprivation, though the biological consequence of the observed effect is unclear.

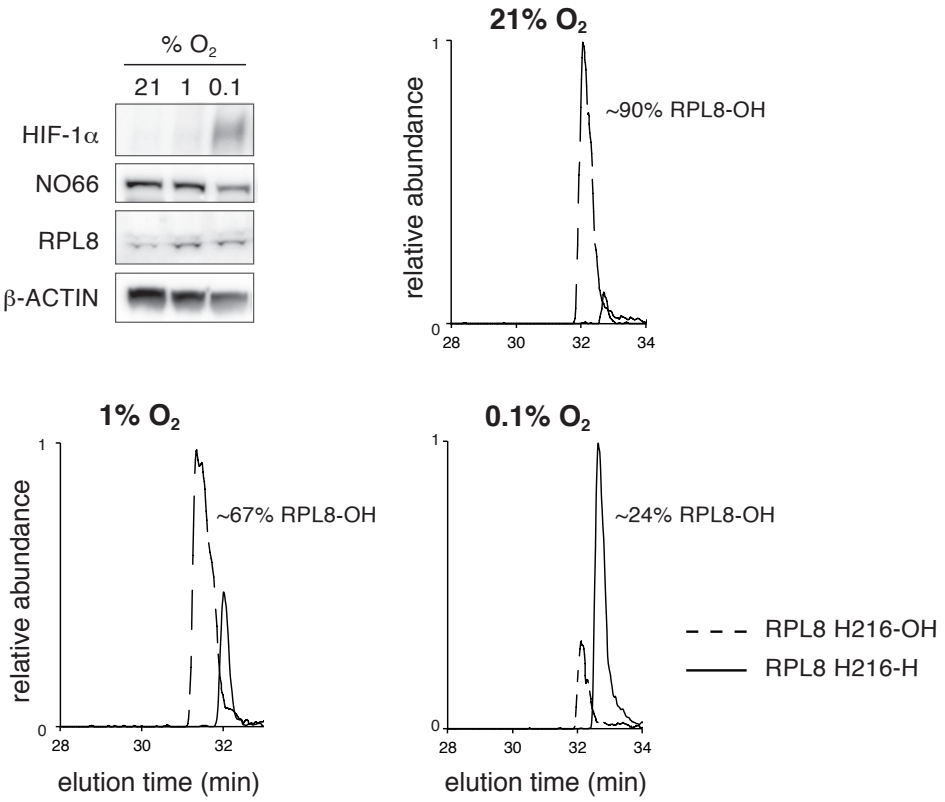


Figure 2.20: RPL8 H216 hydroxylation is reduced under hypoxia. HeLa cells were incubated under 21%, 1%, or 0.1% oxygen for 24 hours. For the duration of the treatment, cells were cultured in SILAC medium which pulse labelled newly synthesised proteins with a heavy isotope variant of arginine. The effectiveness of hypoxia treatments was validated by immunoblotting for HIF1α, as shown in the top left panel. In addition to the stabilisation of HIF1α, NO66 expression was reduced especially under severe hypoxia (0.1% O_2). Remaining panels show EICs of hydroxylated and unhydroxylated RPL8 tryptic peptides$_{201\text{-}226}$ (R+6; $[M+H]^{4+}$; H216-H m/z 686.604; H216-OH m/z 694.600) comparing the effect of varying levels of oxygen on H216 hydroxylation. RPL8 H216 hydroxylation was fully hydroxylated under normoxia, but was reduced to approximately 67% and 24% under 1% and 0.1% hypoxia, respectively.

2.2.8 Biological consequence of NO66 enzymatic activity

NO66 localises to the granular component of the nucleolus (Eilbracht et al., 2004). It interacts with preribosomal particles, and is predicted to play a role in ribosome biogenesis (Eilbracht et al., 2004). Polysome profile analysis measures the relative abundance of 40S, 60S, 80S and polyribosomes, and can be used to visualise any defects in ribosome biogenesis or mRNA translation. The polysomes, consisting of more than one ribosome simultaneously translating an mRNA, are separated from monosomes and ribosomal subunits by velocity sedimentation through a sucrose density gradient. The sucrose gradient is then fractionated, and its UV absorbance at 254nm is measured to obtain the polysome profile. To characterise the function of RPL8 hydroxylation in ribosome biosynthesis and assembly, HEK293T cells reconstituted with wild-type or enzyme-dead NO66 were subjected to polysome profile analysis. However, reconstitution of NO66 into HEK293T cells (Figure 2.18) did not significantly change its polysome profile (Figure 2.21), indicating that the gain of RPL8 hydroxylation did not result in detectable changes in ribosome biogenesis, at least using this approach.

RPL8 plays an important role in the ribosomal machinery. Studies of the yeast RPL8 homologue, RPL2, revealed that it is among the few ribosomal proteins required for ribosome assembly and peptidyl transferase activity (Schulze and Nierhaus, 1982; Diedrich et al., 2000). RPL2 contains a carboxy-terminal extension domain tightly bound to the rRNA core (Klein et al., 2004a). Interestingly, H215 in RPL2 (analogous to H216 in RPL8) locates at the tip of the extension domain, and is in close contact with the P-site of peptidyl transferase center (Meskauskas et al., 2008). Should H216 hydroxylation play a role in peptidyl transferase activity or other ribosomal functions, the intimate link between protein synthesis and cell growth could underly altered growth following NO66 intervention (Suzuki et al., 2007).

To explore this further, we attempted to validate the reported role of NO66 in cell growth by assessing whether the knockdown of NO66 produces a cell proliferation phenotype. MTS (3-(4,5-dimethylthiazol-2-yl)-5-(3-carboxymethoxyphenyl)-2-(4-

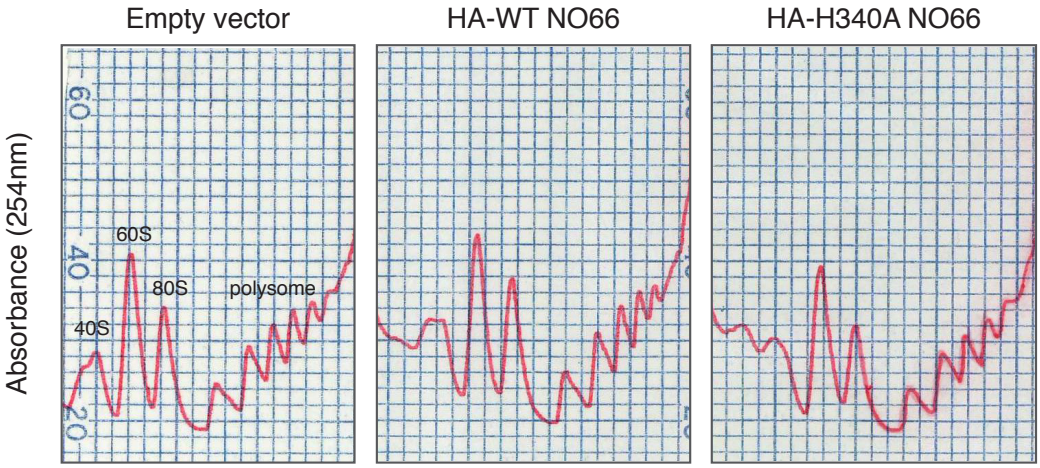


Figure 2.21: Polysome profile analysis of wild-type and NO66 reconstituted HEK293T cells. HEK293T cells stably expression empty vector, HA-WT NO66 or HA-H340A NO66 were treated with cycloheximide, then lysed and passed through a 7-47% sucrose gradient. The gradient was fractionated, and absorbance was measured at 254nm to obtain the polysome profiles. Reconstitution of NO66 expression in HEK293T cells did not signficantly change its polysome profile. For immunoblots validating NO66 expression see Figure 2.18A.

sulfophenyl)-2H-tetrazolium, inner salt) assay (Promega) was used to measure cell growth. Metabolically active cells reduce tetrazolium into a formazan product, which can be measured by colourimetric assays as an inference for cell proliferation. The measurement of cell proliferation using the MTS assay is valid only under the assumption that the loss of NO66 does not significantly alter cell metabolism. This assumption was made since neither NO66 nor RPL8 had any known functions in cell metabolism. While this remains to be a experimental limitation, cell confluency was also qualitatively assessed by eye immediately prior to each MTS measurement to monitor for possible deviations in the MTS readout. To measure the effect of NO66 knowndown on cell proliferation, cells stably expressing shRNA against either NO66 or a control sequence were seeded in 96-well plates, and their proliferation over 6 days was monitored. As shown in Figure 2.22, suppression of NO66 expression by shRNA did not significantly affect cell proliferation. However, the lack of growth phenotype may be due to residual RPL8 hydroxylation, which remained relatively high even after prolonged NO66 knockdown (Figures 2.13). Therefore, cell proliferation was assessed under conditions of NO66 ablation using NO66-reconstituted HEK293T cells and NO66 KO MEFs. The growth of neither HEK293T and MEF cells were significantly affected by NO66 (Figures 2.23 and 2.24). Therefore, at least in the context of our experiments, NO66 and RPL8 H216 hydroxylation are not required for cell growth.

Though NO66 may not directly influence the growth of our cellular models, the loss of RPL8 H216 hydroxylation may have more subtle effects on protein synthesis. Mutation of RPL2 H215 in yeast, which is orthologous to human RPL8 H216, conferred strong resistance against sparsomycin, and partial resistance against anisomycin (Meskauskas et al., 2008). Both antibiotics target the peptidyl transferase center. Anisomycin binds the active peptidyl transferase center, whereas sparsomycin binds near the P-site substrate (Hansen et al., 2003). Therefore, we tested the effect of sparsomycin and anisomycin on the survival of HeLa and A549 cells expressing shRNA targeting NO66. However, NO66 knockdown in HeLa and A549 cells did not result in a differential response to either antibiotic, as shown by dose response curves in Figure

2.25. This data suggests that reduced RPL8 hydroxylation does not significantly alter sensitivity to sparsomycin or anisomycin. Whether abrogated RPL8 hydroxylation in the case of NO66 knockout MEFs and HEK293Ts confers sensitivity to these antibiotics remains undetermined.

2.3 Discussion

Recent studies implicating MINA53 and NO66 in cancer cell growth and other biological pathways have piqued our interest in these JmjC-only oxygenases (Teye et al., 2004; Tsuneoka et al., 2004; Suzuki et al., 2007; Komiya et al., 2010; Sinha et al., 2010). Despite reports of histone demethylation, results on the catalytic activities of MINA53 and NO66 remain conflicting (Lu et al., 2009b; Sinha et al., 2010; Ge et al., 2012). Here, we provide convincing biochemical evidence that NO66 catalyses the histidinyl hydroxylation of 60S ribosomal protein L8.

In vitro studies showed that NO66 did not demethylate histone peptides, but instead hydroxylated a peptide sequence from an interacting ribosomal protein, L8 (Figure 2.2; Ge et al., 2012). Mass spectrometry analysis of endogenous RPL8 showed that it is hydroxylated at H216, which is located in close proximity to the peptidyl transferase centre (Figures 2.5 and 2.7). Importantly, RPL8 H216 hydroxylation is dependent on the expression of NO66, but not its highly related homologue MINA53 (Figures 2.13, 2.14, 2.15, 2.16 and 2.18). NO66 hydroxylase activity against RPL8 is conserved in mice and *D. melanogaster*, and is modestly affected by hypoxia (Figures 2.19 and 2.20). Finally, though NO66 has been previously implicated in cancer cell growth, NO66 suppression did not alter proliferation of our cell models (Figures 2.22, 2.23 and 2.24). Knockdown of the enzyme also did not confer cellular sensitivity towards antibiotics targeting the peptidyl transferase centre (Figure 2.25).

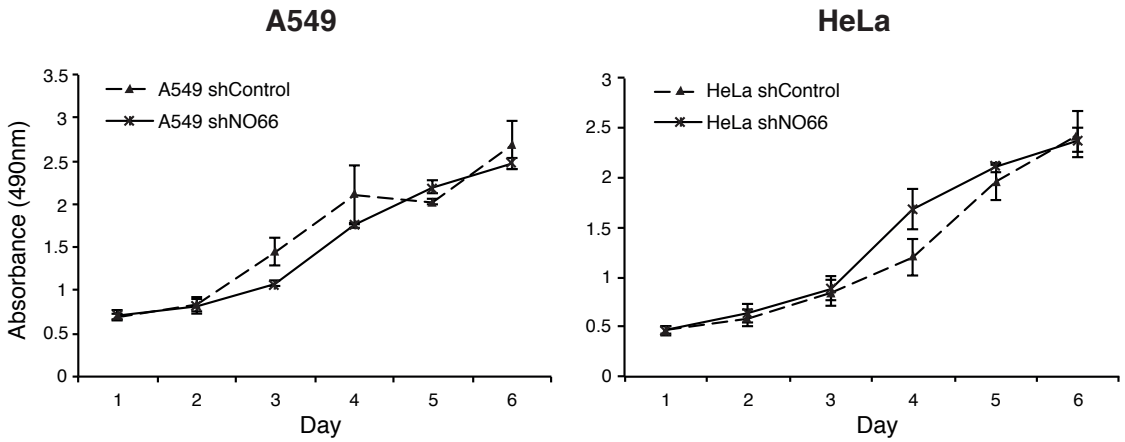


Figure 2.22: Suppression of NO66 in HeLa and A549 cells does not alter cell proliferation. HeLa and A549 cells stably expressing inducible shRNA against either NO66 or a control sequence were treated with doxycycline for 12 days to achieve maximal knockdown. After doxycycline treatment, cells were seeded in 96-well plates in the presence of doxycycline to measure cell proliferation. Cell proliferation was assessed by MTS assay, a colourmetric assay that relies on the metabolic processing of tetrazolium. Representative immunoblot of NO66 protein level post-doxycycline treatment is shown in Figure 2.13A.

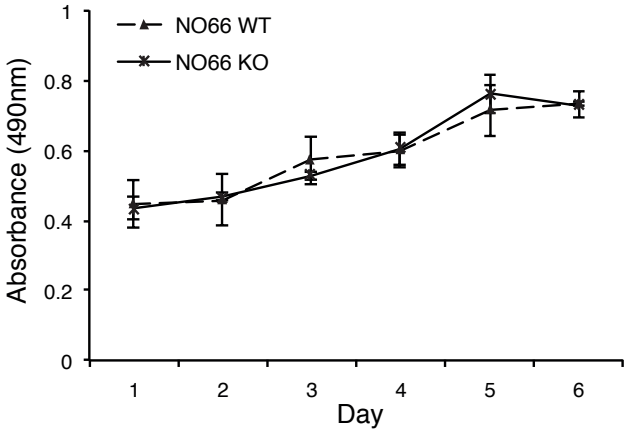


Figure 2.23: Ablation of NO66 expression does not alter MEF growth. Primary MEFs cultured from NO66 WT or KO mice embryos were seeded in 96-well plates for MTS-based growth assay. Neither the absence nor presence of NO66 significantly affected proliferation of MEFs.

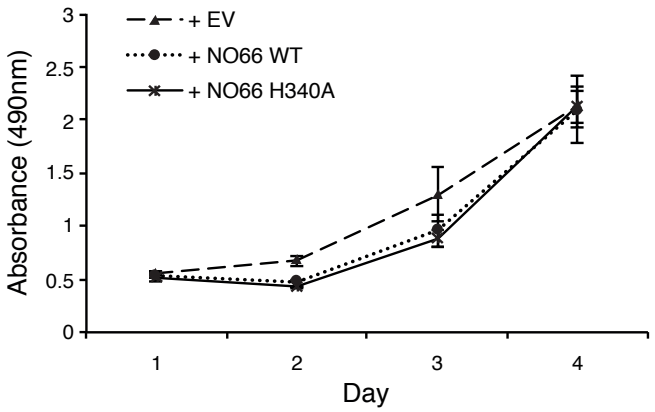


Figure 2.24: Proliferation of HEK293T cells is not affected by NO66 expression. Since NO66 expression is absent in HEK293T cells (Figure 2.18), they were made to stably express empty vector (EV), wild-type or H340A NO66. Expression of either WT or enzyme-dead NO66 did not affect HEK293T cell proliferation, as evidenced by the MTS measurements.

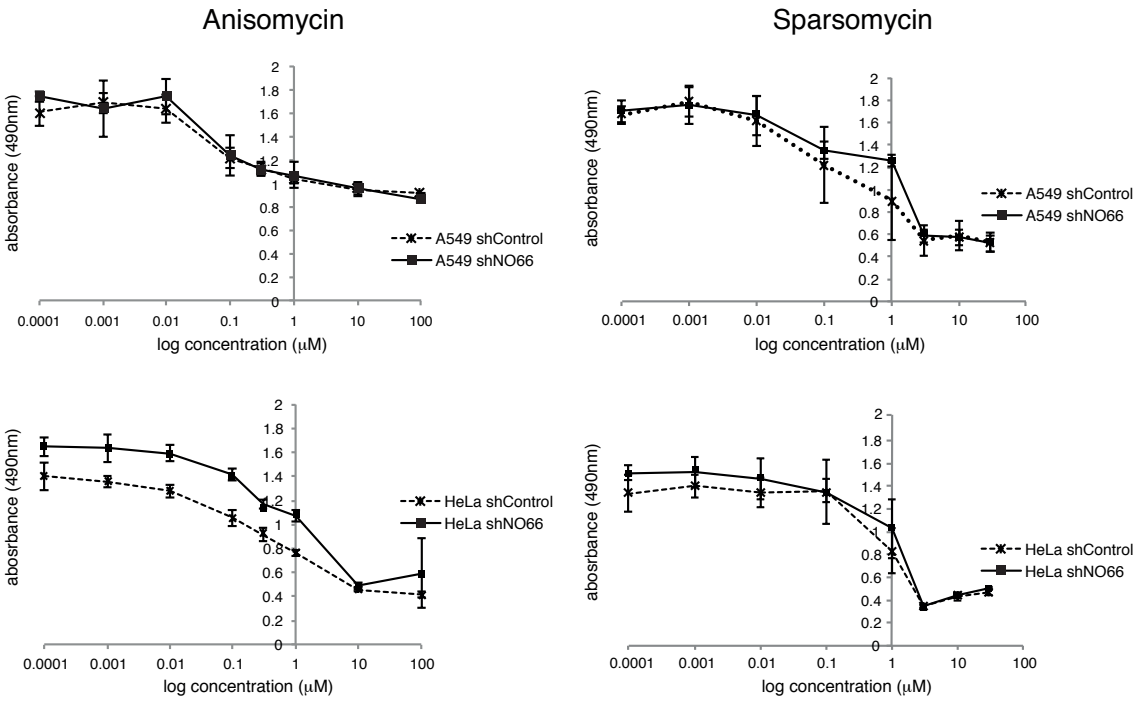


Figure 2.25: NO66 knockdown does not affect cellular sensitivity to antibiotics. A549 and HeLa cells expressing inducible shRNA against either control or NO66 were treated with doxycycline for 12 days and seeded into 96-well microplates for antibiotics screening. Triplicate wells were treated with varying dosage of anisomycin or sparsomycin for 24 hours, following which cell proliferation was measured by MTS assay. The MTS measurements were plotted against antibiotic concentration as shown. NO66 knockdown by shRNA did not significantly affect cell response against either antibiotic.

Other than MINA53 and NO66, it was previously shown that FIH also catalyses histidinyl hydroxylation (Yang et al., 2011a). Hydroxylation and nuclear magnetic resonance (NMR) studies revealed that FIH catalyses hydroxylation at carbon 3 (C3) of a histidine residue belonging to tankyrase-2 (Yang et al., 2011a). NMR of modified RPL8 and RPL27A peptides identified the hydroxylation to be on C3, in support of the evolutionary relationship between the JmjC-only hydroxylases (Ge et al., 2012). The discovery of histidine hydroxylation is of significant biochemical interest, and indicates that the amino acid specificity of 2OG oxygenases is wider than previously believed.

NO66 belongs to a recently identified group of 2OG oxygenases that modifies ribosomal proteins, which altogether has been named ribosomal oxygenases (ROXs). Of the ROXs, both NO66 and MINA53 hydroxylate proteins of the large ribosomal subunit. In prokaryotes, a highly related 2OG oxygenase named YcFD catalyses arginyl hydroxylation of 60S ribosomal protein L16 (Ge et al., 2012). Structural and phylogenetic analyses indicate that NO66 was likely evolved from the prokaryotic ROX YcFD, and MINA53 from NO66 in a much later gene duplication event (Ge et al., 2012; Chowdhury et al., 2014). Interestingly, structural conservation studies indicate that other JmjC domain-containing enzymes were originally evolved from ROXs (Chowdhury et al., 2014).

The evolutionary conservation of ribosomal hydroxylases suggests that ROXs likely play important roles in the protein synthesis machinery. However, other than the hydroxylation of RPS23 by OGFOD1, the exact functions of ribosomal protein hydroxylations remain elusive. It is unclear whether ribosome hydroxylations by NO66, MINA53 and possibly OGFOD1 work together or independently to modulate ribosome function. The cofactor requirements of 2OG oxygenases confer the unique potential to simultaneously regulate all three (or more) ribosome post-translational hydroxylations. Certain physiologically limiting conditions may reduce these modifications, and in turn modulate ribosome function. One such example is the hypoxia sensing pathway, where HIF hydroxylation by the PHDs modulates HIF stability in an oxygen-dependent manner (Ratcliffe, 2013). However, the ribosomal protein hydroxylases are relatively

insensitive to inhibition by hypoxia (Loenarz et al., 2014; Singleton et al., 2014; Figure 2.20), though other conditions such as oxidative stress and iron deprivation may also influence their catalytic functions.

Intriguingly, the only incomplete ribosomal protein hydroxylation identified so far is on RPL8 purified from *D. melanogaster* SL2 cells, for which H216 hydroxylation was estimated to be 55% (Figure 2.19). Whether this partial modification is representative of the physiological status *in vivo*, or reflects sub-optimal growth or nutrient conditions of the cells *in vitro* in unclear. However, further studies of RPL8 hydroxylation in *D. melanogaster* could provide insight into both the regulation of NO66 activity and the function of RPL8 hydroxylation. Perhaps related to the incomplete hydroxylation of RPL8, ShRNA knockdown of NO66 in the *D. melanogaster* wing modestly suppressed its growth (Dr. Pablo Wappner, unpublished data). It is unclear why we have failed to observe a similar phenotype in mammalian cells. Additionally, it is interesting to note that *D. melanogaster* lack the MINA53 gene, raising the possibility that RPL8 and RPL27A hydroxylation are functionally redundant. However, complete inhibition of RPL27A hydroxylation in human cells that naturally lack NO66 protein expression (HEK293T) does not significantly affect growth in both standard tissue culture and nutrient replete conditions (Ge et al., 2012; Dr. Adam Zayer, unpublished data).

The hydroxylation of RPL8 is buried deep within the assembled ribosome, which argues against a signalling function in the cytoplasm. Moreover, the modification is thought to occur during ribosome biogenesis, since NO66 localises to the nucleolus and co-purifies with 60S preribosomal particles (Eilbracht et al., 2004). Therefore, it is conceivable that RPL8 hydroxylation plays a role in ribosome biosynthesis and assembly. Defects in ribosome biogenesis can be measured by direct monitoring of rRNA processing, in addition to polysome profile analysis of the relative abundance of ribosomal subunits. However, the reconstitution of NO66 did not affect the polysome profiles of HEK293T cells, indicating that the presence of RPL8 hydroxylation did not alter ribosome biogenesis, at least under the condition tested (Figure 2.21). However, it is possible that the HEK293T cells have evolved to adapt to the chronic absence of

NO66 and do not require RPL8 hydroxylation, whereas the modification may play a more important role in other cell models. Therefore, acute NO66 knockdown models may provide a more suitable approach to test the involvement of RPL8 hydroxylation in ribosome biogenesis.

The hydroxylation site of RPL8 is in close contact with P-site of the peptidyl transferase centre. Therefore, it would be of interest to characterise the role of RPL8 hydroxylation in ribosomal peptidyl transferase activity. Whilst a direct assay was not performed, we tested for sensitivity of NO66 knockdown cells against antibiotics targeting this region of the ribosome. The suppression of NO66 expression did not render HeLa and A549 cells more sensitive to either sparsomycin or anisomycin (Figure 2.25). This may be explained by insufficient knockdown of NO66. RPL8 hydroxylation remained relatively high (50-60%) in cells expressing inducible shRNA against NO66, even after 12 days of doxycycline treatment (Figure 2.13).

Most ribosomal protein hydroxylations identified so far are near complete under normal physiological conditions, perhaps suggestive of a role in structural maintenance. A cryo-EM structure of the canine ribosome shows that RPL8 H216 is in close proximity to a 28S rRNA loop, and adjacent to a magnesium cation (Mg^{2+}; Figure 2.26; Ge et al., 2012). Mg^{2+} is integral to the assembly and structure of ribosomes, since its positive charge counteracts the negative RNA phosphate backbone and stabilises rRNA tertiary structure (Pyle, 2002; Draper, 2004). Metal cations are also found at the interface between ribosomal proteins and RNA, and are proposed to stabilise protein-RNA interactions (Klein et al., 2004b). H216 in RPL8 is situated within an HXH motif, which resembles a metal chelating motif. Therefore, it is possible that RPL8 H216 hydroxylation helps to chelate Mg^{2+}, and contributes to ribosome structural integrity.

In the mammalian system, NO66 has been implicated in a variety of pathways ranging from osteoblastogenesis to cancer cell growth (Suzuki et al., 2007; Sinha et al., 2010). Both MINA53 and NO66 are reported to be overexpressed in tumours and are required for cancer cell proliferation (Teye et al., 2004; Tsuneoka et al., 2004; Suzuki

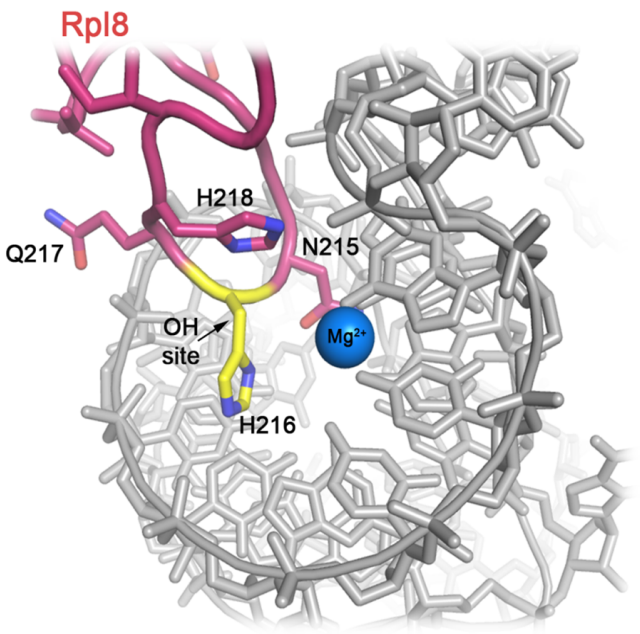


Figure 2.26: The position of RPL8 H216 in the ribosome. Canine cryo-EM ribosome structure showing that RPL8 H216 is in close contact with a magnesium ion. Figure provided by Dr. Rok Sekirnik.

et al., 2007; Komiya et al., 2010). We reasoned that defects in the ribosome machinery due to the lack of RPL8 and RPL27A hydroxylations might be able to explain the proposed effect on growth. However, experiments performed in NO66 knockdown and knockout models suggest no major requirement for cell growth or survival (Figures 2.22, 2.23 and 2.24). Our results contradict previously published findings, though they are consistent with data from our laboratory showing that the loss of MINA53 expression by knockdown or gene ablation did not affect 2D proliferation (Dr. Adam Zayer, unpublished data).

In conclusion, the demonstration of RPL8 hydroxylation by NO66 provides biochemical insights into JmjC-only enzyme function. Together with the discovery of ribosomal hydroxylation by YcFD, MINA53 and OGFOD1, results in this chapter demonstrate a novel role of 2OG oxygenases in the ribosome machinery. Since ribosomal proteins are widely methylated and 2OG oxygenases can catalyse demethylation reactions, the possibility of a wider role for these enzymes in ribosomal modification is of significant interest. Future work should focus on elucidating the physiological consequence of 2OG oxygenase-catalysed ribosomal modifications. To this end, assays that directly measure ribosome performance, such as peptidyl transferase activity, will likely aid understanding of the role of ribosomal hydroxylation in protein synthesis.

Chapter 3

JMJD4 catalyses lysyl hydroxylation of eRF1

3.1 Introduction

The discovery of NO66-catalysed ribosome hydroxylation suggests that its related enzymes may also possess uncharacterised hydroxylase activities. Of members belonging to the JmjC-only family, FIH, MINA53, NO66, JMJD5 and JMJD6 are relatively well characterised. In comparison, little is known about JMJD4, JMJD7, JMJD8 and HSP-BAP1. However, the conservation of Fe(II) and 2OG binding residues in these proteins indicates possible enzymatic activity. Among these putative JmjC-only oxygenases, JMJD4 is especially of interest since its expression is amplified in certain cancers and is required for cell growth (see Chapter 4).

JMJD4 is a well-conserved 2OG oxygenase, with orthologues found in most eukaryotic species other than *Saccharomyces cerevisiae* (Figure 3.1). It shares the highest sequence homology with JMJD6. JMJD6 was originally reported as a histone arginine demethylase (Chang et al., 2007). Later experiments showed that JMJD6 catalyses lysyl hydroxylation of splicing factor U2AF65, and possibly other RS domain-containing proteins and histones (Webby et al., 2009). Interestingly, whereas JMJD6 is found in the nucleus, JMJD4 localises to the cytosol (Hahn et al., 2010; Feng et al., 2014).

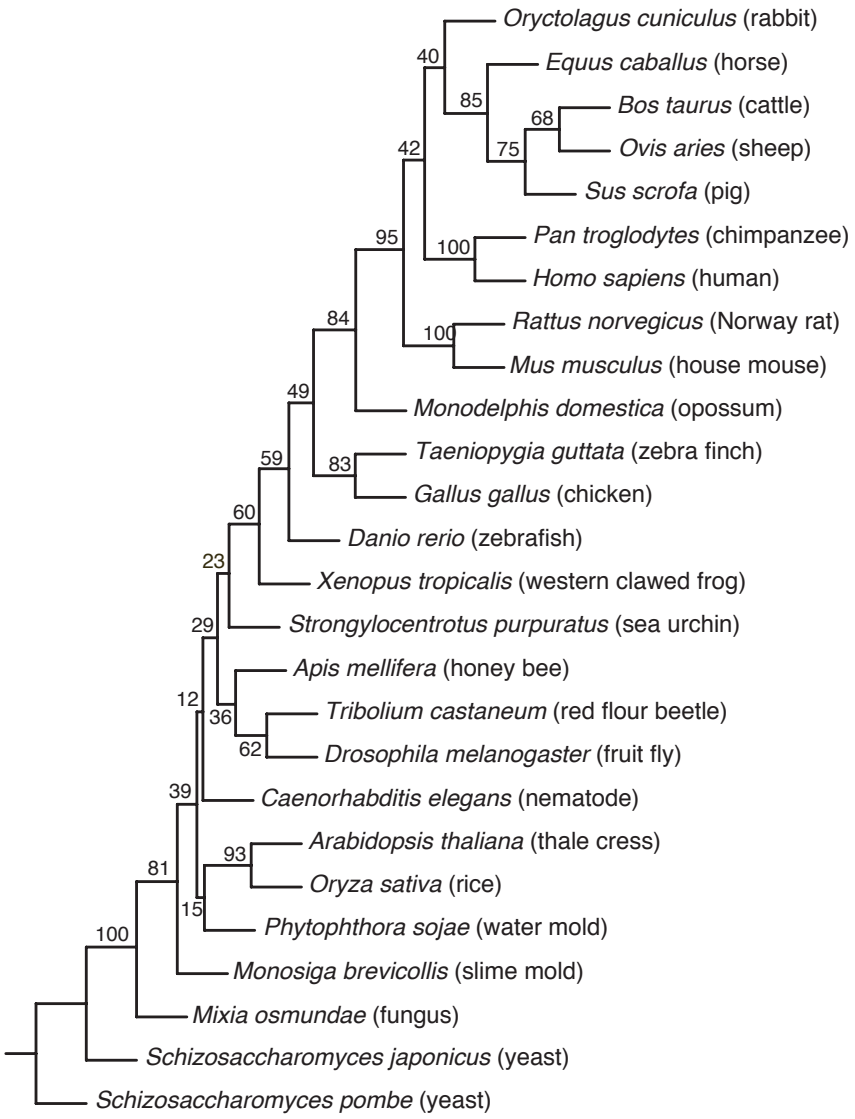


Figure 3.1: Conservation of JMJD4 in eukaryotes. JMJD4 proteins in eukaryotic species were identified using BLAST search of NCBI protein database, and protein sequences were aligned using Clustal Omega. Phylogenetic tree was constructed using PHYLIP (phylogeny inference package). JMJD4 was not identified in *Saccharomyces cerevisiae*. Phylogenetic analyses and figure by Dr. Sarah E. Wilkins, adapted from Feng et al. (2014).

Therefore, JMJD6 and JMJD4 likely do not overlap in substrate specificity.

This chapter describes the discovery and characterisation of JMJD4-catalysed lysyl hydroxylation of eRF1. eRF1 is the eukaryotic release factor responsible for translational termination. Initial proteomic screens using JMJD4 overexpressing HEK293T cells identified eRF1 as an activity-dependent interactor of JMJD4. Overexpression and *in vitro* studies found that eRF1 is hydroxylated at K63 in the presence of JMJD4. Furthermore, endogenous eRF1 is hydroxylated at K63, and the modification is dependent on JMJD4 activity. Finally, the effect of hypoxia and other physiologically limiting conditions on eRF1 hydroxylation was characterised in detail.

3.2 Results

3.2.1 Identification of a JMJD4 candidate substrate

Previous studies of other 2OG oxygenases revealed that they often interact with the substrate in an activity-dependent manner. For example, the interaction between MINA53 and its substrate RPL27A is ablated upon mutation of the predicted Fe(II) binding residue in MINA53 (Dr. Adam Zayer, unpublished data). As such, we screened for JMJD4 candidate substrates by searching for activity-dependent interactors. To this end, HEK293T cells were made to overexpress FLAG-tagged JMJD4, which were either wild-type or mutated at a predicted Fe(II) binding residue (H189A). FLAG-tagged JMJD4 and its interactors were immunopurified, and analysed by LC-MS/MS. A search against a human protein database using the Mascot software identified a number of JMJD4 binding proteins, which were filtered against enzyme-dead JMJD4 control to identify activity-dependent interactors (Table 3.1).

There were no known JMJD6 substrates or histones among the JMJD4-dependent interactors. Instead, two cytoplasmic proteins, eRF1 and eRF3, interacted with WT JMJD4 with the highest affinity. Together, eRF1 and eRF3 form the eukaryotic release factor complex that mediates translational termination. eRF1 recongises the stop

Description	Localisation	PSMs	Peptides	% Coverage
eRF1	Cytoplasmic	213	32	75.1
eRF3A	Cytoplasmic	86	32	56.3
FAM40A	Nuclear	6	3	5.1
GGCX Vitamin K-dependent gamma-carboxylase	ER membrane	5	3	2.5
Transcription elongation factor A protein-like 4	Nuclear	5	3	15.1
DCTN1	Cytoplasmic	3	4	5.4
PARP4 Poly (ADP-ribose) polymerase 4	Cytoplasmic/Nuclear	3	3	2.4
ZNF180 Zinc finger protein 180	Nuclear	3	2	9.0

Table 3.1: List of JMJD4 proteomic interactors. HEK293T cells stably expressing empty vector (EV) control, WT or H189A FLAG-JMJD4 were subjected to anti-FLAG pull-down, after which the immunoprecipitates were digested with trypsin and analysed with LC-MS/MS. The proteomic data was searched against human UniProt (Universal Protein Resource) database using the Mascot search engine. H189 in JMJD4 is predicted to bind to Fe(II), and its mutation should ablate JMJD4 catalytic activity. Results from the three cell lines were cross-referenced to shortlist proteins that only interacted with WT FLAG-JMJD4. The table lists the JMJD4 activity-dependent interactors from a single proteomics experiment in order of abundance, as measured by their peptide coverage and protein score. eRF1 and eRF3 were the most abundant and are highlighted in red. A complete list of JMJD4 interacting proteins is provided in the supplementary CD.

codon and catalyses peptidyl bond hydrolysis. eRF3, on the other hand, stimulates eRF1 activity by acting as a GTPase (Zhouravleva et al., 1995; Frolova et al., 1996). eRF1 was more abundant in the immunoprecipitate sample, indicating that it is the dominant JMJD4 interactor that likely co-purifies eRF3 (Table 3.1). In comparison to eRF1 and eRF3, other shortlisted binding partners were significantly less abundant. Whereas JMJD4 is found in the cytosol (Dr. Mathew Coleman, personal communications), some of these proteins were localised elsewhere in the cell, which suggested that they were likely to be contaminants. Results of the proteomic screen were confirmed by immunoblotting for both release factors in anti-FLAG immunoprecipitated extracts from HEK293T cells. As expected, eRF1 and eRF3 were present in immunoprecipitated complex containing FLAG-JMJD4 (Figure 3.2). The interaction was specific since the release factors did not bind to FLAG-FIH or empty vector control (Figure 3.2). Moreover, immunofluoresence showed that both eRF1 and JMJD4 localise to the cytoplasm (Figure 3.3).

3.2.2 Overexpressed JMJD4 promotes eRF1 hydroxylation

To determine whether JMJD4 hyroxylates eRF1 and/or eRF3, HEK293T cells were transfected with expression vectors encoding V5-tagged eRF1 and HA-tagged eRF3. Concurrently, the cells were transfected with empty vector control or FLAG-tagged JMJD4. The V5-eRF1/eRF3 complex were immunopurified with anti-V5 resin, and resolved using SDS-PAGE. Bands corresponding to eRF1 and eRF3 were excised for protease digestion and LC-MS/MS analysis (Figure 3.4A). Since JMJD4 is predicted to be a lysyl hydroxylase and trypsin cleaves at the carboxyl side of lysine residues, the candidate substrates were digested with Arg-C. MS/MS sequencing identified a +16 dalton mass shift in the eRF1 peptide sequence VAKMLADEFGTASNIKSR (residues 48-65). The mass shift was assigned to the lysine residue at position 63 of eRF1 (K63; Figure 3.4B). Figure 3.4C shows EICs of hydroxylated and unhydroxylated V5-eRF1 Arg-C peptides. Critically, co-expression of FLAG-JMJD4 increased K63 hydroxyla-

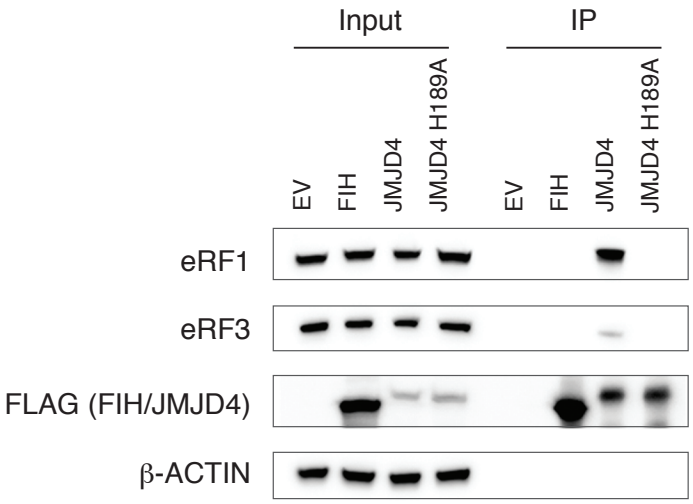


Figure 3.2: JMJD4 interacts with eRF1 in cells. HEK293T cells stably expressing EV, FLAG-FIH, WT or H189A FLAG-tagged JMJD4 were subjected to anti-FLAG immunoprecipitation (IP). The immunoprecipitates were immunoblotted for the presence of endogenous eRF1 and eRF3. 'Input' denotes whole cell extract (5%) prior to immunoprecipitation. In comparison to whole cell extracts, eRF1 and eRF3 were only found in immunoprecipitated fraction containing WT FLAG-JMJD4, but not in that of EV, FLAG-FIH or H189A FLAG-JMJD4. Enrichments of FLAG-tagged enzymes post-affinity purification were confirmed by anti-FLAG immunoblots.

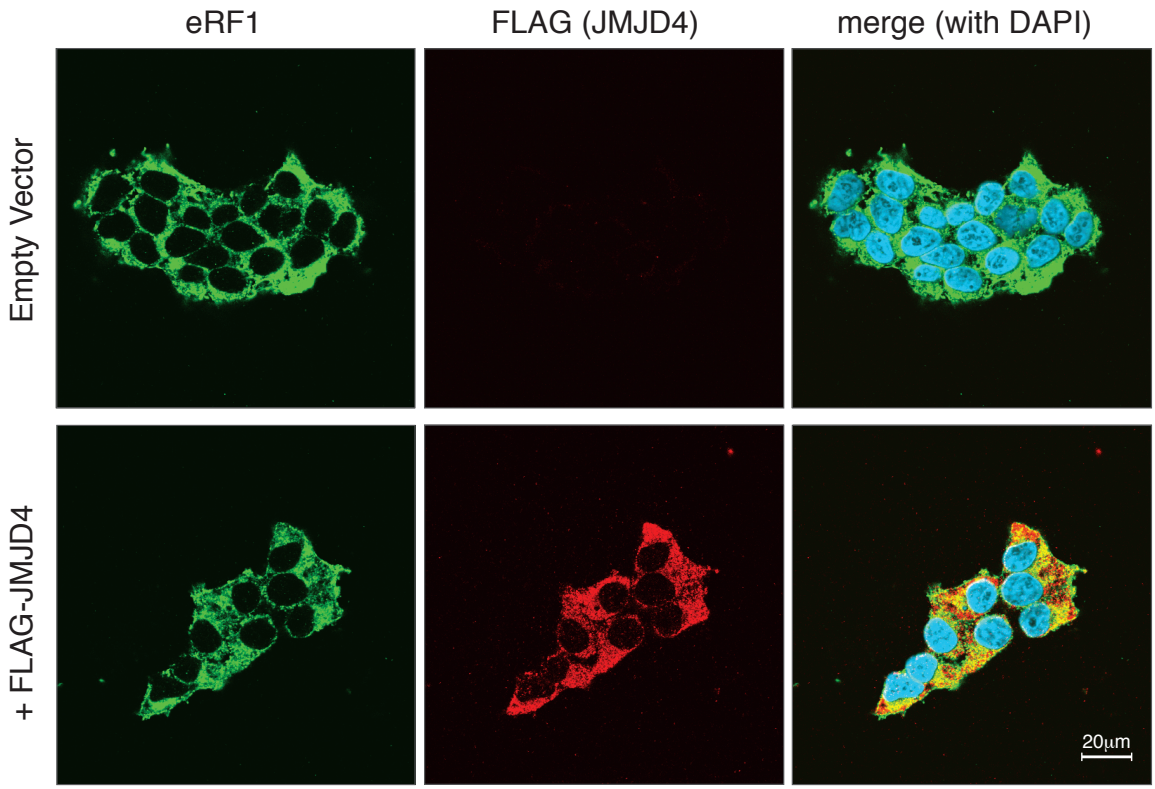
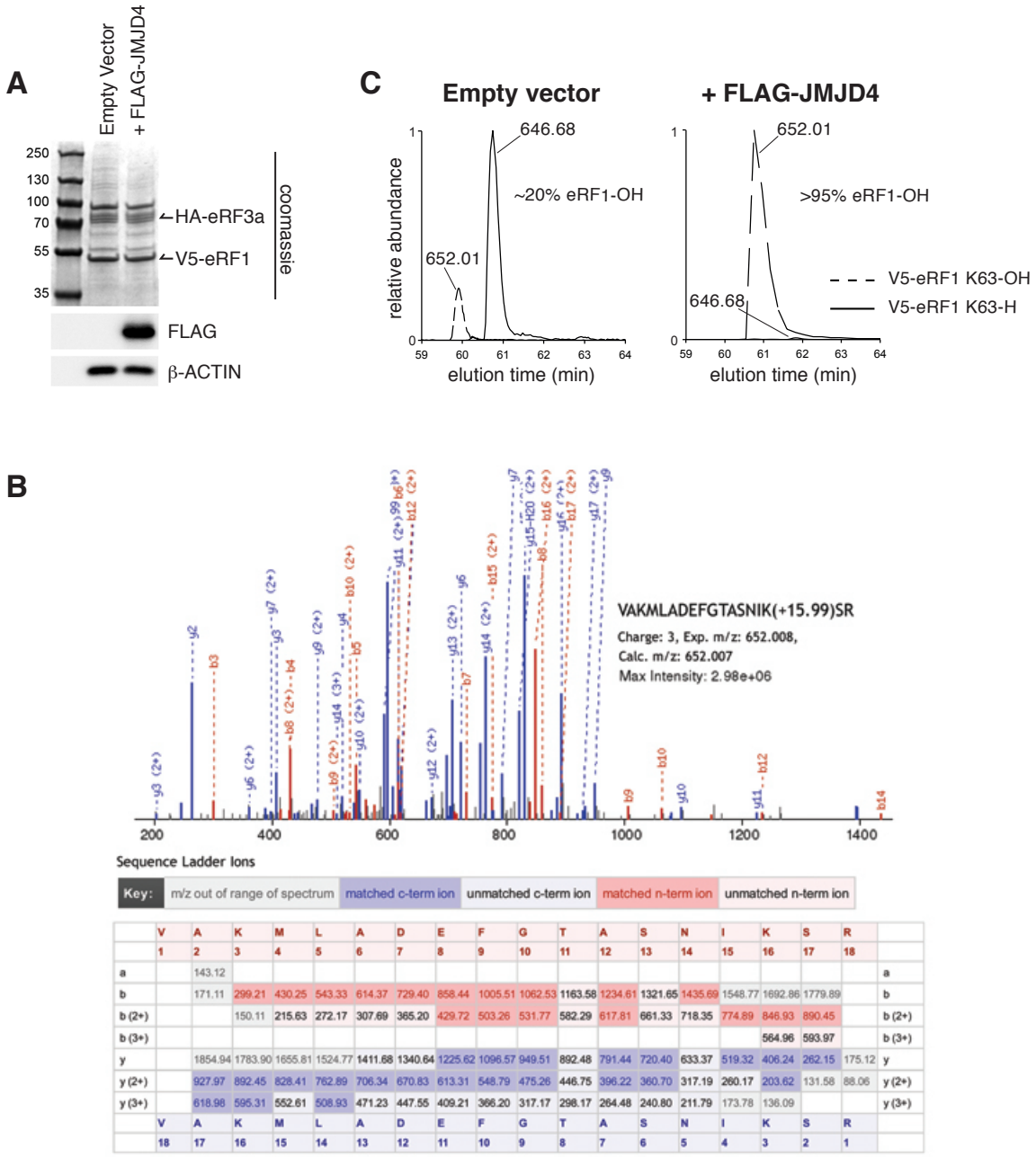


Figure 3.3: JMJD4 and eRF1 co-localise in cells. HEK293T cells stably expressing EV or FLAG-JMJD4 were cultured on immunofluorescence slides overnight, following which they were fixed, permeabilised and immunostained for FLAG (red) and eRF1 (green). Nuclei were visualised using the DNA-binding stain DAPI (blue). Representative confocal immunofluorescence images show that both eRF1 and FLAG-JMJD4 localise to the cytoplasm.



	V	A	K	M	L	A	D	E	F	G	T	A	S	N	I	K	S	R	
	1	2	3	4	5	6	7	8	9	10	11	12	13	14	15	16	17	18	
a		143.12																	a
b		171.11	299.21	430.25	543.33	614.37	729.40	858.44	1005.51	1062.53	1163.58	1234.61	1321.65	1435.69	1548.77	1692.86	1779.89		b
b (2+)			150.11	215.63	272.17	307.69	365.20	429.72	503.26	531.77	582.29	617.81	661.33	718.35	774.89	846.93	890.45		b (2+)
b (3+)																564.96	593.97		b (3+)
y		1854.94	1783.90	1655.81	1524.77	1411.68	1340.64	1225.62	1096.57	949.51	892.48	791.44	720.40	633.37	519.32	406.24	262.15	175.12	y
y (2+)		927.97	892.45	828.41	762.89	706.34	670.83	613.31	548.79	475.26	446.75	396.22	360.70	317.19	260.17	203.62	131.58	88.06	y (2+)
y (3+)		618.98	595.31	552.61	508.93	471.23	447.55	409.21	366.20	317.17	298.17	264.48	240.80	211.79	173.78	136.09			y (3+)
	V	A	K	M	L	A	D	E	F	G	T	A	S	N	I	K	S	R	
	18	17	16	15	14	13	12	11	10	9	8	7	6	5	4	3	2	1	

Figure 3.4: Overexpressed JMJD4 hydroxylates eRF1 at K63. HEK293T cells were transfected with HA-eRF3 and V5-eRF1 in the presence or absence of FLAG-JMJD4, and harvested for anti-HA affinity purification. **A)** The immunopurified complexes were resolved using SDS-PAGE. Bands corresponding to molecular weights of eRF1 and eRF3 were excised, digested with Arg-C and analysed by LC-MS/MS. **B)** MS/MS spectrum of hydroxylated V5-eRF1 peptide$_{48\text{-}65}$ showing the amino acid sequencing. A +16 m/z shift was observed only in fragment ions containing K63, which assigned the position of hydroxylation to the lysine of interest. **C)** EICs of the V5-eRF1 peptide$_{48\text{-}65}$ ($[M+H]^{3+}$; K63-H m/z 646.680; K63-OH m/z 652.008) purified from cells expressing EV or FLAG-JMJD4. It is unclear why the peptide retention times differ between samples, though the identities of the peaks were validated using their m/z ratios and MS spectra. Co-expression of FLAG-JMJD4 resulted in increased abundance of the hydroxylated peptide relative to empty vector control (20 to >95%), as measured by LC-MS quantitation.

tion of V5-eRF1 from 20% to 95% relative to empty vector control. Therefore, the data suggests that JMJD4 hydroxylates eRF1 at K63 under conditions of ectopic over-expression.

3.2.3 Recombinant JMJD4 hydroxylates eRF1 *in vitro*

In order to assess whether eRF1 hydroxylation is directly catalysed by JMJD4, recombinant eRF1 and JMJD4 were expressed in *E. coli*. Bacteria lysates containing the postulated substrate was combined with purified enzyme at a ratio of 10:1 in the presence of Fe(II) and 2OG. The reaction was allowed to proceed for 16 hours at room temperature, following which eRF1 was purified using Ni-NTA agarose beads and resolved using SDS-PAGE for trypsinolysis and LC-MS/MS analysis. LC-MS quantitation using relative peak heights showed that eRF1 K63 was nearly completely hydroxylated in the presence of WT, but not H189A enzyme-dead JMJD4 (Figure 3.5). Moreover, mutation of K63 to either arginine or alanine significantly ablated eRF1 hydroxylation, though JMJD4 exhibited some excess activity towards K63R eRF1 (5% hydroxylation; Figure 3.5). All LC-MS results were confirmed using MS/MS sequencing (Figures 3.6, 3.7 and 3.8). Results from the *in vitro* studies indicate that JMJD4 catalytic activity is specific and confirm previous MS/MS assignment of the modification to K63.

The dynamics of JMJD4 catalytic activity were next characterised by performing a hydroxylation time course. Recombinant eRF1 was incubated with JMJD4 in the presence of the necessary co-factors. At 0, 30, 60, 120 and 480 minutes after incubation, the reaction was quenched by formic acid and digested in-solution with trypsin for LC-MS/MS analysis. As expected, the enzymatic activity of JMJD4 was time-dependent, with the level of eRF1 K63 hydroxylation reaching saturation after 120 minutes (Figure 3.9A). Furthermore, presence of 2OG and Fe(II) were required for the hydroxylation of recombinant eRF1, thus confirming that JMJD4 is a 2OG- and Fe(II)-dependent oxygenase (Figure 3.9B). Interestingly however, ascorbate was not required for the enzymatic activity of JMJD4. Ascorbate has been proposed to stim-

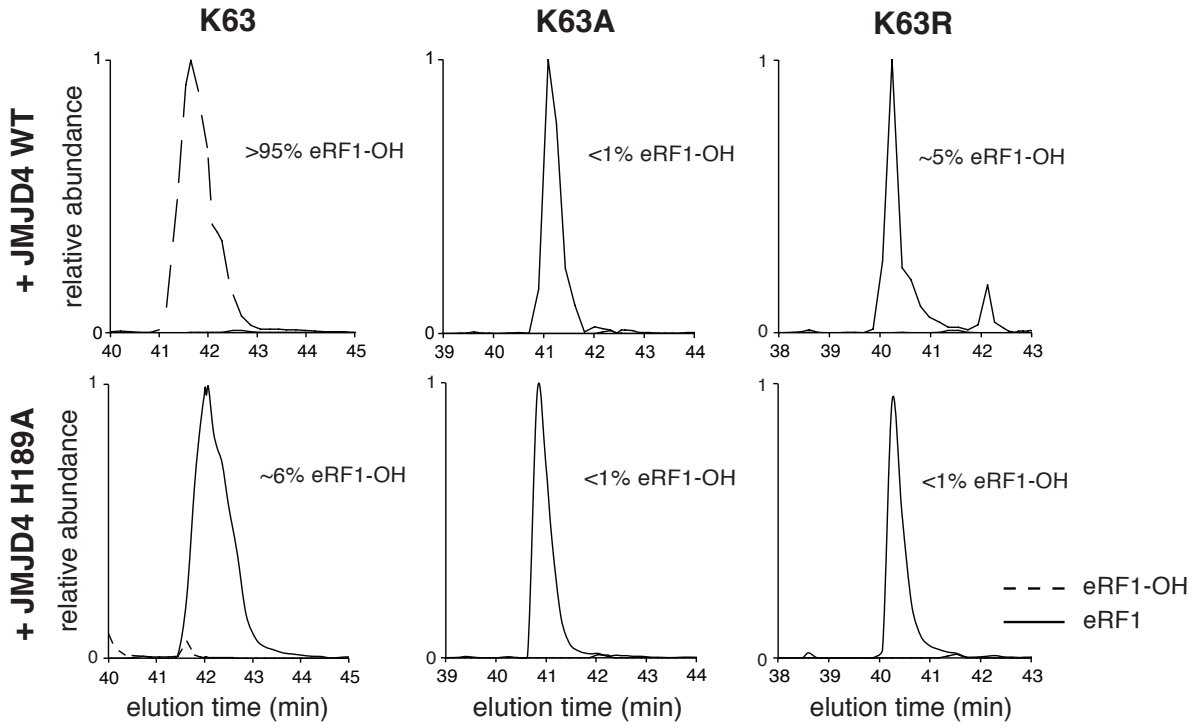


Figure 3.5: Recombinant JMJD4 modifies eRF1 at K63 *in vitro*. Recombinant eRF1 was combined with recombinant JMJD4 in the presence of the required cofactors, and allowed to react for 16 hours at room temperature. Recombinant eRF1 was then purified and trypsinised for LC-MS/MS. The above figure shows EICs of tryptic peptides$_{51\text{-}63}$ from WT or mutant eRF1 reacted with either WT or H189A JMJD4 ($[M+H]^{2+}$; K63-H m/z 698.842; K63-OH m/z 706.840; K63R-H m/z 712.846; K63R-OH m/z 720.843; K63A-H m/z 791.880; K63A-OH m/z 799.878). WT JMJD4 hydroxylated eRF1 to near 100%, and mutation of either K63 in eRF1 or H179 in JMJD4 ablated the hydroxylation. Note that JMJD4 hydroxylated 5% of K36R eRF1, likely due to excessive enzyme activity. Recombinant JMJD4 synthesised by Dr. Luke Yates. *In vitro* hydroxylation performed by Dr. Mathew Coleman.

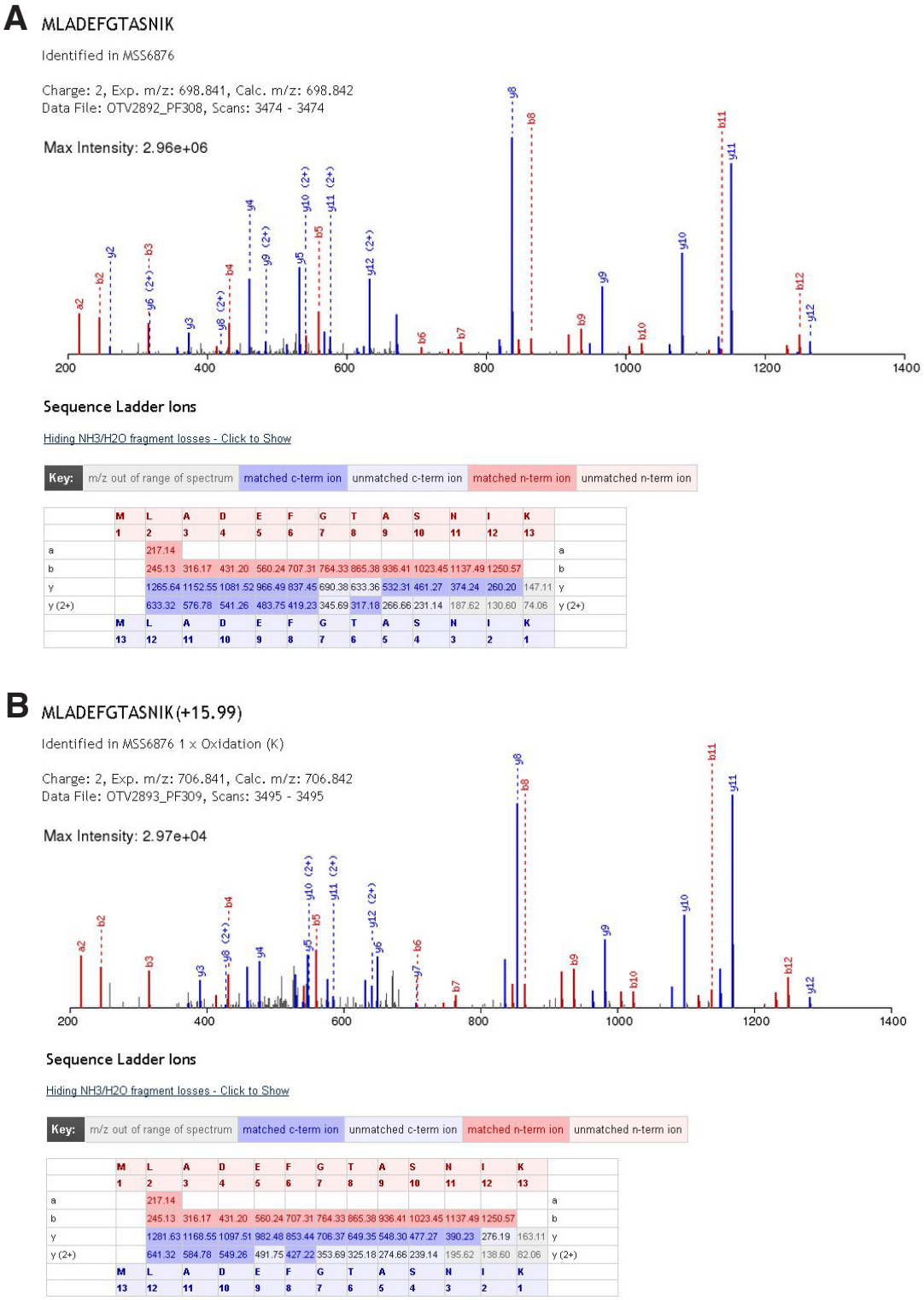


Figure 3.6: MS/MS sequencing of recombinant eRF1 peptide$_{51\text{-}63}$. WT recombinant eRF1 was reacted with either WT or H189A recombinant JMJD4 in the presence of co-factors. **A)** and **B)** show representative MS/MS spectra of unhydroxylated and hydroxylated eRF1 K63 (MLADEFGTASNI<u>K</u>) peptides$_{51\text{-}63}$, respectively. For the hydroxylated peptide, a +16 m/z shift was observed in all y-series but not b-series fragment ions, which assigned the position of hydroxylation to K63.

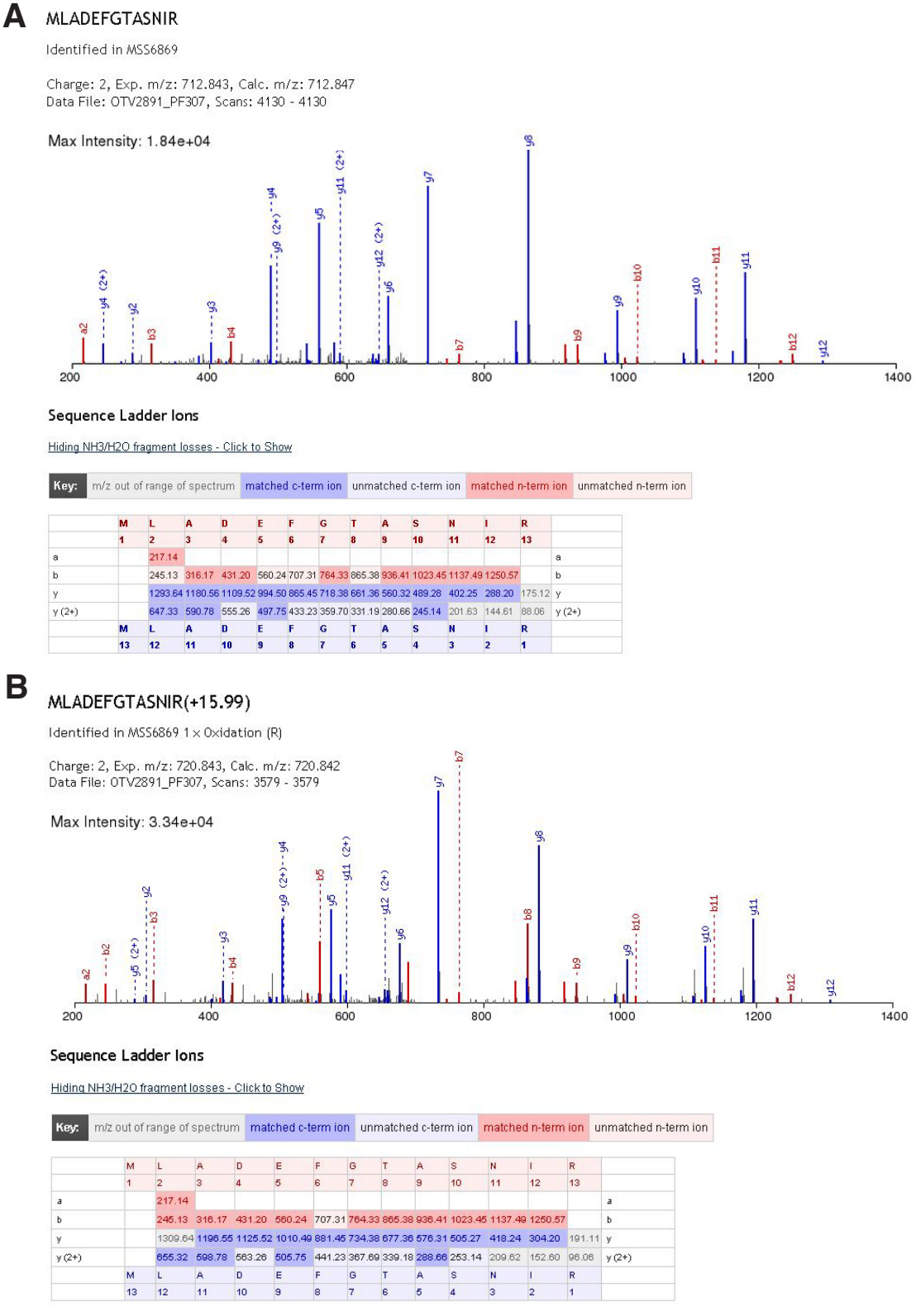
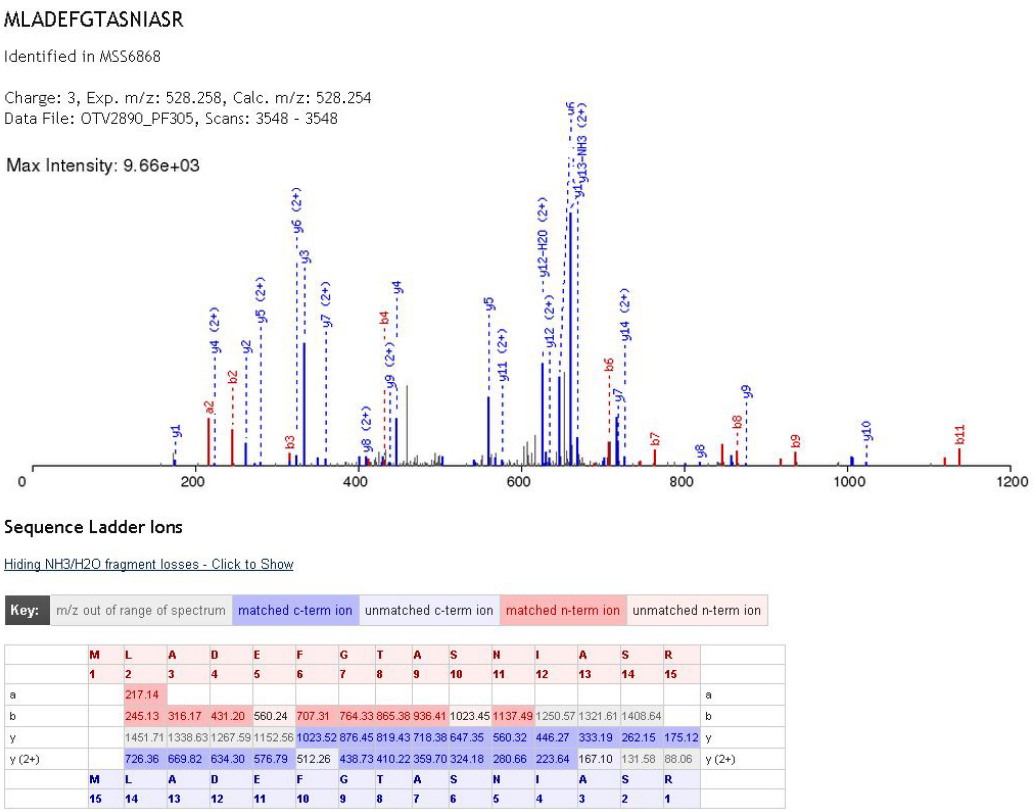


Figure 3.7: MS/MS sequencing of recombinant K63R eRF1 peptide$_{51\text{-}63}$. K63R recombinant eRF1 was reacted with either WT or H189A recombinant JMJD4 in the presence of co-factors. **A)** and **B)** show representative MS/MS spectra of hydroxylated and unhydroxylated K63R eRF1 (MLADEFGTASNIR) peptides$_{51\text{-}63}$, respectively. For the K63R hydroxylated peptide, a +16 m/z shift was observed in all y-series but not b-series fragment ions, which assigned the position of hydroxylation to R63.



	M	L	A	D	E	F	G	T	A	S	N	I	A	S	R	
	1	2	3	4	5	6	7	8	9	10	11	12	13	14	15	
a		217.14														a
b		245.13	316.17	431.20	560.24	707.31	764.33	865.38	936.41	1023.45	1137.49	1250.57	1321.61	1408.64		b
y		1451.71	1338.63	1267.59	1152.56	1023.52	876.45	819.43	718.38	647.35	560.32	446.27	333.19	262.15	175.12	y
y (2+)		726.36	669.82	634.30	576.79	512.26	438.73	410.22	359.70	324.18	280.66	223.64	167.10	131.58	88.06	y (2+)
	M	L	A	D	E	F	G	T	A	S	N	I	A	S	R	
	15	14	13	12	11	10	9	8	7	6	5	4	3	2	1	

Figure 3.8: MS/MS sequencing of recombinant K63A eRF1 peptide$_{51\text{-}65}$. K63A recombinant eRF1 was reacted with either WT or H189A recombinant JMJD4 in the presence of co-factors. Representative MS/MS spectrum of eRF1 K63A (MLADEFGTASNIASR) peptide$_{51\text{-}65}$ showing the absence of K63A hydroxylation.

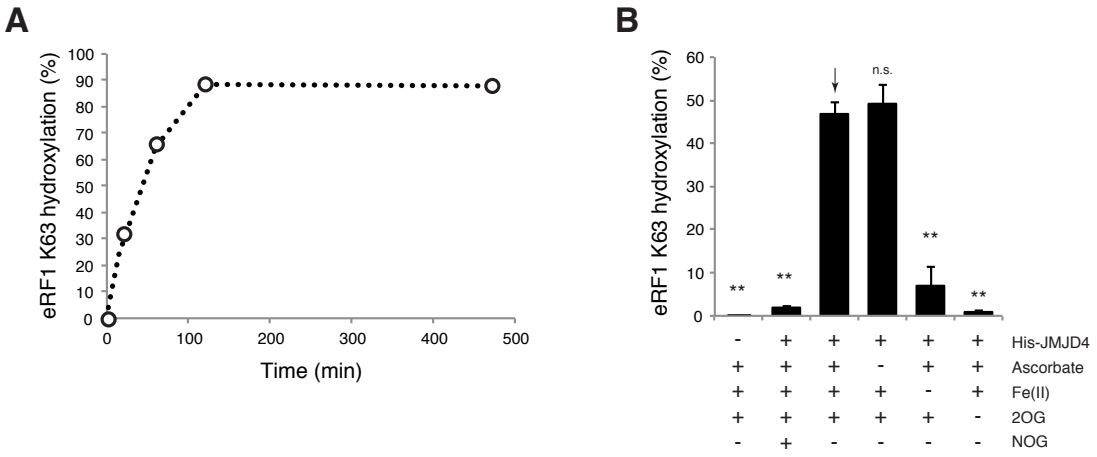


Figure 3.9: JMJD4 is a 2OG- and Fe(II)-dependent oxygenase. A) Recombinant eRF1 was incubated with JMJD4 in the presence of Fe(II), 2OG and ascorbate. At the indicated time points, the reaction was quenched and eRF1 was purified for LC-MS/MS analysis. As expected, recombinant eRF1 was not hydroxylated at the start of the reaction. JMJD4-catalysed hydroxylation increased in a time-dependent manner and plateaued after 120 minutes. **B)** Recombinant eRF1 was incubated with JMJD4 in the presence or absence of cofactors as indicated. The reaction proceeded for 1 hour before it was quenched, and eRF1 was purified and analysed by LC-MS/MS. Hydroxylation of eRF1 K63 was not dependent on ascorbate, though it was ablated in the absence of Fe(II), 2OG or the presence of N-oxalylglycine (NOG). Statistical significance was evaluated using ANOVA followed by Dunnett's post hoc test (n.s. = not significant; ** = $p < 0.01$), and compared against the level of eRF1 hydroxylation in the presence of JMJD4 and all co-factors (arrow).

ulate 2OG oxygenase activity by acting as a reducing agent to maintain the ferrous state of iron (Clifton et al., 2006; Flashman et al., 2010a). However, not all 2OG oxygenases require ascorbate, and *in vitro* conditions may alter cofactor requirements (Clifton et al., 2006). The addition of NOG, a competitive inhibitor and non-reactive analogue of 2OG (Mole et al., 2003), abrogated eRF1 hydroxylation despite the presence of co-factors (Figure 3.9B). These results suggest that JMJD4 directly catalyses eRF1 hydroxylation in a time- and cofactor-dependent manner. In addition, JMJD4 is a *bona fide* 2OG oxygenase susceptible to small molecule inhibition.

3.2.4 Endogenous eRF1 is hydroxylated at K63

Results obtained so far have demonstrated that JMJD4 modifies eRF1 at K63 in overexpression and *in vitro* settings. Next, we sought to determine whether endogenous eRF1 is hydroxylated at K63. Since eRF1 is highly abundant, we were able to immunopurify endogenous eRF1 from cells using a commercially available antibody. eRF1 immunopurified from HEK293T cells was resolved by SDS-PAGE and stained with Coomassie blue. The protein band corresponding to the predicted molecular weight of eRF1 was excised and digested with trypsin for LC-MS/MS analysis (Figure 3.10A). MS/MS sequencing identified a tryptic peptide of sequence MLADEFGTASNI<u>K</u> (residues 51-63) which contained K63. Figure 3.10B shows EICs of the hydroxylated and unhydroxylated eRF1 K63 peptides. Using methods described in Chapter 2, relative quantitation of elution peak heights showed that eRF1 is almost completely hydroxylated at K63.

Figure 3.11 compares MS/MS spectra of unhydroxylated and hydroxylated eRF1 K63 tryptic peptides. In comparison to the unmodified peptide, a +16 mass shift was observed in the modified peptide in the y-ion series from y1 onwards, consistent with the addition of an oxygen atom at K63. However, the y1 fragment ion itself was too small to be detected. Consequently, MS/MS analysis of eRF1 was repeated with Arg-C digestion, which yielded a longer peptide of sequence VAKMLADEFGTASNI<u>K</u>SR (residues 48-65). MS/MS sequencing of the Arg-C peptide also assigned the hydroxy-

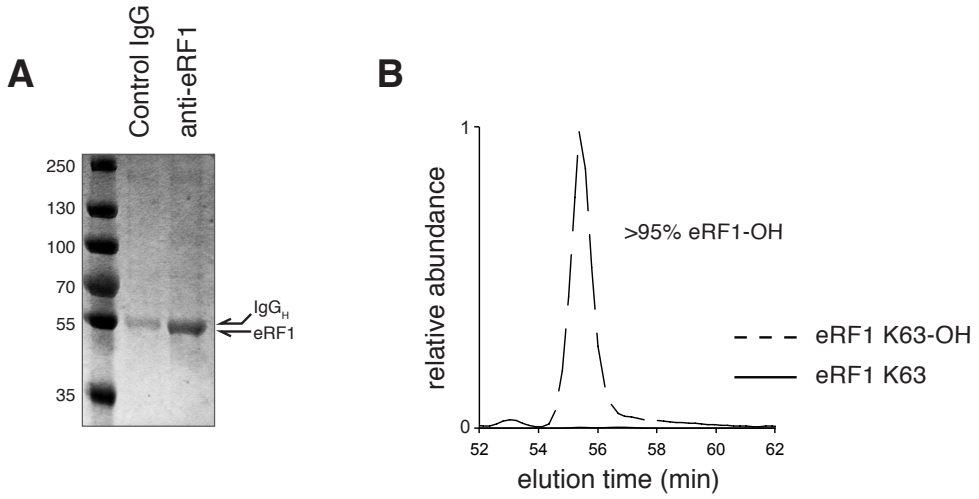


Figure 3.10: Purification and mass spectrometry characterisation of endogenous eRF1. Endogenous eRF1 was immunopurified from HEK293T cells using a commercially available antibody. **A)** The immunopurified complex was resolved using SDS-PAGE and stained with Coomassie Blue. Although eRF1 co-migrates with the IgG heavy chain, immunopurification of eRF1 resulted in a much more strongly stained band than IgG heavy chain alone. Purified eRF1 was excised and digested with trypsin for LC-MS/MS analysis. **B)** EICs comparing K63 hydroxylated and unhydroxylated peptides$_{51\text{-}63}$ ($[M+H]^{2+}$; K63-H m/z 698.842; K63-OH m/z 706.840). Relative LC-MS quantitation revealed that more than 95% of peptides are hydroxylated at K63.

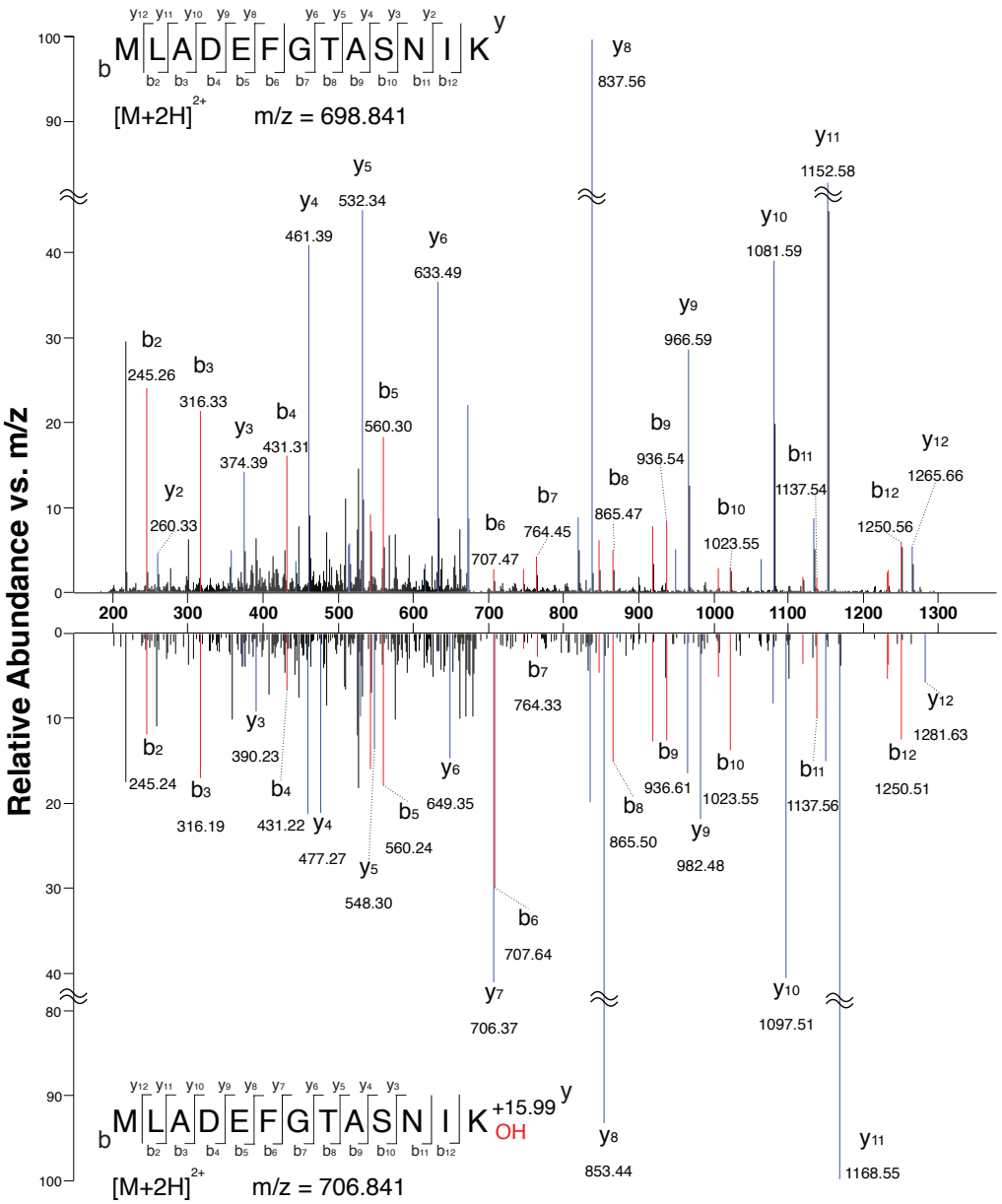


Figure 3.11: MS/MS sequencing of endogenous eRF1 digested with trypsin. Endogenous eRF1 was immunopurified for trypsinolysis and MS/MS sequencing. The figure shows representative MS/MS spectra of unhydroxylated (top panel) and hydroxylated (bottom panel) eRF1 K63-containing tryptic peptides$_{51\text{-}63}$. For the hydroxylated peptide, a +16 m/z shift was observed in all y-series, but not b-series fragment ions, which assigned the position of hydroxylation to K63. MS/MS annotation by Dr. Roman Fischer.

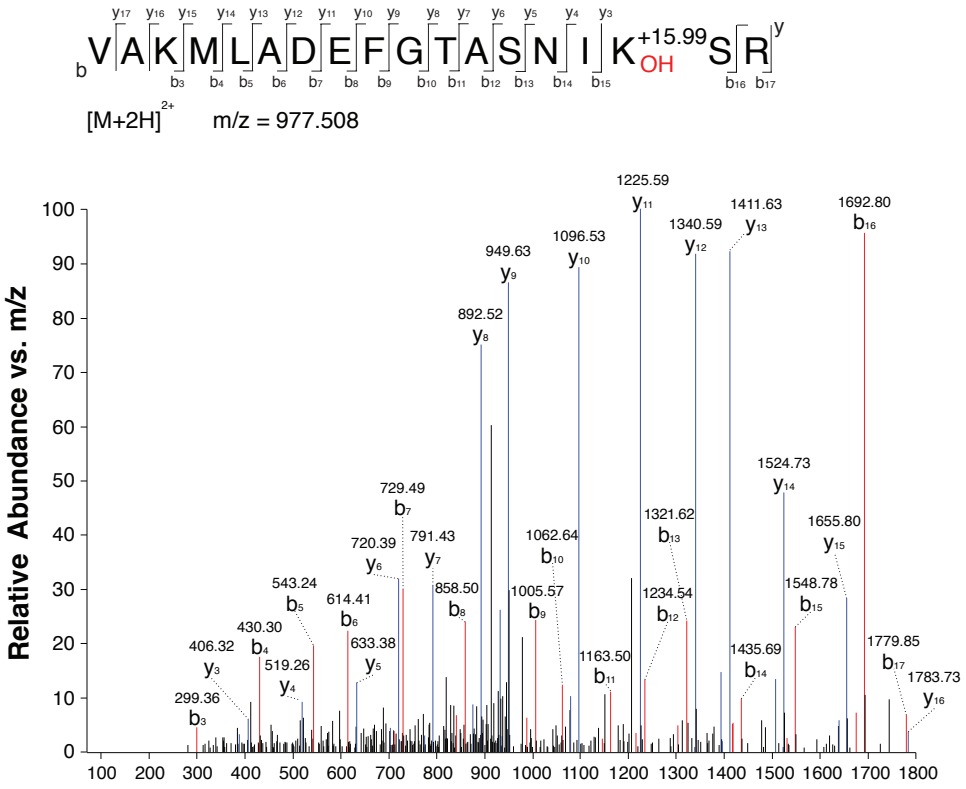


Figure 3.12: MS/MS sequencing of endogenous eRF1 digested with Arg-C. To confirm MS/MS assignment of eRF1 trypsinolysis, endogenous eRF1 was immunopurifed and digested with Arg-C for MS/MS sequencing. Figure shows MS/MS spectrum of a hydroxylated eRF1 K63-containing Arg-C peptide$_{48\text{-}65}$, which assigned position of the hydroxylation to K63. MS/MS annotation by Dr. Roman Fischer.

lation site to K63 (Figure 3.12). Together, these data indicate that endogenous eRF1 is hydroxylated at K63, which corroborate the overexpression and *in vitro* results described previously.

3.2.5 Hydroxylation of eRF1 is ubiquitious and conserved

To characterise the hydroxylation of eRF1 across tissue culture cell lines, endogenous eRF1 was immunopurified from A549, HeLa and U2OS cells for tryptic digest and LC-MS/MS analysis. Similar to HEK293T cells, levels of eRF1 K63 hydroxylation in A549, HeLa and U2OS cells were estimated to be near complete based on LC-MS quantitation (Figure 3.13).

Though eRF1 K63 hydroxylation exists in tissue culture cell lines, less is known about its prevalence in more physiologically relevant settings. To this end, we investigated the tissue distribution of eRF1 K63 hydroxylation. Mice tissues were harvested, pulverised in liquid nitrogen, and suspended in lysis buffer for endogenous eRF1 purification using standard procedures. The immunopurified complex was resolved using SDS-PAGE, and the band corresponding to eRF1 was excised for tryptic digest and analysis by LC-MS/MS. LC-MS quantitation revealed that eRF1 was almost completely hydroxylated in all surveyed mouse tissues, including brain, lung, heart, kidney, liver, spleen and testis (Figure 3.14).

The presence of eRF1 hydroxylation in mice prompted us to examine the species conservation of this post-translational modification. Both JMJD4 and K63 in eRF1 are highly conserved in eukaryotes (Figure 3.1). We purified eRF1 from rabbit reticulocyte lysate (Promega) and determined the level of K63 hydroxylation by LC-MS. Consistent with the conservation of JMJD4 (Figure 3.1), K63 hydroxylation of eRF1 was near complete in rabbit reticulocyte lysate (Figure 3.14). Moreover, eRF1 hydroxylation was also conserved in zebrafish (*Danio rerio*; Figure 3.15). Taken together, the results obtained so far have conclusively demonstrated that endogenous eRF1 is hydroxylated at K63, and that the modification is ubiquitous, conserved and highly abundant.

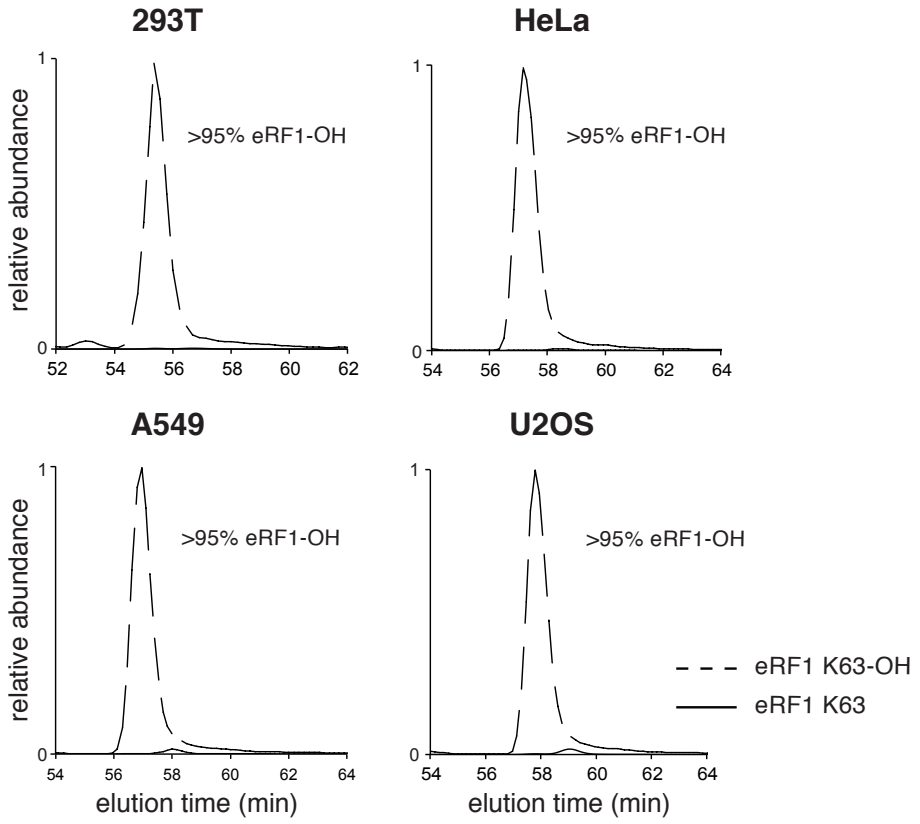


Figure 3.13: eRF1 K63 hydroxylation is widespread in tissue culture cell lines. Endogenous eRF1 was immunopurified from HEK293T, HeLa, A549 and U2OS cells, prior to trypsinolysis and LC-MS/MS analysis. The above figure shows EICs comparing the relative abundance of hydroxylated and unhydroxylated eRF1 K63-containing peptides$_{51\text{-}63}$ from each cell line. Relative quantitation using elution peak intensities showed that endogenous eRF1 was more than 95% hydroxylated in all four cell lines.

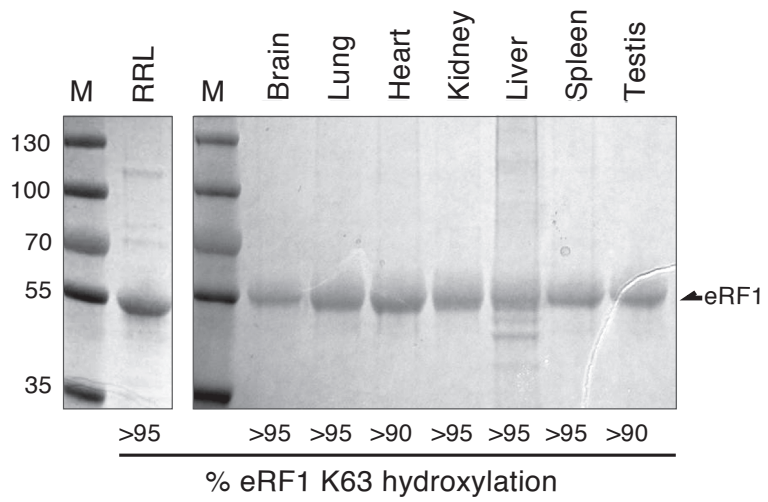
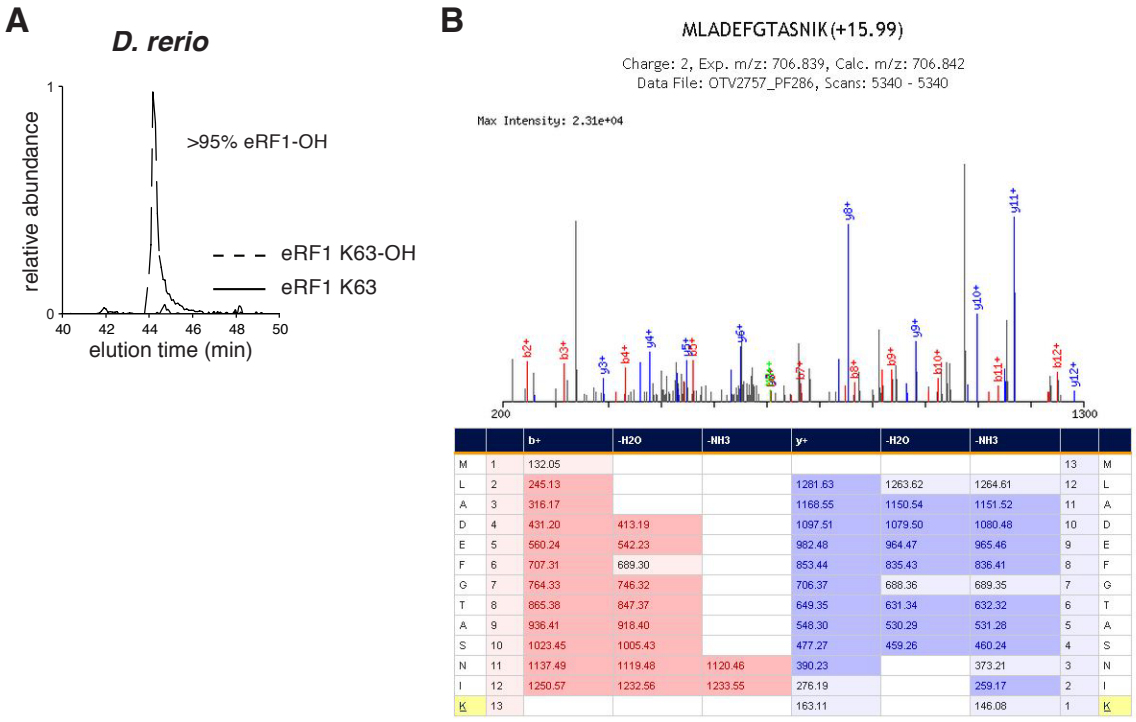


Figure 3.14: eRF1 K63 hydroxylation is ubiquitious and conserved. Endogenous eRF1 was immunopurified from mouse tissues and rabbit reticulocyte lysate for trypsinolysis and MS/MS sequencing. The protein gel shows SDS-PAGE resolution of purified eRF1, which was visualised using Coomassie blue. LC-MS quantitation revealed that eRF1 hydroxylation was near complete in all mouse tissues tested, including brain, lung, heart, kidney, liver, spleen and testis. eRF1 hydroxylation was also present in rabbit reticulocyte lysate, indicating conservation of JMJD4 activity.



		b+	-H2O	-NH3	y+	-H2O	-NH3		
M	1	132.05						13	M
L	2	245.13			1281.63	1263.62	1264.61	12	L
A	3	316.17			1168.55	1150.54	1151.52	11	A
D	4	431.20	413.19		1097.51	1079.50	1080.48	10	D
E	5	560.24	542.23		982.48	964.47	965.46	9	E
F	6	707.31	689.30		853.44	835.43	836.41	8	F
G	7	764.33	746.32		706.37	688.36	689.35	7	G
T	8	865.38	847.37		649.35	631.34	632.32	6	T
A	9	936.41	918.40		548.30	530.29	531.28	5	A
S	10	1023.45	1005.43		477.27	459.26	460.24	4	S
N	11	1137.49	1119.48	1120.46	390.23		373.21	3	N
I	12	1250.57	1232.56	1233.55	276.19		259.17	2	I
K	13				163.11		146.08	1	K

Figure 3.15: eRF1 K63 hydroxylation is conserved in zebrafish. Endogenous eRF1 was immunopurified from zebrafish and digested with trypsin for LC-MS/MS analysis. **A)** EICs of hydroxylated and unhydroxylated eRF1 K63 peptides$_{41\text{-}63}$. Identities of the eluted peaks were confirmed using MS/MS sequencing. Relative LC-MS quantitation showed that eRF1 is almost fully hydroxylated at K63. **B)** Representative MS/MS spectrum of the hydroxylated eRF1 peptide, which assigned the position of hydroxylation to K63.

3.2.6 Endogenous eRF1 hydroxylation requires JMJD4 enzyme activity

Evidence from *in vitro* and overexpression studies indicate that JMJD4 post-translationally hydroxylates eRF1 (Figures 3.4 and 3.5). In order to test if endogenous eRF1 K63 hydroxylation depends on JMJD4 enzyme activity, A549 and HeLa cells were transfected with siRNA duplex against either JMJD4 or a non-targeting control sequence. At 24 hours after the last siRNA transfection, normal culture medium was replaced with SILAC medium to label newly synthesised eRF1 with a heavy isotope variant of lysine . After 24 hours of incubation in SILAC medium, cells were harvested for eRF1 immunopurification and trypsinolysis following standard procedures. Concurrent with LC-MS/MS analysis of eRF1, the effectiveness of siRNA treatment was validated by immunoblotting for JMJD4. LC-MS quantitation revealed that the suppression of endogenous JMJD4 reduced K63 hydroxylation of SILAC-labelled eRF1 to approximately 11% and less than 10% in A549 and HeLa cells, respectively (Figures 3.16 and 3.17). Therefore, we conclude that the expression of JMJD4 is necessary for K63 hydroxylation of eRF1.

To determine whether the observed reduction in eRF1 hydroxylation was due to loss of JMJD4 catalytic activity, A549 and HeLa cells were made to stably express plasmids containing HA-tagged WT or enzyme-dead H189A JMJD4. These JMJD4 mRNAs were made resistant to RNA interference by introducing four silent mutations in consecutive codons within the siRNA targeting sequence. As shown by immunoblots in Figures 3.16A and 3.17A, transfection of anti-JMJD4 siRNA diminished the expression of endogenous JMJD4, but not ectopic siRNA-resistant JMJD4. Upon knockdown of endogenous JMJD4, expression of WT HA-JMJD4 restored eRF1 K63 hydroxylation to approximately 50% and 90% in A549 and HeLa cells, respectively (Figures 3.16B and 3.17B). Critically, the expression of enzyme-dead HA-JMJD4 did not appreciably restore eRF1 K63 hydroxylation in either cell line (Figures 3.16B and 3.17B). It is unclear why JMJD4 reconstitution resulted in such different levels of eRF1 hydroxylation

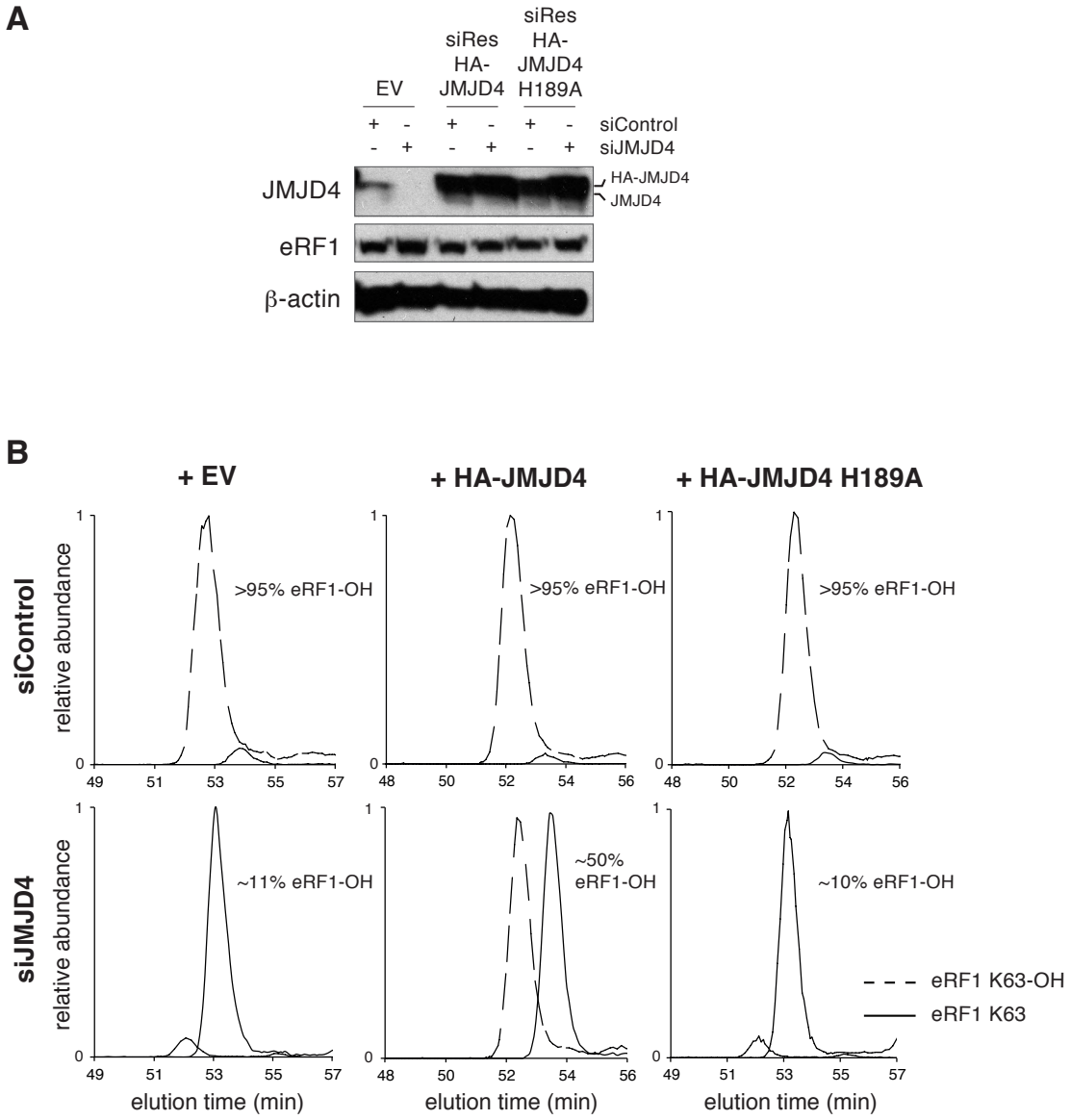


Figure 3.16: Hydroxylation of endogenous eRF1 is dependent on JMJD4 activity in A549 cells. A549 cells were made to stably express siRNA-resistant WT or H189A HA-JMJD4, following which they were transfected with siRNA to suppress the endogenous enzyme. After siRNA transfection, normal cell culture medium was replaced with SILAC medium containing a heavy isope of lysine to measure the hydroxylation of newly synthesised eRF1. At 48 hours post-transfection, eRF1 was immunopurified for LC-MS/MS analysis. **A)** Immunoblots showing the reduction of JMJD4 protein following siRNA treatment, and the expression of ectopic siRNA-resistant JMJD4. **B)** EICs of pulse labeled hydroxylated and unhydroxylated eRF1 tryptic peptides$_{51\text{-}63}$ ($[M+H]^{2+}$; K63-H m/z 701.852; K63-OH m/z 709.850). Note that the peptide masses were shifted +3 m/z due to the presence of heavy lysine (K+6). LC-MS quantitation showed that K63 hydroxylation was significantly reduced upon endogenous JMJD4 suppression (11%), and was restored by the expression of siRNA-resistant WT (50% hydroxylation), but not H179A (10% hydroxylation) JMJD4.

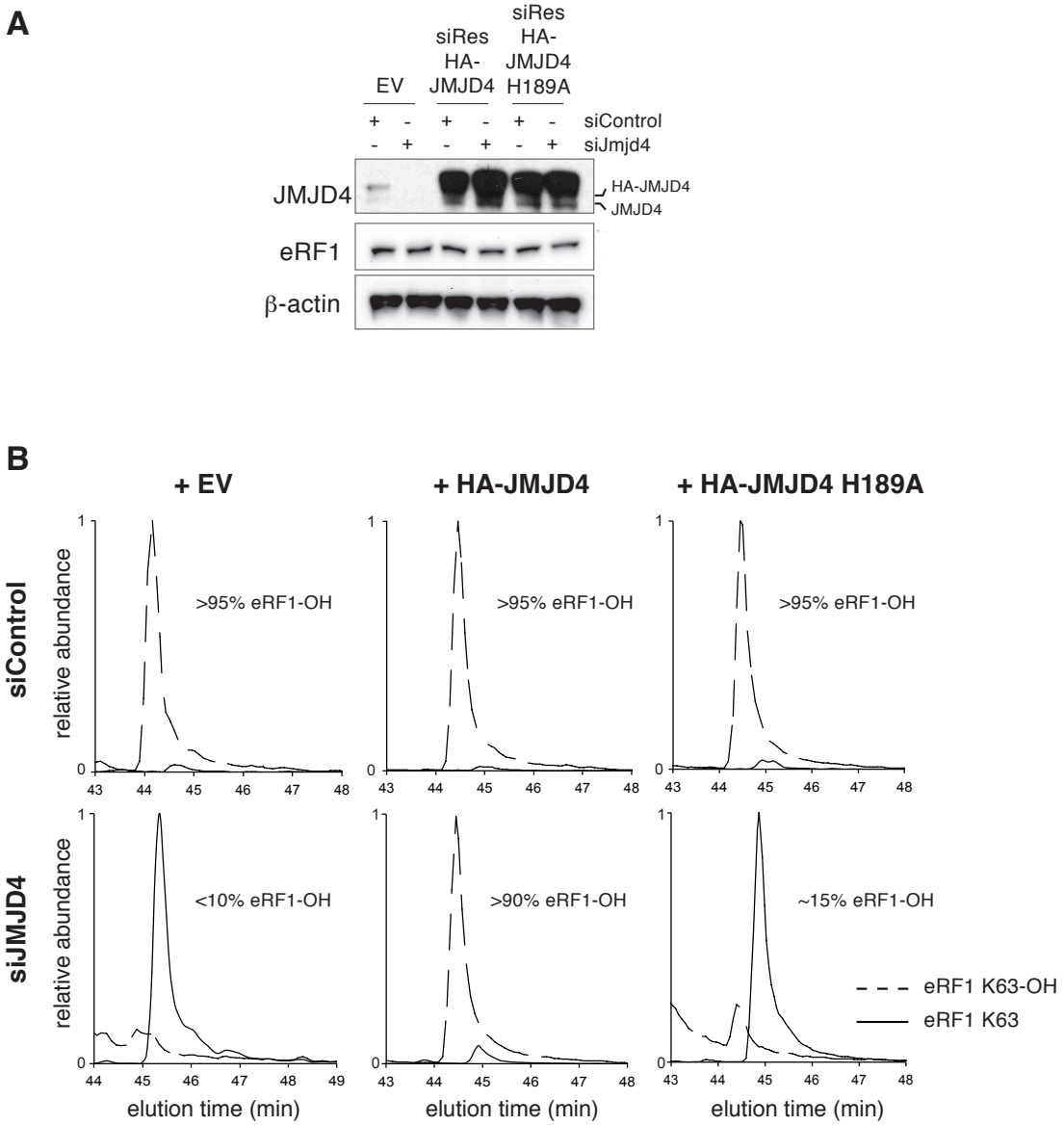


Figure 3.17: Hydroxylation of endogenous eRF1 is dependent on JMJD4 activity in HeLa cells. HeLa cells stably expressing siRNA resistant (siRes) WT or H189A HA-JMJD4 were transfected with siRNA against either endogenous JMJD4 or a control sequence. The cells were cultured in SILAC medium post-siRNA transfection to pulse label newly synthesised eRF1 with a heavy isotope variant of lysine. At 48 hours after the last siRNA transfection, endogenous eRF1 was purified for tryptic digest and LC-MS/MS analysis. **A)** Immunoblots showing suppression of endogenous JMJD4, and ectopic expression of WT and H189A siRNA-resistant JMJD4. **B)** EICs showing the elution profiles of hydroxylated and unhydroxylated SILAC-labelled eRF1 K63 peptides$_{51\text{-}63}$. Relative quantitation of EICs revealed that knockdown of endogenous JMJD4 reduced eRF1 hydroxylation to $<$10%, which was restored by ectopic WT ($>$90% hydroxylation) but not enzyme-dead (15% hydroxylation) siRNA-resistant JMJD4.

in the two cell lines, but perhaps it could be attributed to variations in the percentage of cells achieving stable JMJD4 expression, or the greater level of JMJD4 re-expression in HeLa cells (Figures 3.16A and 3.17A). Nonetheless, our data suggest that endogenous eRF1 K63 hydroxylation is dependent on JMJD4 enzyme activity, which further supports the hypothesis that JMJD4 hydroxylates eRF1 at K63 endogenously.

3.2.7 JMJD4 activity is dependent on oxygen and 2OG

Earlier results established that eRF1 K63 hydroxylation occurs endogenously and is dependent on JMJD4 catalytic activity. In all the cell lines and tissues assayed thus far, the modification was near complete. However, physiological or pathological conditions may exist under which eRF1 hydroxylation is suppressed. Hypoxia is known to inhibit 2OG oxygenases due to their requirement of oxygen as a necessary co-substrate. One such example is the HIF hydroxylases, which catalyse protein hydroxylation in an oxygen-dependent manner (see Chapter 1). To assess the oxygen dependence of JMJD4 activity, HeLa cells were cultured in hypoxia chambers set at 1%, 0.1% and 0% (anoxia) oxygen. During the course of hypoxia treatment, these cells were grown in SILAC medium, which pulse labelled newly synthesised eRF1 using an heavy isotope variant of lysine. After 24 hours of incubation, HeLa cells were harvested from the hypoxia chambers, and eRF1 was immunopurified and trypsinised for analysis by LC-MS/MS. Concurrent to MS sample preparation, efficacy of the hypoxia and anoxia treatments was validated by immunoblotting for HIF1α stabilisation (Figure 3.18A). LC-MS quantitation revealed that 1% and 0.2% oxygen reduced eRF1 K63 hydroxylation in HeLa cells to approximately 90% and 50%, respectively (Figure 3.18B). Furthermore, eRF1 hydroxylation was completely inhibited in the absence (0%) of oxygen (Figure 3.18B).

In addition to hypoxia, HeLa cells were treated with dimethyloxalylglycine (DMOG), a generic inhibitor of 2OG oxygenases (Mole et al., 2003). DMOG is a cell-permeable precursor of NOG, which is a competitive and non-reactive analogue of 2OG. *In vitro*

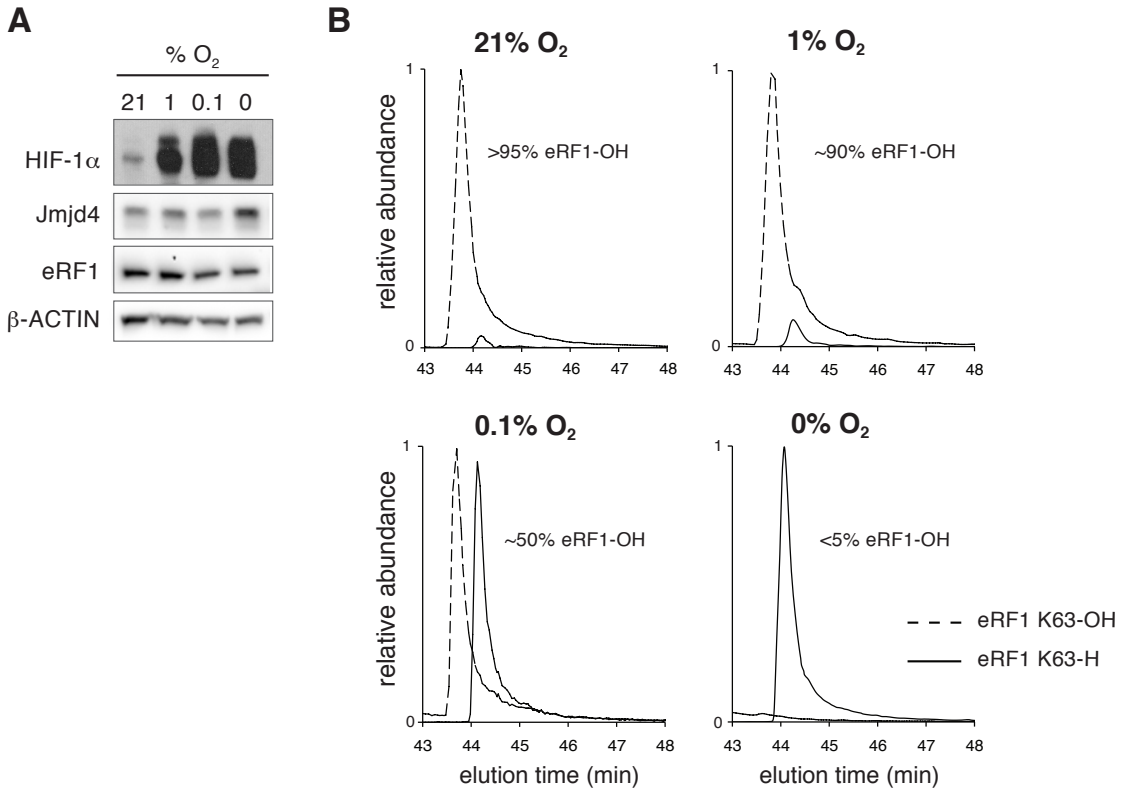


Figure 3.18: eRF1 hydroxylation in HeLa cells is dependent on oxygen. HeLa cells were incubated under conditions of atmospheric, 1%, 0.1% or 0% oxygen in the presence of SILAC medium containing heavy lysine. After 24 hours of incubation, the cells were harvested for endogenous eRF1 purification, trypsinolysis and LC-MS/MS analysis. **A)** Immunoblots show the stabilisation of HIF1α under hypoxia and anoxia conditions, thus confirming efficacy of the respective treatments. An increase in JMJD4 expression was observed under anoxia. **B)** EICs of hydroxylated and unhydroxylated SILAC-labelled eRF1 peptides$_{51\text{-}63}$. Relative quantitaion using LC-MS elution peaks revealed that eRF1 hydroxylation was approximately 90% and 50% in 1% and 0.1% oxygen, respectively, whereas the complete lack of oxygen ablated eRF1 hydroxylation.

data have shown that JMJD4 hydroxylase activity is inhibited by the presence of NOG (Figure 3.9). To test the 2OG dependence of JMJD4 activity in an endogenous setting, HeLa cells were treated with 1mM DMOG for 24 hours. eRF1 synthesised in the presence of DMOG were pulse labelled by culturing cells in SILAC medium containing heavy lysine. Concurrent to LC-MS/MS analysis, whole cell lysates were immunoblotted for the induction of HIF1α to validate efficacy of the DMOG treatment (Figure 3.19A). Addition of the competitive 2OG analogue reduced eRF1 hydroxylation from near complete to approximately 45% in HeLa cells, indicating that JMJD4 activity is dependent on 2OG (Figure 3.19B).

Next, we tested whether the effect of hypoxia and DMOG on JMJD4 activity is observed in other cell lines. U2OS and Hep3B cells were cultured under 1%, 0.1% and 0% oxygen in heavy lysine-containing SILAC medium, following which eRF1 was purified for tryptic digest and LC-MS/MS analysis. In U2OS cells, eRF1 hydroxylation was reduced to approximately 88% and 20% under 1% and 0.1% oxygen, respectively (Figure 3.20). eRF1 hydroxylation in Hep3B cells were similarly decreased to approximately 70% and 9% under 1% and 0.2% oxygen, respectively (Figure 3.21). Additionally, the absence of oxygen completely inhibited eRF1 hydroxylation in both cell lines (Figures 3.20 and 3.21). Parallel experiments showed that DMOG treatment suppressed eRF1 hydroxylation to approximately 27% and 50% in U2OS and Hep3B cells, respectively (Figures 3.20 and 3.21). Taken together, the results suggest that eRF1 hydroxylation is dependent on the presence of oxygen and 2OG. This is consistent with our assumption that JMJD4 is a 2OG- and Fe(II)-dependent oxygenase. Furthermore, despite cell line variations in their responses to hypoxia, significant reduction in eRF1 K63 hydroxylation was only observed under extremely severe hypoxia (0.1% O_2). Therefore, JMJD4 catalytic activity is relatively insensitive to changes in oxygen tension.

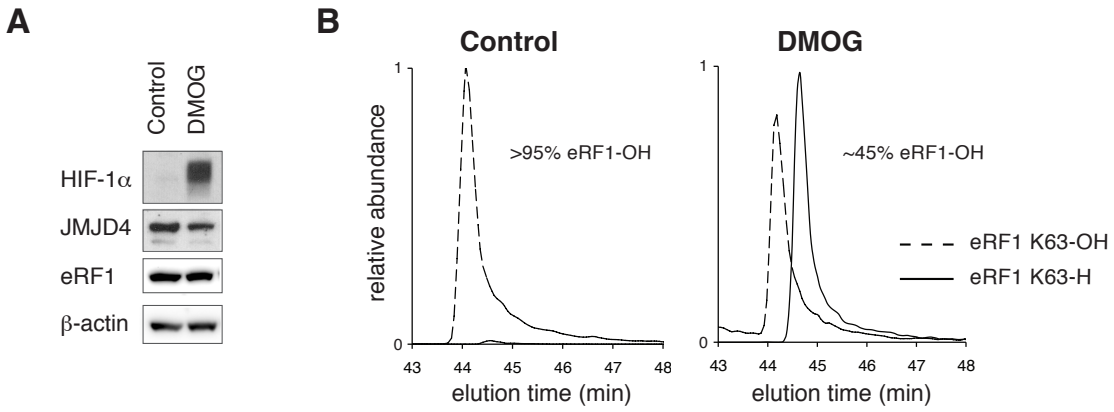


Figure 3.19: eRF1 hydroxylation in HeLa cells is dependent on 2OG. HeLa cells in heavy lysine-containing SILAC medium were treated with DMOG for 24 hours, after which endogenous eRF1 was purified for trypsinolysis and LC-MS/MS analysis. **A)** Immunoblots show stabilisation of HIF1α by DMOG, confirming effectiveness of the inhibitor. **B)** EICs of hydroxylated and unhydroxylated SILAC labelled eRF1 peptides$_{51\text{-}63}$. LC-MS quantitation revealed that DMOG reduced eRF1 hydroxylation from near complete to approximately 45%.

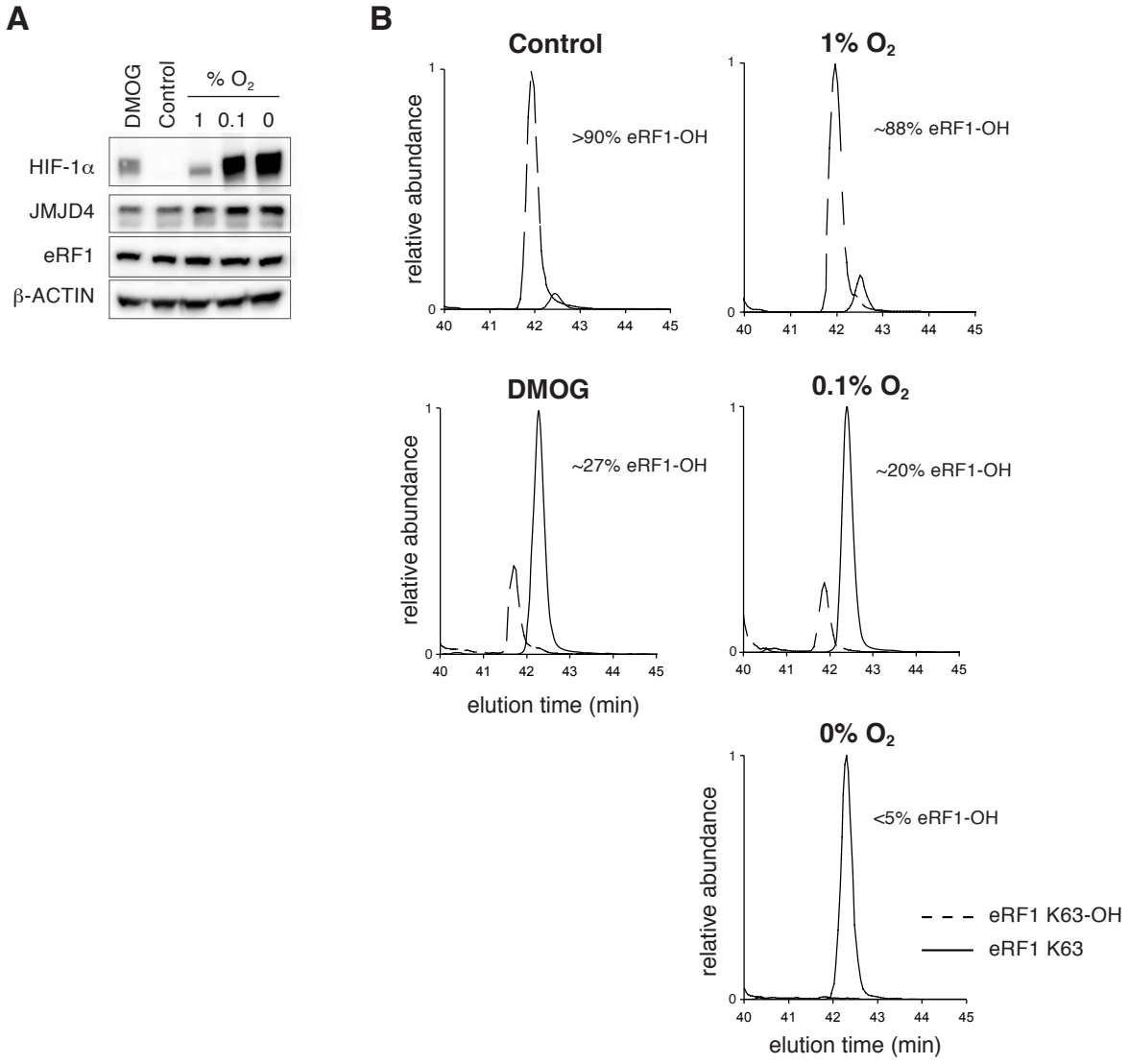


Figure 3.20: Hydroxylation of eRF1 in U2OS cells is dependent on oxygen and 2OG. U2OS cells were incubated in atmospheric, 1%, 0.1% and 0% oxygen or DMOG, in SILAC medium containing a heavy isotope variant of lysine. After 24 hours of treatment, the cells were harvested for eRF1 purification, tryptic digest and LC-MS/MS analysis. **A)** Immunoblots show induction of HIF1α under conditions of hypoxia, anoxia and DMOG treatment. Interestingly, an increase in JMJD4 protein expression was observed in hypoxia and anoxia conditions. **B)** EICs of hydroxylated and unhydroxylated pulse labelled eRF1 peptides$_{51\text{-}63}$. Relative LC-MS quantitation demonstrated that eRF1 hydroxylation was inhibited by hypoxia (1% O_2: 88%; 0.1% O_2: 20%), anoxia (<5%) and DMOG (27%).

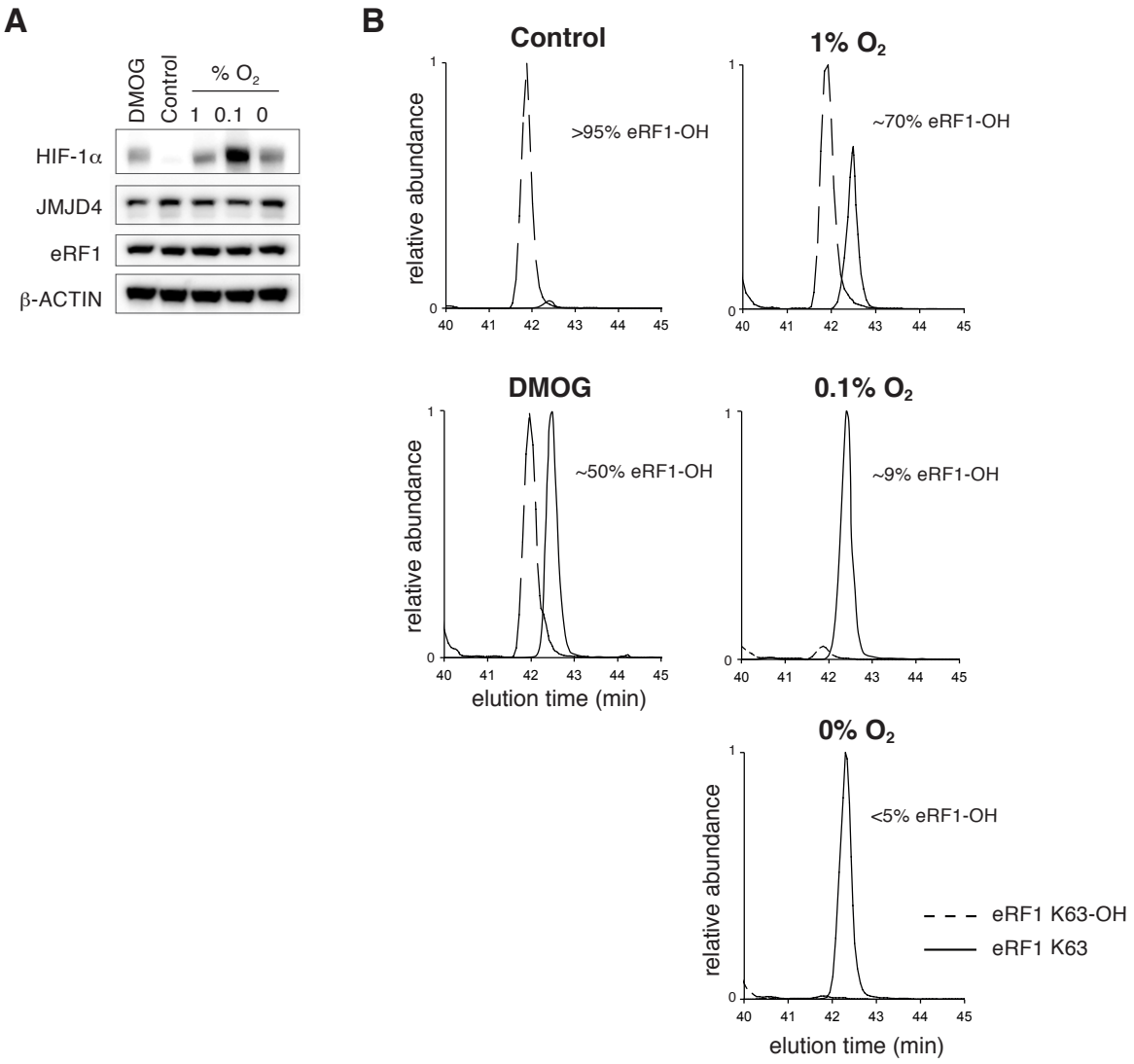


Figure 3.21: Hydroxylation of eRF1 in Hep3B cells is dependent on oxygen and 2OG. Hep3B cells were incubated in atmospheric, 1%, 0.1% and 0% oxygen, or treated with DMOG for 24 hours. For the duration of the treatment, the cells were cultured in SILAC medium containing heavy lysine to pulse label newly synthesised eRF1. eRF1 was purified for trypsinolysis and LC-MS/MS analysis. **A)** Immunoblots show induction of HIF1α under oxygen deficient conditions and DMOG treatment. **B)** EICs of modified and unmodified SILAC labelled eRF1 peptides$_{51\text{-}63}$. LC-MS quantitation showed that eRF1 hydroxylation was reduced to approximately 70% and 9% under 1% and 0.1% oxygen, respectively. eRF1 hydroxylation was abrogated under anoxia, whereas DMOG reduced eRF1 hydroxylation to approximately 50%.

3.2.8 eRF1 hydroxylation is not affected by fumarate accumulation

Other than NOG, non-2OG tricarboxylic (TCA) cycle intermediates may also act as a competitive inhibitors of 2OG oxygenases. In particular, fumarate and succinate are able to compete with 2OG for enzyme binding (Hewitson et al., 2007). Loss-of-function of TCA cycle enzymes fumarate hydratase (FH) or succinate dehydrogenase (SDH) is associated with cellular accumulation of fumarate or succinate, respectively. Such conditions have been reported to inhibit the activities of several 2OG oxygenases, including PHDs, histone demethylases and TET enzymes (Hewitson et al., 2007; Xiao et al., 2012).

Inactivating mutations of FH cause hereditary leiomyomatosis and renal cell carcinoma (HLRCC), a hereditary disorder characterised by kidney cancer and multiple leiomyomas. HLRCC is associated with the inactivation of 2OG oxygenases affecting both epigenetics regulation and hypoxia signalling (Kaelin, 2011; Yang et al., 2013). Therefore, we sought to determine the effect of fumarate accumulation on JMJD4-catalysed eRF1 hydroxylation. To this end, endogenous eRF1 was purified from FH WT and KO MEFs, and KO MEFs reconstituted with either full-length or extra-mitochondrial FH (gift from Dr. Patrick Pollard). Extra-mitochondrial FH lacks the mitochondrial targeting sequence (ΔMTS), and therefore rescues FH-deficiency in the cytoplasm but not in the mitochondria (O'Flaherty et al., 2010). FH deficiency in these cell lines have been shown to cause fumarate accumulation and HIF stabilisation in a FH-dependent manner (O'Flaherty et al., 2010). However, changes in FH level did not appear to influence eRF1 K63 hydroxylation (Figure 3.22A). This suggests that fumarate accumulation alone does not inhibit JMJD4-catalysed eRF1 K63 hydroxylation.

Next, we assessed whether FH-deficiency alters eRF1 K63 hydroxylation under conditions of severe hypoxia, where the partial suppression of JMJD4 due to lack of oxygen may sensitise the enzyme to fumarate. FH WT, KO and reconstituted MEFs

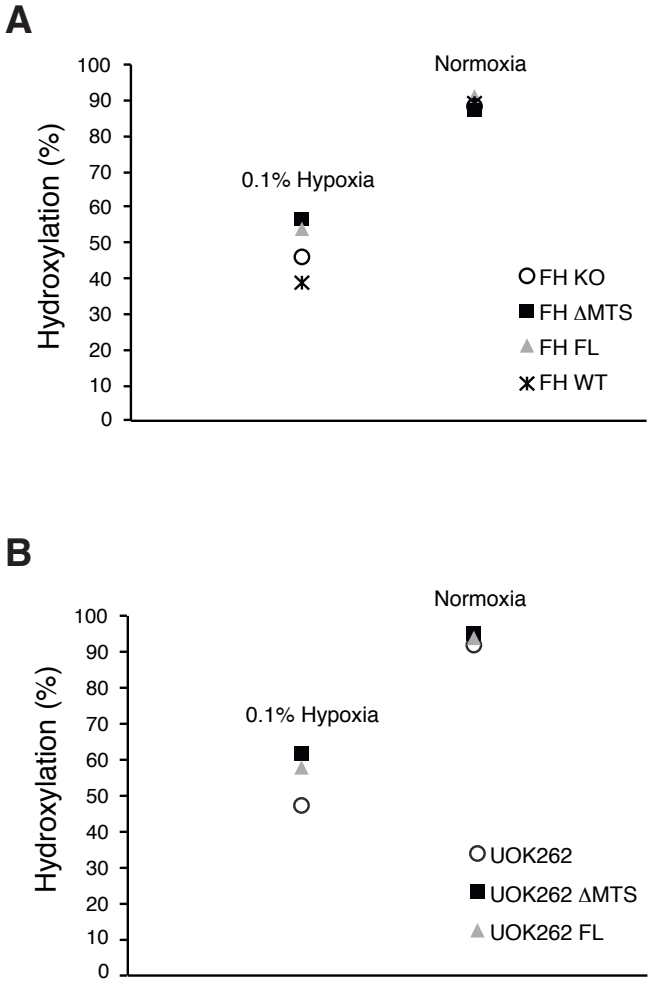


Figure 3.22: K63 hydroxylation of eRF1 is not inhibited by fumarate accumulation. **A)** FH WT, KO, and full-length (FL) and extra-mitochondrial (ΔMTS) FH rescue MEF lines were incubated in normoxia or 0.1% oxygen. During the treatment, the MEFs were cultured in SILAC medium containing heavy lysine. After 24 hours of treatment, endogenous eRF1 was purified and digested with trypsin to measure K63 hydroxylation by LC-MS/MS. Severe hypoxia reduced eRF1 K63 hydroxylation, though the presence or absence of FH did not significantly affect eRF1 hydroxylation levels. **B)** UOK262, a FH-deficient cancer cell line was reconstituted with full-length (FL) or cytoplasmic (ΔMTS) FH. The level of eRF1 K63 hydroxylation was measured in these cells under normoxia and severe hypoxia (0.1% O_2). The FH status of UOK262 cells did not affect eRF1 hydroxylation. Cell lines provided by Dr. Patrick Pollard and Dr. Julie Adam.

were incubated in a hypoxia chamber set at 0.1% oxygen for 24 hours, during which newly synthesised eRF1 were labelled using SILAC medium containing heavy lysine. Endogenous eRF1 was purified and trypsinised for mass spectrometry analysis after the treatment. LC-MS quantitation showed that levels of eRF1 K63 hydroxylation were relatively similar between the four FH MEF lines (Figure 3.22A). FH WT MEFs had the lowest percentage of eRF1 hydroxylation, though it is unclear whether the difference is significant or due to experimental variation. Regardless, our data indicate that FH-deficiency does not affect JMJD4 activity under severe hypoxia (0.1% O_2). Similar experiments were performed using UOK262, a cell line derived from HLRCC-associated kidney cancer (from Dr. Patrick Pollard and Dr. Julie Adam; Yang et al., 2010). eRF1 K63 hydroxylation was comparable in normal and FH-reconstituted UOK262 cells under both normoxia and hypoxia (0.1% O_2) conditions (Figure 3.22B), which supported our results from FH MEF lines.

To determine the effect of fumarate on eRF1 hydroxylation in a more physiologically relevant setting, kidneys were taken from FH WT or KO mice (from Dr. Patrick Pollard and Dr. Julie Adam; Adam et al., 2011) for purification and MS analysis of eRF1. Similar to clinical phenotypes of HLRCC, FH KO mice develop pseudohypoxic renal cysts which create an inhibitory microenvironment for 2OG oxygenases (Pollard et al., 2007). While eRF1 K63 hydroxylation was mildly reduced in FH KO kidney, it remained relatively high at approximately 85% (Figure 3.23). Taken together, our data shows that JMJD4 hydroxylase activity towards eRF1 is highly resistant to inhibition by fumarate accumulation.

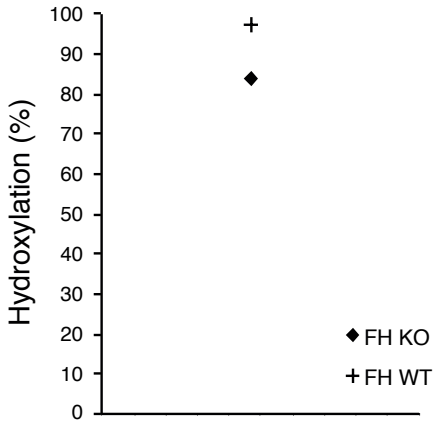


Figure 3.23: eRF1 hydroxylation is mildly reduced in kidney of FH KO mouse. Endogenous eRF1 was purified from kidneys of FH WT and KO mice, following which eRF1 was digested with trypsin for LC-MS quantitation. Minor reduction of eRF1 hydroxylation was observed in the highly cystic and severely hypoxic FH KO kidney. Samples from Dr. Patrick Pollard and Dr. Julie Adam.

3.2.9 eRF1 hydroxylation is saturated in non-Hodgkin lymphoma

Though FH deficiency did not significantly alter eRF1 K63 hydroxylation, we assessed whether eRF1 K63 hydroxylation was altered in solid tumours with severe hypoxia. We reasoned that proliferative and cell signalling dysregulations in cancer, in combination with the hypoxic microenvironment, may alter the activities of 2OG oxygenases such as JMJD4. Endogenous eRF1 was purified from two hypoxic tumour samples from patients with non-Hodgkin lymphoma, and trypsinised for LC-MS/MS analysis. Relative quantitation using LC-MS showed eRF1 was almost completely hydroxylated at K63 in both cases (Figure 3.24). This suggests that JMJD4 hydroxylase activity is not affected by the pathophysiological conditions of these tumours.

3.3 Discussion

Members of the JmJC-only family play diverse roles in pathways ranging from oxygen sensing to mRNA splicing. A subset of JmjC-only proteins remain uncharacterised, even though they feature catalytic domains consistent with that of active 2OG oxygenases. This chapter presents the biochemical characterisation of putative JmjC-only hydroxylase, JMJD4. We have shown that JMJD4 catalyses lysyl hydroxylation of eRF1, the eukaryotic release factor responsible for translational termination (see Chapter 4 introduction). This discovery, in addition to that of the ribosomal hydroxylases, provides further understanding of the JmjC-only oxygenases and highlights their potential as novel regulators of protein synthesis.

The activity-dependent interaction of 2OG oxygenases with their substrates provides a useful method for substrate screening. However, the mutation of a single amino acid is unlikely to ablate the substrate specificity of an enzyme. Iron and 2OG binding to the 2OG oxygenase active site precedes that of the substrate and molecular oxygen (Koehntop et al., 2005; McDonough et al., 2010). It is therefore possible that the lack of

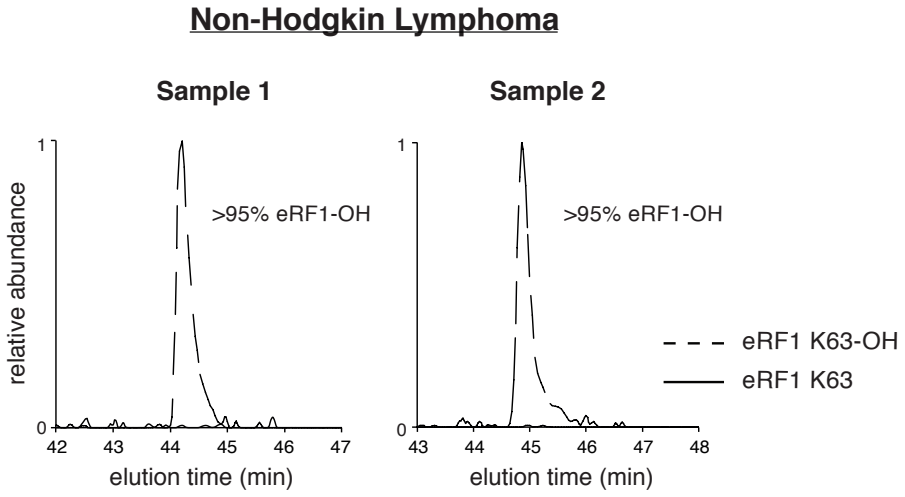


Figure 3.24: eRF1 K63 hydroxylation is not affected by the tumour microenvironment. Endogenous eRF1 was purified from two tumour samples of non-Hodgkin lymphoma for trypsinolysis and LC-MS/MS analysis. EICs of eRF1 peptides$_{51\text{-}63}$ showing that the extent of eRF1 hydroxylation was near complete in hypoxic tumours. Samples from Prof. Adrian Harris (Department of Oncology, University of Oxford).

iron coordination renders the catalytic site inactive and unable to bind to the substrate of interest. This appears to differ between 2OG oxygenases, since catalytcally inactive mutations of certain oxygenases do not affect substrate binding (Schofield group, personal communications). Alternatively, a single point mutation may result in misfolding of the enzyme active site, which could be observed using structural data.

eRF1 was identified as the top candidate substrate in the proteomic search (Figure 3.1). This was supported by our finding that overexpressed eRF1 was hydroxylated at K63 in the presence of overexpressed JMJD4 (Figure 3.4). Moreover, *in vitro* and knockdown studies have shown that JMJD4 specifically hydroxylates eRF1 at K63 in an enzyme- and cofactor-dependent manner (Figures 3.5, 3.9, 3.16 and 3.17). Although the existence of additional hydroxylation targets remains a formal possibility, eRF1 is likely the only substrate of JMJD4 given the lack of other high affinity, activity-dependent interactors. This interestingly contrasts with the biochemical promiscuity of FIH, despite their close evolutionary relationship.

The specificity of JMJD4 activity to lysine is supported by its sequence homology to lysyl hydroxylase JMJD6. Both JMJD6 and collagen lysyl hydroxylases catalyse lysyl hydroxylation at carbon 5 (C5; Webby et al., 2009). The position of eRF1 K63 hydroxylation was determined using amino acid analysis of eRF1 K63 peptides hydroxylated *in vitro* by incubation with recombinant JMJD4 (Feng et al., 2014). Comparison of hydroxylated eRF1 K63 to C3, C4 and C5 hydroxylysine standards revealed that JMJD4-catalysed hydroxylation takes place at C4 rather than C5 (Feng et al., 2014). Arginine has C4 but not C5, which may partly explain the non-specific hydroxylation of K63R by JMJD4. To the best of our knowledge, this is the first known example of C4 lysyl hydroxylation, which further expands existing 2OG oxygenase biochemistry.

The hydroxylation of eRF1 occurs endogenously and is physiologically relevant. eRF1 K63 hydroxylation was found in all cell lines and tissues assayed (Figures 3.13 and 3.14). This indicates that JMJD4 is widely expressed, and that perhaps its activity is needed for normal cellular function. In addition, the level of eRF1 hydroxylation is saturated across all normal physiological contexts, which may argue for a housekeeping

rather than a signalling function. As such, we propose that K63 hydroxylation plays a fundamental role in eRF1 structure or release factor activity. Experiments evaluating the effect of K63 hydroxylation on translational termination will be discussed in detail in chapter 4.

Mass spectrometry characterisation of eRF1 purified from mouse, rabbit and zebrafish samples demonstrated that K63 hydroxylation is evolutionarily conserved (Figures 3.14 and 3.15). These results are in agreement with phylogenetic analyses showing that JMJD4 is conserved in most eukaryotic species (Figure 3.1). The lack of JMJD4 conservation in prokaryotes may be explained by the presence of alternative release factors unrelated to eRF1. In prokaryotes, two class I release factors, RF1 and RF2, are responsible for stop codon recognition (Capecchi, 1967; Scolnick et al., 1968). A third release factor, RF3, is a GTPase that functions similarly to eRF3 (Freistroffer et al., 1997). Though they may share a common ancestry, the prokaryotic release factors bear no sequence or structural similarities to eRF1 (Ito et al., 1996; Vestergaard et al., 2001). Intriguingly, phylogenetic analyses found that JMJD4 is not conserved *S. cerevisiae* (Figure 3.1), though additional biochemical characterisations are required to determine whether eRF1 hydroxylation is present or absent in this particular species.

Despite its requirement for oxygen as a cosubstrate, JMJD4 activity is relatively resistant to inhibition by hypoxia, similar to the related 2OG oxygenase FIH (Tian et al., 2011). K63 hydroxylation in SILAC-labelled eRF1 remained relatively high (70-90%) under 1% oxygen, and was only significantly reduced under severe hypoxia ($>$0.1% O_2). Intriguingly, JMJD4 protein expression was induced under low oxygen conditions in U2OS cells, and in HeLa cells under anoxia (Figures 3.18 and 3.20). This suggests that perhaps the increased JMJD4 expression, and therefore total activity, helps to maintain eRF1 hydroxylation under conditions of hypoxia. Taken together, our results imply that JMJD4 is unlikely to act as an oxygen sensor.

In addition to hypoxia, TCA cycle intermediates such as fumarate and succinate are able to competitively inhibit 2OG oxygenase activity (Hewitson et al., 2007). Under pathological conditions of FH inactivation, inhibition of HIF prolyl hydroxylases by

fumarate results in activation of the hypoxia signalling response (Isaacs et al., 2005; Pollard et al., 2005, 2007). Epigenetic regulation of gene expression is similarly altered due to the suppression of histone demethylase and TET enzyme activities (Xiao et al., 2012). Even though fumarate inhibits a broad number of 2OG oxygenases, JMJD4 activity was unaffected by fumarate accumulation even under severe hypoxia (<0.1%; Figures 3.22 and 3.23). Our findings on JMJD4 are consistent with that of FIH. *In vitro* assays found that TCA cycle intermediates are very weak inhibitors of FIH, possibly due to structural variations in the 2OG binding pocket (Hewitson et al., 2007; Koivunen et al., 2007). The comparable results between JMJD4 and FIH may not be entirely surprising given their evolutionary proximity.

In contrast to FH and SDH, the gain-of-function of isocitrate dehydrogenase (IDH) is frequently associated with cancer (Yan et al., 2009; Abbas et al., 2010; Paschka et al., 2010). Mutant IDH gains the ability to reduce 2OG into 2-hydroxyglutarate (2HG), an oncometabolite that affects the catalytic activities of 2OG oxygenases (Dang et al., 2009; Xu et al., 2011). Cellular accumulation of 2HG results in the hypermethylation of histones and DNA due to the competitive inhibition of histone demethylases and TET enzymes (Xu et al., 2011; Turcan et al., 2012). On the other hand, the effect of 2HG on PHDs appears to be stereoisomer-specific. The R-enantiomer of 2HG which is produced by the mutant IDH stimulates PHD activity, whereas the S-enantiomer is inhibitory (Koivunen et al., 2012; Losman et al., 2013). It would be of interest to determine the effect of 2HG accumulation on JMJD4 catalytic activity, though our attempts to assay eRF1 K63 hydroxylation in IDH mutant cancer samples were unsuccessful due to sample limitations and technical issues.

Taken together, we have shown that JMJD4 hydroxylates eRF1 at K63, and the modification is widespread and physiologically relevant. However, it is not affected by moderate hypoxia (>1% O_2) or FH inactivation. Moreover, hydroxylation of eRF1 maintained saturating levels in hypoxic tumour samples (Figure 3.24), indicating that pathophysiological conditions in at least a subset of cancers do not inhibit JMJD4 activity. This is consistent with the prevalence and abundance of eRF1 K63 hydroxy-

lation in cancer cell lines and normal tissues, and suggests that K63 hydroxylation may play a general housekeeping role in eRF1 structure or function. However, it is possible that JMJD4 is regulated by an alternative physiological signal. Iron deficiency, oxidative stress and other stressors are known to inhibit 2OG oxygenase activity, and could potentially regulate JMJD4-catalysed eRF1 hydroxylation. Future efforts should concentrate on additional characterisations of JMJD4 biochemistry, and more importantly understanding the role of eRF1 K63 hydroxylation in translational termination.

Chapter 4

Role of eRF1 hydroxylation in translational termination

4.1 Introduction

In the previous chapter, the 2OG oxygenase JMJD4 was demonstrated to catalyse lysyl hydroxylation of the eukaryotic release factor eRF1. eRF1, together with the GTPase eRF3, mediates peptidyl-tRNA bond hydrolysis in translational termination (Kisselev and Buckingham, 2000). When a stop codon translocates into the ribosomal aminoacyl(A-) site, it is recognised by eRF1 which binds to the A-site in place of tRNA (Frolova et al., 1994). eRF1 forms a complex with eRF3 and stimulates hydrolysis of the ester bond linking the polypeptide chain to the P-site tRNA, thereby triggering release of the newly synthesised polypeptide (Frolova et al., 1994; Stansfield et al., 1995; Zhouravleva et al., 1995). GTP hydrolysis by eRF3 facilitates eRF1 catalysis and subsequent dissociation from the ribosome (Zhouravleva et al., 1995; Frolova et al., 1996; Eyler et al., 2013).

The structure of eRF1 mimics that of a tRNA, forming a 'Y' shape with three distinctive domains (Song et al., 2000). The M domain (domain-2) features a universally conserved GGQ motif and is required for peptidyl-tRNA bond hydrolysis, while the C domain (domain-3) binds to eRF3 (Frolova et al., 1999; Eurwilaichitr et al., 1999;

Song et al., 2000). The N domain (domain-1) corresponds to the anticodon loop of tRNA and is responsible for stop codon recognition (Song et al., 2000; Bertram et al., 2000). Mutagenesis studies revealed that two conserved motifs in the N domain, NIKS and YCF (YXCXXXF), are important for eRF1 release factor activity (Frolova et al., 2002; Seit-Nebi et al., 2002; Kolosov et al., 2005). The NIKS motif is highly conserved; it forms a loop located at an apex between two α helices (Figure 4.1; Song et al., 2000; Frolova et al., 2002). While the exact role of the NIKS motif in stop codon recognition is under debate, cryo-electron microscopy of the ribosome pretermination complex placed the NIKS motif in proximity to the stop codon (Preis et al., 2014). In addition, a photocrosslinking study demonstrated that NIKS contacts the invariant uridine, with lysine acting as the main crosslinking site (Chavatte et al., 2002).

Importantly, the universally conserved lysine in NIKS motif is K63, the residue hydroxylated by JMJD4. Therefore, we postulate that K63 hydroxylation optimises eRF1 stop codon recognition. We hypothesised that under normal conditions, JMJD4 catalyses hydroxylation of eRF1 at K63 and promotes efficient translational termination. However, upon inhibition of JMJD4 expression or catalytic activity, the lack of eRF1 K63 hydroxylation would result in partial readthrough at the stop codon and leaky translational termination (Figure 4.2).

The work in this chapter describes investigations into the role of JMJD4-catalysed K63 hydroxylation in eRF1 function. A bicistronic reporter system was used to determine the effect of JMJD4 knockdown on translational termination efficiency. In addition, the release factor activities of K63 hydroxylated and unhydroxylated eRF1 were compared using an *in vitro* reconstituted translation system. Finally, we studied the effect of JMJD4 suppression across multiple stop codon sequence contexts, and began to characterise the biological consequences of JMJD4 inhibition.

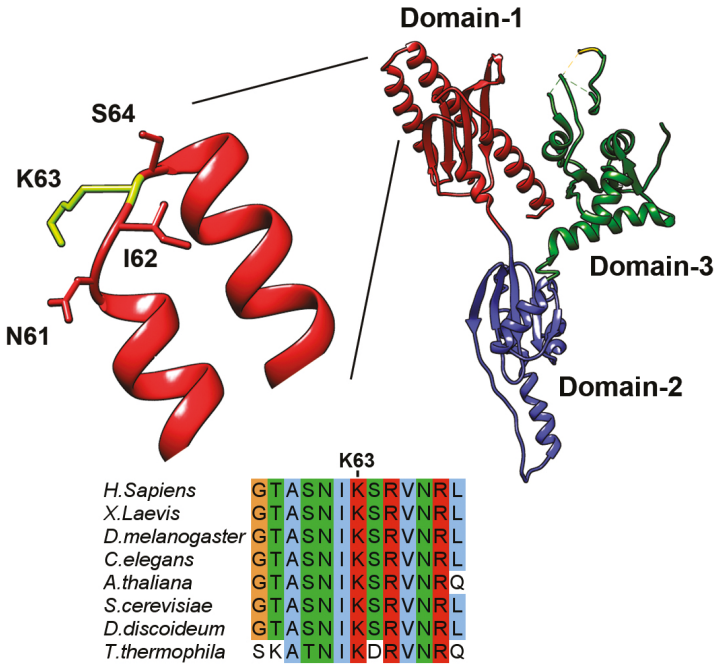


Figure 4.1: Structure and conservation of eRF1 NIKS motif. The structure of eRF1 resembles that of a tRNA (Song et al., 2000). It consists of three domains, of which domain-1 (N-domain) is responsible for stop codon decoding. Stop codon recognition is partially mediated by the NIKS motif located at the extremity of domain-1 between two α helices (top panel; Song et al., 2000; Frolova et al., 2002). The NIKS motif is universally conserved, as shown by sequence alignment across multiple eukaryotic species (bottom panel). Figure adapted from Feng et al. (2014).

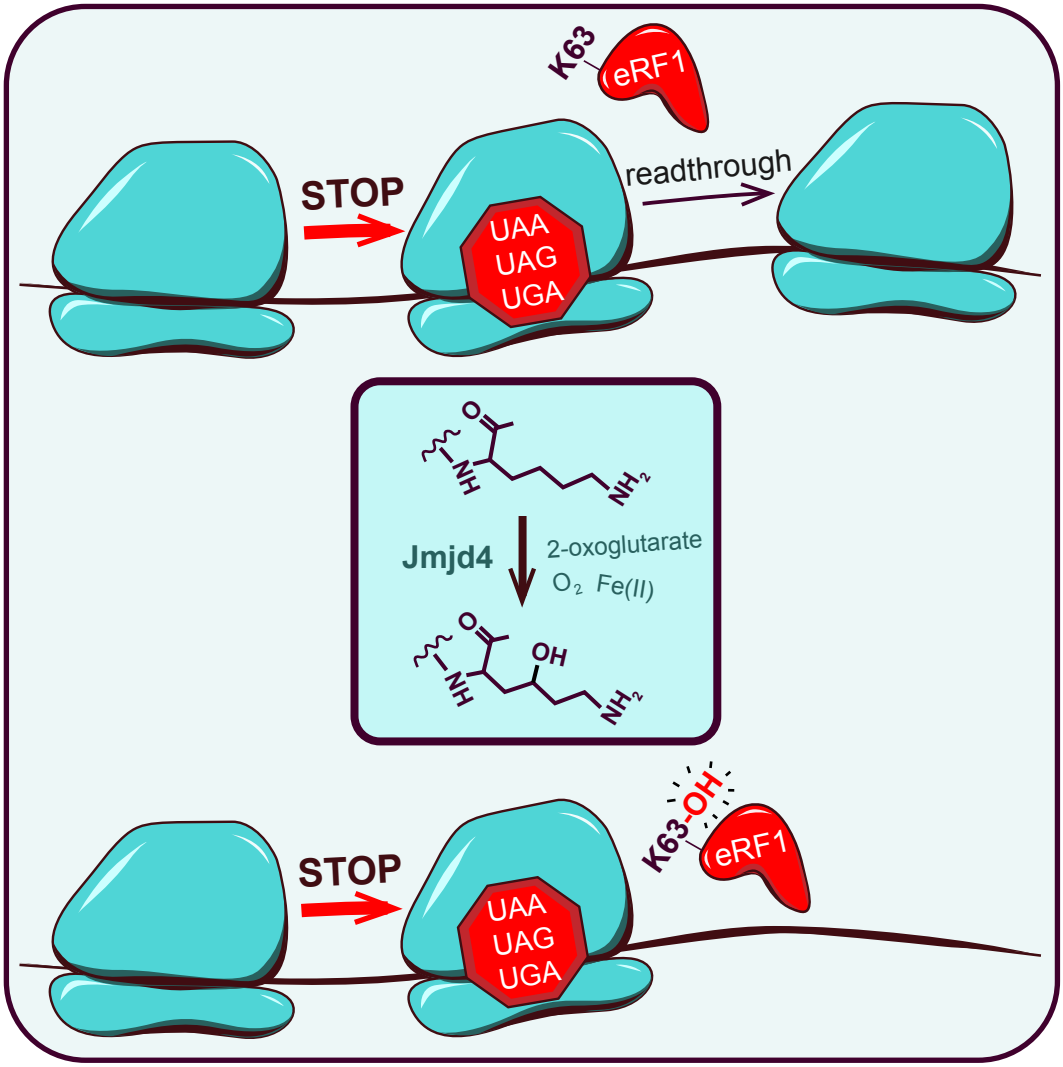


Figure 4.2: Schematic of the proposed role of JMJD4-catalysed eRF1 K63 hydroxylation in translational termination. In the absence of K63 hydroxylation, compromised stop codon recognition by eRF1 leads to inefficient translational termination. Readthrough is proposed to occur at a subset of stop codons (top panel). JMJD4 uses Fe(II), 2OG and atmospheric oxygen to catalyse the hydroxylation of eRF1 at K63 (middle panel). eRF1 functions normally with saturating levels of K63 hydroxylation, and efficiently mediates translational termination (bottom panel).

4.2 Results

4.2.1 Synthetic reporter for measuring stop codon readthrough

To measure translational termination in cells, we employed a dual luciferase reporter system (p2luc; gift from Dr. John F. Atkins, School of Biochemistry, University College Cork). The p2luc reporter was created by cloning tandem in-frame *Renilla* and firefly luciferase genes into a pRL-SV40 plasmid (Grentzmann et al., 1998). The two luciferase genes are separated by a polylinker window, in which one may insert a termination sequence context containing an in-frame stop codon (Figure 4.3A). When translational termination is efficient, eRF1 recognises the in-frame stop codon and protein synthesis generates *Renilla* luciferase as the sole product. However, insufficient translational termination causes readthrough at the stop codons of a subset of reporter transcripts, where the termination signal is decoded by a near-cognate tRNA instead of eRF1. In the case of readthrough, a fusion protein is created which consists of both *Renilla* and firefly luciferase (Figure 4.3B). To measure the fold change in readthrough in response to a treatment, the relative ratio of firefly to *Renilla* luciferase is quantified and normalised against control (Figure 4.3C). A separate 'readthrough' reporter controls for any non-specific effects from the treatment. It has the same polylinker sequence as the reporter of interest, except that the stop codon is replaced by a sense codon (Figure 4.3A).

4.2.2 Loss of JMJD4 activity promotes stop codon readthrough

Translational readthrough at normal stop codons is considered relatively rare (Keeling et al., 2012). However, viruses often use programmed readthrough as means to diversify protein expression (Bertram et al., 2001). To achieve detectable levels of readthrough in our assay, we decided to adopt a leaky termination sequence from tobacco mosaic virus (TMV) that has been widely used to study translational termination (Cassan and Rousset, 2001; Beier and Grimm, 2001; Namy et al., 2002). Translation of the TMV

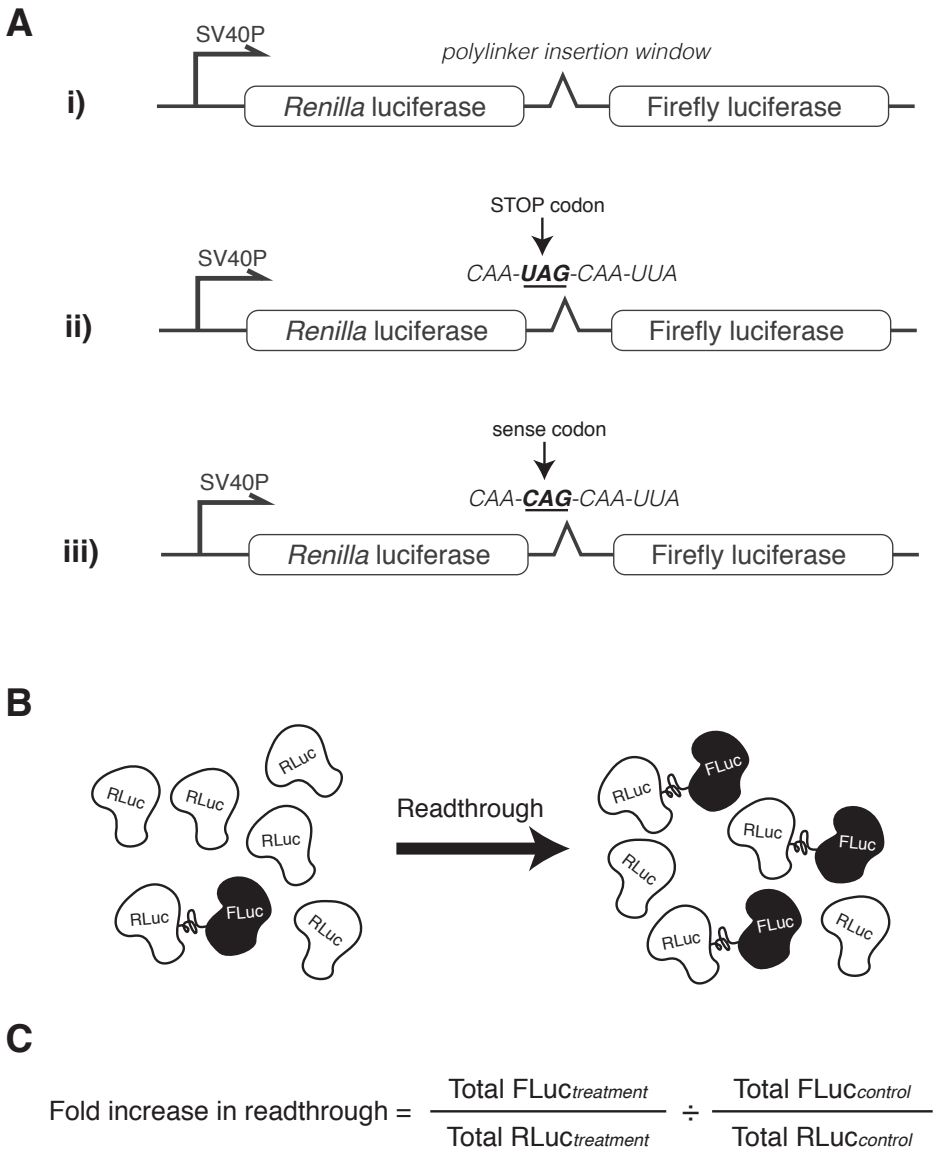


Figure 4.3: Schematic of the p2luc dual-luciferase reporter system. A) The p2luc reporter consists of *Renilla* followed by firefly luciferase. i) The two genes are separated by a polylinker insertion window, where the sequence of interest can be cloned into the reporter. ii) To measure translational termination, a polylinker sequence containing an in-frame stop codon is inserted into p2luc. iii) The 'sense' control reporter contains the same polylinker sequence, except that the stop codon is replaced by a sense codon. **B)** Efficient translational termination of reporter ii) will result in termination at the polylinker sequence, and generation of *Renilla* luciferase only (left). However, in the event of stop codon readthrough, fusion products containing both *Renilla* and firefly luciferase are produced (right). **C)** The relative change in readthrough is quantified by comparing the expression of firefly luciferase under the treatment condition to that of the control. *Renilla* luciferase is used to correct for differences in transfection efficiency between control and treatment conditions.

mRNA yields two polypeptides with molecular weights of 126 kDa and 183 kDa, of which the larger product is generated by readthrough at the first in-frame stop codon (Pelham, 1978; Beier et al., 1984). The leaky termination signal is largely mediated by nucleotides 3' to the TMV stop codon (Skuzeski et al., 1991). We have embedded UAA, UAG and UGA stop codons within the TMV leaky termination context, and cloned them into the p2luc reporter polylinker insertion window. The reporters were transfected into HeLa cells, which were then treated with siRNA against JMJD4, eRF1 or a non-targeting control sequence. The cells were harvested at 48 hours post-reporter transfection to measure the activities of firefly and *Renilla* luciferase. The relative change in stop codon readthrough was calculated as described (Figure 4.3C). As expected, the suppression of eRF1 expression significantly induced readthrough at all three stop codons, consistent with its omnipotent selectivity (Figure 4.4; Frolova et al., 1994). Critically, knockdown of JMJD4 also increased stop codon readthrough relative to siRNA control (Figure 4.4). Moreover, readthrough was induced at all three stop codons, indicating that the expression of JMJD4 is required for a fundemental step in translational termination (Figure 4.4). The observed effects were specific to translational termination, since the suppression of JMJD4 or eRF1 did not alter luciferase expression in the 'sense' control (Figure 4.4).

It was unclear whether the effect of JMJD4 on stop codon readthrough was mediated *via* its hydroxylation of eRF1. Therefore, we sought to determine the role of JMJD4 catalytic activity in translational termination. To this end, the readthrough reporter assay was performed in JMJD4 rescue cell lines. Described in Chapter 3, these were HeLa cells that stably express siRNA-resistant wild-type or enzyme-dead JMJD4. The TMV readthrough reporter containing the UGA stop codon was transfected into the rescue cell lines, following which the expression of endogenous JMJD4 was suppressed using RNAi. Concurrent mass spectrometry evaluation have shown that ectopic expression of siRNA-resistant JMJD4 rescued eRF1 K63 hydroxylation in endogenous JMJD4 knockdown cells from 15% to 90%, and mutation of its conserved Fe(II) binding residue (H189) abolished this effect (Figure 3.17). Consistent with the

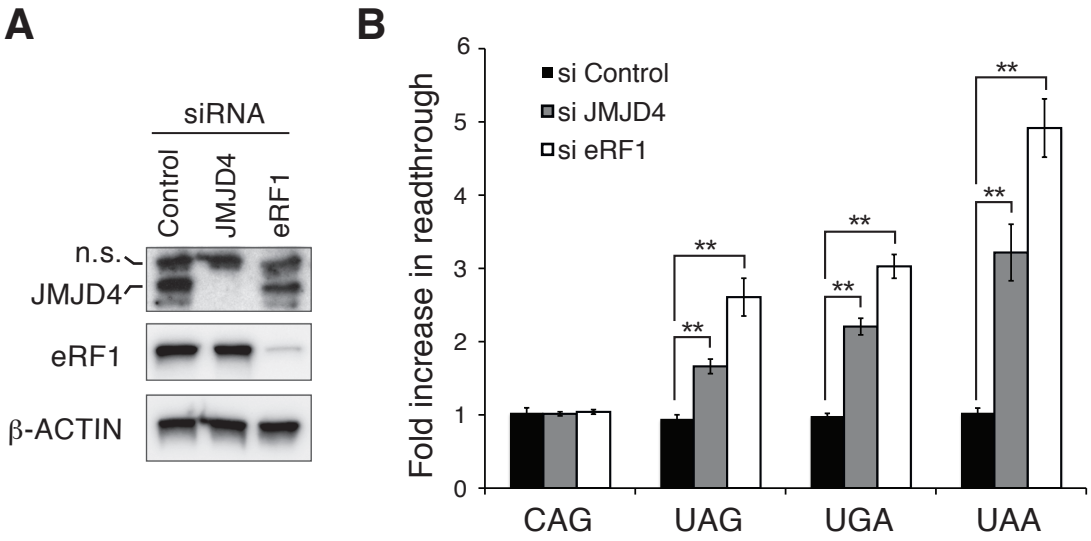


Figure 4.4: Suppression of JMJD4 induces stop codon readthrough. HeLa cells were transfected with bicistronic readthrough reporters, then treated with siRNA against JMJD4, eRF1 or a non-targeting sequence. After siRNA transfections, the cells were harvested to quantify the levels of firefly and *Renilla* luciferase expression. **A)** Immunoblots of whole cell lysates show the levels of JMJD4 and eRF1 knockdown. n.s. = non-specific **B)** Knockdown of JMJD4 and eRF1 induced readthrough at all three stop codons, but did not alter expression of the readthrough control. Statistical significance was evaluated by ANOVA followed by Dunnett's post-hoc analysis (** = $P<0.01$). Experiment performed in collaboration with Dr. Atsushi Yamamoto.

results on eRF1 hydroxylation, reconstitution of WT, but not enzyme-dead JMJD4, returned stop codon readthrough to its basal level (Figure 4.5). Importantly, this effect was specific for JMJD4, as eRF1 siRNA generated the same level of readthrough regardless of ectopic JMJD4 expression. Finally, ectopic expression of siRNA-resistant eRF1 similarly rescued the effect of eRF1 knockdown on translational termination (Figure 4.5). Taken together, these results suggest that the catalytic activity of JMJD4 is required for optimal translational termination, consistent with its hydroxylation of eRF1.

In addition to JMJD4, several related oxygenases are also regulators of gene expression. FIH, JMJD6 and MINA53 hydroxylate proteins involved in transcription, mRNA splicing and translation, respectively (Lando et al., 2002a; Webby et al., 2009; Ge et al., 2012). To determine if the effect of JMJD4 on translational termination is specific, we silenced the expressions of selective JmjC-only oxygenases in HeLa cells using RNA interference, and characterised their effects on the translational readthrough reporter. However, none of the hydroxylases altered readthrough at the leaky termination sequence except for JMJD4 (Figure 4.6). Therefore, the role of JMJD4 in promoting translational termination appears to be unique among closely related 2OG oxygenases. This is in agreement with the observation that the role of JMJD4 in eRF1 K63 hydroxylation is likely to be non-redundant, since the knockdown of JMJD4 almost completely inhibited eRF1 hydroxylation (see Chapter 3).

Addition of novel sequences into transcripts could potentially result in abnormal mRNA processing. For example, insertion of internal ribosome entry site (IRES) elements into a bicistronic reporter would sometimes generate an aberrant splice site, leading to spurious splicing of the transcript which falsely mimics IRES activation (Holcik et al., 2005; Lemp et al., 2012). The p2luc reporter plasmid employed in this work is derived from pRL-SV40 (Promega), which contains an upstream chimeric intron and a cryptic splice site within *Renilla* luciferase. Introduction of an aberrant splice site at the recoding window would cause reduced expression of *Renilla* luciferase and consequent increase of firefly to *Renilla* luciferase ratio, mimicing an apparent de-

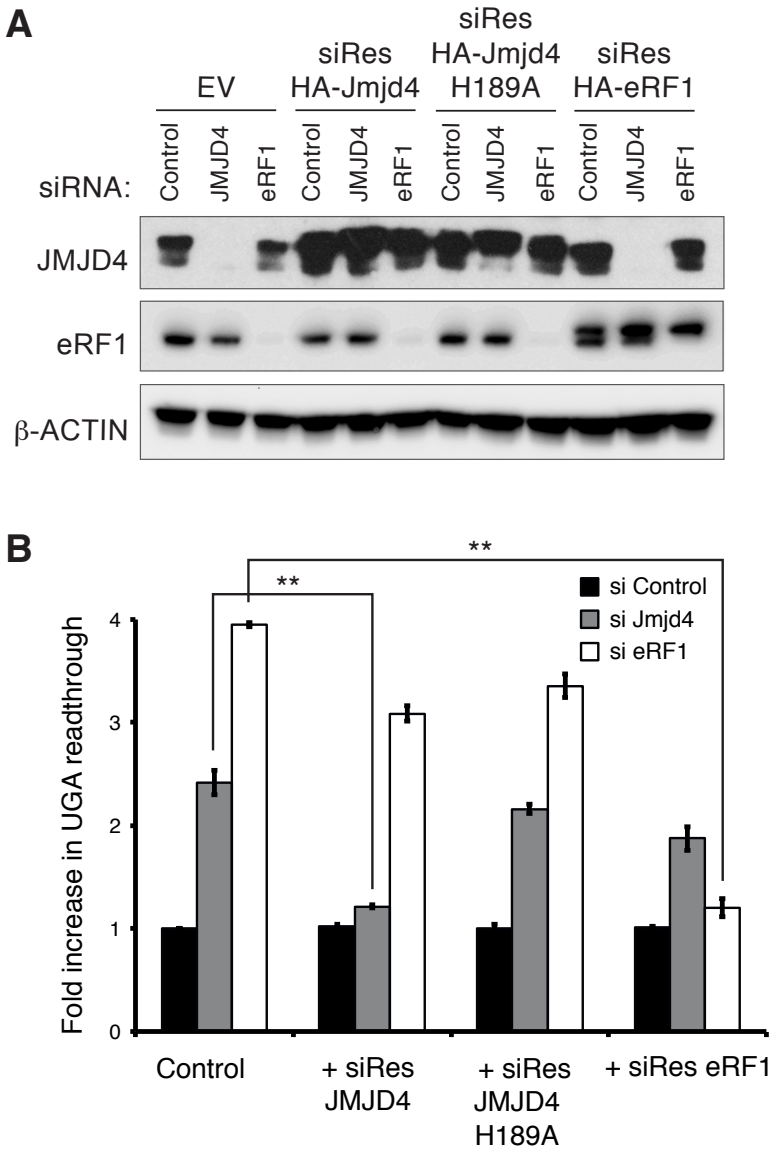


Figure 4.5: JMJD4 activity promotes translational termination efficiency. JMJD4 rescue cell lines were generated by stable expressing empty vector (EV), siRNA-resistant wild-type (WT) or enzyme-dead (H189A) JMJD4 in HeLa cells. Endogenous JMJD4 and eRF1 were silenced using RNAi, following which the bicistronic reporter containing UGA stop codon was transfected into these cells to measure stop codon readthrough. **A)** Immunoblots show the levels of knockdown and re-expression of JMJD4 and eRF1 relative to β-Actin. **B)** Quantitation of fold changes in readthrough of the rescue cell lines. Suppression of both JMJD4 and eRF1 significantly increased stop codon readthrough at the leaky termination sequence. Re-expression of WT, but not H189A JMJD4 ablated this effect. Similarly, reconstitution of eRF1 restored termination efficiency in cells that lack endogenous eRF1, indicating that the observed effects were specific. Statistical significance was evaluated by ANOVA followed by Bonferroni post-hoc test (** = $p < 0.01$). Experiment performed in collaboration with Dr. Atsushi Yamamoto.

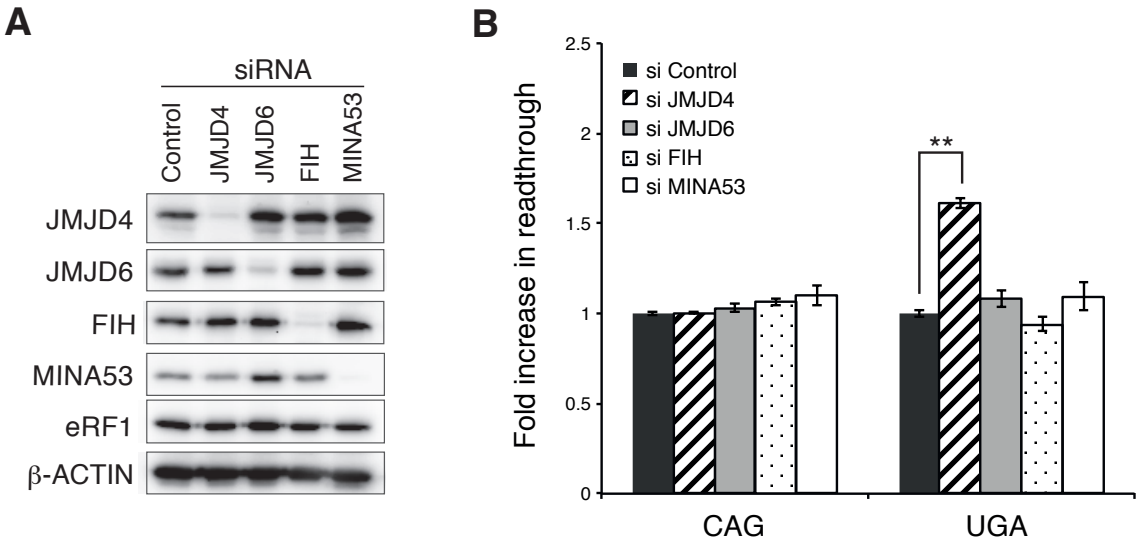


Figure 4.6: JMJD4 specifically affects translational termination. Expressions of JMJD4, JMJD6, FIH and MINA53 in HeLa cells were suppressed using siRNA, following which the cells were transfected with p2luc reporter containing the UGA stop codon in TMV termination sequence. At 48 hours post-transfection, the cells were harvested to quantify the relative levels of firefly to *Renilla* luciferase. **A)** Whole cell lysates were immunoblotted to assess the knockdown levels of respective oxygenases. **B)** Knockdown of JMJD4 induced stop codon readthrough. In comparison, suppression of JMJD6, FIH and MINA53 did not have an appreciable effect on translational termination efficiency. Statistical significance was evaluated by ANOVA followed by Dunnett's post-hoc analysis (** = $p<0.01$).

crease in translational termination efficiency. To test for spurious splicing, we designed a set of reverse-transcription PCR (RT-PCR) primers that spans from the chimeric intron to the start of firefly luciferase (Figure 4.7A). Aberrant splicing would generate a series of small mRNA transcripts with predicted sizes as listed in Figure 4.7A. However, RT-PCR analysis of RNA purified from HeLa cells transfected with readthrough reporters did not identify any unexpected amplification products (Figure 4.7B). Furthermore, treatment of HeLa cells with control or JMJD4 siRNA did not alter splicing of the reporter transcript. Next, we used quantitative-PCR (qPCR) to compare the relative ratio of firefly to *Renilla* luciferase mRNAs. Consistent with data from RT-PCR, treatment of HeLa cells with siRNA against JMJD4 did not change the relative abundance of firefly to *Renilla* luciferase mRNA (Figure 4.8). These data indicate that the JMJD4-dependent changes in the luciferase reporters were likely due to stop codon readthrough rather than aberrant mRNA processing.

4.2.3 K63 hydroxylation optimises eRF1 activity *in vitro*

Results obtained so far suggest that JMJD4 catalysis affects translational termination, consistent with a role for eRF1 K63 hydroxylation. However, it is possible that translational termination is affected indirectly by some other activities of JMJD4 in the cell. Therefore, we aimed to directly measure the effect of K63 hydroxylation on eRF1 activity using a fully reconstituted *in vitro* translation system (Experiment performed by Dr. Elizaveta Sokolova; Alkalaeva et al., 2006). Briefly, ribosomal subunits purified from rabbit reticulocyte lysates were assembled onto mRNA encoding a tetrapeptide. Translational initiation and elongation were reconstituted by adding aminoacyl tRNAs (including [35S]Met-tRNA^{Met}), initiation and elongation factors to the translation system (Pestova et al., 1998; Pestova and Hellen, 2003). In the absence of eRF1, ribosomal complexes are stalled at the pretermination stage and can be purified using sucrose gradient centrifugation. Addition of recombinant eRF1 into the pretermination complexes triggers peptidyl-tRNA bond hydrolysis, which results

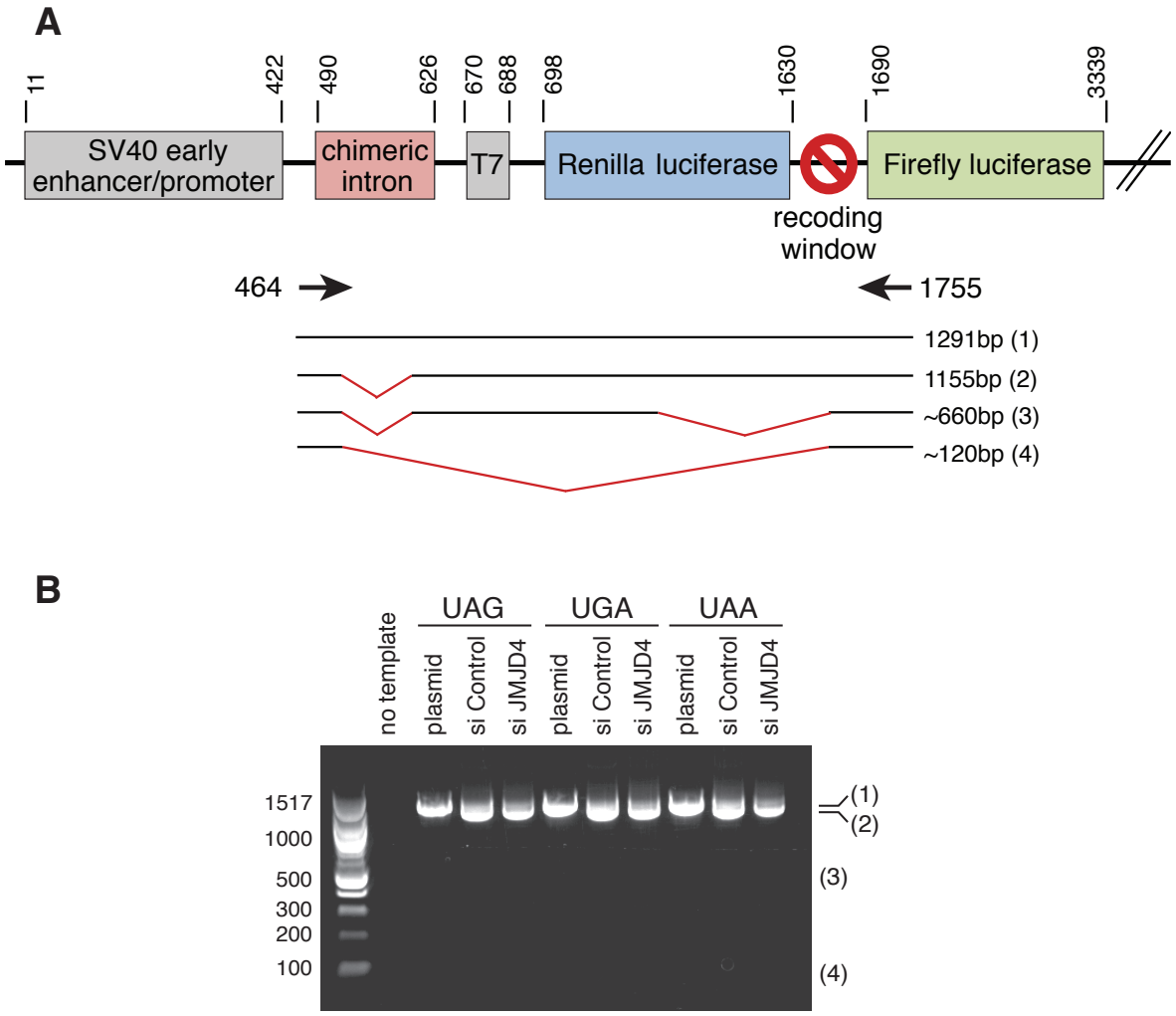


Figure 4.7: End point RT-PCR analysis of p2luc reporter mRNA integrity. A) Schematic of the p2luc dual luciferase reporter. The p2luc reporter features a chimeric intron between SV40 and T7 promoters, in addition to a cryptic splice site within *Renilla* luciferase. A pair of RT-PCR primers was designed to span from the chimeric intron to the beginning of firefly luciferase. RT-PCR amplification of the full-length transcript would yield product (1), whereas normal splicing of the chimeric intron produces product (2). Introduction of a splice site in the recoding window would result in aberrant splicing generating variants (3) and (4). B) RT-PCR analyses validating integrity of the readthrough reporter mRNAs. RNA was purified from HeLa cells transfected with JMJD4 or control siRNA, and respective readthrough reporters. Purified total RNA was treated with DNAse to remove traces of transfected plasmid DNA, followed by cDNA synthesis and RT-PCR. 'Plasmid' denotes positive control p2luc plasmid DNA.

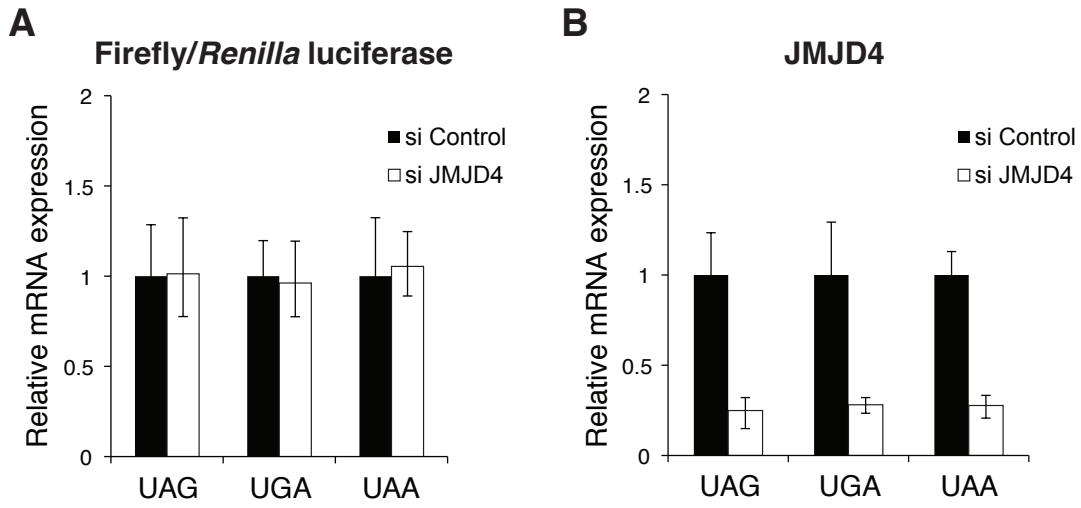


Figure 4.8: Quantitative RT-PCR analysis of p2luc reporter mRNA integrity. qPCR analyses validating integrity of the readthrough reporter mRNAs. Total RNA was purified from HeLa cells treated with control or JMJD4 siRNA and transfected with readthrough reporters. Purified RNA was subjected to DNAse digest to remove transfected plasmid DNA, followed by cDNA synthesis and qPCR. qPCR analysis using SYBR Green primers against firefly or *Renilla* luciferase showed that the ratio of firefly to *Renilla* luciferase was unaffected by JMJD4 siRNA (left). Knockdown of JMJD4 mRNA was confirmed by qPCR (right).

in release of the [35S]methionine labelled peptides. The rate of radiolabelled peptide release is correlated with translational termination efficiency, which allows for quantitation of eRF1 catalytic activity. Mutagenesis studies using the *in vitro* reconstituted translation system have demonstrated the importance of the NIKS motif in eRF1 activity (Kryuchkova et al., 2013). Interestingly however, recombinant eRF1 containing a K63R mutation exhibited the same level of release factor activity as wild-type, K63 unhydroxylated eRF1 (Kryuchkova et al., 2013).

To assess the role of K63 hydroxylation in eRF1 function, we compared termination efficiencies of K63 hydroxylated and unhydroxylated eRF1 using the reconstituted *in vitro* translation system. Recombinant eRF1 reacted with either wild-type or enzyme-dead JMJD4 were purified and incubated with pretermination ribosomal complexes. Concurrent MS analyses showed that wild-type JMJD4 hydroxylated 60% of eRF1 at K63, whereas eRF1 incubated with H189A JMJD4 remained unmodified (Figure 4.9). As previously demonstrated, unhydroxylated eRF1 markedly induced peptidyl release from the pretermination complex (Alkalaeva et al., 2006; Kryuchkova et al., 2013). Critically however, hydroxylation at K63 significantly improved the catalytic efficiency of eRF1 (Figure 4.10). To determine whether the observed effect was specific to K63 hydroxylation, we repeated the experiment using a K63R mutant of eRF1. Incubation with neither wild-type nor H189A JMJD4 resulted in hydroxylation of the mutant eRF1 at K63R (Figure 4.9). Consistent with published data, mutation of K63 to arginine did not alter the basal activity of eRF1 (Kryuchkova et al., 2013). Nonetheless, incubation of K63R eRF1 with wild-type JMJD4 did not improve its termination efficiency, indicating that the observed improvement in eRF1 catalytic efficiency was indeed due to K63 hydroxylation (Figures 4.9 and 4.10).

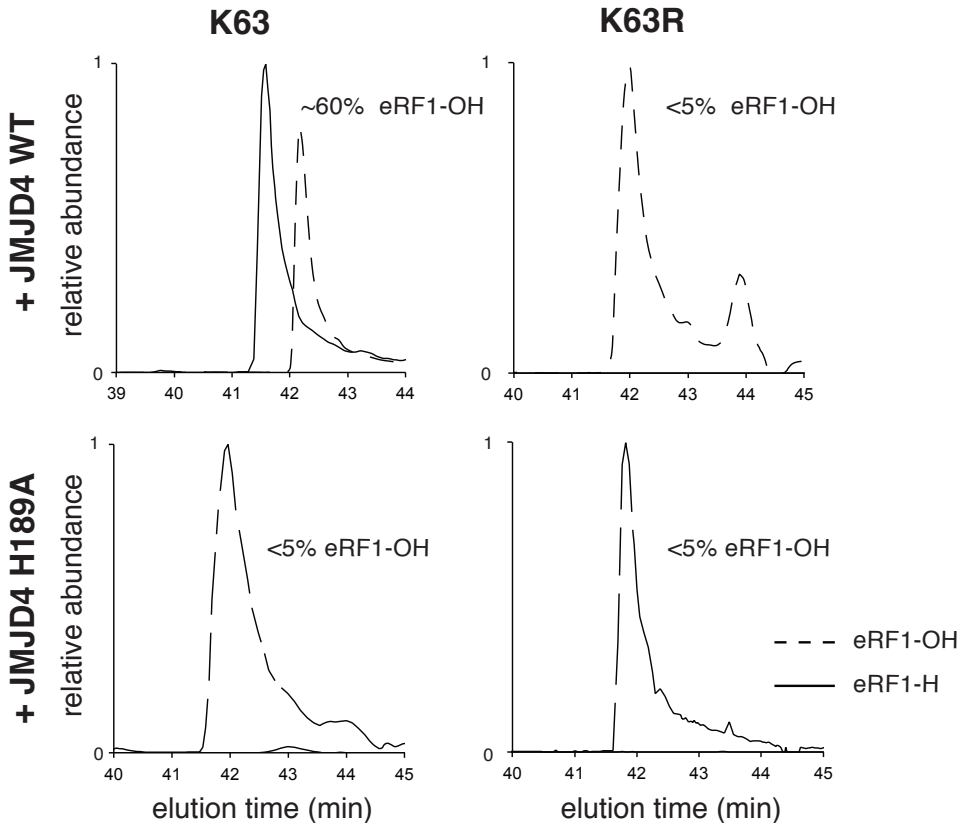


Figure 4.9: Hydroxylation of recombinant eRF1 by recombinant JMJD4 *in vitro*. Partially purified recombinant eRF1 was reacted with recombinant JMJD4 at a ratio of 10:1 in the presence of co-factors for 16 hours in room temperature. Recombinant eRF1 was then isolated from the reaction mixture using two-step chromatography. Purified eRF1 was digested with trypsin in-solution, and analysed for K63 hydroxylation by LC-MS/MS. Figure shows EICs of wild type (K63) or K63R eRF1 incubated with either wild type or H189A JMJD4. *In vitro* reactions and eRF1 purification performed by Dr. Mathew Coleman.

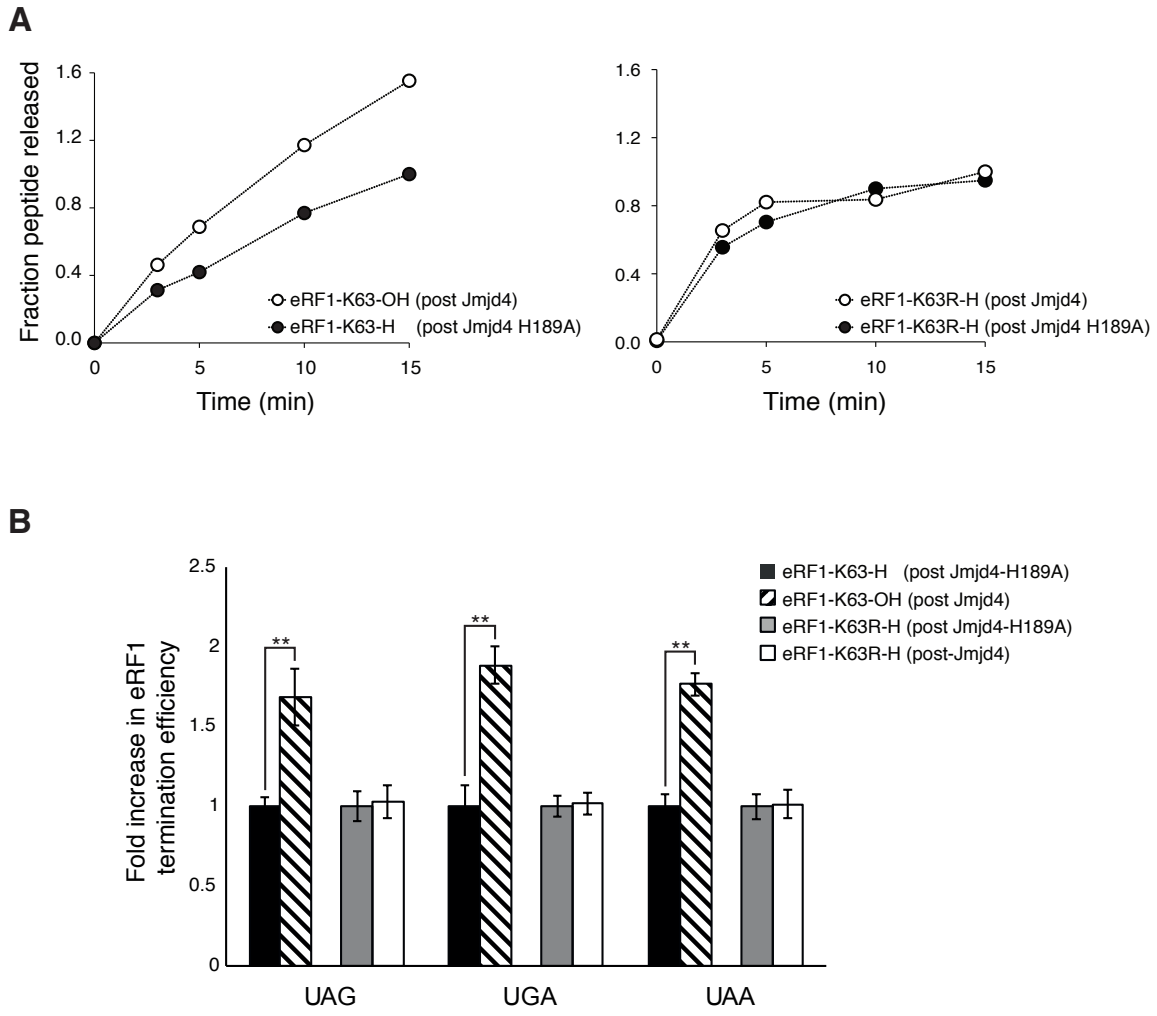


Figure 4.10: K63 hydroxylation promotes eRF1 translational termination efficiency *in vitro*. Partially purified recombinant eRF1 was reacted with either wild type or H189A JMJD4, following which eRF1 was purified for *in vitro* reconstituted translation assay. The addition of recombinant eRF1 to pretermination ribosomal complexes stimulates translational termination, which is quantified by the release of radiolabelled tetrapeptides. **A)** Representative time courses of peptide release. **B)** Catalytic efficiencies (K_{cat}/K_M x 10^4 [$M^{-1}s^{-1}$]) of respective eRF1 proteins. Statistical significance was evaluated using paired two-tailed student's t-test (** = $p<0.001$). *In vitro* reconstituted translation termination assays performed by Dr. Elizaveta Sokolova.

4.2.4 JMJD4 inhibition mediates readthrough at premature termination codons

The role of JMJD4 in translational termination may be generalisable to stop codons in multiple sequence contexts, including premature stop codons that arise from nonsense mutations. Nonsense mutations induce premature translational termination, which results in the production of truncated polypeptides and mRNA decay (Mendell and Dietz, 2001). Nonsense mutations contribute to 5-70% of individual cases in genetic disorders (Sweeney, 2009). Therefore, considerable effort has been invested in the identification of pharmacological agents that mediate readthrough at premature termination codons (Sweeney, 2009). Since JMJD4 activity influences stop codon readthrough, we sought to determine the consequence of JMJD4 inhibition on premature translational termination. To this end, two nonsense mutations from dystrophin and cystic fibrosis transmembrane conductance regulator (CFTR) were cloned into the bicistronic reporter (Figure 4.11A). Mutations of these two proteins are known to cause muscular dystrophy and cystic fibrosis, respectively (Cystic Fibrosis Mutation Database; Online Mendelian Interitance in Man). 12 to 15 nucleotides spanning either side of the stop codon were included as the termination sequence context. HeLa cells were treated with siRNA against either JMJD4 or eRF1, and transfected with nonsense mutation reporters to measure the level of stop codon readthrough. The TMV reporter was transfected in parallel as positive control. Strikingly, inhibition of JMJD4 significantly stimulated readthrough at both nonsense stop codons, and the effect was comparable to positive control eRF1 (Figure 4.11C).

Next, we tested whether the observed readthrough extends to other premature stop codons. Nonsense mutation in tumour suppressor genes is associated with 10-30% of heritable cancer syndromes (Bordeira-Carriço et al., 2012). Premature termination of the adenomatous polyposis coli (APC) tumour suppressor gene is associated with both sporadic and heritable forms of colorectal cancer (Fearnhead et al., 2001). A series of nonsense mutations found in APC were obtained from the COSMIC (Cata-

A

Gene	Description	Amino acid mutation	CDS mutation	Genetic disorder
CFTR	Cystic fibrosis transmembrane conductance regulator	p.W1282*	c.3846G>A	Cystic fibrosis
DMD	dystrophin	p.W3*	c9G>A	Muscular dystrophy

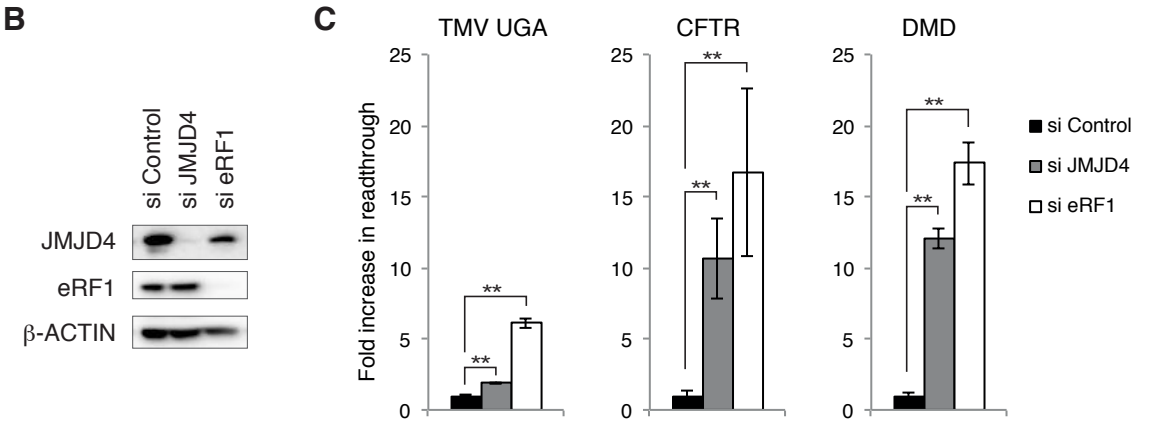


Figure 4.11: JMJD4 suppression mediates readthrough at CFTR and DMD premature termination codons in synthetic reporters. A) Description of two genetic nonsense mutations found in CFTR and DMD genes that are associated with heritable genetic disorders (Cystic Fibrosis Mutation Database; Online Mendelian Interitance in Man). The mutations and their surround termination contexts were cloned into the dual luciferase reporter. The reporters were transfected into HeLa cells treated with JMJD4, eRF1 or control siRNA, following which the luciferase signals were measured to quantify stop codon readthrough. **B)** Immunoblots show efficacy of JMJD4 and eRF1 RNAi treatments. **C)** Knockdown of JMJD4 and eRF1 significantly promoted readthrough at the nonsense stop codons, as measured by firefly to *Renilla* luciferase ratio relative to control. A TMV readthrough reporter was included as positive control. Statistical significance was evaluated by ANOVA followed by Dunnett's post-hoc analysis (** = $p<0.01$).

logue of Somatic Mutations In Cancer) database for cancer cell lines and cloned into the bicistronic reporter system (Figure 4.12A). Importantly, suppression of JMJD4 expression promoted appreciable levels of readthrough at all of the APC premature stop codons (Figures 4.12B and C). Taken together, these data infer that JMJD4 inhibition globally suppresses translational termination at premature stop codons, though additional experiments are required to validate readthrough at an endogenous level.

4.2.5 Depletion of JMJD4 promotes readthrough at endogenous termination sequence contexts

Reporter studies have estimated the rate of readthrough at premature termination codons to be 0.01-1%, but only 0.001-0.1% at normal stop codons (Bonetti et al., 1995; Manuvakhova et al., 2000; Keeling et al., 2012). This is partly due to the surrounding sequence context, which is optimised at naturally occurring stop codons to maximise translational termination efficiency (Manuvakhova et al., 2000; Bonetti et al., 1995; Cassan and Rousset, 2001). However, emerging evidence indicates that translational readthrough in eukaryotes is much more pervasive than previously thought. Regulated readthrough of endogenous genes have been observed in yeast, fungi, *Drosophila* and mammals (Geller and Rich, 1980; Xue and Cooley, 1993; Klagges et al., 1996; Steneberg and Samakovlis, 2001; Namy et al., 2002; Freitag et al., 2012; Yamaguchi et al., 2012). Computational annotation of conserved protein coding regions in the *Drosophila* genome have further identified 283 candidate readthrough extensions (Jungreis et al., 2011). A recent phylogenetic study identified seven candidate readthrough targets from the human genome, all of which were validated using dual luciferase reporters (Jungreis et al., 2011; Loughran et al., 2014).

Additionally, the development of ribosome profiling has allowed for direct measurement of translational readthrough at the genome-scale. Ribosomal profiling is a technique that maps the active translatome at single nucleotide resolution (Ingolia et al., 2009). It relies on nuclease digestion to remove RNA other than short (~30 nucleotide)

A

Amino acid mutation	CDS mutation	Cell line
p.E853*	c.2557G>T	HT-29
p.R1114*	c.3340C>T	LoVo, SW948*
p.Q1367*	c.4099C>T	C2bbe1
p.R1450*	c.4348C>T	SNU-61, SNU-81*, HCC2998*, LS-123*, SW837*, MKN28, SW1417
p.R2166*	c.6496C>T	HCT-15

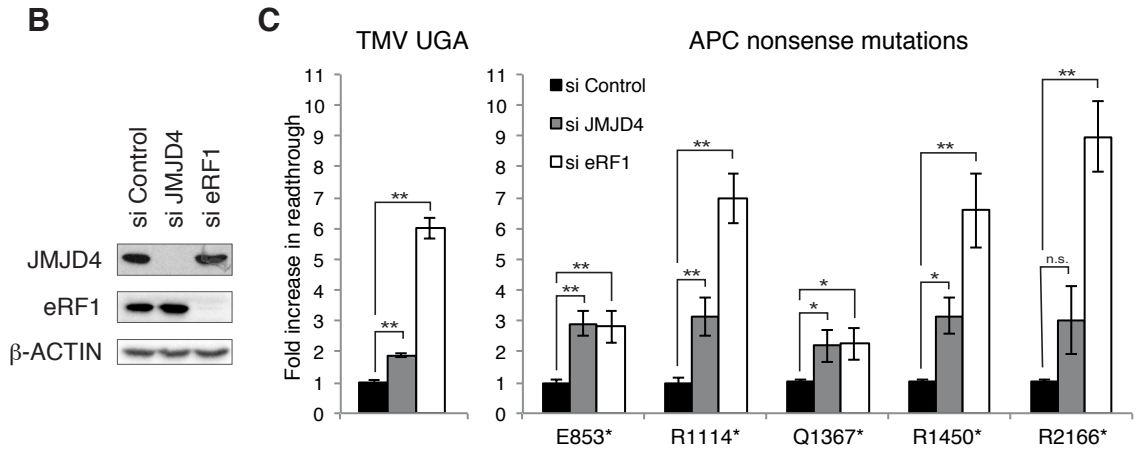


Figure 4.12: JMJD4 suppression mediates readthrough at APC premature termination codons in synthetic reporters. A) Description of APC nonsense mutations found in selective colorectal cancer cell lines (Catalogue of Somatic Mutations In Cancer; COSMIC). The nonsense mutations and their surround sequence contexts were cloned into the bicistronic reporter, following which the reporters were transfected into HeLa cells treated with JMJD4, eRF1 or control siRNA. The firefly and *Renilla* luciferase signals were subsequently measured in these cells to quantify the level of stop codon readthrough. **B)** Immunoblots demonstrating the levels of JMJD4 and eRF1 knockdown. **C)** Suppression of JMJD4 and eRF1 expression induced readthrough at APC nonsense mutation sites, as quantified by luciferase expression relative to control. A TMV readthrough reporter was used as positive control. Statistical significance was evaluated by ANOVA followed by Dunnett's post-hoc analysis (n.s. not significant; * = $p<0.05$; ** = $p<0.01$).

mRNA fragments that are protected by bound ribosomes (Ingolia et al., 2009). These mRNA fragments are termed ribosomal footprints. Deep sequencing of ribosomal footprints provides a 'still shot' of the positional occupancy of translating ribosomes and their respective abundance (Ingolia et al., 2009). In a study by Dunn et al (2013), ribosome profiling of *Drosophila* embryos detected footprints mapped 3' to the annotated stop codons of at least 158 genes, indicative of translational readthrough. Out of the 158 genes, 43 were bioinformatically predicted to undergo readthrough in a separate study (Jungreis et al., 2011; Dunn et al., 2013). The predicted C-terminal amino acid extensions were searched for predicted functional motifs; eight nuclear localisation signals, eight transmembrane helices and one peroxisome targeting signal were identified (Dunn et al., 2013). Moreover, ribosomal profiling of yeast and human cells have also identified numerous translation readthrough events (Dunn et al., 2013). Collectively, these studies provide convincing evidence that stop codon recoding is widespread in eukaryotes, though the functional outcome of translational readthrough remains poorly characterised.

Ribosomal profiling of human foreskin fibroblasts discovered 42 candidate readthrough genes (Dunn et al., 2013). Given the role of JMJD4 in translational termination, we asked whether stop codon readthrough at any of the corresponding stop codon contexts are altered by JMJD4 depletion. To screen for readthrough genes with potentially functional amino acid extensions, we searched for predicted C-terminal extensions encoding for possible functional modifs, as described in Dunn et al. (2013). Two of the predicted readthrough extensions were found to contain transmembrane helices, and no other functional motifs were identified (Figure 4.13A; data not shown).

Next, the termination sequence contexts of nine candidate readthrough genes, including the two encoding transmembrane extensions, were cloned into dual luciferase readthrough reporters (Figure 4.13A). The cloned termination sequence contexts consisted of 18-21 nucleotides on either side of the stop codon. The reporters were transfected into HeLa cells that have been treated with siRNA against JMJD4, eRF1 or non-targeting control. At 48 hours post-reporter transfection, the cells were harvested

A

Name	Description	Readthrough rate	Extension length (bp)	Extension motif
RHOA	GTPase; actin stress fiber formation	7.60×10^{-3}	162	Transmembrane helices
WFDC1	Protease inhibitor	3.18×10^{-2}	72	None
HIS1H2AD	Histone; nucleosome component	3.93×10^{-1}	42	None
DDIT3	Pro-apoptotic transcription factor	1.78×10^{-1}	201	None
GSKIP	GSK3B interactor	6.70×10^{-2}	168	Transmembrane helices
ROMO1	ROS production; cell proliferation	3.29×10^{-2}	54	None
IRF2BP1	IRF2-dependent transcriptional corepressor	2.28×10^{-1}	42	None
THY1	T-cell antigen	2.09×10^{-2}	102	None
BTG1	Cell growth regulator	2.57×10^{-1}	27	None

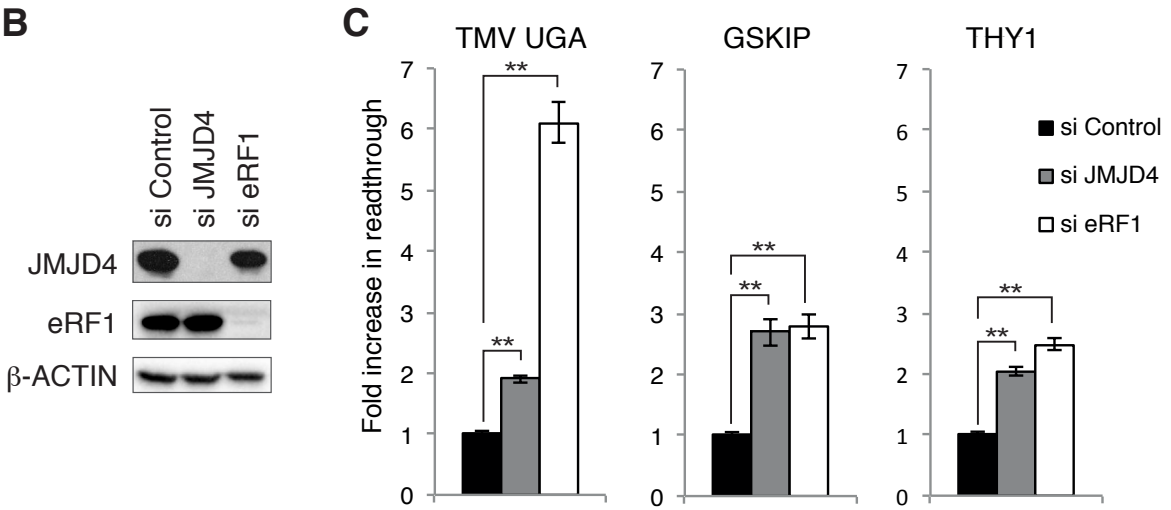


Figure 4.13: Knockdown of JMJD4 induces readthrough at selected endogenous termination sequences. Possible readthrough events at stop codons of endogenous human genes were identified using ribosome profiling (Dunn et al., 2013). Termination sequence contexts of nine candidate readthrough genes were cloned into dual luciferase reporters to measure stop codon readthrough. **A)** Description of the candidate readthrough genes and their predicted extensions (Dunn et al., 2013). Two predicted extension sequences were identified as transmembrane helices using TMHMM Server 2.0 (Transmembrane Helices Hidden Markov Models; Krogh et al., 2001). The reporters were transfected into HeLa cells treated with siRNA against JMJD4, eRF1 or non-targeting control to measure the level of stop codon readthrough. **B)** Immunoblots showing JMJD4 and eRF1 knockdown by RNAi. **C)** Knockdown of JMJD4 and eRF1 resulted in increased readthrough at GSKIP and THY1 termination contexts, as measured by the ratio of firefly to *Renilla* luciferase expression. The remaining readthrough reporters did not achieve detectable luciferase signals above threshold, and were not quantified. Statistical significance was evaluated by ANOVA followed by Dunnett's post-hoc analysis (** = $p<0.01$).

to quantify stop codon readthrough. Firefly luciferase expression was measurable in two of the reporters, though it was below the threshold of detection in the remaining reporters (Figure 4.13C). This is likely due to low rates of stop codon readthrough, since *Renilla* luciferase was adequately expressed in all of the reporters at a level comparable to the TMV control (data not shown). Nevertheless, knockdown of JMJD4 and eRF1 promoted readthrough at the termination sequence contexts of GSKIP and THY1, which encode for a GSKβ inhibitor and a thymocyte surface antigen, respectively (Figure 4.13). However, translational readthrough of these genes is yet to be demonstrated at the endogenous level.

4.2.6 Knockdown of JMJD4 and eRF1 alters cellular polysome profile

We have shown that JMJD4 knockdown promotes translational readthrough in a variety of termination sequence contexts, including that of endogenous genes. This raises the possibility that a widespread deficit in translational termination resulting from JMJD4 inhibition could elicit adaptive responses controlling global protein synthesis and cell proliferation. The effect of translational termination inhibition on global protein synthesis was characterised using polysome profile analysis (see Chapter 2). The expression of JMJD4 and eRF1 was suppressed in HeLa cells using RNAi. At 72 hours post-siRNA transfection, the cells were lysed and subjected to sucrose density gradient centrifugation. Figure 4.14B shows polysome profiles of HeLa cells transfected with control, JMJD4 or eRF1 siRNA. In comparison to the non-targeting control, depletion of JMJD4 is associated with a significant increase in free 60S ribosomal subunits and a subtle decrease in heavy translating polysomes (Figure 4.14). The depletion of eRF1 resulted in an even more marked increase in free 40S and 60S ribosomal subunits and a significant reduction in translating polysomes (Figure 4.14). The observed translational phenotype is remarkably similar to that of translational initiation arrest, since the inhibition of translational initiation is known to cause polysome run-off with an

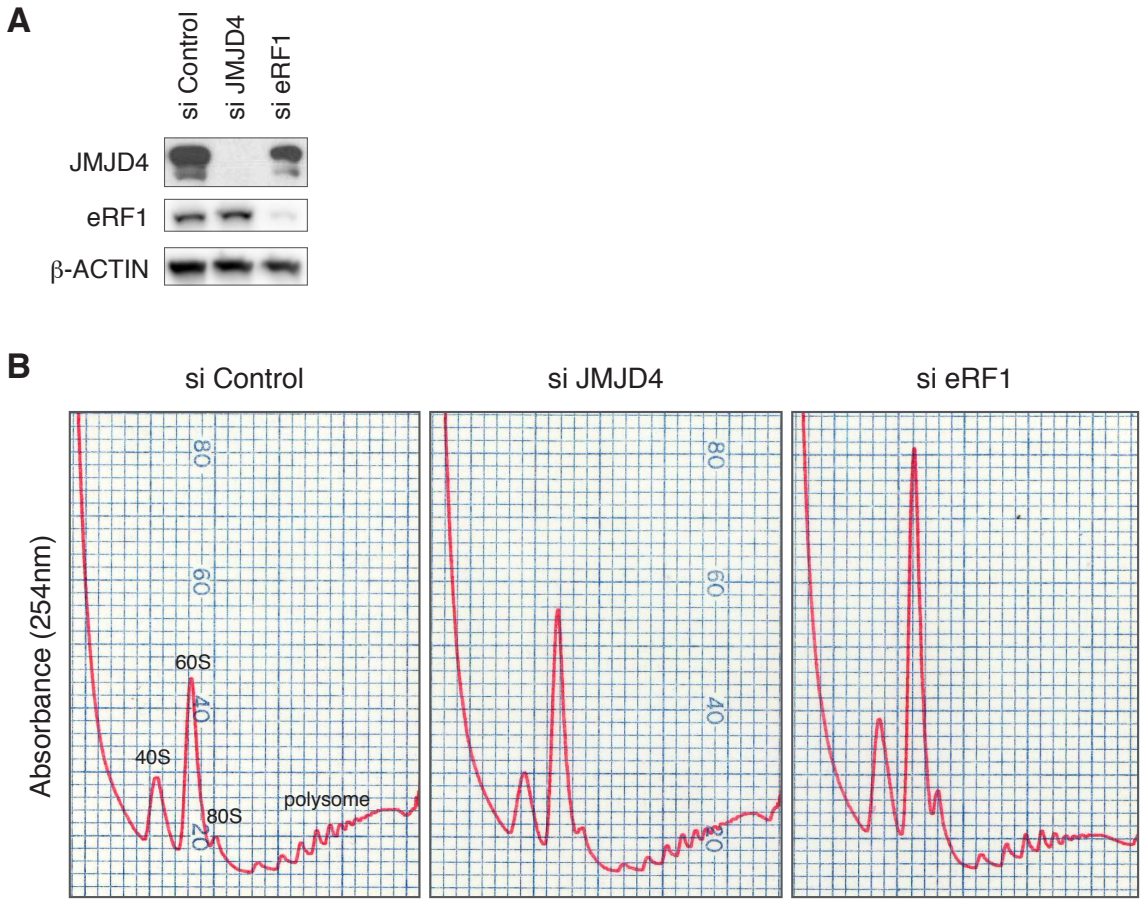


Figure 4.14: Depletion of JMJD4 alters polysome profile of HeLa cells. HeLa cells were transfected with siRNA against JMJD4, eRF1 or a non-targeting control sequence. At 72 hours after siRNA transfection, the cells were treated with cycloheximide to halt protein synthesis, lysed, and passed through a 10-60% (w/v) sucrose gradient. The surcrose gradient was passed through a fractionator, and absorbance was measured at 254nm to obtain the polysome profiles. **A)** Whole cell lysates were immunoblotted to assess the level of JMJD4 and eRF1 knockdown. **B)** Polysome profiles of cells treated with JMJD4, eRF1 or control siRNA. In comparison to control, suppression of JMJD4 expression resulted in a marked increase in 60S ribosomal subunits and negligible reduction of heavy polysomes. eRF1 knockdown resulted in a considerable increase in free 40S and 60S ribosomal subunits and concomitant decrease in translating polysomes.

associated increase in the number of free ribosomes (Mašek et al., 2011). In contrast, ribosome stalling during translational termination should theoretically result in an increase in the amount of polysomes. However, additional characterisations are required to accurately conclude the cause of JMJD4-mediated polysome profile phenotype.

4.2.7 JMJD4 is required for cell proliferation

Polysome profile analysis indicates that the knockdown of JMJD4 affects protein synthesis. Given the intimate link between protein synthesis and growth, we sought to determine whether JMJD4 is also required for cell proliferation. To this end, the expression of endogenous JMJD4 in HeLa cells was suppressed using siRNA, following which the cells were seeded into 96-well plates to measure growth over the span of 5 days. Cell proliferation was determined using MTS assay, which relies on cellular reduction of tetrazolium salt into formazan dyes. As shown by Figure 4.15B, knockdown of JMJD4 significantly inhibited cell proliferation. The suppression of eRF1 expression had a similar effect on cell proliferation, consistent with the importance of eRF1 in yeast for growth (Himmelfarb et al., 1985). Since the MTS assay does not directly quantify cell number (see Chapter 2), the effect of JMJD4 on growth was validated using the CyQUANT cell proliferation assay (Life Technologies). Instead of relying on cellular oxidoreductase activity, the CyQUANT cell proliferation assay uses a fluorescent dye that binds to nucleic acids and directly measures the amount of DNA content in cells. Growth curves measured using the CyQUANT fluorescent dye showed that the depletion of JMJD4 and eRF1 suppresses cell proliferation (Figure 4.15C).

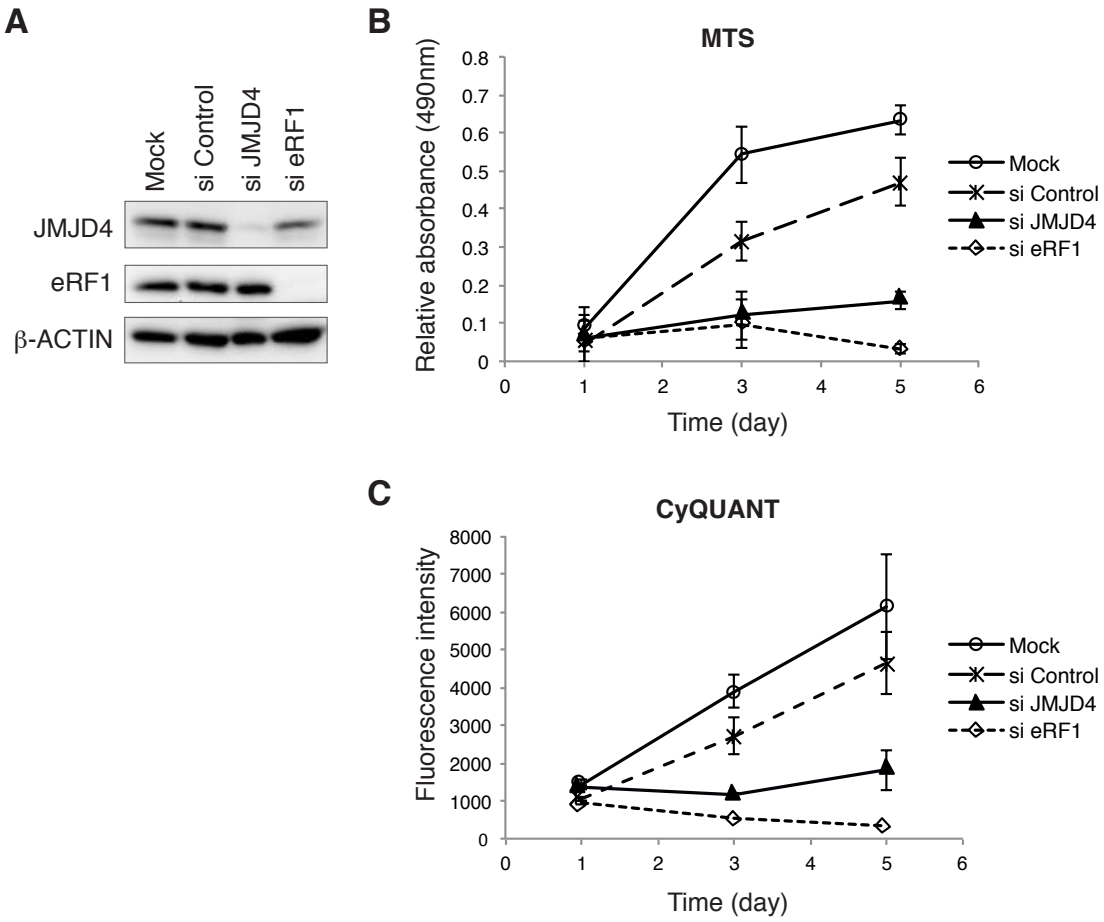


Figure 4.15: JMJD4 knockdown in HeLa cells inhibits proliferation. HeLa cells were treated with siRNA against JMJD4, eRF1 or non-targeting control, following which they were seeded into 96-well plates, and cell proliferation was measured over 5 days to monitor growth. **A)** Immunoblots showing suppression of JMJD4 and eRF1 expression. **B)** Growth curves of control, JMJD4 and eRF1 knockdown cells as measured by MTS tetrazolium assay. **C)** Growth curves of control, JMJD4 and eRF1 knockdown cells as measured by CyQUANT cell proliferation assay. Both assays showed that depletion of JMJD4 and eRF1 markedly reduced proliferation of HeLa cells. Mock = transfection reagent only.

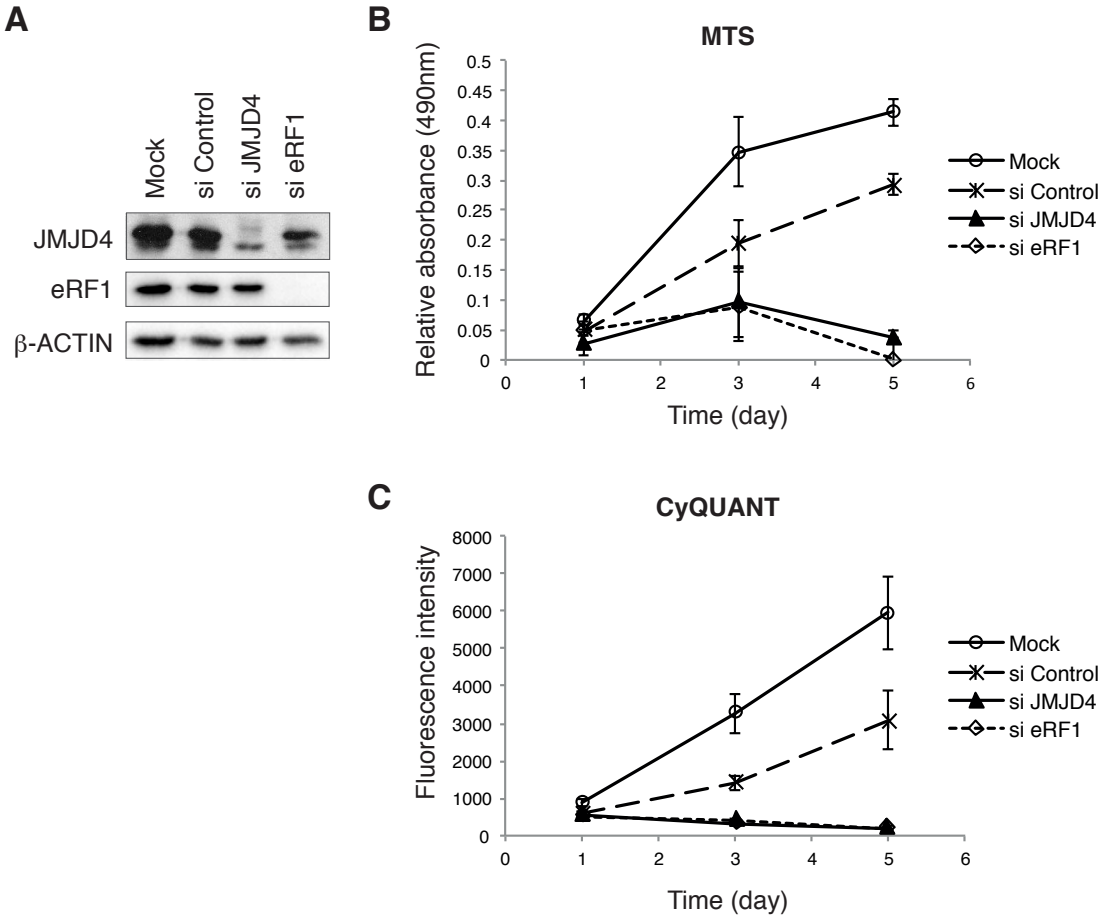


Figure 4.16: JMJD4 expression is required for the proliferation of U2OS cells. Expression of JMJD4 and eRF1 in U2OS cells were suppressed using RNAi, following which the cells were seeded into 96-well plates to monitor growth over the span of 5 days. **A)** Immunoblots demonstrating JMJD4 and eRF1 knockdown. **B)** and **C)** show growth curves of control, JMJD4 and eRF1 knockdown cells as measured by MTS and CyQUANT cell proliferation assays, respectively. Knockdown of JMJD4 and eRF1 significantly inhibited growth of U2OS cells. Mock = transfection reagent only.

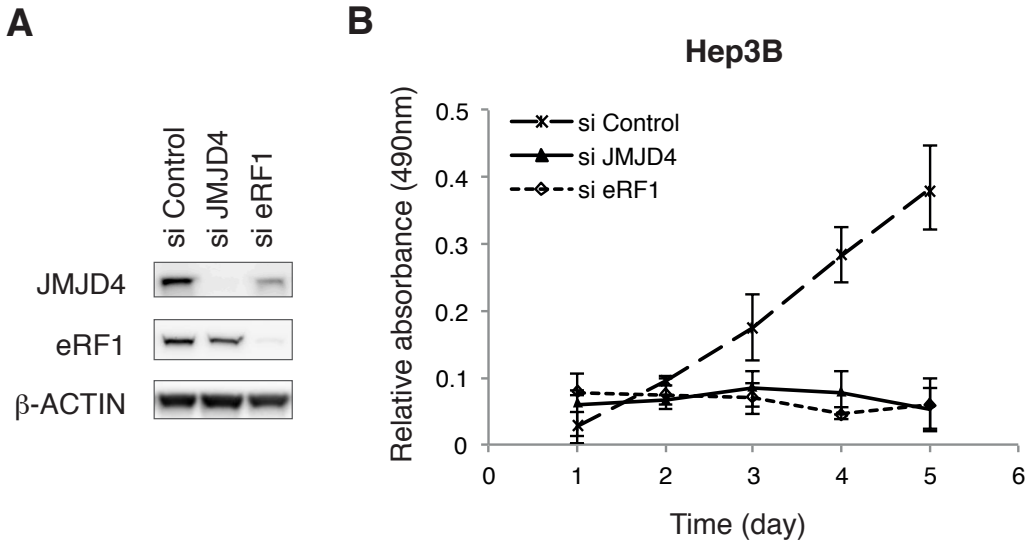


Figure 4.17: Depletion of JMJD4 inhibits Hep3B cell proliferation. Hep3B cells were transfected with control, JMJD4 or eRF1 siRNA, and seeded into 96-well plates to monitor cell growth over the span of 5 days. **A)** Immunoblots of whole cell lysates showing efficacy of JMJD4 and eRF1 siRNA treatments. **B)** growth curves of control, JMJD4 and eRF1 depleted cells as measured by MTS tetrazolium assay. Knockdown of both JMJD4 and eRF1 markedly suppressed growth of Hep3B cells.

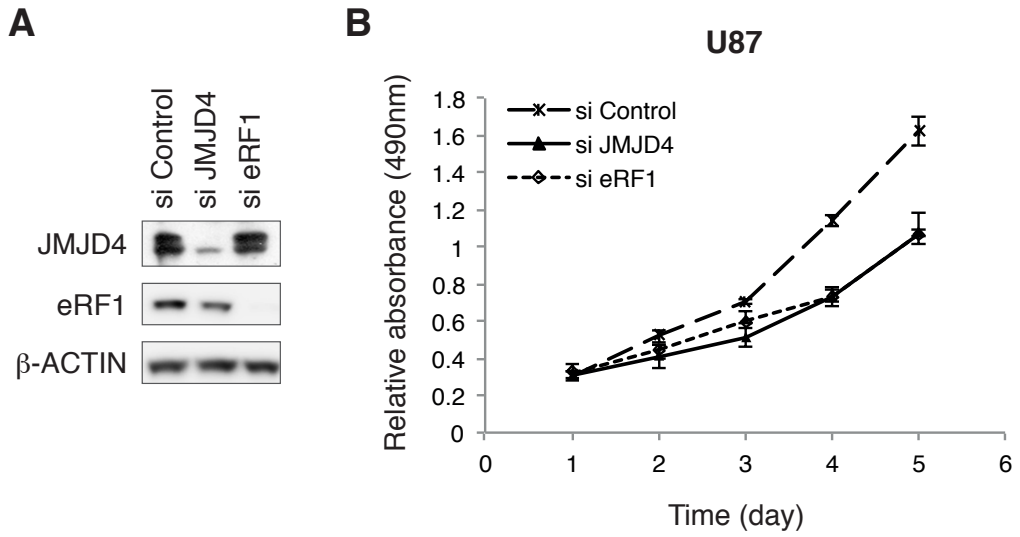


Figure 4.18: JMJD4 is important for U87 cell proliferation. U87 cells were treated with control, JMJD4 or eRF1 siRNA, and seeded into 96-well plates to measure cell proliferation. **A)** Immunoblots of whole cell lysates showing JMJD4 and eRF1 knockdown. **B)** Growth curves of control, JMJD4 and eRF1 knockdown cells, as measured by MTS assay over the span of 5 days. Suppression of JMJD4 and eRF1 expression significantly reduced U87 cell proliferation.

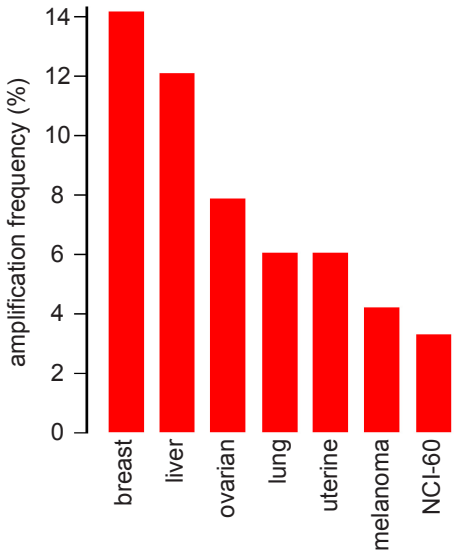


Figure 4.19: *Jmjd4* gene amplification in cancer. Amplification of *Jmjd4* was observed across multiple cancers, in addition to NCI-60 panel of cell lines. Figure obtained using the cBio Cancer Genomics portal (http://www.cbioportal.org; Cerami et al., 2012).

Next, we assessed whether the JMJD4-dependent effect on growth is observed in other culture cell lines. U2OS cells were transfected with siRNA against JMJD4, eRF1 or a non-targeting control sequence, following which cell proliferation was measured using the MTS or CyQUANT cell proliferation assay. Knockdown of both JMJD4 and eRF1 effectively suppressed the proliferation of U2OS cells (Figure 4.16). Similarly, a requirement for JMJD4 was observed for the proliferation of Hep3B and U87 cells (Figures 4.17 and 4.18). Though growth was only moderately inhibited in U87 cells, the effect of JMJD4 on growth was comparable to that of eRF1 (4.18). These results indicate that the expression of JMJD4 plays an important role in cell growth in culture.

Mutations or altered expression of genes involved in growth contributes to the dysregulation of cell growth in cancer (Hanahan and Weinberg, 2000). Results from cultured cell lines showed a requirement for JMJD4 in cell growth *in vitro*. Therefore, we tested whether JMJD4 is abnormally altered in cancer. The cBio Cancer Genomics portal (http://www.cbioportal.org; Cerami et al., 2012) was used to visualise any genetic changes in JMJD4 in more than 10,000 tumour samples from 48 cancer studies. Interestingly, the *Jmjd4* gene was amplified in 3-14% of tumour samples across multiple cancer types, including breast, liver, ovarian, lung, uterine, melanomas and cancer cell lines (Figure 4.19). This suggests that the expression of JMJD4 may play a potentially important role in cancer, which is likely related to its requirement in cell growth.

4.3 Discussion

Stop codon decoding by eRF1 is mediated by the apex of its N-domain (Figure 4.1; Bertram et al., 2000). Of the amino acids implicated in stop codon recognition, two highly conserved motifs, NIKS and YCF, are the most critical (Frolova et al., 2002; Seit-Nebi et al., 2002; Kolosov et al., 2005). In chapter 3, JMJD4 was shown to hydroxylate the lysine residue of the NIKS motif. Therefore, JMJD4-catalysed hydroxylation was postulated to facilitate eRF1 stop codon recognition and thereby translational termination.

A dual luciferase reporter system was used to measure translational termination (Grentzmann et al., 1998). The p2luc reporter has been widely employed to study stop codon readthrough and other events of translational recoding (Bidou et al., 2004; Salas-Marco and Bedwell, 2004; Henderson et al., 2006; Wills et al., 2006; Ivanov et al., 2008; Wang et al., 2012). Recoding efficiencies of HIV and antizyme frameshifting measured by the p2luc reporter are in agreement with measurements made using other approaches (Grentzmann et al., 1998). Using the p2luc reporter, we showed that siRNA knockdown of JMJD4 increases readthrough at stop codons embedded within a leaky termination sequence, derived from tobacco mosaic virus (Figure 4.4). Moreover, the effect of JMJD4 on stop codon readthrough was dependent on its catalytic activity (Figure 4.5). In support of the hypothesis that the observed readthrough is mediated *via* eRF1 modification, the hydroxylation of recombinant eRF1 at K63 significantly improved its catalytic efficiency *in vitro* (Figures 4.9 and 4.10).

The knockdown of JMJD4 promoted readthrough at all three stop codons (UAA, UAG and UGA; Figure 4.4). This is in agreement with the proposal that K63 in the NIKS motif contacts the invariant uridine at the first position of a stop codon (Chavatte et al., 2002), and the observation that mutation of the NIKS motif affects termination efficiency at all three stop codons (Frolova et al., 2002; Kryuchkova et al., 2013). Therefore, the lack of stop codon selectivity by JMJD4 is consistent with its effects on translational termination being mediated by eRF1 K63 hydroxylation. Furthermore, the depletion of JMJD4 increased stop codon readthrough at multiple termination sequence contexts (Figures 4.11, 4.12 and 4.13), thus supporting a role for K63 hydroxylation in a fundamental aspect of eRF1 function.

Emerging evidence indicates that regulated stop codon readthrough in eukaryotes is a physiologically relevant mechanism of gene regulation (Geller and Rich, 1980; Xue and Cooley, 1993; Klagges et al., 1996; Steneberg and Samakovlis, 2001; Namy et al., 2002; Freitag et al., 2012; Yamaguchi et al., 2012; Dunn et al., 2013). Studies of regulated stop codon readthrough have been historically restricted to bioinformatic approaches (Namy et al., 2002; Jungreis et al., 2011; Loughran et al., 2014). However, recent tech-

nological advances have led to the development of ribosomal profiling, a powerful technique that can directly measure endogenous translational readthrough (Ingolia et al., 2009; Dunn et al., 2013). Using a list of candidate readthrough genes obtained from ribosome profiling of human foreskin fibroblasts (Dunn et al., 2013), we have shown that JMJD4 inhibition promoted readthrough at the termination sequence contexts of two endogenous genes (Figure 4.13). GSKIP and THY1 are unrelated genes involved in Wnt signalling and cell-cell interactions, respectively (Lin et al., 2009; Haeryfar and Hoskin, 2004; Rege and Hagood, 2006). Unfortunately, it was not possible to investigate the potential C-terminal extensions of endogenous proteins within the time frame of this thesis. The physiological significance of the results obtained from the artefical reporters therefore remains unclear. Nonetheless, our results indicate that JMJD4 expression is implicated in endogenous termination sequence contexts, and further supports our argument that JMJD4 has a global effect on translational termination. To date, three mammalian readthrough candidates, rabbit β-globin, myelin protein zero (MPZ) and Aquaporin 4 (APQ4) have been shown to produce full-length polypeptides containing C-terminal readthrough extensions (Geller and Rich, 1980; Chittum et al., 1998; Yamaguchi et al., 2012; Loughran et al., 2014). It would therefore be of interest to also determine whether JMJD4 inhibition induces readthrough of these candidates at the endogenous level.

In addition to endogenous termination sequences, the suppression of JMJD4 also resulted in stop codon readthrough of nonsense mutations. Using synthetic bicistronic reporters, we showed that the suppression of JMJD4 induced readthrough at premature stop codons associated with cystic fibrosis, muscular dystrophy and colorectal cancer (Figures 4.11 and 4.12). Termination at premature stop codons results in the production of truncated polypeptides, mRNA destabilisation due to nonsense-mediated decay, and consequent gene inactivation (Mendell and Dietz, 2001). There has been a growing interest in pharmacological agents that promote readthrough at premature termination codons, which include aminoglycosides antibiotics and more specifically developed compounds such as PTC124 (Welch et al., 2007; Sweeney, 2009; Floquet et al., 2011b,a).

However, widespread clinical application of aminoglycosides has been prevented due to serious side effects including renal toxicity (Mingeot-Leclercq and Tulkens, 1999), and the efficacy of PTC124 is under debate (Auld et al., 2009). Therefore, there is a demand to discover novel targets and small molecules with potential as readthrough agents. Since JMJD4 is amenable to small molecule inhibition (see Chapter 3), the discovery of eRF1 hydroxylation may provide a novel therapeutic opportunity that warrants further investigation. In the future, it will be necessary to undertake additional experiments to determine whether JMJD4 inhibition can partially rescue the translation of full-length nonsense-mutated endogenous proteins. This may well be possible, since translational termination at premature stop codons is considerably less efficient than at endogenous termination signals (Keeling et al., 2012). Finally, the possibility that JMJD4 inhibition may co-operate with other readthrough agents is of interest.

Given the cofactor requirements of 2OG oxygenase activity, the hydroxylation of eRF1 by JMJD4 may provide a mechanism for the physiological regulation of translational termination. Since eRF1 hydroxylation is essentially complete (see Chapter 3), any regulation must occur as a result of decreased hydroxylation in response to reduced JMJD4 expression or co-factor availability. However, JMJD4 appears to be relatively refractory to endogenous 2OG competitors such as fumarate, or reduced oxygen tension (see Chapter 3). Indeed, our attempts to investigate the effect of hypoxia on translation termination were unsuccessful due to confounding factors associated with the severe oxygen deprivation required to impair JMJD4 activity (data not shown).

A severe defect in global translational termination efficiency is predicted to compromise protein sequence fidelity through aberrant readthrough, destabilise mRNA transcripts by decay, and alter global protein synthesis. Indeed, polysome profile analyses indicate that the knockdown of eRF1 significantly increased the number of ribosomal subunits, and reduced the amount of translating polysomes (Figure 4.14). In comparison to eRF1, the depletion of JMJD4 produced similar, though appreciably smaller changes to the polysome profile (Figure 4.14). The observed polysome phenotype

may be consistent with defective translational initiation. Classically, the inhibition of translational initiation reduces the number of translating ribosomes, and increases the amount of free ribosomes in the cell (Mašek et al., 2011). However, it is important to note that additional characterisations are required to accurately pinpoint the protein synthesis defect behind the observed polysome phenotype.

Translational initiation is considered to be the rate limiting step in mRNA translation, and is tightly controlled by a number of signalling pathways (Sonenberg and Hinnebusch, 2009). Under conditions of stress such as amino acid deprivation, ER stress, viral infection and heme deprivation, the phosphorylation of eIF2α prevents the recycling of initiation factor eIF2 and reduces the rate of global translational initiation (Sonenberg and Hinnebusch, 2009; Spriggs et al., 2010). Furthermore, the reduced rate of cap-dependent translational initiation mediates translational reprogramming, which increases mRNA translation of the stress-response transcription factor ATF4 (Vattem and Wek, 2004). On the other hand, the mammalian target of rapamycin (mTOR) pathway responds to growth and nutrient stimuli, and up-regulates protein synthesis *via* the phosphorylation of multiple translation factors (Ma and Blenis, 2009). For example, the phosphorylation of eIF4E-binding proteins (4E-BPs) by mTOR weakens their binding to eIF4E, and increases eIF4E availability for cap-dependent translational initiation (Sonenberg and Hinnebusch, 2009). It is thus conceivable that aberrant translational termination generates misfolded protein products, which in turn leads to ER stress and eIF2α phosphorylation. However, preliminary experiments indicate that JMJD4 knockdown does not induce eIF2α phosphorylation or activate ATF4 (data not shown). Similarly, JMJD4 knockdown did not inhibit the mTOR pathway (data not shown). Therefore, additional experiments such as gene expression profiling are required to better understand the cellular response to the loss of eRF1 K63 hydroxylation.

Perhaps consistent with the observed changes in protein synthesis, siRNA knockdown of both eRF1 and JMJD4 significantly impaired cell proliferation (Figures 4.15, 4.16, 4.17 and 4.18). However, a direct link between eRF1 hydroxylation and cell

proliferation was not demonstrated. It is possible that JMJD4 hydroxylates other proteins involved in growth, or possesses functions unrelated to its enzyme activity. However, the lack of other high affinity activity-dependent interactors argues against the existence of JMJD4 hydroxylation targets other than eRF1. Future investigations should focus on elucidating the molecular mechanisms by which defective translational termination regulates cell growth control.

Amplification of the *Jmjd4* gene in tumours suggests a possible role in the development of cancer (Figure 4.19). Increased JMJD4 expression may serve to maintain eRF1 hydroxylation in the hypoxic and metabolically imbalanced tumour microenvironment. This is supported by the observation that eRF1 K63 hydroxylation was near complete in all cultured cell lines and clinical tumour samples (see Chapter 3), and that JMJD4 is required for cell proliferation (Figures 4.15, 4.16, 4.17 and 4.18). Since 2OG oxygenases are susceptible to small molecule inhibition, understanding of the link between JMJD4 activity, its role in cell growth and potential relevance to cancer is of significant therapeutic interest.

Chapter 5

Discussions, conclusions and future work

5.1 Introduction

Oxidative modifications catalysed by 2OG oxygenases play important roles in the regulation of gene expression. In addition to epigenetic regulation, gene transcription and mRNA splicing, accumulating evidence suggests that 2OG oxygenases are also involved in the regulation of protein synthesis. This thesis provides additional proof that 2OG oxygenases hydroxylate components of the protein synthesis machinery. We have identified novel catalytic functions for NO66 and JMJD4, two 2OG oxygenases belonging to the JmjC-only family. Chapter 2 describes the biochemical activity of NO66, which catalyses the histidinyl hydroxylation of ribosomal protein L8. Chapter 3 shows that JMJD4 hydroxylates eRF1, the eukaryotic release factor required for translational termination. Chapter 4 details the role of JMJD4 and eRF1 hydroxylation in translational termination. In this chapter, we will be discussing the broader implications of this work, as well as potential future directions.

5.2 Post-translational modifications of the ribosome

Known post-translational modifications of ribosomal proteins include acetylation, methylation, phosphorylation and more (Odintsova et al., 2003; Yu et al., 2005). These modifications are associated with both regulatory and structural functions. A well-characterised example of ribosomal protein modifications is the multi-phosphorylation of RPS6 downstream of the mTOR pathway, in response to growth and mitogen stimulation (Krieg et al., 1988; Ruvinsky and Meyuhas, 2006). Substitution of RPS6 phosphorylation sites with alanine reduces cell size and alters glucose metabolism in mice (Ruvinsky et al., 2005). On the other hand, certain ribosomal protein methylations are proposed to stabilise ribosomal protein-RNA interactions (Clarke, 2013). In yeast, ribosomal protein methylations have been implicated in ribosome biosynthesis and assembly, translational accuracy and growth (Bachand and Silver, 2004; Shirai et al., 2010; Al-Hadid et al., 2014). A role in ribosomal biogenesis has also been reported for ribosomal protein methylations in humans (Ren et al., 2010).

The diversity and scope of post-translational modifications in the ribosome highlight their capacity to regulate ribosome function. The pattern of post-translational modifications in the ribosome is context-dependent and highly regulated (Yu et al., 2005; Ramagopal, 1991). In contrast to the classic notion that the ribosome is an automated machine, the presence of ribosomal protein modifications indicate that it is in fact heterogeneous and dynamic (Xue and Barna, 2012). The discovery of ribosomal protein hydroxylations by 2OG oxygenases further adds to the overall complexity. Ribosomal protein hydroxylations could functionally interact with other post-translational modifications. Additionally, hydroxylations could maintain ribosome structure, facilitate protein synthesis or regulate ribosome biogenesis. Considering that ribosomal proteins are widely methylated at lysine and arginine rich motifs, the potential for ribosomal demethylations by 2OG oxygenases is of interest.

5.3 Post-translational modifications in translational termination

In addition to ribosomal proteins, other protein synthesis factors are also post-translationally modified. Historically, the best studied examples are perhaps the regulation of translational initiation by the phosphorylation of eIF2α, and substrates of the mTOR pathway (see Chapter 4 discussion). In comparison, less is known about post-translational modifications that target translational termination. eRF1 was reported to be glutamine methylated at the GGQ motif of the M domain, by the HEMK2 methyltransferase in complex with its obligate binding partner Trm112 (Figaro et al., 2008; Liger et al., 2011). The GGQ motif is universally conserved across all three domains of life, despite the lack of release factor conservation between prokaryotes and eukaryotes (Graille et al., 2012). The GGQ motif is indispensible for eRF1 function, since it promotes peptidyl bond hydrolysis in the peptidyl transferse centre (Song et al., 2000; Seit-Nebi et al., 2001; Mora et al., 2003). Methylation of the glutamine is similarly conserved, indicating an importance in release factor function (Dinçbas-Renqvist et al., 2000). Mice knockout of HEMK2 is embryonic lethal at day 6.5, though a direct link to translational termination was not demonstrated (Liu et al., 2010). On the other hand, methylation of the GGQ motif has been shown to influence translational termination efficiency in yeast and *E. coli* (Mora et al., 2007; Polevoda et al., 2006). Interestingly, the HEMK2 binding partner Trm112 is also required for the methyltransferase activity of ALKBH8 (Fu et al., 2010), raising the intriguing possibility of cross-talk between tRNA modifications and the GGQ methylation of eRF1.

With the exception of yeast, the regulation of translational termination in eukaryotes remains largely unexplored. Given the emerging importance of regulated stop codon readthrough, translational termination may play a more critical role in translational control than previously realised. However, we were unable to identify a physiological context that modulates JMJD4 hydroxylase activity. This suggests that JMJD4-catalysed eRF1 hydroxylation may act as a housekeeping modification, and

constitutively facilitate stop codon recognition. Alternatively, it is possible that eRF1 hydroxylation mediates stop codon recoding in the termination sequence contexts of a specific subset of genes. Interestingly, translational decoding appears to be a 'hydroxylation hotspot'. OGFO1 hydroxylates RPS23 at a prolyl residue close to the A-site, and its activity has been shown to affect translational accuracy (Loenarz et al., 2014; Singleton et al., 2014). ALKBH8 and TYW5 modify nucleotides at the tRNA anticodon loop (Noma et al., 2010; Fu et al., 2010; van den Born et al., 2011). It is possible that hydroxylations catalysed by these 2OG oxygenases work synergistically to mediate translational recoding under certain physiological contexts. Combined inhibition of JMJD4, OGFOD1, TYW5 and/or ALKBH8 may provide a useful experimental model to test this hypothesis.

5.4 Physiological significance of NO66- and JMJD4-catalysed post-translational hydroxylations

The unique cofactor requirements of 2OG oxygenases provide them with the capability to 'sense' perturbations in the physiological environment, and regulate gene expression accordingly (Figure 5.1). Ever since the landmark discovery of oxygen-dependent HIF hydroxylations, considerable efforts have been invested in search for other oxygen-sensitive, 2OG oxygenase-catalysed modifications. Despite the common requirement for oxygen as a cosubstrate, NO66 and JMJD4 activities are relatively insensitive to inhibition by hypoxia. This is in agreement with findings for FIH and OGFOD1 (Tian et al., 2011; Singleton et al., 2014), and argues against a general function for 2OG oxygenases in oxygen sensing.

However, 2OG oxygenase activities are also intricately connected to other aspects of cell physiology. For example, oxidative radicals are capable of inactivating 2OG oxygenases *via* oxidation of the Fe(II) catalytic core (Masson et al., 2012). On the other hand, the presence of ascorbate facilitates 2OG oxygenase activity by maintaining Fe(II) at

its reduced state (Clifton et al., 2006; Flashman et al., 2010a). Interestingly, FIH is significantly more susceptible to inhibition by hydrogen peroxide in comparison to the PHD enzymes, indicating possible regulation of the JmJC-only enzymes by cellular redox status (Masson et al., 2012). The accumulation of TCA cycle intermediates in pathological situations results in the competitive inhibition of certain 2OG oxygenases, though fumarate hydratase inactivation did not significantly influence JMJD4 activity (discussed in Chapter 3). In addition to being a TCA cycle intermediate, 2OG is also a key component in amino acid synthesis. Therefore, it is possible that metabolism is also involved in the regulation of 2OG oxygenase activities. Even though we were unable to identify a physiological context that inhibits NO66 or JMJD4, other signals such as iron availability, redox status and metabolic changes could modulate these enzymes in ways that are yet to be recognised.

The sensitivity of 2OG oxygenases to physiological perturbations is perhaps linked to their frequent involvement in cell growth and cancer (Figure 5.1). Activation of the HIF signalling pathway has long been associated with angiogenesis, invasion and other adaptive responses in tumours (Semenza, 2010). In contrast, loss-of-function of the TET enzymes is commonly found in cancer, and is associated with poor patient prognosis (Ko et al., 2010; Yang et al., 2012; Huang and Rao, 2014). Certain histone demethylases such as JMJD2C, JARID1B and FBXL10 are overexpressed in cancer and implicated in cell growth (Højfeldt et al., 2013). Similarly, JMJD4 expression is amplified in multiple tumour types, and is required for cell growth in culture (see Chapter 4). Given the susceptibility of 2OG oxygenases to small molecule inhibitions (Rose et al., 2011), JMJD4 may be a promising therapeutic target for cancer and disorders associated with nonsense mutations. However, additional experiments are required to fully characterise the effects of JMJD4 inhibition in normal versus diseased cells.

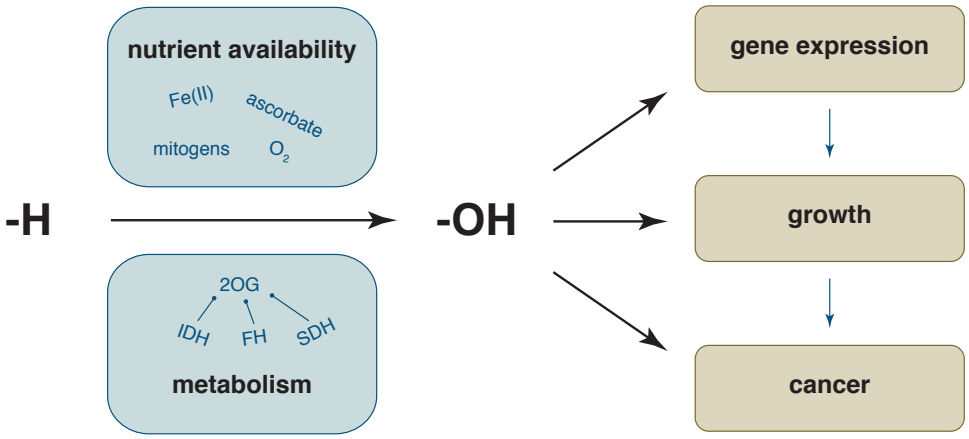


Figure 5.1: The interaction between 2OG oxygenase activity and the physiological environment. Hydroxylations catalysed by 2OG oxygenases are influenced by changes in oxygen tension, metabolism and nutrient availability. Consequently, 2OG oxygenases are able to integrate changes in the physiological stimuli to modulate gene expression, growth and tumourigenesis. IDH = isocitrate dehydrogenase; SDH = succinate dehydrogenase; FH = fumarate hydratase. Inactivation of these enzymes causes the accumulation of TCA cycle intermediates that competitively inhibit 2OG oxygenases.

5.5 Final conclusions

This thesis has shown that JmjC-only oxygenases NO66 and JMJD4 hydroxylate components of the protein synthesis machinery. Our results, together with previously known ribosomal and nucleotide modifications, indicate that 2OG oxygenase-catalysed modifications are prevalent and important in protein synthesis. The activities of these enzymes have been implicated in tRNA synthesis, mRNA metabolism, ribosomal function and translational termination.

In conclusion, the work in this thesis further extends the scope of 2OG oxygenase function in regulated gene expression. Future efforts should focus on characterising the physiological regulation of NO66- and JMJD4-catalysed hydroxylations, and determining the role of ribosomal protein hydroxylations in protein synthesis. The potential regulation of stop codon recoding by JMJD4-catalysed eRF1 hydroxylation is also of interest. Furthermore, elucidating the connections between JMJD4 activity, translational termination and cell growth has practical relevance to the possible involvement of JMJD4 in cancer and disorders associated with nonsense mutations.

Chapter 6

Materials and Methods

6.1 Reagents

Unless specified otherwise, all chemicals and solutions were purchased from Sigma-Aldrich.

6.1.1 Solutions

Milli-Q grade Water Water was purified using the Milli-Q Intergral water purification system (Millipore). Tap water was first passed through a 0.2µm filter followed by an ultrafiltration cartridge (BioPak) to produce ultrapure water, also referred to here as 'Milli-Q grade water'.

Phosphate buffered saline (PBS; 10X) 1.37M NaCl, 27mM KCl, 43mM Na_2HPO_4, 14mM KH_2PO_4, pH adjusted to 7.4. 1X PBS was made by diluting 10X concentrated stock with Milli-Q grade water. 1X PBS-Tween (PBST) was made by adding 0.1% Tween-20 (v/v) to 1X PBS.

Tris-borate-EDTA (TBE) buffer 1X TBE running buffer was made by diluting 10X TBE concentrated stock with Milli-Q grade water to a final concentration of 89mM Tris-borate and 2mM EDTA, pH 8.3.

SDS-PAGE resolving gel buffer (4X) 1.5M Tris-HCl pH 8.8, 0.4% (w/v) SDS.

SDS-PAGE stacking gel buffer (4X) 0.5M Tris-HCl pH 6.8, 0.4% (w/v) SDS.

SDS-PAGE loading buffer (6X) 350mM Tris-HCl pH 6.8, 10% (w/v) SDS, 50% (v/v) glycerol, 0.6M dithiothreitol (DTT), 0.1% (w/v) bromophenol blue.

SDS-PAGE running buffer (10X) 0.25M Tris-base, 1.9M glycerine, 1% (w/v) SDS. 1X SDS-PAGE running buffer was made by diluting 10X concentrated stock in Milli-Q grade water.

Protein transfer buffer (20x) 0.2M Tris-base, 2M glycerine. 1X transfer buffer was made by adding 50ml 20X concentrated stock, 100ml methanol, and Milli-Q grade water to a final volume of 1L.

Jie's lysis buffer 20mM Tris-HCl pH 7.4, 100mM NaCl, 5mM $MgCl_2$, 0.5% (v/v) NP-40. Protease inhibitor (Sigma-Aldrich) and phosphatase inhibitor (Roche) cocktails were added immediately prior to cell lysis.

Polysome buffer (10X) 150mM Tris-HCl pH 7.4, 3M NaCl, 150mM $MgCl_2$. 1X polysome lysis buffer was made by diluting 10X stock concentrate in Milli-Q grade water to volume and adding 1% (v/v) Triton X-100. 1µg ml^{-1} cycloheximide and 10mg ml^{-1} heparin were added to the polysome lysis buffer immediately prior to use.

Passive lysis buffer 1X passive lysis buffer was prepared from 5X passive lysis buffer (Promega) diluted with 4 volumes of Milli-Q grade water.

Ribosome lysis buffer 20mM Tris-HCl pH 7.8, 100mM NaCl, 20mM KCl, 10mM $MgCl_2$, 6mM 2-Mercaptoethanol, 5% (w/v) sucrose, 1% (v/v) Triton-X100.

Ribosome sucrose cushion 20mM pH7.8 Tris-HCl, 100mM NaCl, 20mM KCl, 10mM MgCl2, 6mM 2-Mercaptoethanol, 32% (w/v) sucrose, 1% (v/v) Triton-X100.

Ribosome resuspension buffer 50mM Tris pH 7.8, 5mM $MgCl_2$, 25mM KCl.

3-(4,5-dimethyl-2-yl)-5-(3-carboxymethoxyphenyl)-2-(4-sulfophenyl)-2H- tetrazolium, inner salt (MTS) solution MTS solution was prepared by dissolving 42mg of CellTiter 96® AQueous MTS reagent powder (Promega) in 21ml of Dulbecco's PBS. The solution was pH adjusted to 6-6.5 using 1N HCl, passed through a 0.2µm filter, and aliquoted to store at -20°C protected from light.

Phenazine methosulfate (PMS) solution 0.92mg of PMS was dissolved in 1ml of Dulbecco's PBS. The PMS solution was 0.2µm filtered, and aliquoted to store at -20°C protected from light.

6.2 Bacterial techniques

6.2.1 Solutions and reagents

Luria-Bertani medium (LB) LB medium was made by diluting 20g of LB powder in 1L of Milli-Q grade water, then autoclaved at 121°C and 100kPa for 15 minutes. To make LB agar plates, 15g of agar (Invitrogen) was added to 1L of LB solution. The LB agar solution was autoclaved, then allowed to cool to 60°C prior to the addition of selection antibiotics and pouring of the agar plates.

SOC (Super Optimal Broth) Medium SOC medium was purchased from Life Technologies.

Antibiotics Selection antibiotics were either ampicillin or kanamycin, used at working concentrations of 100µg ml^{-1} and 50µg ml^{-1}, respectively.

6.2.2 Bacterial culture

NEB (New England Biolabs) Turbo Competent *E. coli* cells were used for all cloning purposes.

6.2.3 Transformation

NEB Turbo Competent *E. coli* cells were stored at -80°C and thawed on ice prior to use. For each transformation, 20µl of culture was combined with either 5µl of ligation reaction or 50ng of plasmid DNA. The mixture was gently tapped to mix, and incubated on ice for 30 minutes. The cells were then heat shocked at 42°C for 30 seconds, and rested on ice for 5 minutes before 0.6ml of SOC medium was added to the transformation mixture. The cells were recovered at 37°C, in a shaking incubator at 220 rpm for 1 hour. For plasmid DNA purifications, the transformed cells were directly added to LB solution containing selection antibiotics, and incubated at 37°C overnight. For ligation reactions, the cells were spun at 5000 rpm for 30 seconds following which the supernatant was decanted, and the bacteria pellet was plated onto agar plate containing selection antibiotics. The bacteria were either cultured at 37°C for 10 hours, or 32°C for 16 hours to allow colony formation.

6.2.4 Plasmid DNA purification

Small-scale plasmid DNA isolation from transformed *E. Coli* cells was performed using GeneJET Plasmid Miniprep kit (Thermo Scientific), and large-scale plasmid DNA purification was carried out using GeneJET Plasmid Maxiprep kit (Thermo Scientific), both following manufacturer's protocols. Briefly, transformed bacteria were cultured overnight in 4ml or 250ml of LB medium and appropriate selection antibiotics, then lysed in a SDS-alkaline solution. Cell debris was removed by centrifugation, and the cleared lysate was passed through a silica column to allow DNA binding. Plasmid DNA was washed and then eluted from the silica membrane using Milli-Q grade water. Plasmid DNA concentration was determined using the NanoDrop ND-1000 spectrophotometer, by measuring the absorbance at 260nm and 280nm.

6.3 Nucleic acid techniques

6.3.1 Polymerase chain reaction (PCR)

A standard PCR reaction contained 50ng DNA template, 20pM of each primer, 0.2mM dNTPs, 2.5U *Pfu* DNA polymerase (Thermo Scientific), 5µl 10X *Pfu* buffer and Milli-Q grade water to a final volume of 50µl. DNA amplification was performed using a PTC-200 PCR Thermo Cycler (MJ Research). The following program was used: 96°C for 45 seconds, 60°C for 60 seconds, 72°C for 120 seconds per 1kbp of DNA being amplified. After 35 cycles, the DNA sample was visualised using agarose gel electrophoresis.

6.3.2 Agarose gel electrophoresis

Agarose gel was prepared by dissolving 1%, 1.5% or 2% (w/v) agarose in TBE buffer, in addition to 2µg ml^{-1} ethidium bromide. DNA samples were prepared with 1X gel loading dye (6X stock; New England Biolabs), loaded into the agarose gel, and electrophoresed at 100V for small gels, and 120V for large gels.

6.3.3 DNA purification from agarose gel and PCR reactions

Resolved agarose gel was visualised using a UV transilluminator (UV Products), and DNA bands were excised using a scalpel. DNA was purified from the agarose gel using GeneJET gel extraction kit (Thermo Scientific) following manufacturer's protocol. The GeneJET PCR purification kit was used (Thermo Scientific) was used to purify DNA directly from solution, following manufacturer's instructions. Both protocols involve concentration of DNA onto a silica-based column and subsequent elution.

6.3.4 Restriction enzyme digestion

1µg plasmid DNA or 45µl PCR products were digested with 10-20U of High-Fidelity restriction endonucleases (New England Biolabs), in 1X reaction buffer and 100µg ml^{-1} bovine serum albumin (BSA) at a total volume of 20µl or 70µl, respectively. The

digestion reactions were carried out at 37°C and manufacturer's recommended reaction time. If required, 5' ends of digested plasmid DNA were dephosphorylated using 10U calf intestinal alkaline phosphatase (New England Biolabs), incubated at 37°C for 1 hour.

6.3.5 Ligation

Ligation reactions were carried out using 20U T4 DNA ligase (New England Biolabs) in 1X T4 DNA ligase buffer to a final volume of 20µl. PCR products were mixed with digested and dephosphorylated vector at 3:1, 6:1 and 9:1 molar ratios. The ligation reaction was incubated at 1 hour in room temperature, or overnight at 16°C.

6.3.6 Site-directed mutagenesis (SDM)

A standard SDM reaction contained 50ng DNA template, 20pM of each primer, 1mM dNTPs, 2.5U of *Pfu* DNA polymerase (Thermo Scientific), 1X *Pfu* reaction buffer and optional 5% (v/v) DMSO to a final volume of 50µl. Depending on the primer sequence, the SDM reaction was performed at three possible annealing temperatures. The program is as follows: 95°C for 30 seconds, 60°C for 1 minute, 58°C, 60°C or 62°C for 16 minutes for 20 cycles. After DNA amplification, template DNA was digested by adding 40U *Dpn I* to the reaction, and incubated at 37°C for 1 hour. The PCR products were subsequently resolved using agarose gel electrophoresis, and corresponding DNA bands were excised, purified and transformed into NEB Turbo Competent *E. coli* cells.

6.3.7 DNA sequencing

Integrity of the cloned plasmids were validated by DNA sequencing using appropriate primers. Sequencing was performed by Sanger sequencing service (Source Bioscience).

6.3.8 Genotype PCR

The genotype PCR reaction mixture contains 10µl HotStarTaq Master Mix (Qiagen), 2µl lysates prepared from NO66 WT or KO MEFs, 30pM of 3' loxp FW, 3' loxp RV and 5' loxp 1 or 2 primers each, and Milli-Q grade water to make up a total volume of 20µl. The PCR program is as follows: 94°C for 30 seconds, 56°C for 30 seconds, 72°C for 30 seconds. After 25 cycles, the amplified PCR products were visualised using agarose gel electrophoresis on a 2% (w/v) agarose gel. Genotype PCR primer sequences are listed in Table 6.1.

Table 6.1: Oligonucleotide primers used for genotype PCR of NO66 WT and KO MEFs.

Name	Primer (5' - 3')
NO66 3' loxp FW	AGTTTGACCCCTGCACCTTTG
NO66 3' loxp RV	GCCCCGGAAGTACACATTTAATC
NO66 5' loxp 1	TGCCTTCCTTGACCCTGGAA
NO66 5' loxp 2	AGGATTGGGAAGACAATAGCAG

6.3.9 RNA extraction

Total RNA was extracted using the TRIzol® reagent. Growth medium was removed from adherent cells, and the cells were washed twice in ice-cold PBS. Remaining PBS was aspirated, and 1ml of TRIzol® reagent was added to each well of a 6-well plate. The mixture was pipetted up and down to mix, and incubated at room temperature for 5 minutes or freeze-thawed at -80°C. Next, 200µl of chloroform was added to the lysate, which was then mixed by inversion 15 times, and incubated at room temperature for 15 minutes. The mixture was then separated by centrifugation at 13,000 rpm for 15 minutes at 4°C, after which the top phase containing RNA was carefully transferred into a fresh tube. 500µl of isopropanol was added to precipitate the RNA, and incubated at room temperature for 5-10 minutes. The RNA precipitates were sedimented by centrifugation at 13,000 rpm for 10 minutes at 4°C. The RNA pellet was washed using 1ml of 75% ethanol, and sedimented again by centrifugation at 7500 rpm for 5

minutes at 4°C. Residual 75% ethanol was decanted with care, and the RNA pellet was evaporated to dryness on a 30°C heat block. Next, RNA were resuspended in 30µl of Ambion® nuclease-free water (Life Technologies), and incubated at 65°C for 15 minutes on a Thermomixer® (Eppendorf) set at 1000 rpm to remove any secondary structures. Final RNA concentration was determined using the NanoDrop ND-1000 spectrophotometer.

6.3.10 cDNA synthesis

cDNA synthesis was performed using the High-Capacity cDNA Reverse Transcription kit (Applied Biosystems). A standard reaction contained 1µg RNA template, 2µl 10X Reverse Transcription buffer, 4mM dNTPs, 2µl 10X random primers, 50U MultiScribe Reverse Transcriptase, 20U RNAse inhibitor (Applied Biosystems) and Ambion® nuclease-free water (Life Technologies) at a total volume of 20µl. Reverse transcription was performed using a PTC-200 PCR Thermo Cycler (MJ Research) with the following program: 25°C for 10 minutes, 37°C for 120 minutes, then 85°C for 5 minutes to heat inactivate the reverse transcriptase.

6.3.11 Real-time quantitative PCR (RT-qPCR)

RT-qPCR reactions were performed using the StepOnePlus Real Time PCR System (Applied Biosystems).

To quantify JMJD4 mRNA expression, a Taqman®-based qPCR reaction was carried out using 50ng cDNA, 5µl 2X Taqman® Fast Universal PCR master mix (Applied Biosystems), 0.5µl JMJD4 Taqman® probe, 0.5µl control (Cyclophilin A) Taqman® probe, and Ambion® nuclease-free water (Life Technologies) combined to a final volume of 10µl. The qPCR program is as follows: 95°C for 3 seconds, 60°C for 30 seconds, and repeat for 40 cycles. JMJD4 mRNA expression was normalised against Cyclophilin A control, and fold change was determined using the comparative C_t method (Schmittgen and Livak, 2008).

To quantify the relative ratio of firefly to *Renilla* luciferase mRNA expression, a SYBR® Green-based qPCR reaction was carried out using oligonucleotide primers shown in Table 6.2. A standard reaction consisted of 50ng cDNA, 5µl 2X SYBR® Green master mix (Applied Biosystems), 500pM of forward and reverse primers each, and Ambion® nuclease-free water (Life Technologies) combined to a total volume of 10µl. The qPCR program is as follows: 95°C for 15 seconds, 60°C for 1 minute, and repeat for 40 cycles. Fold change in firefly relative to *Renilla* luciferase mRNA expression was calculated using the comparative C_t method (Schmittgen and Livak, 2008).

Table 6.2: Oligonucleotide primers used for RT-qPCR.

Name	Primer (5' - 3')
Firefly luciferase FW	CGTGCCAGAGTCTTTCGACA
Firefly luciferase RV	ACAGGCGGTGCGATGAG
Renilla luciferase FW	AAGAGCGAAGAGGGCGAGAA
Renilla luciferase RV	TGCGGACAATCTGGACGAC

6.3.12 End point reverse transcription PCR (RT-PCR)

RNA was extracted as described in section 'RNA extraction', and treated with Ambion® TURBO DNA-free DNase kit (Life Technologies) prior to reverse transcription to remove traces of transfected plasmid DNA. Briefly, 2U of TURBO DNase was added to the RNA sample with 10X TURBO DNase buffer diluted to volume. The digest was incubated at 37°C for 30 minutes, followed by addition of 0.1 volume of DNase inactivation reaction reagent. The reaction was incubated at room temperature for 5 minutes with occasional mixing, then centrifuged at 11,000 rpm for 1.5 minutes to pellet the DNase inactivation reagent. RNA supernatant was transferred to a fresh tube for cDNA synthesis.

The following primers were used to monitor integrity of the Renilla-stop-firefly mRNA: forward 5'-CAGAAGTTGGTCGTGAGGCA-3' and reverse 5'- TCCAGCGGTTCCATCCTCTA -3'. The end-point RT-PCR reaction contained 50ng cDNA tem-

plate, 0.5U Q5 high-fidelity DNA polymerase (New England Biolabs), 5µl 5X Q5 reaction buffer, 200µM dNTPs, 500pM of forward and reverse primers each, and Ambion® nuclease-free water (Life Technologies) in a total volume of 25µl. The PCR reaction was performed using a PTC-200 PCR Thermo Cycler (MJ Research) with the following program: 98°for 10 seconds, 65°C for 30 seconds, 72°C for 1 minute. After 30 cycles, the PCR products were separated by electrophoresis on a 1.5% (w/v) agarose gel and visualised with a UV transilluminator.

6.4 Mammalian cell culture techniques

6.4.1 Cell culture

All cells were cultured in Dulbecco's Modified Eagle's Medium (DMEM), supplemented with 10% fetal bovine serum (FBS), 2mM L-glutamine, 50 IU ml^{-1} penicillin, 50µg ml^{-1} streptomycin and selection antibiotics if required. Cells were maintained in tissue culture incubators set at 37°C and 5% CO_2.

6.4.2 Hypoxia and DMOG treatments in cell culture

Cells were cultured in INVIVO^2 400 hypoxia workstations (Ruskinn Technology), set at appropriate levels of O_2 and 5% CO_2 balanced with N_2. After 24 hours of hypoxia treatment, cells were harvested inside the hypoxia workstation in the presence of 1mM NOG (Santa Cruz Biotechnology). To inhibit 2OG oxygenase activity, cells were treated with 1mM DMOG (Frontier Scientific) for 24 hours.

6.4.3 Plasmid transfection

For forward transfections, adherent cells were seeded 24 hours prior to transfection to achieve 30-50% confluency at the time of transfection.

For HeLa cells, plasmids were transfected using FuGENE® HD transfection reagent (Promega) following manufacturer's protocol. The transfection mixture was prepared

at a ratio of 500ng of DNA to 1.5µl of FuGENE® HD in 50µl of Opti-MEM® reduced serum medium (Life Technologies), for cells in 1ml of growth medium. Plasmids were first diluted in Opti-MEM® and mixed gently by tapping. Then, the transfection reagent was added to the solution. The mixture was gently tapped to mix and centrifuged at 5000 rpm for 5 seconds, then incubated at room temperature for 30 minutes. During the incubation period, adherent cells were changed into fresh culture medium where possible. The transfection mixture was added dropwise to cell culture and mixed. Cells were returned to standard culture conditions for 24-48 hours prior to analysis.

TurboFect transfection reagent (Fermentas) was used to transfect plasmids into A549 cells. For 1ml of cell culture medium, 500ng of plasmid DNA was mixed with 1µl of turbofect in 50µl of Opti-MEM®. The transfection mixture was incubated for 30 minutes at room temperature, then added dropwise into the growth medium. At 24 hours after transfection, the growth medium was replaced with fresh DMEM to minimise cell toxicity.

6.4.4 siRNA transfection

siRNA was transfected using the Oligofectamine transfection reagent (Life Technologies), following a protocol adapted from manufacturer's recommendations. To minimise siRNA-mediated toxicity, cells were cultured in growth medium without any antibiotics. For cells cultured in 2ml of growth medium, 1µl of siRNA (50µM; final concentration 25pM) was diluted in 200µl of Opti-MEM® reduced serum medium to make up mixture 'A', while 12µl of Oligofectamine transfection reagent were diluted in 48µl of Opti-MEM® medium to make up mixture 'B'. Both mixtures were gently mixed and centrifuged at 5000rpm for 5 seconds. Following 5 minutes of incubation at room temperature, the two mixtures were combined, mixed and spun down. The combined mixture was incubated at room temperature for 40 minutes prior to dropwise addition into growth medium.

Unless specified otherwise, cells were transfected twice at 24-hour intervals to achieve maximal knockdown. Depending on the experiment, both forward and reverse transfections were used. All siRNA were purchased from Sigma-Aldrich, and are listed in Table 6.3.

Table 6.3: siRNA duplexes. Start position denotes approximate sequence start position of the targeted RefSeq sequence, provided by Sigma-Aldrich.

Target transcript	siRNA description	Start position
Negative Control	MISSION® siRNA Universal Negative Control # 2	
JMJD4 (NM_023007)	MISSION® siRNA SASI_Hs01_00053631	475
eRF1 (NM_004730A)	MISSION® siRNA SASI_Hs01_00015827	396

6.4.5 Generation of stable cell lines

Stable expression plasmids were transfected into either HEK293T cells together with packaging vectors, or Phenoix cells using FuGENE® HD transfection reagent as previously described. Growth medium containing the transfection mixture was replaced with fresh DMEM at 24 hours post-transfection. At 72 hours post-transfection, growth medium containing retrovirus was harvested, passed through a 0.45µm filter, and mixed with equal volume of normal growth medium. The combined media was added to cells of interest, which were seeded on the previous day to achieve 30-50% confluency. The cells were incubated in retroviral medium for 24 hours in standard tissue culture conditions, after which the infected cells were recovered in normal growth medium for 24 hours, and then selected using the appropriate antibiotics to establish stable cell lines. In the case of doxycycline-inducible cell lines, they were cultured in medium containing Tet system-approved FBS (Clontech Laboratories) after viral infection. Working concentrations of the selection antibiotics are as follows: puromycin (InvivoGen) 1µg ml^{-1}, blasticidin S (InvivoGen) 5µg ml^{-1}, hygromycin (Roche) 200µg ml^{-1}.

6.4.6 Cell proliferation assays

Cells were seeded into 96-well plates in 100µl of growth medium 24 hours prior to growth assay. HEK293T cells were seeded at 5000 cells per well. A549, U2OS, Hep3B and MEF cells were seeded at 2000 cells per well. HeLa and U87 cells were seeded at 1000 cells per well. Nunc® Edge 96-well plates (Thermo Scientific) were used for MTS assay, and black Nunc® Microwell 96-well Optical-Bottom plates (Thermo Scientific) were used for CyQUANT® assay to minimise fluorescence bleed-through.

To measure cell growth using the MTS assay, frozen aliquots of MTS solution were mixed with PMS solution at a ratio of 4ml MTS to 200µl phenazine methosulfate (PMS). 20µl of the combined solution was added to each well. The plates were then incubated under standard tissue culture conditions for 1 hour in the case of HEK293T, HeLa and U87 cells, and 2 hours in the case of A549, U2OS, Hep3B and MEF cell lines. Results were quantified by measuring the solution absorbance at 490nm using the FLUOstar Omega microplate reader (BMG Labtech). Cell proliferation was followed for 5 days to obtain the growth curve. Average absorbance was calculated from triplicates, subtracted from blank (growth medium only), and plotted in Microsoft Excel 2013 to visualise cell growth.

Cell growth was quantified using the CyQUANT® Direct Cell Proliferation Assay (Life Technologies) following manufacturer's instructions. To prepare 15ml of 2X detection reagent, 48µl of CyQUANT® Direct nucleic acid stain was combined with 240µl of CyQUANT® Direct background suppressor I in 11.7ml of PBS. 100µl of detection reagent was added to each well, following which the cells were incubated under standard culture conditions for 1 hour. Cell number was measured by fluorescence using the FLUOstar Omega microplate reader (BMG Labtech), with excitation and emission wavelengths set at 485nm and 530nm, respectively. Cell proliferation was followed for 5 days to obtain the growth curve. Average fluorescence was calculated from triplicates and plotted in Microsoft Excel 2013 to visualise cell growth.

6.4.7 Synthetic lethality screening

Cells were seeded into 96-well plates at a concentration of 5000 cells in 100µl of growth medium per plate. On the following day, normal growth medium was replaced with medium containing anisomycin or sparsomycin, diluted over a range of 0.0001-100µM. The cells were incubated in the presence of anisomycin or sparsomycin under standard tissue culture conditions for 24 hours, following which cell proliferation was assessed using MTS assay as described in the section 'cell proliferation assays'. 490nm absorbance was obtained for each condition in triplicates. The values were averaged, blank corrected and plotted in Microsoft Excel 2013 over the log of antibiotic concentration.

6.4.8 Readthrough reporter assay

Cells were twice transfected with siRNA duplexes as described in section 'siRNA transfections'. At 24 hours after the final siRNA transfection, they were seeded into 12-well plates at a concentration of 0.5 x 10^5 cells per well in 0.5ml of growth medium. Simultaneously, the cells were reverse transfected with p2luc reporter plasmids using FuGENE® HD transfection reagent. On the following day, growth media was replaced with 1ml of fresh media per well. At 48 hours after reporter transfection, the cells were washed with ice-cold PBS, and harvested in 50µl of 1X passive lysis buffer for dual luciferase reporter analysis. Firefly and *Renilla* luciferase signals were measured using the Dual-Luciferase reporter assay system (Promega) with a FLUOstar Omega microplate reader (BMG Labtech). Briefly, 50µl of Luciferase Assay Reagent II (Promega) was injected into each well of a white opaque bottom 96-well microplate containing 5µl of lysate, then firefly luciferase signal was quantified by recording luminescence measurements at 1-second intervals over 12 seconds at a gain of 3600. *Renilla* luciferase signal was measured by injecting 50µl of Stop & Glo Reagent (Promega) in the same well, then luminescence was measured at 1-second intervals over 12 seconds at a gain of 3000. The sum of luminescence over 12 seconds for firefly and *Renilla* luciferase was used to calculate the rate of readthrough, then averaged across triplicate experiments.

6.4.9 Immunofluorescence

HEK293T cells were seeded into 35 mm poly-d-lysine coated glass bottom dishes (MatTek), and allowed to attach overnight to achieve 40-60% confluency. To prepare cells for immunofluorescence, growth medium was aspirated and the cells were rinsed twice in PBS. The cells were fixed by immersing in 4% (w/v) paraformaldehyde for 10 minutes, followed by two washes in PBS. Next, the cells were permeabilised by incubation in PBS containing 0.5% (v/v) Triton X-100 for 10 minutes, followed by two washes in PBS containing 0.5% (v/v) Triton X-100 and 1% (w/v) BSA (PBSTB). The permeabilised cells were incubated in primary antibodies diluted in PBSTB as follows: rabbit anti-eRF1 (Sigma-Aldrich) 1:250; mouse anti-FLAG clone M2 (Sigma-Aldrich) 1:500. Following 1 hour of primary antibody incubation, the cells were washed three times in PBSTB, and incubated with secondary antibodies conjugated with Alexa Fluor dyes for 1 hour protected from light. The secondary antibodies are as follows: anti-mouse Alexa Fluor 594 (Life Technologies) and anti-Rabbit Alexa Fluor 488 (Life Technologies), both diluted by 1:500 in PBSTB. Following secondary antibody incubation, the cells were washed three times in PBSTB and two times in PBS. The cells were mounted using Vectashield® mounting medium with DAPI (4',6-diamidino-2-phenylindolel; Vector Labs) to visualise the nuclei.

6.4.10 Microscopy imaging

Confocal fluorescence images were taken with a Zeiss LSM510 MetaHead confocal microscope using LSM 510 software v4.2 (Carl Zeiss GmbH). Widefield fluorescence images were visualised using a Nikon wide-field TE2000U microscope, and acquired with a Hamamatsu C4742-96 low-noise B&W CCD camera using IPLab software version 3.7.

6.4.11 Preparation of cell lysates

Adherent cells were washed twice with ice-cold PBS, then harvested in ribosome lysis buffer for ribosomal protein purification, passive lysis buffer for readthrough reporter assays, and Jie's lysis buffer for all other immunoblotting and immunoprecipitation experiments. All lysis buffers were supplemented with 1X protease inhibitor cocktail immediately prior to harvest. 100µl of lysis buffer per well was added to 6-well plates, and 50µl of lysis buffer per well was added to 12-well plates. For immunoprecipitation and ribosomal protein purification, 1ml of lysis buffer was added to a 15cm^2 dish. Cells were scraped into lysis buffer on ice. Following a freeze-thaw cycle, insoluble cell debris were pelleted by centrifugation at 13,000 rpm for 15 minutes at 4°C.

6.4.12 Polysome profile analysis

Polysome profiling protocol was adapted from Professor Anne Willis (MRC Toxicology, University of Leicester).

Sucrose gradients were prepared from seven different solutions containing 10%, 18%, 26%, 34%, 42%, 50% or 60% (w/v) sucrose in 1X polysome buffer supplemented with 100µg ml^{-1} cycloheximide and 1mg ml^{-1} heparin. The sucrose solutions were layered in 25x89mm open-top polyallomer tubes (Seton Scientific) in the order of decreasing sucrose concentration, at a volume of 1.7ml for 60% sucrose, and 5.5ml for all other sucrose concentrations. The centrifuge tubes were placed in dry ice, and each sucrose layer was frozen solid prior to the addition of the next layer. The frozen sucrose gradient was stored at -80°C, and thawed overnight at 4°C prior to the polysome profiling experiments.

HeLa cells were transfected with siRNA duplexes as described, and incubated in standard tissue culture conditions for 48 hours to achieve 50-70% confluency. At two hours prior to harvest, the growth medium was replaced with fresh DMEM to stimulate protein translation. Cycloheximide was added to the growth medium at a final concentration of 100µg ml^{-1} to inhibit polysome run-off. Following 15 minutes of incubation

in cycloheximide, the growth medium was decanted and the cells were washed twice in ice-cold PBS. Next, the cells were scraped into polysome lysis buffer; 1ml of polysome lysis buffer was used for a single 15cm^2 plate. The cells were lysed by passing through a homogeniser for 15 strokes, then insoluble debris were pelleted by centrifugation at 13,000 rpm for 1 minute in a pre-chilled centrifuge at 4°C. RNA concentration in the polysome lysates was approximated using the NanoDrop ND-1000 spectrophotometer.

Samples were equalised based on the estimated RNA concentrations, and gently loaded onto the sucrose gradient without disrupting the gradient itself. The centrifuge tubes were placed in the swing buckets of a SW28 rotor (Beckman Coulter), and centrifuged at 28,000 rpm for 5 hours at 4°C in vacuum. Following ultracentrifugation, the centrifuge tube was mounted onto the tube piercer of a density gradient fractionator (Teledyne Isco). The bottom of the tube was pierced with a needle, and Fluorinert® FC-40 was pumped upwards at a constant flow (6ml min^{-1}) to push the sucrose gradient upwards through the optical unit of a UA-6 detector (Teledyne Isco). OD at 254nm was monitored and recorded to generate a continuous absorbance profile.

6.5 Protein techniques

6.5.1 Relative protein quantitation

Protein concentration in cell lysates were quantified using the Pierce BCA protein assay kit (Thermo Scientific) following manufacturer's protocols. 5µl of cell lysates were aliquoted into each well of a clear, U-bottom 96-well plate (Falcon). Working reagent was made by mixing BCA reagent A (containing bicinchoninic acid, sodium bicarbonate, sodium carbonate and sodium tartrate in alkaline solution) with BCA reagent B (4% v/v copper sulfate) at a ratio of 50:1. 40µl working reagent was aliquoted into each well, following which the plate mixed and incubated at 37°C for 30 minutes. Protein concentration was quantified using the FLUOstar Omega microplate reader (BMG Labtech) by measuring solution absorbance at 562nm. The absorbance values

were blank corrected using the lysis buffer control for relative protein quantitation.

6.5.2 Sodium dodecyl sulfate polyacrylamide gel electrophoresis (SDS-PAGE)

SDS-PAGE was performed using the Mini-PROTEAN® 3 apparatus (Bio-Rad). Polyacrylamide gels were hand-casted using Mini-PROTEAN® Tetra handcast systems (Bio-Rad). Resolving gel contained 1X SDS-PAGE resolving gel buffer (diluted from 4X) with 10 or 15% acrylamide (diluted from 30% acrylamide/bis-acrylamide solution; Bio-Rad). Stacking gel contained 1X SDS-PAGE stacking gel buffer (diluted from 4X) with 3.9% acrylamide (diluted from 30% acrylamide/bis-acrylamide solution; Bio-Rad). All gels contain 0.1% (w/v) SDS. Polymerisation was catalysed by the addition of ammonium persulfate (APS; 0.1% w/v) and Tetramethylethylenediamine (TEMED; 0.1% v/v).

Protein samples were prepared in 1X SDS-PAGE loading buffer, and heated at 90°C for 10 minutes prior to loading. Protein samples were loaded alongside PageRuler Plus prestained protein ladder (Thermo Scientific) to visualise the molecular weights. The gels were electrophoresed at a constant voltage of 110V in 1X SDS-PAGE running buffer, following which they were washed with Milli-Q grade water, and either immunoblotted or stained using Imperial Protein Stain (Thermo Scientific) following manufacturer's instructions.

6.5.3 Immunoblotting

Protein resolved using SDS-PAGE were electroblotted onto Immbilon-P polyvinylidene fluoride (PVDF) microporous membrane (Millipore) using the Mini Trans-Blot® cell (Bio-Rad). The polyacrylamide gel and PDVF membrane were equilibrated using 1X protein transfer buffer. The transfer casette was assembled by layering the gel and the membrane between 3MM chromatography papers (Whatman) and foam pads (Bio-Rad) while submerged in 1X protein transfer buffer to minimise the introduction of

any air bubbles. The assembled transfer cassette, together with an ice block, was placed inside the transfer tank filled with 1X protein transfer buffer, and transferred at a constant current of 100mA for 60 minutes. Quality of the protein transfer was assessed by Ponceau S staining.

The transferred membrane was blocked in PBST with 5% (w/v) milk for 1 hour at room temperature. The membranes were subsequently probed with primary antibodies diluted in blocking solution. All antibodies are listed in Table 6.4. The membranes were incubated in primary antibody for at least 1 hour in room temperature, or overnight at 4°C. After primary antibody incubation, the membranes were washed three times in PBST for 5 minutes each. Next, the membranes were incubated in blocking solution containing horseradish peroxidase (HRP)-conjugated secondary antibody diluted at a ratio of 1:2000, for 60 minutes at room temperature. The membranes were washed again in PBST for 3X 5 minutes, and bound antibodies were visualised using SuperSignal West Dura or Femto chemiluminescent substrates (Thermo Scientific) on a BioSpectrum AC imaging system (UV Products). All incubation and washing steps were performed on a rocker.

6.6 Proteomic techniques

6.6.1 SILAC (Stable Isotopic Labelling of Amino acids in Cell culture)

Cells were passaged in SILAC media (PAA) supplemented with 10% (v/v) dialysed fetal bovine albumin (Appleton), 2mM L-glutamine, 50 IU ml^{-1} penicillin, 50µg ml^{-1} streptomycin, and either heavy (U-13C6; Lys6, Cambridge Isotope Laboratories) or light (normal isotope) isotopic forms of L-Lysine (0.68µM) and L-Arginine (0.54µM). The cells were pulse labelled for 24 hours, then harvested for eRF1 or RPL8 purification and mass spectrometry analysis.

Table 6.4: Antibodies for immunoblotting.

Antigen	Antibody	Dilution	Source
NO66	mouse mAb	1:4	In house (Eilbracht et al., 2004)
RPL8	goat pAb	1:1,000	Abcam (ab63941)
MINA53	rabbit pAb	1:1,000	Abcam (ab37175)
JMJD4	mouse mAb	1:50	In house (generated by Helen Turley)
JMJD4	rabbit pAb	1:1,000	Sigma-Aldrich (HPA027260)
eRF1 (B-11)	mouse mAb	1:1,000	Santa Cruz (sc-365686)
eRF1	rabbit pAb	1:1,000	Sigma-Aldrich (E8156)
eRF3	rabbit pAb	1:1,000	Sigma-Aldrich (E4781)
HIF1α	mouse mAb	1:1,000	BD Transduction Labs (610959)
FIH	mouse mAb	1:200	In house (Stolze et al., 2004)
PSR (N-20)	goat pAb	1:1,000	Santa Cruz (sc-11632)
HRP-conjugated antibodies			
β-Actin	mouse mAb	1:25,000	Abcam (ab49900)
HA	mouse mAb	1:4,000	Sigma (H6533)
FLAG (M2)	mouse mAb	1:3,000	Sigma (A8592)
Anti-mouse	goat pAb	1:2,000	Dako (P0447)
Anti-rabbit	swine pAb	1:2,000	Dako (P0399)
Anti-goat	rabbit pAb	1:2,000	Dako (P0449)

6.6.2 Immunoprecipitation

Cells were lysed in Jie's buffer as described in section 'preparation of cell lysates'.

NO66 proteomic pulldown was performed by adding anti-HA affinity resin or control anti-V5 affinity resin to lysates from HEK293T cells overexpressing empty vector control or HA-NO66. JMJD4 proteomic pulldowns from HEK293T cells overexpressing empty vector control, FLAG-JMJD4 or FLAG-H189A JMJD4 were performed by adding anti-FLAG affinity resin to cell lysates. Immunopurification of overexpressed eRF1/eRF3 complex from HEK293T cells transfected with V5-eRF1 and HA-eRF3 in the presence or absence of FLAG-JMJD4 was performed by adding anti-V5 affinity resin to clear cell lysates. In all three instances, affinity resins were added at a ratio of 10µl bed volume of beads to 1ml of cell lysates. The immunoprecipitation samples were mixed on a rotator overnight at 4°C, following which the beads were washed five times with 1-2ml of Jie's lysis buffer, with sedimentation carried out in between by brief centrifugation. After the last wash, lysis buffer was removed as completely as possible without any loss of beads. The immunoprecipitate samples were eluted using 10 bed

volumes of ammonium hydroxide (0.5M NH_4OH with 0.5mM EDTA). Eluted proteins were concentrated using methanol-chloroform precipitation for in-solution digestion.

To immunoprecipitate endogenous eRF1 from cultured cells, cells were cultured in two $15cm^2$ plates until confluent, then harvested in Jie's lysis buffer as previously described. In the case of tissue and tumour samples, they were frozen, smashed, homogenised in Jie's lysis buffer, and centrifuged to pellet any insoluble debris. Next, 20µg of mouse anti-eRF1 antibodies (Santa Cruz Biotechnology) were added to each sample, and mixed on a rotator at 4°C overnight. On the following day, 15µl bed volume of fast flow protein G-agarose beads (Upstate Biotechnology) were added to each sample, and mixed on a rotator at 4°C for 1h to allow antibody binding. Next, the agrose beads were washed five times with 1-2ml of Jie's lysis buffer, with sedimentation by centrifugation between each step. The immunoprecipitates were eluted in 40µl 2X SDS-PAGE sample buffer by boiling and vortex mixing, then resolved using SDS-PAGE for in-gel digestion.

6.6.3 Methanol-chloroform precipitation

To purify proteins using methanol-chloroform extraction, 400µl of methanol was added to 100µl of sample and immediately mixed by vortexing. Next, 100µl of chloroform was added to the mixture followed by 300µl of Milli-Q grade water, with vortex mixing between each step. The sample was centrifuged at 13,000 rpm for 5 minutes to separate, and the top phase was discarded. 400µl of methanol was subsequently added to the sample, which was immediately vortex mixed and centrifuged at 13,000 rpm for 3 minutes to pellet the protein precipitates. The remaining methanol was aspirated, and the protein pellet was dried completely using a vacuum centrifuge. The proteins were then resuspended in 20µl of 6M urea in 100mM pH 7.8 Tris-HCl for in-solution digest.

6.6.4 Purification of ribosomal proteins

Cells were cultured until 90% confluency in 8-10 15cm^2 plates, following which they were lysed in ribosome lysis buffer as described in section 'preparation of cell lysates'. Mouse liver was pulverised in liquid nitrogen and homogenised in ribosome lysis buffer. Clarified cell lysates were passed through a 45µm filter, and the filtrate was carefully loaded onto 25ml of ribosome sucrose cushion in a 25x89mm open-top polyclear tube (Seton Scientific). The tubes were placed into the swing buckets of a SW28 rotor (Beckman Coulter), and centrifuged at 28,000 rpm for 3 hours at 4°C in vacuum. Following ultracentrifugation, the supernatant was decanted to leave the crude ribosome pellet. The ribosomes were resuspended in 1ml of ribosome resuspension buffer, and pipetted up and down to mix. 5µl of 1M $MgCl_2$ was quickly added to the solution, and mixed by vortex. Next, 0.7ml of ethanol was added to the solution, mixed by vortex, and then centrifuged at 7000 rpm for 2 minutes at 4°C. The resultant ribosome pellet was resuspended in 250µl of ribosome resuspension buffer, following which 25µl of 1M $MgCl_2$ and 550µl of glacial acetic acid was added to the mixture, with vortex mixing between each addition. The mixture was rotated at 4°C for 45 minutes to precipitate the RNA. RNA precipitates were sedimented by centrifugation at 10,000 rpm for 10 minutes at 4°C. The resulting supernatant was transferred into fresh tubes and incubated with 4 volumes of ice-cold acetone for 2 hours at -20°C to precipitate the ribosomal proteins. Precipitated proteins were sedimented by centrifugation at 10,000 rpm for 10 minutes at 4°C. The protein pellet was washed in 1ml of ice-cold acetone, and centrifuged again at 10,000 rpm for 10 minutes. Remaining acetone was aspirated, and the protein pellet was evaporated into dryness using a vacuum centrifuge.

The dry protein pellet was resuspended in 100µl of solution containing 2% (v/v) acetic acid and 10% (v/v) acetonitrile, and loaded onto a Vydac214TP C4 250mmx4.6mm HPLC column (Grace discovery). The column was pre-equilibrated with 10% acetonitrile and 90% H_2O, with 0.1% trifluoroacetic acid. The proteins were separated using the following gradient: 10% acetonitrile at 0-10 minutes, 10-20% acetonitrile from 10-

25 minutes, and 20-43% acetonitrile from 25-180 minutes, at a flow rate of 1ml/min in 0.1% trifluoroacetic acid. Protein absorbance was measured at 214nm, and fractions between 95 and 130 minutes were collected at 1.5 minute intervals. The fractions were dotted onto a PDVF membrane, then blocked and immunoblotted with a goat anti-RPL8 antibody (Abcam). HPLC fraction containing RPL8 was first dried in a vacuum centrifuge, then resuspended in 40µl of 6M urea in 100mM pH 7.8 Tris-HCl for tryptic digest and mass spectrometry analysis.

6.6.5 In-gel protein digestion

Protein samples were resolved using SDS-PAGE and stained as described in section 'SDS-PAGE'. The protein band of interest was excised using a scalpel and sliced into $1mm^2$ cubes. The gel pieces were washed twice and resuspended in the wash solution (50% v/v methanol and 5% v/v acetic acid), and rotated at 4°C overnight. On the following day, the wash solution was replaced and the gel pieces were rotated for additional 5 hours. After the wash solution was aspirated, 200µl acetonitrile was added to dehydrate the gel pieces. Complete dehydration occurs after approximately 5 minutes with occasional vortexing, following which acetonitrile was aspirated, and the gel pieces were rehydrated using 30µl of 10mM DTT in 100mM NH_4HCO_3. Following 30 minutes of incubation in 10mM DTT, remaining DTT solution was removed and 30µl of 100mM iodoacetamide in 100mM NH_4HCO_3 was added to carmaidomethylate the reduced disulfide bonds. Following 30 minutes of incubation, remaining solutions were removed from the samples. Next, the gel pieces were dehydrated in 200µl acetonitrile, rehydrated in 200µl 50mM NH_4HCO_3, and dehydrated again in 200µl acetonitrile. The remaining acetonitrile was aspirated after the last dehydration step, and the gel pieces were dried completely in a vacuum centrifuge. For in-gel protein digestion, proteomics grade trypsin singles or 1µg of sequencing grade Arg-C (Roche) were resuspended in 30µl of freshly prepared 50mM NH_4HCO_3, and added to the sample to rehydrate the gel pieces. The digests were incubated overnight at 37°C. On the following day, digested

peptides were eluted by incubation in 30µl of 50mM NH_4HCO_3 for 10 minutes with occasional vortexing, followed by two additional elutions in 30µl of extraction buffer (80% v/v acetonitrile and 5% v/v acetic acid), and a final elution in 20µl acetonitrile. The eluted fractions were pooled together, dried in a vacuum centrifuge, and resuspended in 16µl of solution containing 2% (v/v) acetonitrile and 0.1% (v/v) formic acid for LC-MS/MS.

6.6.6 In-solution protein digestion

To digest proteins in-solution, 2µl of 200mM DTT in 100mM Tris-HCl, pH 7.8 was added to the protein sample, and incubated at room temperature for 1 hour. Next, 8µl of 200mM iodoacetamide in 100mM Tris-HCl, pH 7.8 was added to the sample, which was vortex mixed and incubated for another hour at room temperature. Following the incubation step, 8µl of 200mM DTT was added to consume any remaining iodoacetamide, and the sample was incubated at room temperature for 30-60 minutes. Subsequently, Milli-Q grade water was added to the sample to reduce urea to a final concentration of 0.6M. Trypsin singles were resuspended in 20µl of 50mM NH_4HCO_3 and added to the sample. The digest was incubated at 37°C overnight. On the following day, the digested peptides were purified using the Pierce PepClean C18 spin column (Thermo Scientific) according to manufacturer's protocol. The final elutant was evaporated using a vacuum centrifuge, and resuspended in 20µl of buffer containing 2% acetonitrile (v/v) and 0.1% (v/v) formic acid for LC-MS/MS analysis.

6.6.7 Mass Spectrometry analysis using Thermos LTQ Orbitrap Velos

Dr. Benedikt Kessler, Dr. Nicola Ternette and Dr. Roman Fischer at Target Discovery Institute, University of Oxford operated the instrument.

Digested samples were analysed by LC-MS/MS on a nanoAcquity system (Waters) coupled to LTQ Orbitrap Velos mass spectrometer (Thermo Scientific), at a resolution

of 30,000. Samples were loaded onto a 75µm I.D. x 25cm C18 nanoAcquity UPLC column (Waters) with 1.7µm particle size. The peptides were separated by a linear gradient of 1-40% acetonitrile, at a flow rate of 250 nl min^{-1} for 120 minutes. Top 20 peptides were selected and MS/MS spectra were acquired in CID mode. ProteoWizard MSConvert software (http://proteowizard.sourceforge.net) was used to extract 200 most intense MS/MS peaks from raw files to generate MGF files. For MS/MS analysis, data was searched against the IPI human database (version 3.87, 91464 entries) in Mascot (http://www.matrixscience.com) version 2.3.01. The search allowed 5ppm/0.1 Da mass deviations and one miscleavage. The search included cysteine carbamidomethylation as a fixed modification. Variable modifications included oxidation of methionine and histidine or lysine, and deamidation of asparagine and glutamine. Proteomic candidate searches were additionally processed using the Central Proteomics Facilities Pipeline (Trudgian et al., 2010).

Raw LC-MS/MS data generated by the Thermos LTQ Orbitrap Velos mass spectrometer were analysed using Xcalibur software version 2.1 (Thermo Scientific). Expected peptide m/z values were calculated using ProteinProspector version 5.12.3 (Mass Spectrometry Facility, UCSF), and were used to extract ion chromatograms with a mass tolerance of ±5 ppm. Hydroxylation levels were approximated based on relative quantitation of elution peak heights.

6.7 Other techniques

6.7.1 *In vitro* hydroxylation assays

In vitro NO66 peptide hydroxylation assays and related reagent preparations were carried out by Dr. Wei Ge (Chemistry Research Laboratory, University of Oxford).

Recombinant JMJD4 was prepared by Dr. Luke Yates (Division of Structural Biology, University of Oxford) and Dr. Sarah Wilkins (Chemistry Research Laboratory, University of Oxford). Recombinant eRF1 was prepared by Dr. Mathew Coleman

(School of Cancer Sciences, University of Birmingham).

Small-scale *in vitro* eRF1 hydroxylation reactions were initiated by the addition of 200ng recombinant His-JMJD4 to 2µg of recombinant His-eRF1 in 200µl of assay buffer containing 50mM Tris-HCl pH 7.4, in the presence or absence of 0.8mM L-ascorbate, 16µM $FeSO_4$, 160µM 2OG, 1mM DTT and 1mM NOG, as specified by the experimental conditions. The mixture was incubated at 37°C for an indicated amount of time, after which the reaction was quenched with 0.1% (v/v) formic acid. Proteins were purified from the reaction mixture using methanol-chloroform precipitation, and resuspended for in-solution digest followed by mass spectrometry.

Large-scale hydroxylation reactions and subsequent eRF1 purifications were carried out by Dr. Mathew Coleman (School of Cancer Sciences, University of Birmingham). Briefly, bacterial pellets expressing recombinant JMJD4 or eRF1 were lysed in 50mM Tris-HCl pH 8, 200mM KCl, 0.5% (v/v) Triton-X-100, 10% (v/v) glycerol, 0.2mg/ml lysozyme, 1X protease inhibitors and 6mM 2-mercaptoethanol. The bacterial lysates were sonicated, and then centrifuged at 13,000 rpm for 20 minutes at 4°C to remove insoluble materials. Supernatants containing JMJD4 were mixed with that of eRF1 at a ratio of 1:10, and allowed to react for 16 hours at room temperature in the presence of 10mM 2OG and 80µM Fe(II). eRF1 was subsequently purified using a two-step chromatography method involving Ni-NTA and MonoQ columns. *In vitro* reconstituted translational termination experiments were performed by Dr. Elizaveta Sokolova (Engelhardt Institute of Molecular Biology, the Russian Academy of Sciences). The *in vitro* reconstituted translation system was performed as described in Alkalaeva et al. (2006), and discussed in detail in Chapter 4.

6.7.1.1 Statistical analyses

Readthrough reporter data were analysed using IBM SPSS Statistics software version 21.0. Paired two-tailed Student's t-test was performed for single comparisons. For multiple comparisons, analysis of variance (ANOVA) was performed followed by Dunnett's or Bonferroni post-hoc analysis. All results are presented as mean ± SEM.

6.8 Plasmids and oligonucleotide primers

6.8.1 oligonucleotides primers used for construction of plasmids

All oligonucleotide primers were custom synthesised by Sigma-Aldrich.

Table 6.5: Oligonucleotide primers used for cloning.

Name	Primer (5' - 3')
J4HA_TIPz_Asc_F	GCGTTTGGCGCGCCATGGATTACCCATACGATGTTCCAGATTACGCTGACCGCGAGACG
J4HA_TIPz_Sbf_R	AAAATACCTGCAGGCTATGGGGCCGCAGCAGC
E1HA_TIPz_Asc_F	ATGCGTGGCGCGCCATGGATTACCCATACGATGTTCCAGATTACGCTGCGGACGACCCCAGTGCT
E1HA_TIPz_Sbf_R	AAAATACCTGCAGGCTAGTAGTCATCAAGGTCAAA
J4_siRes_SDM_F	CTCTCAGAGACTATATTACTTATTGGAAAGAGTAC
J4_siRes_SDM_R	GTACTCTTTCCAATAAGTAATATAGTCTCTGAGAG
E1_siRes_SDM_F	ACATCTGTACAACAGAGGCTTAAGCTTTATAACAAA
E1_siRes_SDM_R	TTTGTTATAAAGCTTAAGCCTCTGTTGTACAGATGT

Table 6.6: Oligonucleotide primers used for cloning of p2luc readthrough reporters.

Name	Primer (5' - 3')
TMV_TAA_F	TCGACGGCAGGAACACAATAACAATTACAGATTG
TMV_TAA_R	GATCCAATCTGTAATTGTTATTGTGTTCCTGCCG
TMV_TAG_F	TCGACGGCAGGAACACAATAGCAATTACAGATTG
TMV_TAG_R	GATCCAATCTGTAATTGCTATTGTGTTCCTGCCG
TMV_TGA_F	TCGACGGCAGGAACACAATGACAATTACAGATTG
TMV_TGA_R	GATCCAATCTGTAATTGTCATTGTGTTCCTGCCG
CF_W1282X_F	TCGACGACTTTGCAACAGTGAAGGAAAGCCTTTG
CF_W1282X_R	GATCCAAAGGCTTTCCTTCACTGTTGCAAAGTCG
DMD_W3X_F	TCGACGTTCAAAATGCTTTGATGGGAAGAAGTAG
DMD_W3X_R	GATCCTACTTCTTCCCATCAAAGCATTTTGAACG
APC_E853X_F	TCGACGGATAGAAGTTTGTAGAGAGAACGCGGAG
APC_E853X_R	GATCCTCCGCGTTCTCTCTACAAACTTCTATCCG
APC_R1114X_F	TCGACGTCAGAAACAAATTGAGTGGGTTCTAATG
APC_R1114X_R	GATCCATTAGAACCCACTCAATTTGTTTCTGACG
APC_Q1367X_F	TCGACGAAAAGTGGTGCTTAGACACCCAAAAGTG
APC_Q1367X_R	GATCCACTTTTGGGTGTCTAAGCACCACTTTTCG
APC_R1450X_F	TCGACGGCTCAAACCAAGTGAGAAGTACCTAAAG
APC_R1450X_R	GATCCTTTAGGTACTTCTCACTTGGTTTGAGCCG
APC_R2166X_F	TCGACGAATAAAGGCCCATGAATTCTAAAACCAG
APC_R2166X_R	GATCCTGGTTTTAGAATTCATGGGCCTTTATTCG
GSKIP_F	TCGACGTTGAAAAGAGATGGACAGTCATGACTACACTTTTTCCTTTCAG
GSKIP_R	GATCCTGAAAGGAAAAAGTGTAGTCATGACTGTCCATCTCTTTTCAACG
THY1_F	TCGACGGCCACGGATTTCATGTCCCTGTGACTGGTGGGGCCCATGGAGG
THY1_R	GATCCCTCCATGGGCCCCACCAGTCACAGGGACATGAAATCCGTGGCCG

6.8.1.1 Plasmids for expression in mammalian cells

pEF6 Full-length human NO66 WT, NO66 H340A or eRF1 cDNA in pEF6 with C-terminal HA tag. From Dr. Mathew Coleman.

pTRIBz shRNA against NO66 or luciferase control cloned in a modified version of pTRIPz (Open Biosystems), where the IRES-Puro-WRE cassette was replaced by an IRES-Blast-WRE cassette (pTRIBZ; gift from T. Tenev, London). ShRNA control target sites AGCTCCCGTGAATTGGAATCC and GGATTCCAATTCAGCGGGAGCCT; shRNA NO66 target sites ATCACGTTCTTACCTTGATAAG and CTTATCAAGGTAAGAACGTGAG. shRNA design by Dr. Atsushi Yamamoto.

pEF1-V5-HIS Full-length human eRF1 cDNA in pEF1-V5-HIS (Life Technologies). From Dr. Mathew Coleman.

pGIPz Full length human JMJD4 WT, JMJD4 H189A or FIH cDNA with N-terminal 3XFLAG tag, in place of GFP cDNA in pGIPz vector (Open Biosystems). From Dr. Mathew Coleman.

pTIPz Full-length human WT or H189A JMJD4 were cloned into *SbfI/Asc* restriction sites of the pTIPz inducible vector. pTIPz was derived from pTRIPz (Open Biosystems) by removing the RFP expression casette, modified by Dr. Matthew Cockman.

p2Luc Complementary oligonucleotide primers with restriction site overhangs were annealed by heating to 95°C then slowly cooled to room temperature, and ligated into *SalI/BamHI* restriction sites of P2luc (gift from Dr. John F. Atkins).

Bibliography

P. A. Aas, M. Otterlei, P. Ø. Falnes, C. B. Vågbø, F. Skorpen, M. Akbari, O. Sundheim, M. Bjørås, G. Slupphaug, E. Seeberg, and H. E. Krokan. Human and bacterial oxidative demethylases repair alkylation damage in both RNA and DNA. *Nature*, 421(6925):859–863, 2003.

S. Abbas, S. Lugthart, F. G. Kavelaars, A. Schelen, J. E. Koenders, A. Zeilemaker, W. J. van Putten, A. W. Rijneveld, B. Löwenberg, and P. J. Valk. Acquired mutations in the genes encoding IDH1 and IDH2 both are recurrent aberrations in acute myeloid leukemia: prevalence and prognostic value. *Blood*, 116(12):2122–2126, 2010.

J. Adam, E. Hatipoglu, L. O'Flaherty, N. Ternette, N. Sahgal, H. Lockstone, D. Baban, E. Nye, G. W. Stamp, K. Wolhuter, M. Stevens, R. Fischer, P. Carmeliet, P. H. Maxwell, C. W. Pugh, N. Frizzell, T. Soga, B. M. Kessler, M. El-Bahrawy, P. J. Ratcliffe, and P. J. Pollard. Renal cyst formation in Fh1-deficient mice is independent of the Hif/Phd pathway: roles for fumarate in KEAP1 succination and Nrf2 signaling. *Cancer Cell*, 20(4):524–537, 2011.

K. Agger, P. A. Cloos, J. Christensen, D. Pasini, S. Rose, J. Rappsilber, I. Issaeva, E. Canaani, A. E. Salcini, and K. Helin. UTX and JMJD3 are histone H3K27 demethylases involved in HOX gene regulation and development. *Nature*, 449(7163):731–734, 2007.

W. Aik, M. A. McDonough, A. Thalhammer, R. Chowdhury, and C. J. Schofield. Role of the jelly-roll fold in substrate binding by 2-oxoglutarate oxygenases. *Current Opinion in Structural Biology*, 22(6):691–700, 2012.

Q. Al-Hadid, K. Roy, W. Munroe, M. C. Dzialo, G. F. Chanfreau, and S. G. Clarke. Histidine methylation of yeast ribosomal protein Rpl3p is required for proper 60S subunit assembly. *Molecular and Cellular Biology*, 34(15):2903–16, 2014.

E. Z. Alkalaeva, A. V. Pisarev, L. Y. Frolova, L. L. Kisselev, and T. V. Pestova. In vitro reconstitution of eukaryotic translation reveals cooperativity between release factors eRF1 and eRF3. *Cell*, 125(6):1125–1136, 2006.

P. Annunen, T. Helaakoski, J. Myllyharju, J. Veijola, T. Pihlajaniemi, and K. I. Kivirikko. Cloning of the human prolyl 4-hydroxylase α subunit isoform α (II) and characterization of the type II enzyme tetramer. *Journal of Biological chemistry*, 272(28):17342–17348, 1997.

P. Annunen, H. Autio-Harmainen, and K. I. Kivirikko. The novel type II prolyl 4-hydroxylase is the main enzyme form in chondrocytes and capillary endothelial cells, whereas the type I enzyme predominates in most cells. *Journal of Biological Chemistry*, 273(11):5989–5992, 1998.

R. J. Appelhoff, Y.-M. Tian, R. R. Raval, H. Turley, A. L. Harris, C. W. Pugh, P. J. Ratcliffe, and J. M. Gleadle. Differential function of the prolyl hydroxylases PHD1, PHD2, and PHD3 in the regulation of hypoxia-inducible factor. *Journal of Biological Chemistry*, 279 (37):38458–38465, 2004.

J. Aragonés, M. Schneider, K. Van Geyte, P. Fraisl, T. Dresselaers, M. Mazzone, R. Dirkx, S. Zacchigna, H. Lemieux, N. H. Jeoung, D. Lambrechts, T. Bishop, P. Lafuste, A. Diez-Juan, S. K. Harten, P. Van Noten, K. De Bock, C. William, M. Tjwa, A. Grosfield, R. Navet, L. Moons, T. Vandendriessche, C. Deroose, B. Wijeyekoon, J. Nuyts, B. Jordan, R. Silasi-Mansat, F. Lupu, M. Dewerchin, C. Pugh, P. Salmon, L. Mortelmans, B. Gallez, F. Gorus, J. Buyse, F. Sluse, R. A. Harris, E. Gnaiger, P. Hespel, P. Van Hecke, F. Schuit, P. Van Veldhoven, P. J. Ratcliffe, M. Baes, P. Maxwell, and P. Carmeliet. Deficiency or inhibition of oxygen sensor Phd1 induces hypoxia tolerance by reprogramming basal metabolism. *Nature Genetics*, 40(2):170–180, 2008.

D. S. Auld, N. Thorne, W. F. Maguire, and J. Inglese. Mechanism of PTC124 activity in cell-based luciferase assays of nonsense codon suppression. *Proceedings of the National Academy of Sciences*, 106(9):3585–3590, 2009.

F. Bachand and P. A. Silver. PRMT3 is a ribosomal protein methyltransferase that affects the cellular levels of ribosomal subunits. *The EMBO Journal*, 23(13):2641–2650, 2004.

D. Balciunas and H. Ronne. Evidence of domain swapping within the jumonji family of transcription factors. *Trends in Biochemical Sciences*, 25(6):274–276, 2000.

D. Baldridge, U. Schwarze, R. Morello, J. Lennington, T. K. Bertin, J. M. Pace, M. G. Pepin, M. Weis, D. R. Eyre, J. Walsh, D. Lambert, A. Green, H. Robinson, M. Michelson, G. Houge, C. Lindman, J. Martin, J. Ward, E. Lemyre, J. J. Mitchell, D. Krakow, D. L. Rimoin, D. H. Cohn, P. H. Byers, and B. Lee. CRTAP and LEPRE1 mutations in recessive osteogenesis imperfecta. *Human Mutation*, 29(12):1435–1442, 2008.

D. Baldridge, J. Lennington, M. Weis, E. P. Homan, M.-M. Jiang, E. Munivez, D. R. Keene, W. R. Hogue, S. Pyott, P. H. Byers, D. Krakow, D. H. Cohn, D. R. Eyre, B. Lee, and R. Morello. Generalized connective tissue disease in Crtap-/-mouse. *PloS One*, 5(5):e10560, 2010.

J. Barman-Aksözen, C. Béguin, A. M. Dogar, X. Schneider-Yin, and E. I. Minder. Iron availability modulates aberrant splicing of ferrochelatase through the iron-and 2-oxoglutarate dependent dioxygenase Jmjd6 and U2AF(65). *Blood Cells, Molecules, and Diseases*, 51(3): 151–161, 2013.

A. M. Barnes, E. M. Carter, W. A. Cabral, M. Weis, W. Chang, E. Makareeva, S. Leikin, C. N. Rotimi, D. R. Eyre, C. L. Raggio, and J. C. Marini. Lack of cyclophilin B in osteogenesis imperfecta with normal collagen folding. *New England Journal of Medicine*, 362(6):521–528, 2010.

H. Beier and M. Grimm. Misreading of termination codons in eukaryotes by natural nonsense suppressor tRNAs. *Nucleic Acids Research*, 29(23):4767–4782, 2001.

H. Beier, M. Barciszewska, G. Krupp, R. Mitnacht, and H. J. Gross. UAG readthrough during TMV RNA translation: isolation and sequence of two tRNAsTyr with suppressor activity from tobacco plants. *The EMBO Journal*, 3(2):351, 1984.

R. A. Berg and D. J. Prockop. The thermal transition of a non-hydroxylated form of collagen: Evidence for a role for hydroxyproline in stabilizing the triple-helix of collagen. *Biochemical and Biophysical Research Communications*, 52(1):115–120, 1973.

E. Berra, E. Benizri, A. Ginouvès, V. Volmat, D. Roux, and J. Pouysségur. HIF prolyl-hydroxylase 2 is the key oxygen sensor setting low steady-state levels of HIF-1α in normoxia. *The EMBO Journal*, 22(16):4082–4090, 2003.

G. Bertram, H. Bell, D. Ritchie, G. Fullerton, and I. Stansfield. Terminating eukaryote translation: domain 1 of release factor eRF1 functions in stop codon recognition. *RNA*, 6 (09):1236–1247, 2000.

G. Bertram, S. Innes, O. Minella, J. P. Richardson, and I. Stansfield. Endless possibilities: translation termination and stop codon recognition. *Microbiology*, 147(2):255–269, 2001.

L. Bidou, I. Hatin, N. Perez, V. Allamand, J. Panthier, and J. Rousset. Premature stop codons involved in muscular dystrophies show a broad spectrum of readthrough efficiencies in response to gentamicin treatment. *Gene Therapy*, 11(7):619–627, 2004.

T. Bishop, D. Gallagher, A. Pascual, C. A. Lygate, J. P. de Bono, L. G. Nicholls, P. Ortega-Saenz, H. Oster, B. Wijeyekoon, A. I. Sutherland, A. Grosfield, J. Aragones, M. Schneider, K. van Geyte, D. Teixeira, A. Diez-Juan, J. Lopez-Barneo, K. M. Channon, P. H. Maxwell, C. W. Pugh, A. M. Davis, P. Carmeliet, and P. J. Ratcliffe. Abnormal sympathoadrenal development and systemic hypotension in PHD3-/- mice. *Molecular and Cellular Biology*, 28(10):3386–3400, 2008.

J.-N. Boeckel, V. Guarani, M. Koyanagi, T. Roexe, A. Lengeling, R. T. Schermuly, P. Gellert, T. Braun, A. Zeiher, and S. Dimmeler. Jumonji domain-containing protein 6 (Jmjd6) is required for angiogenic sprouting and regulates splicing of VEGF-receptor 1. *Proceedings of the National Academy of Sciences*, 108(8):3276–3281, 2011.

F.-M. Boisvert, S. van Koningsbruggen, J. Navascués, and A. I. Lamond. The multifunctional nucleolus. *Nature Reviews Molecular Cell Biology*, 8(7):574–585, 2007.

B. Bonetti, L. Fu, J. Moon, and D. M. Bedwell. The efficiency of translation termination is determined by a synergistic interplay between upstream and downstream sequences in Saccharomyces cerevisiae. *Journal of Molecular Biology*, 251(3):334–345, 1995.

R. Bordeira-Carriço, A. P. Pêgo, M. Santos, and C. Oliveira. Cancer syndromes and therapy by stop-codon readthrough. *Trends in Molecular Medicine*, 18(11):667–678, 2012.

J. Böse, A. D. Gruber, L. Helming, S. Schiebe, I. Wegener, M. Hafner, M. Beales, F. Köntgen, and A. Lengeling. The phosphatidylserine receptor has essential functions during embryogenesis but not in apoptotic cell removal. *Journal of Biology*, 3:15, 2004.

A. P. Bracken and K. Helin. Polycomb group proteins: navigators of lineage pathways led astray in cancer. *Nature Reviews Cancer*, 9(11):773–784, 2009.

C. P. Bracken, A. O. Fedele, S. Linke, W. Balrak, K. Lisy, M. L. Whitelaw, and D. J. Peet. Cell-specific regulation of hypoxia-inducible factor (HIF)-1α and HIF-2α stabilization and transactivation in a graded oxygen environment. *Journal of Biological Chemistry*, 281(32): 22575–22585, 2006.

M. Brauchle, Z. Yao, R. Arora, S. Thigale, I. Clay, B. Inverardi, J. Fletcher, P. Taslimi, M. G. Acker, B. Gerrits, J. Voshol, A. Bauer, D. Schübeler, T. Bouwmeester, and H. Ruffner. Protein complex interactor analysis and differential activity of KDM3 subfamily members towards H3K9 methylation. *PloS One*, 8(4):e60549, 2013.

G. L. Brien, G. Gambero, D. J. O'Connell, E. Jerman, S. A. Turner, C. M. Egan, E. J. Dunne, M. C. Jurgens, K. Wynne, L. Piao, A. J. Lohan, N. Ferguson, X. Shi, K. M. Sinha, B. J. Loftus, G. Cagney, and A. P. Bracken. Polycomb PHF19 binds H3K36me3 and recruits PRC2 and demethylase NO66 to embryonic stem cell genes during differentiation. *Nature Structural & Molecular Biology*, 19(12):1273–1281, 2012.

R. K. Bruick and S. L. McKnight. A conserved family of prolyl-4-hydroxylases that modify HIF. *Science*, 294(5545):1337–1340, 2001.

W. A. Cabral, W. Chang, A. M. Barnes, M. Weis, M. A. Scott, S. Leikin, E. Makareeva, N. V. Kuznetsova, K. N. Rosenbaum, C. J. Tifft, D. I. Bulas, C. Kozma, P. A. Smith, D. R. Eyre, and J. C. Marini. Prolyl 3-hydroxylase 1 deficiency causes a recessive metabolic bone disorder resembling lethal/severe osteogenesis imperfecta. *Nature Genetics*, 39(3):359–365, 2007.

M. C. Cantarini, S. M. de la Monte, M. Pang, M. Tong, A. D'Errico, F. Trevisani, and J. R. Wands. Aspartyl-asparagyl β hydroxylase over-expression in human hepatoma is linked to activation of insulin-like growth factor and notch signaling mechanisms. *Hepatology*, 44(2): 446–457, 2006.

M. R. Capecchi. Polypeptide chain termination in vitro: isolation of a release factor. *Proceedings of the National Academy of Sciences*, 58(3):1144, 1967.

M. Cassan and J.-P. Rousset. UAG readthrough in mammalian cells: effect of upstream and downstream stop codon contexts reveal different signals. *BMC Molecular Biology*, 2(1):3, 2001.

E. Cerami, J. Gao, U. Dogrusoz, B. E. Gross, S. O. Sumer, B. A. Aksoy, A. Jacobsen, C. J. Byrne, M. L. Heuer, E. Larsson, Y. Antipin, B. Reva, A. P. Goldberg, C. Sander, and N. Schultz. The cBio cancer genomics portal: an open platform for exploring multidimensional cancer genomics data. *Cancer Discovery*, 2(5):401–404, 2012.

B. Chang, Y. Chen, Y. Zhao, and R. K. Bruick. JMJD6 is a histone arginine demethylase. *Science*, 318(5849):444–447, 2007.

L. Chavatte, A. Seit-Nebi, V. Dubovaya, and A. Favre. The invariant uridine of stop codons contacts the conserved NIKSR loop of human eRF1 in the ribosome. *The EMBO Journal*, 21(19):5302–5311, 2002.

B. Chen, M. Yu, Q. Chang, Y. Lu, C. Thakur, D. Ma, Z. Yi, and F. Chen. Mdig represses H19 large intergenic non-coding RNA (lincRNA) by down-regulating H3k9me3 and heterochromatin. *Oncotarget*, 4(9):1427, 2013.

H. S. Chittum, W. S. Lane, B. A. Carlson, P. P. Roller, F.-D. T. Lung, B. J. Lee, and D. L. Hatfield. Rabbit β-globin is extended beyond its UGA stop codon by multiple suppressions and translational reading gaps. *Biochemistry*, 37(31):10866–10870, 1998.

R. Chowdhury, N. C. Brissett, T. Krojer, C.-h. Ho, S. S. Ng, I. J. Clifton, W. Ge, N. J. Kershaw, G. C. Fox, J. R. Muniz, M. Vollmar, C. Phillips, E. S. Pilka, K. L. Kavanagh, F. von Delft, U. Oppermann, M. A. McDonough, A. J. Doherty, and C. J. Schofield. Ribosomal oxygenases are structurally conserved from prokaryotes to humans. *Nature*, 510:422–426, 2014.

J. Christensen, K. Agger, P. A. Cloos, D. Pasini, S. Rose, L. Sennels, J. Rappsilber, K. H. Hansen, A. E. Salcini, and K. Helin. RBP2 belongs to a family of demethylases, specific for tri-and dimethylated lysine 4 on histone 3. *Cell*, 128(6):1063–1076, 2007.

M. Cikala, O. Alexandrova, C. N. David, M. Pröschel, B. Stiening, P. Cramer, and A. Bröttger. The phosphatidylserine receptor from Hydra is a nuclear protein with potential Fe (ii) dependent oxygenase activity. *BMC Cell Biology*, 5(1):26, 2004.

S. G. Clarke. Protein methylation at the surface and buried deep: thinking outside the histone box. *Trends in Biochemical Sciences*, 38(5):243–252, 2013.

I. J. Clifton, M. A. McDonough, D. Ehrismann, N. J. Kershaw, N. Granatino, and C. J. Schofield. Structural studies on 2-oxoglutarate oxygenases and related double-stranded β-helix fold proteins. *Journal of Inorganic Biochemistry*, 100(4):644–669, 2006.

P. M. Clissold and C. P. Ponting. JmjC: cupin metalloenzyme-like domains in jumonji, hairless and phospholipase $A_2\beta$. *Trends in Biochemical Sciences*, 26(1):7–9, 2001.

P. A. Cloos, J. Christensen, K. Agger, A. Maiolica, J. Rappsilber, T. Antal, K. H. Hansen, and K. Helin. The putative oncogene GASC1 demethylates tri-and dimethylated lysine 9 on histone H3. *Nature*, 442(7100):307–311, 2006.

M. E. Cockman, N. Masson, D. R. Mole, P. Jaakkola, G.-W. Chang, S. C. Clifford, E. R. Maher, C. W. Pugh, P. J. Ratcliffe, and P. H. Maxwell. Hypoxia inducible factor-α binding and ubiquitylation by the von Hippel-Lindau tumor suppressor protein. *Journal of Biological Chemistry*, 275(33):25733–25741, 2000.

M. E. Cockman, D. E. Lancaster, I. P. Stolze, K. S. Hewitson, M. A. McDonough, M. L. Coleman, C. H. Coles, X. Yu, R. T. Hay, S. C. Ley, C. W. Pugh, N. J. Oldham, N. Masson, C. J. Schofield, and P. J. Ratcliffe. Posttranslational hydroxylation of ankyrin repeats in iκB proteins by the hypoxia-inducible factor (HIF) asparaginyl hydroxylase, factor inhibiting HIF (FIH). *Proceedings of the National Academy of Sciences*, 103(40):14767–14772, 2006.

M. E. Cockman, J. D. Webb, and P. J. Ratcliffe. FIH-dependent asparaginyl hydroxylation of ankyrin repeat domain-containing proteins. *Annals of the New York Academy of Sciences*, 1177(1):9–18, 2009.

M. L. Coleman, M. A. McDonough, K. S. Hewitson, C. Coles, J. Mecinović, M. Edelmann, K. M. Cook, M. E. Cockman, D. E. Lancaster, B. M. Kessler, N. J. Oldham, P. J. Ratcliffe, and C. J. Schofield. Asparaginyl hydroxylation of the Notch ankyrin repeat domain by factor inhibiting hypoxia-inducible factor. *Journal of Biological Chemistry*, 282(33):24027–24038, 2007.

G. L. Cuthbert, S. Daujat, A. W. Snowden, H. Erdjument-Bromage, T. Hagiwara, M. Yamada, R. Schneider, P. D. Gregory, P. Tempst, A. J. Bannister, and T. Kouzarides. Histone deimination antagonizes arginine methylation. *Cell*, 118(5):545–553, 2004.

L. Dang, D. W. White, S. Gross, B. D. Bennett, M. A. Bittinger, E. M. Driggers, V. R. Fantin, H. G. Jang, S. Jin, M. C. Keenan, K. M. Marks, R. M. Prins, P. S. Ward, K. E. Yen, L. M. Liau, J. D. Rabinowitz, L. C. Cantley, C. B. Thompson, M. G. Vander Heiden, and S. M. Su. Cancer-associated idh1 mutations produce 2-hydroxyglutarate. *Nature*, 462 (7274):739–744, 2009.

C. E. Dann, R. K. Bruick, and J. Deisenhofer. Structure of factor-inhibiting hypoxia-inducible factor 1: An asparaginyl hydroxylase involved in the hypoxic response pathway. *Proceedings of the National Academy of Sciences*, 99(24):15351–15356, 2002.

F. Dayan, D. Roux, M. C. Brahimi-Horn, J. Pouyssegur, and N. M. Mazure. The oxygen sensor factor-inhibiting hypoxia-inducible factor-1 controls expression of distinct genes through the bifunctional transcriptional character of hypoxia-inducible factor-1α. *Cancer Research*, 66 (7):3688–3698, 2006.

F. De Santa, M. G. Totaro, E. Prosperini, S. Notarbartolo, G. Testa, and G. Natoli. The histone H3 lysine-27 demethylase Jmjd3 links inflammation to inhibition of polycomb-mediated gene silencing. *Cell*, 130(6):1083–1094, 2007.

P. A. Del Rizzo, S. Krishnan, and R. C. Trievel. Crystal structure and functional analysis of JMJD5 indicate an alternate specificity and function. *Molecular and Cellular Biology*, 32 (19):4044–4052, 2012.

G. Diedrich, C. M. Spahn, U. Stelzl, M. A. SchaÈfer, T. Wooten, D. E. Bochkariov, B. S. Cooperman, R. R. Traut, and K. H. Nierhaus. Ribosomal protein L2 is involved in the association of the ribosomal subunits, tRNA binding to A and P sites and peptidyl transfer. *The EMBO Journal*, 19(19):5241–5250, 2000.

C. Dina, D. Meyre, S. Gallina, E. Durand, A. Körner, P. Jacobson, L. M. Carlsson, W. Kiess, V. Vatin, C. Lecoeur, J. Delplanque, E. Vaillant, F. Pattou, J. Ruiz, J. Weill, C. Levy-Marchal, F. Horber, N. Potoczna, S. Hercberg, C. Le Stunff, Bougnères, P. Kovacs, M. Marre, B. Balkau, S. Cauchi, J.-C. Chèvre, and P. Froguel. Variation in FTO contributes to childhood obesity and severe adult obesity. *Nature Genetics*, 39(6):724–726, 2007.

V. Dinçbas-Renqvist, Å. Engström, L. Mora, V. Heurgué-Hamard, R. Buckingham, and M. Ehrenberg. A post-translational modification in the GGQ motif of RF2 from Escherichia coli stimulates termination of translation. *The EMBO Journal*, 19(24):6900–6907, 2000.

J. E. Dinchuk, R. J. Focht, J. A. Kelley, N. L. Henderson, N. I. Zolotarjova, R. Wynn, N. T. Neff, J. Link, R. M. Huber, T. C. Burn, M. J. Rupar, M. R. Cunningham, B. H. Selling, J. Ma, A. A. Stern, G. F. Hollis, R. B. Stein, and P. A. Friedman. Absence of post-translational aspartyl β-hydroxylation of epidermal growth factor domains in mice leads to developmental defects and an increased incidence of intestinal neoplasia. *Journal of Biological Chemistry*, 277(15):12970–12977, 2002.

X. Ding, H. Pan, J. Li, Q. Zhong, X. Chen, S. M. Dry, and C.-Y. Wang. Epigenetic activation of AP1 promotes squamous cell carcinoma metastasis. *Science Signaling*, 6(273):ra28, 2013.

T. Drakenberg, P. Fernlund, P. Roepstorff, and J. Stenflo. β-Hydroxyaspartic acid in vitamin K-dependent protein C. *Proceedings of the National Academy of Sciences*, 80(7):1802–1806, 1983.

D. E. Draper. A guide to ions and RNA structure. *RNA*, 10(3):335–343, 2004.

T. Duncan, S. C. Trewick, P. Koivisto, P. A. Bates, T. Lindahl, and B. Sedgwick. Reversal of DNA alkylation damage by two human dioxygenases. *Proceedings of the National Academy of Sciences*, 99(26):16660–16665, 2002.

J. G. Dunn, C. K. Foo, N. G. Belletier, E. R. Gavis, and J. S. Weissman. Ribosome profiling reveals pervasive and regulated stop codon readthrough in Drosophila melanogaster. *eLife*, 2:e01179, 2013.

J. M. Dunwell, A. Culham, C. E. Carter, C. R. Sosa-Aguirre, and P. W. Goodenough. Evolution of functional diversity in the cupin superfamily. *Trends in Biochemical Sciences*, 26 (12):740–746, 2001.

P. S. Ebert and D. J. Prockop. The hydroxylation of proline to hydroxyproline during the synthesis of collagen in chick embryos. *Biochemical and Biophysical Research Communications*, 8(4):305–309, 1962.

D. Ehrismann, E. Flashman, D. Genn, N. Mathioudakis, K. Hewitson, P. Ratcliffe, and C. Schofield. Studies on the activity of the hypoxia-inducible-factor hydroxylases using an oxygen consumption assay. *Biochemical Journal*, 401:227–234, 2007.

J. Eilbracht, M. Reichenzeller, M. Hergt, M. Schnölzer, H. Heid, M. Stöhr, W. W. Franke, and M. S. Schmidt-Zachmann. NO66, a highly conserved dual location protein in the nucleolus and in a special type of synchronously replicating chromatin. *Molecular Biology of the Cell*, 15(4):1816–1832, 2004.

J. Eilbracht, S. Kneissel, A. Hofmann, and M. S. Schmidt-Zachmann. Protein NO52,Äîa constitutive nucleolar component sharing high sequence homologies to protein NO66. *European Journal of Cell Biology*, 84(2):279–294, 2005.

M. Ema, S. Taya, N. Yokotani, K. Sogawa, Y. Matsuda, and Y. Fujii-Kuriyama. A novel bHLH-PAS factor with close sequence similarity to hypoxia-inducible factor 1α regulates the VEGF expression and is potentially involved in lung and vascular development. *Proceedings of the National Academy of Sciences*, 94(9):4273–4278, 1997.

A. C. Epstein, J. M. Gleadle, L. A. McNeill, K. S. Hewitson, J. O'Rourke, D. R. Mole, M. Mukherji, E. Metzen, M. I. Wilson, A. Dhanda, Y.-M. Tian, N. Masson, D. L. Hamilton, P. Jakkola, R. Barstead, J. Hodgkin, P. H. Maxwell, C. W. Pugh, C. J. Schofield, and P. J. Ratcliffe. *C. elegans* EGL-9 and mammalian homologs define a family of dioxygenases that regulate HIF by prolyl hydroxylation. *Cell*, 107(1):43–54, 2001.

L. Eurwilaichitr, F. M. Graves, I. Stansfield, and M. F. Tuite. The C-terminus of eRF1 defines a functionally important domain for translation termination in Saccharomyces cerevisiae. *Molecular Microbiology*, 32(3):485–496, 1999.

D. E. Eyler, K. A. Wehner, and R. Green. Eukaryotic release factor 3 is required for multiple turnovers of peptide release catalysis by eukaryotic release factor 1. *Journal of Biological Chemistry*, 288(41):29530–29538, 2013.

P. Ø. Falnes, R. F. Johansen, and E. Seeberg. AlkB-mediated oxidative demethylation reverses DNA damage in Escherichia coli. *Nature*, 419(6903):178–182, 2002.

N. S. Fearnhead, M. P. Britton, and W. F. Bodmer. The ABC of APC. *Human Molecular Genetics*, 10(7):721–733, 2001.

T. Feng, A. Yamamoto, S. E. Wilkins, E. Sokolova, L. A. Yates, M. Münzel, P. Singh, R. J. Hopkinson, R. Fischer, M. E. Cockman, J. Shelley, D. C. Trudgian, J. Schödel, J. S. O. McCullagh, W. Ge, B. M. Kessler, R. J. Gilbert, L. Y. Frolova, E. Alkalaeva, P. J. Ratcliffe, C. J. Schofield, and M. L. Coleman. Optimal translational termination requires C4 lysyl hydroxylation of eRF1. *Molecular Cell*, 53(4):645–654, 2014.

W. Feng, M. Yonezawa, J. Ye, T. Jenuwein, and I. Grummt. PHF8 activates transcription of rRNA genes through H3K4me3 binding and H3K9me1/2 demethylation. *Nature Structural & Molecular Biology*, 17(4):445–450, 2010.

R. J. Fernandes, A. W. Farnand, G. R. Traeger, M. A. Weis, and D. R. Eyre. A role for prolyl 3-hydroxylase 2 in post-translational modification of fibril-forming collagens. *Journal of Biological Chemistry*, 286(35):30662–30669, 2011.

S. Figaro, N. Scrima, R. H. Buckingham, and V. Heurgué-Hamard. HemK2 protein, encoded on human chromosome 21, methylates translation termination factor eRF1. *FEBS Letters*, 582(16):2352–2356, 2008.

J. Fischer, L. Koch, C. Emmerling, J. Vierkotten, T. Peters, J. C. Brüning, and U. Rüther. Inactivation of the Fto gene protects from obesity. *Nature*, 458(7240):894–898, 2009.

E. Flashman, S. Davies, K. Yeoh, and C. Schofield. Investigating the dependence of the hypoxia-inducible factor hydroxylases (factor inhibiting HIF and prolyl hydroxylase domain 2) on ascorbate and other reducing agents. *Biochemical Journal*, 427:135–142, 2010a.

E. Flashman, L. M. Hoffart, R. B. Hamed, J. M. Bollinger Jr, C. Krebs, and C. J. Schofield. Evidence for the slow reaction of hypoxia-inducible factor prolyl hydroxylase 2 with oxygen. *FEBS Journal*, 277(19):4089–4099, 2010b.

C. Floquet, J. Deforges, J.-P. Rousset, and L. Bidou. Rescue of non-sense mutated p53 tumor suppressor gene by aminoglycosides. *Nucleic Acids Research*, 39(8):3350–3362, 2011a.

C. Floquet, J.-P. Rousset, and L. Bidou. Readthrough of premature termination codons in the adenomatous polyposis coli gene restores its biological activity in human cancer cells. *PloS One*, 6(8):e24125, 2011b.

B. D. Fodor, S. Kubicek, M. Yonezawa, R. J. O,ÄôSullivan, R. Sengupta, L. Perez-Burgos, S. Opravil, K. Mechtler, G. Schotta, and T. Jenuwein. Jmjd2b antagonizes H3K9 trimethylation at pericentric heterochromatin in mammalian cells. *Genes & Development*, 20(12): 1557–1562, 2006.

T. M. Frayling, N. J. Timpson, M. N. Weedon, E. Zeggini, R. M. Freathy, C. M. Lindgren, J. R. Perry, K. S. Elliott, H. Lango, N. W. Rayner, B. Shields, L. W. Harries, J. C. Barrett, S. Ellard, C. J. Groves, B. Knight, A.-M. Patch, A. R. Ness, S. Ebrahim, D. A. Lawlor, S. M. Ring, Y. Ben-Shlomo, M.-R. Jarvelin, U. Sovio, A. J. Bennett, D. Melzer, L. Ferrucci, R. J. F. Loos, I. Barroso, N. J. Wareham, F. Karpe, K. R. Owen, L. R. Cardon, M. Walker, G. A. Hitman, C. N. A. Palmer, A. S. F. Doney, A. D. Morris, and G. D. Smith. A common variant in the FTO gene is associated with body mass index and predisposes to childhood and adult obesity. *Science*, 316(5826):889–894, 2007.

D. V. Freistroffer, M. Y. Pavlov, J. MacDougall, R. H. Buckingham, and M. Ehrenberg. Release factor RF3 in E. coli accelerates the dissociation of release factors RF1 and RF2 from the ribosome in a GTP-dependent manner. *The EMBO Journal*, 16(13):4126–4133, 1997.

J. Freitag, J. Ast, and M. Bölker. Cryptic peroxisomal targeting via alternative splicing and stop codon read-through in fungi. *Nature*, 485(7399):522–525, 2012.

D. Frescas, D. Guardavaccaro, F. Bassermann, R. Koyama-Nasu, and M. Pagano. JHDM1B/FBXL10 is a nucleolar protein that represses transcription of ribosomal RNA genes. *Nature*, 450(7167):309–313, 2007.

L. Frolova, X. Le Goff, H. H. Rasmussen, S. Cheperegin, G. Drugeon, M. Kress, I. Arman, A.-L. Haenni, J. E. Celis, M. Phllippe, J. Justesen, and L. Kisselev. A highly conserved eukaryotic protein family possessing properties of polypeptide chain release factor. *Nature*, 372:701–703, 1994.

L. Frolova, X. Le Goff, G. Zhouravleva, E. Davydova, M. Philippe, and L. Kisselev. Eukaryotic polypeptide chain release factor eRF3 is an eRF1-and ribosome-dependent guanosine triphosphatase. *RNA*, 2(4):334–341, 1996.

L. Frolova, A. Seit-Nebi, and L. Kisselev. Highly conserved NIKS tetrapeptide is functionally essential in eukaryotic translation termination factor eRF1. *RNA*, 8(2):129–136, 2002.

L. Y. Frolova, R. Y. Tsivkovskii, G. F. Sivolobova, N. Y. Oprina, O. I. Serpinsky, V. M. Blinov, S. I. Tatkov, and L. L. Kisselev. Mutations in the highly conserved GGQ motif of class 1 polypeptide release factors abolish ability of human eRF1 to trigger peptidyl-tRNA hydrolysis. *RNA*, 5(8):1014–1020, 1999.

Y. Fu, Q. Dai, W. Zhang, J. Ren, T. Pan, and C. He. The AlkB domain of mammalian ABH8 catalyzes hydroxylation of 5-methoxycarbonylmethyluridine at the wobble position of tRNA. *Angewandte Chemie International Edition*, 122(47):9069–9072, 2010.

S. Fukahori, H. Yano, M. Tsuneoka, Y. Tanaka, M. Yagi, M. Kuwano, T. Tajiri, T. Taguchi, M. Tsuneyoshi, and M. Kojiro. Immunohistochemical expressions of Cap43 and Mina53 proteins in neuroblastoma. *Journal of Pediatric Surgery*, 42(11):1831–1840, 2007.

W. Ge, A. Wolf, T. Feng, C.-h. Ho, A. Zayer, N. Granatino, M. E. Cockman, C. Loenarz, N. D. Loik, A. P. Hardy, T. D. W. Claridge, R. B. Hamed, R. Chowdhury, L. Gong, C. V. Robinson, D. C. Trudgian, M. Jiang, M. M. Mackeen, J. S. Mccullagh, Y. Gordiyenko, A. Thalhammer, A. Yamamoto, M. Yang, P. Liu-Yi, Z. Zhang, M. Schmidt-Zachmann, B. M. Kessler, R. P. J, G. M. Preston, M. L. Coleman, and C. J. Schofield. Oxygenase-catalyzed ribosome hydroxylation occurs in prokaryotes and humans. *Nature Chemical Biology*, 8(12):960–962, 2012.

A. I. Geller and A. Rich. A UGA termination suppression tRNATrp active in rabbit reticulocytes. *Nature*, 283(5742):41–46, 1980.

K. Gelse, E. Pöschl, and T. Aigner. Collagens,Äîstructure, function, and biosynthesis. *Advanced Drug Delivery Reviews*, 55(12):1531–1546, 2003.

T. Gerken, C. A. Girard, Y.-C. L. Tung, C. J. Webby, V. Saudek, K. S. Hewitson, G. S. Yeo, M. A. McDonough, S. Cunliffe, L. A. McNeill, J. Galvanovskis, P. Rorsman, P. Robins, X. Prieur, A. P. Coll, M. Ma, Z. Jovanovic, I. S. Farooqi, B. Sedgwick, I. Barroso, T. Lindahl, C. P. Ponting, F. M. Ashcroft, S. O'Rahilly, and C. J. Schofield. The obesity-associated FTO gene encodes a 2-oxoglutarate-dependent nucleic acid demethylase. *Science*, 318(5855):1469–1472, 2007.

M. Ghosh, R. Loper, M. H. Gelb, and C. C. Leslie. Identification of the expressed form of human cytosolic phospholipase A2β (cPLA2β): cPLA2β3 is a novel variant localised to mitochondria and early endosomes. *Journal of Biological Chemistry*, 281(24):16615–16624, 2006.

A. C. Gill, M. A. Ritchie, L. G. Hunt, S. E. Steane, K. G. Davies, S. P. Bocking, A. G. Rhie, A. D. Bennett, and J. Hope. Post-translational hydroxylation at the N-terminus of the prion protein reveals presence of PPII structure in vivo. *The EMBO Journal*, 19(20): 5324–5331, 2000.

K. L. Gorres and R. T. Raines. Prolyl 4-hydroxylase. *Critical Reviews in Biochemistry and Molecular Biology*, 45(2):106–124, 2010.

M. Graille, S. Figaro, S. Kervestin, R. H. Buckingham, D. Liger, and V. Heurgué-Hamard. Methylation of class I translation termination factors: structural and functional aspects. *Biochimie*, 94(7):1533–1543, 2012.

G. Grentzmann, J. A. Ingram, P. J. Kelly, R. F. Gesteland, and J. F. Atkins. A dual-luciferase reporter system for studying recoding signals. *RNA*, 4(4):479–486, 1998.

R. S. Gronke, W. J. VanDusen, V. M. Garsky, J. W. Jacobs, M. K. Sardana, A. M. Stern, and P. A. Friedman. Aspartyl beta-hydroxylase: in vitro hydroxylation of a synthetic peptide based on the structure of the first growth factor-like domain of human factor IX. *Proceedings of the National Academy of Sciences*, 86(10):3609–3613, 1989.

Y. Gu, S. Moran, J. Hogenesch, L. Wartman, and C. Bradfield. Molecular characterization and chromosomal localization of a third alpha-class hypoxia inducible factor subunit, HIF3alpha. *Gene Expression*, 7(3):205, 1998.

R. Ha-Vinh, Y. Alanay, R. A. Bank, A. B. Campos-Xavier, A. Zankl, A. Superti-Furga, and L. Bonafé. Phenotypic and molecular characterization of Bruck syndrome (osteogenesis imperfecta with contractures of the large joints) caused by a recessive mutation in PLOD2. *American Journal of Medical Genetics*, 131(2):115–120, 2004.

S. M. Haeryfar and D. W. Hoskin. Thy-1: more than a mouse pan-T cell marker. *The Journal of Immunology*, 173(6):3581–3588, 2004.

P. Hahn, I. Wegener, A. Burrells, J. Böse, A. Wolf, C. Erck, D. Butler, C. J. Schofield, A. Bröttger, and A. Lengeling. Analysis of Jmjd6 cellular localization and testing for its involvement in histone demethylation. *PloS One*, 5(10):e13769, 2010.

G. Han, J. Li, Y. Wang, X. Li, H. Mao, Y. Liu, and C. D. Chen. The hydroxylation activity of Jmjd6 is required for its homo-oligomerization. *Journal of Cellular Biochemistry*, 113 (5):1663–1670, 2012.

D. Hanahan and R. A. Weinberg. The hallmarks of cancer. *Cell*, 100(1):57–70, 2000.

J. L. Hansen, P. B. Moore, and T. A. Steitz. Structures of five antibiotics bound at the peptidyl transferase center of the large ribosomal subunit. *Journal of Molecular Biology*, 330(5):1061–1075, 2003.

S. Hara, J. Hamada, C. Kobayashi, Y. Kondo, and N. Imura. Expression and characterization of hypoxia-inducible factor (HIF)-3α in human kidney: suppression of HIF-mediated gene expression by HIF-3α. *Biochemical and Biophysical Research Communications*, 287(4): 808–813, 2001.

A. P. Hardy, I. Prokes, L. Kelly, I. D. Campbell, and C. J. Schofield. Asparaginyl β-hydroxylation of proteins containing ankyrin repeat domains influences their stability and function. *Journal of Molecular Biology*, 392(4):994–1006, 2009.

E. Hausmann. Cofactor requirements for the enzymatic hydroxylation of lysine in a polypeptide precursor of collagen. *Biochimica et Biophysica Acta (BBA)-Protein Structure*, 133(3): 591–593, 1967.

T. Hautala, M. G. Byers, R. L. Eddy, T. B. Shows, K. I. Kivirikko, and R. Myllyla. Cloning of human lysyl hydroxylase: Complete cDNA-derived amino acid sequence and assignment of the gene (*plod*) to chromosome 1p36. 3→ p36. 2. *Genomics*, 13(1):62–69, 1992.

Y.-F. He, B.-Z. Li, Z. Li, P. Liu, Y. Wang, Q. Tang, J. Ding, Y. Jia, Z. Chen, L. Li, Y. Sun, X. Li, Q. Dai, C.-X. Song, K. Zhang, C. He, and G.-L. Xu. Tet-mediated formation of 5-carboxylcytosine and its excision by TDG in mammalian DNA. *Science*, 333(6047):1303–1307, 2011.

J. Heikkinen, M. Risteli, C. Wang, J. Latvala, M. Rossi, M. Valtavaara, and R. Myllylä. Lysyl hydroxylase 3 is a multifunctional protein possessing collagen glucosyltransferase activity. *Journal of Biological Chemistry*, 275(46):36158–36163, 2000.

A. Heim, C. Grimm, U. Müller, S. Häußler, M. M. Mackeen, J. Merl, S. M. Hauck, B. M. Kessler, C. J. Schofield, A. Wolf, and A. Bröttger. Jumonji domain containing protein 6 (Jmjd6) modulates splicing and specifically interacts with arginine–serine-rich (RS) domains of SR-and SR-like proteins. *Nucleic Acids Research*, 42(12):7833,Äì–7850, 2014.

T. Helaakoski, P. Annunen, K. Vuori, I. Macneil, T. Pihlajaniemi, and K. Kivirikko. Cloning, baculovirus expression, and characterization of a second mouse prolyl 4-hydroxylase α-subunit isoform: Formation of an $\alpha 2\beta 2$ tetramer with the protein disulfide-isomerase/β subunit. *Proceedings of the National Academy of Sciences*, 92(10):4427–4431, 1995.

C. M. Henderson, C. B. Anderson, and M. T. Howard. Antisense-induced ribosomal frameshifting. *Nucleic Acids Research*, 34(15):4302–4310, 2006.

K. S. Hewitson, L. A. McNeill, M. V. Riordan, Y.-M. Tian, A. N. Bullock, R. W. Welford, J. M. Elkins, N. J. Oldham, S. Bhattacharya, J. M. Gleadle, P. J. Ratcliffe, C. W. Pugh, and C. J. Schofield. Hypoxia-inducible factor (HIF) asparagine hydroxylase is identical to factor inhibiting HIF (FIH) and is related to the cupin structural family. *Journal of Biological Chemistry*, 277(29):26351–26355, 2002.

K. S. Hewitson, B. M. Liénard, M. A. McDonough, I. J. Clifton, D. Butler, A. S. Soares, N. J. Oldham, L. A. McNeill, and C. J. Schofield. Structural and mechanistic studies on the inhibition of the hypoxia-inducible transcription factor hydroxylases by tricarboxylic acid cycle intermediates. *Journal of Biological Chemistry*, 282(5):3293–3301, 2007.

L. Hillringhaus, W. W. Yue, N. R. Rose, S. S. Ng, C. Gileadi, C. Loenarz, S. H. Bello, J. E. Bray, C. J. Schofield, and U. Oppermann. Structural and evolutionary basis for the dual substrate selectivity of human kdm4 histone demethylase family. *Journal of Biological Chemistry*, 286(48):41616–41625, 2011.

H. Himmelfarb, E. Maicas, and J. Friesen. Isolation of the SUP45 omnipotent suppressor gene of Saccharomyces cerevisiae and characterization of its gene product. *Molecular and Cellular Biology*, 5(4):816–822, 1985.

C. A. Hirsch and H. H. Hiatt. Turnover of liver ribosomes in fed and in fasted rats. *Journal of Biological Chemistry*, 241(24):5936–5940, 1966.

M. Hirsilä, P. Koivunen, V. Günzler, K. I. Kivirikko, and J. Myllyharju. Characterization of the human prolyl 4-hydroxylases that modify the hypoxia-inducible factor. *Journal of Biological Chemistry*, 278(33):30772–30780, 2003.

L. M. Hoffart, E. W. Barr, R. B. Guyer, J. M. Bollinger, and C. Krebs. Direct spectroscopic detection of a CH-cleaving high-spin Fe (iv) complex in a prolyl-4-hydroxylase. *Proceedings of the National Academy of Sciences*, 103(40):14738–14743, 2006.

J. W. Højfeldt, K. Agger, and K. Helin. Histone lysine demethylases as targets for anticancer therapy. *Nature Reviews Drug Discovery*, 12:917–930, 2013.

M. Holcik, T. Graber, S. M. Lewis, C. A. Lefebvre, E. Lacasse, and S. Baird. Spurious splicing within the XIAP 5'UTR occurs in the Rluc/Fluc but not the βgal/CAT bicistronic reporter system. *RNA*, 11(11):1605–1609, 2005.

S. Hong, Y.-W. Cho, L.-R. Yu, H. Yu, T. D. Veenstra, and K. Ge. Identification of JmjC domain-containing UTX and JMJD3 as histone H3 lysine 27 demethylases. *Proceedings of the National Academy of Sciences*, 104(47):18439–18444, 2007.

X. Hong, J. Zang, J. White, C. Wang, C.-H. Pan, R. Zhao, R. C. Murphy, S. Dai, P. Henson, J. W. Kappler, J. Hagman, and G. Zhang. Interaction of JMJD6 with single-stranded RNA. *Proceedings of the National Academy of Sciences*, 107(33):14568–14572, 2010.

D. A. Hsia, C. G. Tepper, M. R. Pochampalli, E. Y. Hsia, C. Izumiya, S. B. Huerta, M. E. Wright, H.-W. Chen, H.-J. Kung, and Y. Izumiya. KDM8, a H3K36me2 histone demethylase that acts in the cyclin A1 coding region to regulate cancer cell proliferation. *Proceedings of the National Academy of Sciences*, 107(21):9671–9676, 2010.

C. Huang, Y. Xiang, Y. Wang, X. Li, L. Xu, Z. Zhu, T. Zhang, Q. Zhu, K. Zhang, N. Jing, and C. D. Chen. Dual-specificity histone demethylase KIAA1718 (KDM7A) regulates neural differentiation through FGF4. *Cell Research*, 20(2):154–165, 2010.

Y. Huang and A. Rao. Connections between TET proteins and aberrant DNA modification in cancer. *Trends in Genetics*, 30(10):464–474, 2014.

J. Hulse, S. Ellis, and L. Henderson. Carnitine biosynthesis. beta-hydroxylation of trimethyllysine by an alpha-ketoglutarate-dependent mitochondrial dioxygenase. *Journal of Biological Chemistry*, 253(5):1654–1659, 1978.

J. J. Hutton Jr, A. Tappel, and S. Udenfriend. Requirements for α-ketoglutarate, ferrous ion and ascorbate by collagen proline hydroxylase. *Biochemical and Biophysical Research Communications*, 24(2):179–184, 1966.

J. J. Hutton Jr, A. Tappel, and S. Udenfriend. Cofactor and substrate requirements of collagen proline hydroxylase. *Archives of Biochemistry and Biophysics*, 118(1):231–240, 1967.

N. Ince, M. Suzanne, and J. R. Wands. Overexpression of human aspartyl (asparaginyl) β-hydroxylase is associated with malignant transformation. *Cancer Research*, 60(5):1261–1266, 2000.

N. T. Ingolia, S. Ghaemmaghami, J. R. Newman, and J. S. Weissman. Genome-wide analysis in vivo of translation with nucleotide resolution using ribosome profiling. *Science*, 324 (5924):218–223, 2009.

J. S. Isaacs, Y. J. Jung, D. R. Mole, S. Lee, C. Torres-Cabala, Y.-L. Chung, M. Merino, J. Trepel, B. Zbar, J. Toro, P. J. Ratcliffe, W. M. Linehan, and L. Neckers. HIF overexpression correlates with biallelic loss of fumarate hydratase in renal cancer: novel role of fumarate in regulation of HIF stability. *Cancer Cell*, 8(2):143–153, 2005.

A. Ishimura, K.-i. Minehata, M. Terashima, G. Kondoh, T. Hara, and T. Suzuki. Jmjd5, an H3K36me2 histone demethylase, modulates embryonic cell proliferation through the regulation of Cdkn1a expression. *Development*, 139(4):749–759, 2012.

H. Ishizaki, H. Yano, M. Tsuneoka, S. Ogasawara, J. Akiba, N. Nishida, S. Kojiro, S. Fukahori, F. Moriya, K. Matsuoka, and M. Kojiro. Overexpression of the myc target gene Mina53 in advanced renal cell carcinoma. *Pathology International*, 57(10):672–680, 2007.

K. Ito, K. Ebihara, M. Uno, and Y. Nakamura. Conserved motifs in prokaryotic and eukaryotic polypeptide release factors: tRNA-protein mimicry hypothesis. *Proceedings of the National Academy of Sciences*, 93(11):5443–5448, 1996.

S. Ito, A. C. D,ÄôAlessio, O. V. Taranova, K. Hong, L. C. Sowers, and Y. Zhang. Role of Tet proteins in 5mC to 5hmC conversion, ES-cell self-renewal and inner cell mass specification. *Nature*, 466(7310):1129–1133, 2010.

S. Ito, L. Shen, Q. Dai, S. C. Wu, L. B. Collins, J. A. Swenberg, C. He, and Y. Zhang. Tet proteins can convert 5-methylcytosine to 5-formylcytosine and 5-carboxylcytosine. *Science*, 333(6047):1300–1303, 2011.

M. Ivan, K. Kondo, H. Yang, W. Kim, J. Valiando, M. Ohh, A. Salic, J. M. Asara, W. S. Lane, and W. G. Kaelin Jr. HIFα targeted for VHL-mediated destruction by proline hydroxylation: implications for O2 sensing. *Science*, 292(5516):464–468, 2001.

P. V. Ivanov, N. H. Gehring, J. B. Kunz, M. W. Hentze, and A. E. Kulozik. Interactions between UPF1, eRFs, PABP and the exon junction complex suggest an integrated model for mammalian NMD pathways. *The EMBO Journal*, 27(5):736–747, 2008.

S. Iwase, F. Lan, P. Bayliss, L. de la Torre-Ubieta, M. Huarte, H. H. Qi, J. R. Whetstine, A. Bonni, T. M. Roberts, and Y. Shi. The X-linked mental retardation gene *SMCX/JARID1C* defines a family of histone H3 lysine 4 demethylases. *Cell*, 128(6):1077–1088, 2007.

P. Jaakkola, D. R. Mole, Y.-M. Tian, M. I. Wilson, J. Gielbert, S. J. Gaskell, A. von Kriegsheim, H. F. Hebestreit, M. Mukherji, C. J. Schofield, and P. J. Ratcliffe. Targeting of HIF-α to the von Hippel-Lindau ubiquitylation complex by O2-regulated prolyl hydroxylation. *Science*, 292(5516):468–472, 2001.

K. Janke, U. Brockmeier, K. Kuhlmann, M. Eisenacher, J. Nolde, H. E. Meyer, H. Mairbäurl, and E. Metzen. Factor inhibiting HIF-1 (FIH-1) modulates protein interactions of apoptosis-stimulating p53 binding protein 2 (ASPP2). *Journal of Cell Science*, 126(12):2629–2640, 2013.

G. A. Jansen, R. Oftnan, S. Ferdinandusse, L. Ijlst, A. O. Muijsers, O. H. Skjeldal, O. Stokke, C. Jakobs, G. T. Besley, J. E. Wraith, and R. J. A. Wanders. Refsum disease is caused by mutations in the phytanoyl–CoA hydroxylase gene. *Nature Genetics*, 17(2):190–193, 1997.

G. Jia, C.-G. Yang, S. Yang, X. Jian, C. Yi, Z. Zhou, and C. He. Oxidative demethylation of 3-methylthymine and 3-methyluracil in single-stranded dna and rna by mouse and human FTO. *FEBS letters*, 582(23):3313–3319, 2008.

G. Jia, Y. Fu, X. Zhao, Q. Dai, G. Zheng, Y. Yang, C. Yi, T. Lindahl, T. Pan, Y.-G. Yang, and C. He. N6-methyladenosine in nuclear RNA is a major substrate of the obesity-associated FTO. *Nature Chemical Biology*, 7(12):885–887, 2011.

M. Jiang, Y. Ma, H. Cheng, X. Ni, L. Guo, Y. Xie, and Y. Mao. Molecular cloning and characterization of a novel human gene (HSPBAP1) from human fetal brain. *Cytogenetic and Genome Research*, 95(1-2):48–51, 2001.

C. Johansson, A. Tumber, K. Che, P. Cain, R. Nowak, C. Gileadi, and U. Oppermann. The roles of jumonji-type oxygenases in human disease. *Epigenomics*, 6(1):89–120, 2014.

M. A. Jones, M. F. Covington, L. DiTacchio, C. Vollmers, S. Panda, and S. L. Harmer. Jumonji domain protein JMJD5 functions in both the plant and human circadian systems. *Proceedings of the National Academy of Sciences*, 107(50):21623–21628, 2010.

I. Jungreis, M. F. Lin, R. Spokony, C. S. Chan, N. Negre, A. Victorsen, K. P. White, and M. Kellis. Evidence of abundant stop codon readthrough in Drosophila and other metazoa. *Genome Research*, 21(12):2096–2113, 2011.

W. Kaelin. Cancer and altered metabolism: potential importance of hypoxia-inducible factor and 2-oxoglutarate-dependent dioxygenases. In *Cold Spring Harbor Symposia on Quantitative Biology*, volume 76, pages 335–345. Cold Spring Harbor Laboratory Press, 2011.

M. J. Katz, J. M. Acevedo, C. Loenarz, D. Galagovsky, P. Liu-Yi, M. Pérez-Pepe, A. Thalhammer, W. Ge, M. Melani, M. G. Thomas, S. Simonetta, G. Boccaccio, C. J. Schofield, M. E. Cockman, R. P. J, and P. Wappner. Sudestada1, a Drosophila ribosomal prolyl-hydroxylase required for mRNA translation, cell homeostasis, and organ growth. *Proceedings of the National Academy of Sciences*, 111(11):4025–4030, 2014.

K. M. Keeling, D. Wang, S. E. Conard, and D. M. Bedwell. Suppression of premature termination codons as a therapeutic approach. *Critical Reviews in Biochemistry and Molecular Biology*, 47(5):444–463, 2012.

L. Kelly, M. A. McDonough, M. L. Coleman, P. J. Ratcliffe, and C. J. Schofield. Asparagine β-hydroxylation stabilizes the ankyrin repeat domain fold. *Molecular BioSystems*, 5(1): 52–58, 2009.

S.-M. Kim, J.-Y. Kim, N.-W. Choe, I.-H. Cho, J.-R. Kim, D.-W. Kim, J.-E. Seol, S. E. Lee, H. Kook, K.-I. Nam, H. Kook, Y.-Y. Bhak, and S.-B. Seo. Regulation of mouse steroidogenesis by WHISTLE and JMJD1C through histone methylation balance. *Nucleic Acids Research*, 38(19):6389–6403, 2010.

N. V. Kirienko and D. S. Fay. SLR-2 and JMJC-1 regulate an evolutionarily conserved stress-response network. *The EMBO Journal*, 29(4):727–739, 2010.

L. L. Kisselev and R. H. Buckingham. Translational termination comes of age. *Trends in Biochemical Sciences*, 25(11):561–566, 2000.

B. R. Klagges, G. Heimbeck, T. A. Godenschwege, A. Hofbauer, G. O. Pflugfelder, R. Reifegerste, D. Reisch, M. Schaupp, S. Buchner, and E. Buchner. Invertebrate synapsins: a single gene codes for several isoforms in Drosophila. *The Journal of Neuroscience*, 16(10): 3154–3165, 1996.

D. J. Klein, P. B. Moore, and T. A. Steitz. The roles of ribosomal proteins in the structure assembly, and evolution of the large ribosomal subunit. *Journal of Molecular Biology*, 340 (1):141–177, 2004a.

D. J. Klein, P. B. Moore, and T. A. Steitz. The contribution of metal ions to the structural stability of the large ribosomal subunit. *RNA*, 10(9):1366–1379, 2004b.

R. J. Klose, E. M. Kallin, and Y. Zhang. JmjC-domain-containing proteins and histone demethylation. *Nature Reviews Genetics*, 7(9):715–727, 2006a.

R. J. Klose, K. Yamane, Y. Bae, D. Zhang, H. Erdjument-Bromage, P. Tempst, J. Wong, and Y. Zhang. The transcriptional repressor JHDM3A demethylates trimethyl histone H3 lysine 9 and lysine 36. *Nature*, 442(7100):312–316, 2006b.

R. J. Klose, Q. Yan, Z. Tothova, K. Yamane, H. Erdjument-Bromage, P. Tempst, D. G. Gilliland, Y. Zhang, and W. G. Kaelin Jr. The retinoblastoma binding protein RBP2 is an H3K4 demethylase. *Cell*, 128(5):889–900, 2007.

H. J. Knowles, R. R. Raval, A. L. Harris, and P. J. Ratcliffe. Effect of ascorbate on the activity of hypoxia-inducible factor in cancer cells. *Cancer Research*, 63(8):1764–1768, 2003.

M. Ko, Y. Huang, A. M. Jankowska, U. J. Pape, M. Tahiliani, H. S. Bandukwala, J. An, E. D. Lamperti, K. P. Koh, R. Ganetzky, X. S. Liu, L. Aravind, S. Agarwal, J. P. Maciejewski, and A. Rao. Impaired hydroxylation of 5-methylcytosine in myeloid cancers with mutant TET2. *Nature*, 468(7325):839–843, 2010.

K. D. Koehntop, J. P. Emerson, and L. Que Jr. The 2-His-1-carboxylate facial triad: a versatile platform for dioxygen activation by mononuclear non-heme iron (II) enzymes. *Journal of Biological Inorganic Chemistry*, 10(2):87–93, 2005.

P. Koivunen, M. Hirsilä, V. Günzler, K. I. Kivirikko, and J. Myllyharju. Catalytic properties of the asparaginyl hydroxylase (FIH) in the oxygen sensing pathway are distinct from those of its prolyl 4-hydroxylases. *Journal of Biological Chemistry*, 279(11):9899–9904, 2004.

P. Koivunen, M. Hirsilä, K. I. Kivirikko, and J. Myllyharju. The length of peptide substrates has a marked effect on hydroxylation by the hypoxia-inducible factor prolyl 4-hydroxylases. *Journal of Biological Chemistry*, 281(39):28712–28720, 2006.

P. Koivunen, M. Hirsilä, A. M. Remes, I. E. Hassinen, K. I. Kivirikko, and J. Myllyharju. Inhibition of hypoxia-inducible factor (HIF) hydroxylases by citric acid cycle intermediates: possible links between cell metabolism and stabilization of HIF. *Journal of Biological Chemistry*, 282(7):4524–4532, 2007.

P. Koivunen, S. Lee, C. G. Duncan, G. Lopez, G. Lu, S. Ramkissoon, J. A. Losman, P. Joensuu, U. Bergmann, S. Gross, J. Travins, S. Weiss, R. Looper, K. L. Ligon, R. G. W. Verhaak, H. Yan, and W. G. Kaelin Jr. Transformation by the (R)-enantiomer of 2-hydroxyglutarate linked to EGLN activation. *Nature*, 483(7390):484–488, 2012.

P. Kolosov, L. Frolova, A. Seit-Nebi, V. Dubovaya, A. Kononenko, N. Oparina, J. Justesen, A. Efimov, and L. Kisselev. Invariant amino acids essential for decoding function of polypeptide release factor eRF1. *Nucleic Acids Research*, 33(19):6418–6425, 2005.

K. Komiya, N. Sueoka-Aragane, A. Sato, T. Hisatomi, T. Sakuragi, M. Mitsuoka, T. Sato, S. Hayashi, H. Izumi, M. Tsuneoka, and E. Sueoka. Mina53, a novel c-Myc target gene, is frequently expressed in lung cancers and exerts oncogenic property in NIH/3T3 cells. *Journal of Cancer Research and Clinical Oncology*, 136(3):465–473, 2010.

R. D. Kornberg and Y. Lorch. Twenty-five years of the nucleosome, fundamental particle of the eukaryote chromosome. *Cell*, 98(3):285–294, 1999.

J. Krieg, J. Hofsteenge, and G. Thomas. Identification of the 40S ribosomal protein S6 phosphorylation sites induced by cycloheximide. *Journal of Biological Chemistry*, 263(23): 11473–11477, 1988.

A. Krogh, B. Larsson, G. Von Heijne, and E. L. Sonnhammer. Predicting transmembrane protein topology with a hidden Markov model: application to complete genomes. *Journal of Molecular Biology*, 305(3):567–580, 2001.

P. Kryuchkova, A. Grishin, B. Eliseev, A. Karyagina, L. Frolova, and E. Alkalaeva. Two-step model of stop codon recognition by eukaryotic release factor eRF1. *Nucleic Acids Research*, 41(8):4573–4586, 2013.

C. Kuiper, I. G. Molenaar, G. U. Dachs, M. J. Currie, P. H. Sykes, and M. C. Vissers. Low ascorbate levels are associated with increased hypoxia-inducible factor-1 activity and an aggressive tumor phenotype in endometrial cancer. *Cancer Research*, 70(14):5749–5758, 2010.

L. Kukkola, R. Hieta, K. I. Kivirikko, and J. Myllyharju. Identification and characterization of a third human, rat, and mouse collagen prolyl 4-hydroxylase isoenzyme. *Journal of Biological Chemistry*, 278(48):47685–47693, 2003.

Y. Kunisaki, S. Masuko, M. Noda, A. Inayoshi, T. Sanui, M. Harada, T. Sasazuki, and Y. Fukui. Defective fetal liver erythropoiesis and T lymphopoiesis in mice lacking the phosphatidylserine receptor. *Blood*, 103(9):3362–3364, 2004.

F. Lan, P. E. Bayliss, J. L. Rinn, J. R. Whetstine, J. K. Wang, S. Chen, S. Iwase, R. Alpatov, I. Issaeva, E. Canaani, T. M. Roberts, H. Y. Chang, and Y. Shi. A histone H3 lysine 27 demethylase regulates animal posterior development. *Nature*, 449(7163):689–694, 2007.

D. Lando, D. J. Peet, J. J. Gorman, D. A. Whelan, M. L. Whitelaw, and R. K. Bruick. FIH-1 is an asparaginyl hydroxylase enzyme that regulates the transcriptional activity of hypoxia-inducible factor. *Genes & Development*, 16(12):1466–1471, 2002a.

D. Lando, D. J. Peet, D. A. Whelan, J. J. Gorman, and M. L. Whitelaw. Asparagine hydroxylation of the HIF transactivation domain: a hypoxic switch. *Science*, 295(5556):858–861, 2002b.

L. Lavaissiere, S. Jia, M. Nishiyama, S. de la Monte, A. M. Stern, J. R. Wands, and P. A. Friedman. Overexpression of human aspartyl (asparaginyl) beta-hydroxylase in hepatocellular carcinoma and cholangiocarcinoma. *The Journal of Clinical Investigation*, 98(6):1313, 1996.

M. G. Lee, J. Norman, A. Shilatifard, and R. Shiekhattar. Physical and functional association of a trimethyl H3K4 demethylase and Ring6a/MBLR, a polycomb-like protein. *Cell*, 128 (5):877–887, 2007.

N. A. Lemp, K. Hiraoka, N. Kasahara, and C. R. Logg. Cryptic transcripts from a ubiquitous plasmid origin of replication confound tests for cis-regulatory function. *Nucleic Acids Research*, 40(15):7280–7290, 2012.

J. Li, A. Mahajan, and M.-D. Tsai. Ankyrin repeat: a unique motif mediating protein-protein interactions. *Biochemistry*, 45(51):15168–15178, 2006.

M.-M. Li, A. Nilsen, Y. Shi, M. Fusser, Y.-H. Ding, Y. Fu, B. Liu, Y. Niu, Y.-S. Wu, C.-M. Huang, M. Olofsson, K.-X. Jin, X.-Z. Xu, C. He, M.-Q. Dong, J. M. R. Danielsen, A. Klungland, and Y.-G. Yang. ALKBH4-dependent demethylation of actin regulates actomyosin dynamics. *Nature Communications*, 4:1832, 2013.

M. E. Lieb, K. Menzies, M. C. Moschella, R. Ni, and M. B. Taubman. Mammalian EGLN genes have distinct patterns of mRNA expression and regulation. *Biochemistry and Cell Biology*, 80(4):421–426, 2002.

D. Liger, L. Mora, N. Lazar, S. Figaro, J. Henri, N. Scrima, R. H. Buckingham, H. van Tilbeurgh, V. Heurgué-Hamard, and M. Graille. Mechanism of activation of methyltransferases involved in translation by the Trm112 'hub' protein. *Nucleic Acids Research*, 39 (14):6249–6259, 2011.

C.-C. Lin, C.-H. Chou, S.-L. Howng, C.-Y. Hsu, C.-C. Hwang, C. Wang, C.-M. Hsu, and Y.-R. Hong. GSKIP, an inhibitor of GSK3β, mediates the N-cadherin/β-catenin pool in the differentiation of SH-SY5Y cells. *Journal of Cellular Biochemistry*, 108(6):1325–1336, 2009.

G. Lindstedt and S. Lindstedt. Cofactor requirements of γ-butyrobetaine hydroxylase from rat liver. *Journal of Biological Chemistry*, 245(16):4178–4186, 1970.

C. Liu, R. R. Gilmont, R. Benndorf, and M. J. Welsh. Identification and characterization of a novel protein from Sertoli cells, PASS1, that associates with mammalian small stress protein hsp27. *Journal of Biological Chemistry*, 275(25):18724–18731, 2000.

L. Liu, H. Kim, A. Casta, Y. Kobayashi, L. S. Shapiro, and A. M. Christiano. Hairless is a histone H3K9 demethylase. *The FASEB Journal*, 28(4):1534–1542, 2014.

P. Liu, S. Nie, B. Li, Z.-Q. Yang, Z.-M. Xu, J. Fei, C. Lin, R. Zeng, and G.-L. Xu. Deficiency in a glutamine-specific methyltransferase for release factor causes mouse embryonic lethality. *Molecular and Cellular Biology*, 30(17):4245–4253, 2010.

W. Liu, Q. Ma, K. Wong, W. Li, K. Ohgi, J. Zhang, A. K. Aggarwal, and M. G. Rosenfeld. Brd4 and JMJD6-associated anti-pause enhancers in regulation of transcriptional pause release. *Cell*, 155(7):1581–1595, 2013.

A. Loboda, A. Jozkowicz, and J. Dulak. HIF-1 versus HIF-2,Äîis one more important than the other? *Vascular Pharmacology*, 56(5):245–251, 2012.

C. Loenarz, W. Ge, M. L. Coleman, N. R. Rose, C. D. Cooper, R. J. Klose, P. J. Ratcliffe, and C. J. Schofield. PHF8, a gene associated with cleft lip/palate and mental retardation, encodes for an Nε-dimethyl lysine demethylase. *Human Molecular Genetics*, 19(2):217–222, 2010.

C. Loenarz, A. Thalhammer, W. Ge, E. Spivakovsky, M. M. Mackeen, M. A. McDonough, M. E. Cockman, B. M. Kessler, P. J. Ratcliffe, A. Wolf, and C. J. Schofield. Hydroxylation of the eukaryotic ribosomal decoding center affects translational accuracy. *Proceedings of the National Academy of Sciences*, 111(11):4019–4024, 2014.

J.-A. Losman, R. E. Looper, P. Koivunen, S. Lee, R. K. Schneider, C. McMahon, G. S. Cowley, D. E. Root, B. L. Ebert, and W. G. Kaelin. (r)-2-hydroxyglutarate is sufficient to promote leukemogenesis and its effects are reversible. *Science*, 339(6127):1621–1625, 2013.

G. Loughran, M.-Y. Chou, I. P. Ivanov, I. Jungreis, M. Kellis, A. M. Kiran, P. V. Baranov, and J. F. Atkins. Evidence of efficient stop codon readthrough in four mammalian genes. *Nucleic Acids Research*, 42(14):8928–8938, 2014.

T. Lu, M. W. Jackson, A. D. Singhi, E. S. Kandel, M. Yang, Y. Zhang, A. V. Gudkov, and G. R. Stark. Validation-based insertional mutagenesis identifies lysine demethylase FBXL11 as a negative regulator of NFκB. *Proceedings of the National Academy of Sciences*, 106 (38):16339–16344, 2009a.

T. Lu, M. W. Jackson, B. Wang, M. Yang, M. R. Chance, M. Miyagi, A. V. Gudkov, and G. R. Stark. Regulation of NF-κB by NSD1/FBXL11-dependent reversible lysine methylation of p65. *Proceedings of the National Academy of Sciences*, 107(1):46–51, 2010.

Y. Lu, Q. Chang, Y. Zhang, K. Beezhold, Y. Rojanasakul, H. Zhao, V. Castranova, X. Shi, and F. Chen. Lung cancer-associated JmjC domain protein mdig suppresses formation of tri-methyl lysine 9 of histone H3. *Cell Cycle*, 8(13):2101–2109, 2009b.

X. M. Ma and J. Blenis. Molecular mechanisms of mTOR-mediated translational control. *Nature reviews Molecular cell biology*, 10(5):307–318, 2009.

P. C. Mahon, K. Hirota, and G. L. Semenza. FIH-1: a novel protein that interacts with HIF-1α and VHL to mediate repression of HIF-1 transcriptional activity. *Genes & Development*, 15(20):2675–2686, 2001.

Y. Makino, R. Cao, K. Svensson, G. Bertilsson, M. Asman, H. Tanaka, Y. Cao, A. Berkenstam, and L. Poellinger. Inhibitory PAS domain protein is a negative regulator of hypoxia-inducible gene expression. *Nature*, 414(6863):550–554, 2001.

Y. Makino, A. Kanopka, W. J. Wilson, H. Tanaka, and L. Poellinger. Inhibitory PAS domain protein (IPAS) is a hypoxia-inducible splicing variant of the hypoxia-inducible factor-3α locus. *Journal of Biological Chemistry*, 277(36):32405–32408, 2002.

Y. Makino, R. Uenishi, K. Okamoto, T. Isoe, O. Hosono, H. Tanaka, A. Kanopka, L. Poellinger, M. Haneda, and C. Morimoto. Transcriptional up-regulation of inhibitory PAS domain protein gene expression by hypoxia-inducible factor 1 (HIF-1). *Journal of Biological Chemistry*, 282(19):14073–14082, 2007.

M. Malumbres and M. Barbacid. RAS oncogenes: the first 30 years. *Nature Reviews Cancer*, 3(6):459–465, 2003.

M. Manuvakhova, K. Keeling, and D. M. Bedwell. Aminoglycoside antibiotics mediate context-dependent suppression of termination codons in a mammalian translation system. *RNA*, 6(7):1044–1055, 2000.

E. Marcon, Z. Ni, S. Pu, A. L. Turinsky, S. S. Trimble, J. B. Olsen, R. Silverman-Gavrila, L. Silverman-Gavrila, S. Phanse, H. Guo, G. Zhong, X. Guo, P. Young, S. Bailey, D. Roudeva, D. Zhao, J. Hewel, J. Li, S. Graslund, M. Paduch, A. A. Kossiakoff, M. Lupien, A. Emili, S. J. Wodak, and J. Greenblatt. Human-chromatin-related protein interactions identify a demethylase complex required for chromosome segregation. *Cell Reports*, 8(1): 297–310, 2014.

C. Martin and Y. Zhang. The diverse functions of histone lysine methylation. *Nature Reviews Molecular Cell Biology*, 6(11):838–849, 2005.

T. Mašek, L. Valášek, and M. Pospíšek. Polysome analysis and RNA purification from sucrose gradients. In *RNA*, pages 293–309. Springer, 2011.

N. Masson, R. S. Singleton, R. Sekirnik, D. C. Trudgian, L. J. Ambrose, M. X. Miranda, Y.-M. Tian, B. M. Kessler, C. J. Schofield, and P. J. Ratcliffe. The FIH hydroxylase is a cellular peroxide sensor that modulates HIF transcriptional activity. *EMBO Reports*, 13 (3):251–257, 2012.

P. H. Maxwell, C. W. Pugh, and P. J. Ratcliffe. Inducible operation of the erythropoietin 3'enhancer in multiple cell lines: evidence for a widespread oxygen-sensing mechanism. *Proceedings of the National Academy of Sciences*, 90(6):2423–2427, 1993.

M. A. McDonough, C. Loenarz, R. Chowdhury, I. J. Clifton, and C. J. Schofield. Structural studies on human 2-oxoglutarate dependent oxygenases. *Current Opinion in Structural Biology*, 20(6):659–672, 2010.

B. McMullen, K. Fujikawa, and W. Kisiel. The occurrence of β-hydroxyaspartic acid in the vitamin K-dependent blood coagulation zymogens. *Biochemical and Biophysical Research Communications*, 115(1):8–14, 1983.

J. T. Mendell and H. C. Dietz. When the message goes awry: disease-producing mutations that influence mRNA content and performance. *Cell*, 107(4):411–414, 2001.

A. Meskauskas, J. R. Russ, and J. D. Dinman. Structure/function analysis of yeast ribosomal protein L2. *Nucleic Acids Research*, 36(6):1826–1835, 2008.

E. Metzger, M. Wissmann, N. Yin, J. M. Müller, R. Schneider, A. H. Peters, T. Günther, R. Buettner, and R. Schüle. LSD1 demethylates repressive histone marks to promote androgen-receptor-dependent transcription. *Nature*, 437(7057):436–439, 2005.

S. J. Mihalik, J. C. Morrell, D. Kim, K. A. Sacksteder, P. A. Watkins, and S. J. Gould. Identification of PAHX, a Refsum disease gene. *Nature Genetics*, 17(2):185–189, 1997.

Y. A. Minamishima, J. Moslehi, N. Bardeesy, D. Cullen, R. T. Bronson, and W. G. Kaelin. Somatic inactivation of the PHD2 prolyl hydroxylase causes polycythemia and congestive heart failure. *Blood*, 111(6):3236–3244, 2008.

M.-P. Mingeot-Leclercq and P. M. Tulkens. Aminoglycosides: nephrotoxicity. *Antimicrobial Agents and Chemotherapy*, 43(5):1003–1012, 1999.

D. R. Mole, I. Schlemminger, L. A. McNeill, K. S. Hewitson, C. W. Pugh, P. J. Ratcliffe, and C. J. Schofield. 2-oxoglutarate analogue inhibitors of HIF prolyl hydroxylase. *Bioorganic & Medicinal Chemistry Letters*, 13(16):2677–2680, 2003.

S. M. Monte, S. Tamaki, M. C. Cantarini, N. Ince, M. Wiedmann, J. J. Carter, S. A. Lahousse, S. Califano, T. Maeda, T. Ueno, A. D'Errice, F. Trevisano, and J. R. Wands. Aspartyl-(asparaginyl)-β-hydroxylase regulates hepatocellular carcinoma invasiveness. *Journal of Hepatology*, 44(5):971–983, 2006.

L. Mora, V. Heurgué-Hamard, S. Champ, M. Ehrenberg, L. L. Kisselev, and R. H. Buckingham. The essential role of the invariant GGQ motif in the function and stability in vivo of bacterial release factors RF1 and RF2. *Molecular Microbiology*, 47(1):267–275, 2003.

L. Mora, V. Heurgué-Hamard, M. de Zamaroczy, S. Kervestin, and R. H. Buckingham. Methylation of bacterial release factors RF1 and RF2 is required for normal translation termination in vivo. *Journal of Biological Chemistry*, 282(49):35638–35645, 2007.

S. Mordechai, L. Gradstein, A. Pasanen, R. Ofir, K. El Amour, J. Levy, N. Belfair, T. Lifshitz, S. Joshua, G. Narkis, K. Elbedour, J. Myllyharju, and O. S. Birk. High myopia caused by a mutation in *leprel1*, encoding prolyl 3-hydroxylase 2. *The American Journal of Human Genetics*, 89(3):438–445, 2011.

R. Morello, T. K. Bertin, Y. Chen, J. Hicks, L. Tonachini, M. Monticone, P. Castagnola, F. Rauch, F. H. Glorieux, J. Vranka, H. P. Bachinger, J. M. Pace, U. Schwarze, P. H. Byers, M. Weis, R. J. Fernandes, D. R. Eyre, Z. Yao, B. F. Boyce, and B. Lee. CRTAP is required for prolyl 3-hydroxylation and mutations cause recessive osteogenesis imperfecta. *Cell*, 127(2):291–304, 2006.

O. Namy, G. Duchateau-Nguyen, and J.-P. Rousset. Translational readthrough of the PDE2 stop codon modulates cAMP levels in Saccharomyces cerevisiae. *Molecular Microbiology*, 43(3):641–652, 2002.

S. S. Ng, K. L. Kavanagh, M. A. McDonough, D. Butler, E. S. Pilka, B. M. Lienard, J. E. Bray, P. Savitsky, O. Gileadi, F. von Delft, N. R. Rose, J. Offer, J. C. Scheinost, T. Borowski, M. Sundstrom, C. J. Schofield, and U. Oppermann. Crystal structures of histone demethylase JMJD2a reveal basis for substrate specificity. *Nature*, 448(7149):87–91, 2007.

A. Noma, R. Ishitani, M. Kato, A. Nagao, O. Nureki, and T. Suzuki. Expanding role of the jumonji C domain as an RNA hydroxylase. *Journal of Biological Chemistry*, 285(45): 34503–34507, 2010.

T. I. Odintsova, E.-C. Müller, A. V. Ivanov, T. A. Egorov, R. Bienert, S. N. Vladimirov, S. Kostka, A. Otto, B. Wittmann-Liebold, and G. G. Karpova. Characterization and analysis of posttranslational modifications of the human large cytoplasmic ribosomal subunit proteins by mass spectrometry and Edman sequencing. *Journal of Protein Chemistry*, 22 (3):249–258, 2003.

L. O'Flaherty, J. Adam, L. C. Heather, A. V. Zhdanov, Y.-L. Chung, M. X. Miranda, J. Croft, S. Olpin, K. Clarke, C. W. Pugh, J. Griffiths, D. Papkovsky, H. Ashrafian, P. J. Ratcliffe, and P. J. Pollard. Dysregulation of hypoxia pathways in fumarate hydratase-deficient cells is independent of defective mitochondrial metabolism. *Human Molecular Genetics*, 19(19): 3844–3851, 2010.

J. D. Ogle, R. B. Arlinghaus, and M. A. Logan. 3-Hydroxyproline, a new amino acid of collagen. *Journal of Biological Chemistry*, 237(12):3667–3673, 1962.

S. Oh and R. Janknecht. Histone demethylase JMJD5 is essential for embryonic development. *Biochemical and Biophysical Research Communications*, 420(1):61–65, 2012.

M. Ohh, C. W. Park, M. Ivan, M. A. Hoffman, T.-Y. Kim, L. E. Huang, N. Pavletich, V. Chau, and W. G. Kaelin. Ubiquitination of hypoxia-inducible factor requires direct binding to the β-domain of the von Hippel–Lindau protein. *Nature Cell Biology*, 2(7):423–427, 2000.

M. Okamoto, M. Van Stry, L. Chung, M. Koyanagi, X. Sun, Y. Suzuki, O. Ohara, H. Kitamura, A. Hijikata, M. Kubo, and M. Bix. Mina, an Il4 repressor, controls T helper type 2 bias. *Nature Immunology*, 10(8):872–879, 2009.

Y. Pan, K. D. Mansfield, C. C. Bertozzi, V. Rudenko, D. A. Chan, A. J. Giaccia, and M. C. Simon. Multiple factors affecting cellular redox status and energy metabolism modulate hypoxia-inducible factor prolyl hydroxylase activity in vivo and in vitro. *Molecular and Cellular Biology*, 27(3):912–925, 2007.

P. Paschka, R. F. Schlenk, V. I. Gaidzik, M. Habdank, J. Krönke, L. Bullinger, D. Späth, S. Kayser, M. Zucknick, K. Götze, et al. IDH1 and IDH2 mutations are frequent genetic alterations in acute myeloid leukemia and confer adverse prognosis in cytogenetically normal acute myeloid leukemia with NPM1 mutation without FLT3 internal tandem duplication. *Journal of Clinical Oncology*, 28(22):3636–3643, 2010.

K. Passoja, K. Rautavuoma, L. Ala-Kokko, T. Kosonen, and K. I. Kivirikko. Cloning and characterization of a third human lysyl hydroxylase isoform. *Proceedings of the National Academy of Sciences*, 95(18):10482–10486, 1998.

L. Pauling and R. B. Corey. The structure of fibrous proteins of the collagen-gelatin group. *Proceedings of the National Academy of Sciences*, 37(5):278,Äì–281, 1951.

H. R. Pelham. Leaky UAG termination codon in tobacco mosaic virus RNA. *Nature*, 272: 469,Äì–471, 1978.

T. V. Pestova and C. U. Hellen. Translation elongation after assembly of ribosomes on the Cricket paralysis virus internal ribosomal entry site without initiation factors or initiator tRNA. *Genes & Development*, 17(2):181–186, 2003.

T. V. Pestova, S. I. Borukhov, and C. U. Hellen. Eukaryotic ribosomes require initiation factors 1 and 1A to locate initiation codons. *Nature*, 394(6696):854–859, 1998.

B. Peterkofsky and S. Udenfriend. Conversion of proline to collagen hydroxyproline in a cell-free system from chick embryo. *Journal of Biological Chemistry*, 238(12):3966–3977, 1963.

T. Pihlajaniemi, T. Helaakoski, K. Tasanen, R. Myllylä, M. Huhtala, J. Koivu, and K. Kivirikko. Molecular cloning of the beta-subunit of human prolyl 4-hydroxylase. This subunit and protein disulphide isomerase are products of the same gene. *The EMBO Journal*, 6(3):643, 1987.

E. Pokidysheva, K. D. Zientek, Y. Ishikawa, K. Mizuno, J. A. Vranka, N. T. Montgomery, D. R. Keene, T. Kawaguchi, K. Okuyama, and H. P. Bächinger. Posttranslational modifications in type I collagen from different tissues extracted from wild type and prolyl 3-hydroxylase 1 null mice. *Journal of Biological Chemistry*, 288(34):24742–24752, 2013.

E. Pokidysheva, S. Boudko, J. Vranka, K. Zientek, K. Maddox, M. Moser, R. Fässler, J. Ware, and H. P. Bächinger. Biological role of prolyl 3-hydroxylation in type IV collagen. *Proceedings of the National Academy of Sciences*, 111(1):161–166, 2014.

B. Polevoda, L. Span, and F. Sherman. The yeast translation release factors Mrf1p and Sup45p (eRF1) are methylated, respectively, by the methyltransferases Mtq1p and Mtq2p. *Journal of Biological Chemistry*, 281(5):2562–2571, 2006.

P. Pollard, J. Briere, N. Alam, J. Barwell, E. Barclay, N. Wortham, T. Hunt, M. Mitchell, S. Olpin, S. J. Moat, I. P. Hargreaves, S. J. Heales, Y. L. Chung, J. R. Griffiths, A. Dalgleish, J. A. McGrath, M. J. Gleeson, S. V. Hodgson, R. Poulsom, P. Rustin, and I. P. M. Tomlinson. Accumulation of Krebs cycle intermediates and over-expression of HIF1α in tumours which result from germline FH and SDH mutations. *Human Molecular Genetics*, 14(15):2231–2239, 2005.

P. J. Pollard, B. Spencer-Dene, D. Shukla, K. Howarth, E. Nye, M. El-Bahrawy, M. Deheragoda, M. Joannou, S. McDonald, A. Martin, P. Igarashi, S. Varsani-Brown, I. Rosewell, R. Poulsom, P. Maxwell, G. W. Stamp, and I. P. M. Tomlinson. Targeted inactivation of *fh1* causes proliferative renal cyst development and activation of the hypoxia pathway. *Cancer Cell*, 11(4):311–319, 2007.

V. Ponnaluri, D. T. Vavilala, S. Putty, W. G. Gutheil, and M. Mukherji. Identification of non-histone substrates for JMJD2A,ÄîC histone demethylases. *Biochemical and Biophysical Research Communications*, 390(2):280–284, 2009.

A. Preis, A. Heuer, C. Barrio-Garcia, A. Hauser, D. E. Eyler, O. Berninghausen, R. Green, T. Becker, and R. Beckmann. Cryoelectron microscopic structures of eukaryotic translation termination complexes containing eRF1-eRF3 or eRF1-ABCE1. *Cell Reports*, 2014.

J. C. Price, E. W. Barr, B. Tirupati, J. M. Bollinger, and C. Krebs. The first direct characterization of a high-valent iron intermediate in the reaction of an α-ketoglutarate-dependent dioxygenase: a high-spin Fe (iv) complex in taurine/α-ketoglutarate dioxygenase (TauD) from Escherichia coli. *Biochemistry*, 42(24):7497–7508, 2003.

D. J. Prockop and K. Juva. Synthesis of hydroxyproline in vitro by the hydroxylation of proline in a precursor of collagen. *Proceedings of the National Academy of Sciences*, 53(3): 661, 1965.

J. Prockop. Collagens: molecular biology, diseases, and potentials for therapy. *Annual Review of Biochemistry*, 64(1):403–434, 1995.

C. T. Przysiecki, J. E. Staggers, H. G. Ramjit, D. G. Musson, A. M. Stern, C. D. Bennett, and P. A. Friedman. Occurrence of beta-hydroxylated asparagine residues in non-vitamin K-dependent proteins containing epidermal growth factor-like domains. *Proceedings of the National Academy of Sciences*, 84(22):7856–7860, 1987.

C. Pugh, C. Tan, R. Jones, and P. Ratcliffe. Functional analysis of an oxygen-regulated transcriptional enhancer lying 3' to the mouse erythropoietin gene. *Proceedings of the National Academy of Sciences*, 88(23):10553–10557, 1991.

M. T. Puig-Hervás, S. Temtamy, M. Aglan, M. Valencia, V. Martínez-Glez, M. J. Ballesta-Martínez, V. López-González, A. M. Ashour, K. Amr, V. Pulido, E. Guillén-Navarro, P. Lapunzina, J. Capparrós-Martin, and V. L. Ruiz-Perez. Mutations in PLOD2 cause autosomal-recessive connective tissue disorders within the Bruck syndrome,ÄîOsteogenesis imperfecta phenotypic spectrum. *Human Mutation*, 33(10):1444–1449, 2012.

A. M. Pyle. Metal ions in the structure and function of RNA. *Journal of Biological Inorganic Chemistry*, 7(7-8):679–690, 2002.

H. H. Qi, P. P. Ongusaha, J. Myllyharju, D. Cheng, O. Pakkanen, Y. Shi, S. W. Lee, J. Peng, and Y. Shi. Prolyl 4-hydroxylation regulates Argonaute 2 stability. *Nature*, 455(7211): 421–424, 2008.

H. H. Qi, M. Sarkissian, G.-Q. Hu, Z. Wang, A. Bhattacharjee, D. B. Gordon, M. Gonzales, F. Lan, P. P. Ongusaha, M. Huarte, N. K. Yaghi, H. Lim, B. A. Garcia, L. Brizuela, K. Zhao, T. M. Roberts, and Y. Shi. Histone H4K20/H3K9 demethylase PHF8 regulates zebrafish brain and craniofacial development. *Nature*, 466(7305):503–507, 2010.

S. Ramagopal. Covalent modifications of ribosomal proteins in growing and aggregation-competent Dictyostelium discoideum: phosphorylation and methylation. *Biochemistry and Cell Biology*, 69(4):263–268, 1991.

T. A. Rand, S. Petersen, F. Du, and X. Wang. Argonaute2 cleaves the anti-guide strand of siRNA during RISC activation. *Cell*, 123(4):621–629, 2005.

P. J. Ratcliffe. HIF-1 and HIF-2: working alone or together in hypoxia? *The Journal of Clinical Investigation*, 117(4):862–865, 2007.

P. J. Ratcliffe. Oxygen sensing and hypoxia signalling pathways in animals: the implications of physiology for cancer. *The Journal of Physiology*, 591(8):2027–2042, 2013.

T. A. Rege and J. S. Hagood. Thy-1 as a regulator of cell-cell and cell-matrix interactions in axon regeneration, apoptosis, adhesion, migration, cancer, and fibrosis. *The FASEB journal*, 20(8):1045–1054, 2006.

J. Ren, Y. Wang, Y. Liang, Y. Zhang, S. Bao, and Z. Xu. Methylation of ribosomal protein S10 by protein-arginine methyltransferase 5 regulates ribosome biogenesis. *Journal of Biological Chemistry*, 285(17):12695–12705, 2010.

N. R. Rose, M. A. McDonough, O. N. King, A. Kawamura, and C. J. Schofield. Inhibition of 2-oxoglutarate dependent oxygenases. *Chemical Society Reviews*, 40(8):4364–4397, 2011.

H. Ruotsalainen, L. Sipilä, E. Kerkelä, H. Pospiech, and R. Myllylä. Characterization of cDNAs for mouse lysyl hydroxylase 1, 2 and 3, their phylogenetic analysis and tissue-specific expression in the mouse. *Matrix Biology*, 18(3):325–329, 1999.

H. Ruotsalainen, L. Sipilä, M. Vapola, R. Sormunen, A. M. Salo, L. Uitto, D. K. Mercer, S. P. Robins, M. Risteli, A. Aszodi, et al. Glycosylation catalyzed by lysyl hydroxylase 3 is essential for basement membranes. *Journal of Cell Science*, 119(4):625–635, 2006.

I. Ruvinsky and O. Meyuhas. Ribosomal protein S6 phosphorylation: from protein synthesis to cell size. *Trends in Biochemical Sciences*, 31(6):342–348, 2006.

I. Ruvinsky, N. Sharon, T. Lerer, H. Cohen, M. Stolovich-Rain, T. Nir, Y. Dor, P. Zisman, and O. Meyuhas. Ribosomal protein S6 phosphorylation is a determinant of cell size and glucose homeostasis. *Genes & Development*, 19(18):2199–2211, 2005.

J. Salas-Marco and D. M. Bedwell. GTP hydrolysis by eRF3 facilitates stop codon decoding during eukaryotic translation termination. *Molecular and Cellular Biology*, 24(17):7769–7778, 2004.

A. M. Salo, H. Cox, P. Farndon, C. Moss, H. Grindulis, M. Risteli, S. P. Robins, and R. Myllylä. A connective tissue disorder caused by mutations of the lysyl hydroxylase 3 gene. *The American Journal of Human Genetics*, 83(4):495–503, 2008.

T. D. Schmittgen and K. J. Livak. Analyzing real-time PCR data by the comparative CT method. *Nature Protocols*, 3(6):1101–1108, 2008.

J. E. Schneider, J. Böse, S. D. Bamforth, A. D. Gruber, C. Broadbent, K. Clarke, S. Neubauer, A. Lengeling, and S. Bhattacharya. Identification of cardiac malformations in mice lacking Ptdsr using a novel high-throughput magnetic resonance imaging technique. *BMC Developmental Biology*, 4(1):16, 2004.

C. J. Schofield and P. J. Ratcliffe. Oxygen sensing by HIF hydroxylases. *Nature Reviews Molecular Cell Biology*, 5(5):343–354, 2004.

H. Schulze and K. H. Nierhaus. Minimal set of ribosomal components for reconstitution of the peptidyltransferase activity. *The EMBO Journal*, 1(5):609, 1982.

E. Scolnick, R. Tompkins, T. Caskey, and M. Nirenberg. Release factors differing in specificity for terminator codons. *Proceedings of the National Academy of Sciences*, 61(2):768, 1968.

A. Seit-Nebi, L. Frolova, J. Justesen, and L. Kisselev. Class-1 translation termination factors: invariant GGQ minidomain is essential for release activity and ribosome binding but not for stop codon recognition. *Nucleic Acids Research*, 29(19):3982–3987, 2001.

A. Seit-Nebi, L. Frolova, and L. Kisselev. Conversion of omnipotent translation termination factor eRF1 into ciliate-like UGA-only unipotent eRF1. *EMBO Reports*, 3(9):881–886, 2002.

G. L. Semenza. Defining the role of hypoxia-inducible factor 1 in cancer biology and therapeutics. *Oncogene*, 29(5):625, 2010.

G. L. Semenza and G. L. Wang. A nuclear factor induced by hypoxia via de novo protein synthesis binds to the human erythropoietin gene enhancer at a site required for transcriptional activation. *Molecular and Cellular Biology*, 12(12):5447, 1992.

G. L. Semenza, M. K. Nejfelt, S. M. Chi, and S. E. Antonarakis. Hypoxia-inducible nuclear factors bind to an enhancer element located 3' to the human erythropoietin gene. *Proceedings of the National Academy of Sciences*, 88(13):5680–5684, 1991.

P. S. Sepe, S. A. Lahousse, B. Gemelli, H. Chang, T. Maeda, J. R. Wands, and S. M. de la Monte. Role of the aspartyl-asparaginy β-hydroxylase gene in neuroblastoma cell motility. *Laboratory Investigation*, 82(7):881–891, 2002.

D. J. Seward, G. Cubberley, S. Kim, M. Schonewald, L. Zhang, B. Tripet, and D. L. Bentley. Demethylation of trimethylated histone H3 lys4 in vivo by JARID1 JmjC proteins. *Nature Structural & Molecular Biology*, 14(3):240–242, 2007.

Y. Shi, F. Lan, C. Matson, P. Mulligan, J. R. Whetstine, P. A. Cole, R. A. Casero, and Y. Shi. Histone demethylation mediated by the nuclear amine oxidase homolog LSD1. *Cell*, 119 (7):941–953, 2004.

A. Shirai, M. Sadaie, K. Shinmyozu, and J.-i. Nakayama. Methylation of ribosomal protein L42 regulates ribosomal function and stress-adapted cell growth. *Journal of Biological Chemistry*, 285(29):22448–22460, 2010.

M. D. Shoulders and R. T. Raines. Collagen structure and stability. *Annual Review of Biochemistry*, 78:929, 2009.

A. Sidow, M. S. Bulotsky, A. W. Kerrebrock, R. T. Bronson, M. J. Daly, M. P. Reeve, T. L. Hawkins, B. W. Birren, R. Jaenisch, and E. S. Lander. Serrate2 is disrupted in the mouse limb-development mutant syndactylism. *Nature*, 389(6652):722–725, 1997.

R. S. Singleton, P. Liu-Yi, F. Formenti, W. Ge, R. Fischer, J. Adam, P. J. Pollard, A. Wolf, A. Thalhammer, C. Loenarz, E. Flashman, A. Yamamoto, M. L. Coleman, B. M. Kessler, P. Wappner, C. J. Schofield, P. J. Ratcliffe, and M. E. Cockman. OGFOD1 catalyzes prolyl hydroxylation of RPS23 and is involved in translation control and stress granule formation. *Proceedings of the National Academy of Sciences*, 111(11):4031–4036, 2014.

K. M. Sinha, H. Yasuda, M. M. Coombes, S. Y. Dent, and B. de Crombrugghe. Regulation of the osteoblast-specific transcription factor Osterix by NO66, a jumonji family histone demethylase. *The EMBO Journal*, 29(1):68–79, 2010.

K. M. Sinha, H. Yasuda, X. Zhou, and B. deCrombrugghe. Osterix and NO66 histone demethylase control the chromatin of Osterix target genes during osteoblast differentiation. *Journal of Bone and Mineral Research*, 29(4):855–865, 2014.

J. M. Skuzeski, L. M. Nichols, R. F. Gesteland, and J. F. Atkins. The signal for a leaky UAG stop codon in several plant viruses includes the two downstream codons. *Journal of Molecular Biology*, 218(2):365–373, 1991.

C. Söderhäll, I. Marenholz, T. Kerscher, F. Rüschendorf, J. Esparza-Gordillo, M. Worm, C. Gruber, G. Mayr, M. Albrecht, K. Rohde, H. Schulz, U. Wahn, N. Hubner, and Y.-A. Lee. Variants in a novel epidermal collagen gene (COL29A1) are associated with atopic dermatitis. *PLoS Biology*, 5(9):e242, 2007.

N. Sonenberg and A. G. Hinnebusch. Regulation of translation initiation in eukaryotes: mechanisms and biological targets. *Cell*, 136(4):731–745, 2009.

H. Song, P. Mugnier, A. K. Das, H. M. Webb, D. R. Evans, M. F. Tuite, B. A. Hemmings, and D. Barford. The crystal structure of human eukaryotic release factor eRF1–mechanism of stop codon recognition and peptidyl-tRNA hydrolysis. *Cell*, 100(3):311–321, 2000.

K. A. Spriggs, M. Bushell, and A. E. Willis. Translational regulation of gene expression during conditions of cell stress. *Molecular Cell*, 40(2):228–237, 2010.

I. Stansfield, K. Jones, V. Kushnirov, A. Dagkesamanskaya, A. Poznyakovski, S. Paushkin, C. Nierras, B. Cox, M. Ter-Avanesyan, and M. Tuite. The products of the SUP45 (eRF1) and SUP35 genes interact to mediate translation termination in Saccharomyces cerevisiae. *The EMBO Journal*, 14(17):4365, 1995.

P. Steneberg and C. Samakovlis. A novel stop codon readthrough mechanism produces functional headcase protein in Drosophila trachea. *EMBO Reports*, 2(7):593–597, 2001.

J. Stenflo, A. Lundwall, and B. Dahlbäck. β-Hydroxyasparagine in domains homologous to the epidermal growth factor precursor in vitamin K-dependent protein s. *Proceedings of the National Academy of Sciences*, 84(2):368–372, 1987.

J. Stenflo, A. Ohlin, W. Owen, and W. Schneider. β-Hydroxyaspartic acid or beta-hydroxyasparagine in bovine low density lipoprotein receptor and in bovine thrombomodulin. *Journal of Biological Chemistry*, 263(1):21–24, 1988.

J. Stenflo, E. Holme, S. Lindstedt, N. Chandramouli, L. Huang, J. P. Tam, and R. Merrifield. Hydroxylation of aspartic acid in domains homologous to the epidermal growth factor precursor is catalyzed by a 2-oxoglutarate-dependent dioxygenase. *Proceedings of the National Academy of Sciences*, 86(2):444–447, 1989.

J. Stenflo, Y. Stenberg, and A. Muranyi. Calcium-binding EGF-like modules in coagulation proteinases: function of the calcium ion in module interactions. *Biochimica et Biophysica Acta (BBA)-Protein Structure and Molecular Enzymology*, 1477(1):51–63, 2000.

M. R. Stetten. Some aspects of the metabolism of hydroxyproline, studied with the aid of isotopic nitrogen. *Journal of Biological Chemistry*, 181(1):31–37, 1949.

I. P. Stolze, Y.-M. Tian, R. J. Appelhoff, H. Turley, C. C. Wykoff, J. M. Gleadle, and P. J. Ratcliffe. Genetic analysis of the role of the asparaginyl hydroxylase factor inhibiting hypoxia-inducible factor (HIF) in regulating HIF transcriptional target genes. *Journal of Biological Chemistry*, 279(41):42719–42725, 2004.

M. S. Sunnerhagen, E. Persson, I. Dahlqvist, T. Drakenberg, J. Stenflo, M. Mayhew, M. Robin, P. Handford, J. Tilley, and I. Campbell. The effect of aspartate hydroxylation on calcium binding to epidermal growth factor-like modules in coagulation factors IX and X. *Journal of Biological Chemistry*, 268(31):23339–23344, 1993.

C. Suzuki, K. Takahashi, S. Hayama, N. Ishikawa, T. Kato, T. Ito, E. Tsuchiya, Y. Nakamura, and Y. Daigo. Identification of Myc-associated protein with JmjC domain as a novel therapeutic target oncogene for lung cancer. *Molecular Cancer Therapeutics*, 6(2):542–551, 2007.

H. L. Sweeney. Suppression of premature stop codons for the treatment of a subset of patients with genetic disorders. *Journal of Medical Sciences*, 2(1):1–4, 2009.

M. Tahiliani, P. Mei, R. Fang, T. Leonor, M. Rutenberg, F. Shimizu, J. Li, A. Rao, and Y. Shi. The histone H3K4 demethylase SMCX links REST target genes to X-linked mental retardation. *Nature*, 447(7144):601–605, 2007.

M. Tahiliani, K. P. Koh, Y. Shen, W. A. Pastor, H. Bandukwala, Y. Brudno, S. Agarwal, L. M. Iyer, D. R. Liu, L. Aravind, and A. Rao. Conversion of 5-methylcytosine to 5-hydroxymethylcytosine in mammalian DNA by MLL partner TET1. *Science*, 324(5929): 930–935, 2009.

K. Takaluoma, J. Lantto, and J. Myllyharju. Lysyl hydroxylase 2 is a specific telopeptide hydroxylase, while all three isoenzymes hydroxylate collagenous sequences. *Matrix Biology*, 26(5):396–403, 2007.

K. Takeda, V. C. Ho, H. Takeda, L.-J. Duan, A. Nagy, and G.-H. Fong. Placental but not heart defects are associated with elevated hypoxia-inducible factor α levels in mice lacking prolyl hydroxylase domain protein 2. *Molecular and Cellular Biology*, 26(22):8336–8346, 2006.

K. Takeda, H. L. Aguila, N. S. Parikh, X. Li, K. Lamothe, L.-J. Duan, H. Takeda, F. S. Lee, and G.-H. Fong. Regulation of adult erythropoiesis by prolyl hydroxylase domain proteins. *Blood*, 111(6):3229–3235, 2008.

X.-P. Tan, Q. Zhang, W.-G. Dong, X.-W. Lei, and Z.-R. Yang. Upregulated expression of Mina53 in cholangiocarcinoma and its clinical significance. *Oncology Letters*, 3(5):1037–1041, 2012.

H. Tarhonskaya, A. M. Rydzik, I. K. Leung, N. D. Loik, M. C. Chan, A. Kawamura, J. S. McCullagh, T. D. Claridge, E. Flashman, and C. J. Schofield. Non-enzymatic chemistry enables 2-hydroxyglutarate-mediated activation of 2-oxoglutarate oxygenases. *Nature Communications*, 5, 2014.

K. Teye, M. Tsuneoka, N. Arima, Y. Koda, Y. Nakamura, Y. Ueta, K. Shirouzu, and H. Kimura. Increased expression of a Myc target gene Mina53 in human colon cancer. *The American Journal of Pathology*, 164(1):205–216, 2004.

P. Tiainen, A. Pasanen, R. Sormunen, and J. Myllyharju. Characterization of recombinant human prolyl 3-hydroxylase isoenzyme 2, an enzyme modifying the basement membrane collagen IV. *Journal of Biological Chemistry*, 283(28):19432–19439, 2008.

H. Tian, S. L. McKnight, and D. W. Russell. Endothelial PAS domain protein 1 (EPAS1), a transcription factor selectively expressed in endothelial cells. *Genes & Development*, 11 (1):72–82, 1997.

Y.-M. Tian, K. K. Yeoh, M. K. Lee, T. Eriksson, B. M. Kessler, H. B. Kramer, M. J. Edelmann, C. Willam, C. W. Pugh, C. J. Schofield, and P. J. Ratcliffe. Differential sensitivity of hypoxia inducible factor hydroxylation sites to hypoxia and hydroxylase inhibitors. *Journal of Biological Chemistry*, 286(15):13041–13051, 2011.

P. Trojer, J. Zhang, M. Yonezawa, A. Schmidt, H. Zheng, T. Jenuwein, and D. Reinberg. Dynamic histone H1 isotype 4 methylation and demethylation by histone lysine methyltransferase G9a/KMT1C and the Jumonji domain-containing JMJD2/KDM4 proteins. *Journal of Biological Chemistry*, 284(13):8395–8405, 2009.

D. C. Trudgian, B. Thomas, S. J. McGowan, B. M. Kessler, M. Salek, and O. Acuto. CPFP: a central proteomics facilities pipeline. *Bioinformatics*, 26(8):1131–1132, 2010.

K. Tryggvason, K. Majamaa, J. Risteli, and K. I. Kivirikko. Partial purification and characterization of chick-embryo prolyl 3-hydroxylase. *Biochemical Journal*, 183:303–307, 1979.

Y.-i. Tsukada, J. Fang, H. Erdjument-Bromage, M. E. Warren, C. H. Borchers, P. Tempst, and Y. Zhang. Histone demethylation by a family of JmjC domain-containing proteins. *Nature*, 439(7078):811–816, 2006.

Y.-i. Tsukada, T. Ishitani, and K. I. Nakayama. KDM7 is a dual demethylase for histone H3 lys 9 and Lys 27 and functions in brain development. *Genes & Development*, 24(5): 432–437, 2010.

M. Tsuneoka, Y. Koda, M. Soejima, K. Teye, and H. Kimura. A novel myc target gene, mina53, that is involved in cell proliferation. *Journal of Biological Chemistry*, 277(38): 35450–35459, 2002.

M. Tsuneoka, H. Fujita, N. Arima, K. Teye, T. Okamura, H. Inutsuka, Y. Koda, K. Shirouzu, and H. Kimura. Mina53 as a potential prognostic factor for esophageal squamous cell carcinoma. *Clinical Cancer Research*, 10(21):7347–7356, 2004.

S. Turcan, D. Rohle, A. Goenka, L. A. Walsh, F. Fang, E. Yilmaz, C. Campos, A. W. Fabius, C. Lu, P. S. Ward, et al. IDH1 mutation is sufficient to establish the glioma hypermethylator phenotype. *Nature*, 483(7390):479–483, 2012.

M. Unoki, A. Masuda, N. Dohmae, K. Arita, M. Yoshimatsu, Y. Iwai, Y. Fukui, K. Ueda, R. Hamamoto, M. Shirakawa, H. Sasaki, and Y. Nakamura. Lysyl 5-hydroxylation, a novel histone modification, by Jumonji domain containing 6 (JMJD6). *Journal of Biological Chemistry*, 288(9):6053–6062, 2013.

M. Valtavaara, H. Papponen, A.-M. Pirttilä, K. Hiltunen, H. Helander, and R. Myllylä. Cloning and characterization of a novel human lysyl hydroxylase isoform highly expressed in pancreas and muscle. *Journal of Biological Chemistry*, 272(11):6831–6834, 1997.

M. Valtavaara, C. Szpirer, J. Szpirer, and R. Myllylä. Primary structure, tissue distribution, and chromosomal localization of a novel isoform of lysyl hydroxylase (lysyl hydroxylase 3). *Journal of Biological Chemistry*, 273(21):12881–12886, 1998.

E. van den Born, C. B. Vågbø, L. Songe-Møller, V. Leihne, G. F. Lien, G. Leszczynska, A. Malkiewicz, H. E. Krokan, F. Kirpekar, A. Klungland, and P. Ø. Falnes. ALKBH8-mediated formation of a novel diastereomeric pair of wobble nucleosides in mammalian tRNA. *Nature Communications*, 2:172, 2011.

A. J. van der Slot, A.-M. Zuurmond, A. F. Bardoel, C. Wijmenga, H. E. Pruijs, D. O. Sillence, J. Brinckmann, D. J. Abraham, C. M. Black, N. Verzijl, J. DeGroot, R. Hanemaaijer, J. M. TeKoppele, T. W. J. Huizinga, and R. A. Band. Identification of PLOD2 as telopeptide lysyl hydroxylase, an important enzyme in fibrosis. *Journal of Biological Chemistry*, 278 (42):40967–40972, 2003.

F. S. van Dijk, I. M. Nesbitt, E. H. Zwikstra, P. G. Nikkels, S. R. Piersma, S. A. Fratantoni, C. R. Jimenez, M. Huizer, A. C. Morsman, J. M. Cobben, M. H. H. van Roij, M. W. Elting, J. I. M. L. Verbeke, L. C. D. Wijnaendts, N. J. Shaw, W. Hogler, C. McKeown, E. A. Sistermans, A. Dalton, H. Meijers-Heijboer, and G. Pals. *PPIB* mutations cause severe osteogenesis imperfecta. *The American Journal of Human Genetics*, 85(4):521–527, 2009.

K. M. Vattem and R. C. Wek. Reinitiation involving upstream ORFs regulates ATF4 mRNA translation in mammalian cells. *Proceedings of the National Academy of Sciences of the United States of America*, 101(31):11269–11274, 2004.

B. Vestergaard, L. B. Van, G. R. Andersen, J. Nyborg, R. H. Buckingham, and M. Kjeldgaard. Bacterial polypeptide release factor RF2 is structurally distinct from eukaryotic eRF1. *Molecular Cell*, 8(6):1375–1382, 2001.

J. A. Vranka, L. Y. Sakai, and H. P. Bächinger. Prolyl 3-hydroxylase 1, enzyme characterization and identification of a novel family of enzymes. *Journal of Biological Chemistry*, 279 (22):23615–23621, 2004.

J. A. Vranka, E. Pokidysheva, L. Hayashi, K. Zientek, K. Mizuno, Y. Ishikawa, K. Maddox, S. Tufa, D. R. Keene, R. Klein, and H. P. Bächinger. Prolyl 3-hydroxylase 1 null mice display abnormalities in fibrillar collagen-rich tissues such as tendons, skin, and bones. *Journal of Biological Chemistry*, 285(22):17253–17262, 2010.

L. J. Walport, R. J. Hopkinson, M. Vollmar, S. K. Madden, C. Gileadi, U. Oppermann, C. J. Schofield, and C. Johansson. Human UTY (KDM6C) is a male-specific nϵ-methyl lysyl-demethylase. *Journal of Biological Chemistry*, 289(26):18302,Äì–18313, 2014.

C. Wang, H. Luosujärvi, J. Heikkinen, M. Risteli, L. Uitto, and R. Myllylä. The third activity for lysyl hydroxylase 3: galactosylation of hydroxylysyl residues in collagens in vitro. *Matrix Biology*, 21(7):559–566, 2002.

D. Wang, V. Belakhov, J. Kandasamy, T. Baasov, S.-C. Li, Y.-T. Li, D. M. Bedwell, and K. M. Keeling. The designer aminoglycoside NB84 significantly reduces glycosaminoglycan accumulation associated with MPS IH in the Idua-W392X mouse. *Molecular Genetics and Metabolism*, 105(1):116–125, 2012.

G. L. Wang and G. L. Semenza. General involvement of hypoxia-inducible factor 1 in transcriptional response to hypoxia. *Proceedings of the National Academy of Sciences*, 90(9): 4304–4308, 1993.

G. L. Wang, B.-H. Jiang, E. A. Rue, and G. L. Semenza. Hypoxia-inducible factor 1 is a basic-helix-loop-helix-PAS heterodimer regulated by cellular O2 tension. *Proceedings of the National Academy of Sciences*, 92(12):5510–5514, 1995.

H.-J. Wang, Y.-J. Hsieh, W.-C. Cheng, C.-P. Lin, Y.-s. Lin, S.-F. Yang, C.-C. Chen, Y. Izumiya, J.-S. Yu, H.-J. Kung, and W.-C. Wang. JMJD5 regulates PKM2 nuclear translocation and reprograms HIF-1α–mediated glucose metabolism. *Proceedings of the National Academy of Sciences*, 111(1):279–284, 2014a.

X. Wang, Z. Lu, A. Gomez, G. C. Hon, Y. Yue, D. Han, Y. Fu, M. Parisien, Q. Dai, G. Jia, T. Ren, and C. He. N6-methyladenosine-dependent regulation of messenger RNA stability. *Nature*, 2013.

Y. Wang, J. Wysocka, J. Sayegh, Y.-H. Lee, J. R. Perlin, L. Leonelli, L. S. Sonbuchner, C. H. McDonald, R. G. Cook, Y. Dou, R. G. Roeder, S. Clarke, M. R. Stallcup, C. D. Allis, and S. A. Coonrod. Human PAD4 regulates histone arginine methylation levels via demethylimination. *Science*, 306(5694):279–283, 2004.

Y. Wang, Y. Li, J. I. Toth, M. D. Petroski, Z. Zhang, and J. C. Zhao. N6-methyladenosine modification destabilizes developmental regulators in embryonic stem cells. *Nature Cell Biology*, 16:191–198, 2014b.

J. D. Webb, A. Murányi, C. W. Pugh, P. J. Ratcliffe, and M. L. Coleman. MYPT1, the targeting subunit of smooth-muscle myosin phosphatase, is a substrate for the asparaginyl hydroxylase factor inhibiting hypoxia-inducible factor (FIH). *Biochemical Journal*, 420: 327–333, 2009.

C. J. Webby, A. Wolf, N. Gromak, M. Dreger, H. Kramer, B. Kessler, M. L. Nielsen, C. Schmitz, D. S. Butler, J. R. Yates III, C. M. Delahunty, P. Hahn, A. Lengeling, M. Mann, N. J. Proudfoot, C. J. Schofield, and A. Böttger. Jmjd6 catalyses lysyl-hydroxylation of U2AF65, a protein associated with RNA splicing. *Science*, 325(5936):90–93, 2009.

E. M. Welch, E. R. Barton, J. Zhuo, Y. Tomizawa, W. J. Friesen, P. Trifillis, S. Paushkin, M. Patel, C. R. Trotta, S. Hwang, R. G. Wilde, G. Karp, J. Takasugi, G. Chen, S. Jongs, H. Ren, Y.-C. Moon, D. Corson, A. A. Turpoff, J. A. Campbell, M. M. Conn, A. Khan, N. G. Almstead, J. Hedrick, A. Mollin, N. Risher, M. Weetail, S. Yeh, A. A. Branstrom, J. M. Colacino, J. Babiak, D. Ju, William, S. Hirawat, V. J. Northcutt, L. L. Miller, H. F. Spatrick, Phyllis, M. Kawana, H. Feng, A. Jacobson, S. W. Peltz, and H. L. Sweeney. PTC124 targets genetic disorders caused by nonsense mutations. *Nature*, 447(7140):87–91, 2007.

H. Wen, J. Li, T. Song, M. Lu, P.-Y. Kan, M. G. Lee, B. Sha, and X. Shi. Recognition of histone H3K4 trimethylation by the plant homeodomain of PHF2 modulates histone demethylation. *Journal of Biological Chemistry*, 285(13):9322–9326, 2010.

M. P. Westbye, E. Feyzi, P. A. Aas, C. B. Vågbø, V. A. Talstad, B. Kavli, L. Hagen, O. Sundheim, M. Akbari, N.-B. Liabakk, G. Slupphaug, M. Otterlei, and H. E. Krokan. Human AlkB homolog 1 is a mitochondrial protein that demethylates 3-methylcytosine in DNA and RNA. *Journal of Biological Chemistry*, 283(36):25046–25056, 2008.

J. R. Whetstine, A. Nottke, F. Lan, M. Huarte, S. Smolikov, Z. Chen, E. Spooner, E. Li, G. Zhang, M. Colaiacovo, and Y. Shi. Reversal of histone lysine trimethylation by the JMJD2 family of histone demethylases. *Cell*, 125(3):467–481, 2006.

P. Williamson and R. A. Schlegel. Hide and seek: the secret identity of the phosphatidylserine receptor. *Journal of Biology*, 3(4):14, 2004.

N. M. Wills, B. Moore, A. Hammer, R. F. Gesteland, and J. F. Atkins. A functional –1 ribosomal frameshift signal in the human paraneoplastic Ma3 gene. *Journal of Biological Chemistry*, 281(11):7082–7088, 2006.

Z.-Q. Xi, J.-J. Sun, X.-F. Wang, M.-W. Li, X.-Z. Liu, L.-Y. Wang, X. Zhu, F. Xiao, J.-M. Li, Y. Gong, and L.-F. Guan. HSPBAP1 is found extensively in the anterior temporal neocortex of patients with intractable epilepsy. *Synapse*, 61(9):741–747, 2007.

M. Xiao, H. Yang, W. Xu, S. Ma, H. Lin, H. Zhu, L. Liu, Y. Liu, C. Yang, Y. Xu, S. Zhao, D. Ye, Y. Xiong, and K.-L. Guan. Inhibition of α-KG-dependent histone and DNA demethylases by fumarate and succinate that are accumulated in mutations of FH and SDH tumor suppressors. *Genes & Development*, 26(12):1326–1338, 2012.

W. Xu, H. Yang, Y. Liu, Y. Yang, P. Wang, S.-H. Kim, S. Ito, C. Yang, P. Wang, M.-T. Xiao, L.-x. Liu, W.-q. Jiang, J. Liu, J.-y. Zhang, B. Wang, S. Frye, Y. Zhang, Y.-h. Xu, Q.-y. Lei, K.-L. Guan, s.-m. Zhao, and Y. Xiong. Oncometabolite 2-hydroxyglutarate is a competitive inhibitor of α-ketoglutarate-dependent dioxygenases. *Cancer cell*, 19(1):17–30, 2011.

F. Xue and L. Cooley. Kelch encodes a component of intercellular bridges in Drosophila egg chambers. *Cell*, 72(5):681–693, 1993.

S. Xue and M. Barna. Specialized ribosomes: a new frontier in gene regulation and organismal biology. *Nature Reviews Molecular cell biology*, 13(6):355–369, 2012.

Y. Yamaguchi, A. Hayashi, C. W. Campagnoni, A. Kimura, T. Inuzuka, and H. Baba. L-MPZ, a novel isoform of myelin P0, is produced by stop codon readthrough. *Journal of Biological Chemistry*, 287(21):17765–17776, 2012.

K. Yamane, C. Toumazou, Y.-i. Tsukada, H. Erdjument-Bromage, P. Tempst, J. Wong, and Y. Zhang. JHDM2A, a JmjC-containing H3K9 demethylase, facilitates transcription activation by androgen receptor. *Cell*, 125(3):483–495, 2006.

K. Yamane, K. Tateishi, R. J. Klose, J. Fang, L. A. Fabrizio, H. Erdjument-Bromage, J. Taylor-Papadimitriou, P. Tempst, and Y. Zhang. PLU-1 is an H3K4 demethylase involved in transcriptional repression and breast cancer cell proliferation. *Molecular Cell*, 25 (6):801–812, 2007.

M. Yamauchi and M. Sricholpech. Lysine post-translational modifications of collagen. *Essays in Biochemistry*, 52(1):113–133, 2012.

H. Yan, D. W. Parsons, G. Jin, R. McLendon, B. A. Rasheed, W. Yuan, I. Kos, I. Batinic-Haberle, S. Jones, G. J. Riggins, H. Friedman, D. Reardon, J. Herndon, K. W. Kinzler, V. E. Velculescu, B. Vogelstein, and D. D. Bigner. IDH1 and IDH2 mutations in gliomas. *New England Journal of Medicine*, 360(8):765–773, 2009.

H. Yang, Y. Liu, F. Bai, J. Zhang, S. Ma, J. Liu, Z. Xu, H. Zhu, Z. Ling, D. Ye, K. Guan, and Y. Xiong. Tumor development is associated with decrease of TET gene expression and 5-methylcytosine hydroxylation. *Oncogene*, 32(5):663–669, 2012.

M. Yang, R. Chowdhury, W. Ge, R. B. Hamed, M. A. McDonough, T. D. Claridge, B. M. Kessler, M. E. Cockman, P. J. Ratcliffe, and C. J. Schofield. Factor-inhibiting hypoxia-inducible factor (FIH) catalyses the post-translational hydroxylation of histidinyl residues within ankyrin repeat domains. *FEBS Journal*, 278(7):1086–1097, 2011a.

M. Yang, W. Ge, R. Chowdhury, T. D. Claridge, H. B. Kramer, B. Schmierer, M. A. McDonough, L. Gong, B. M. Kessler, P. J. Ratcliffe, M. L. Coleman, and C. J. Schofield. Asparagine and aspartate hydroxylation of the cytoskeletal ankyrin family is catalyzed by factor-inhibiting hypoxia-inducible factor. *Journal of Biological Chemistry*, 286(9):7648–7660, 2011b.

M. Yang, T. Soga, and P. J. Pollard. Oncometabolites: linking altered metabolism with cancer. *Journal of Clinical Investigation*, 123(9):3652–3658, 2013.

Y. Yang, V. A. Valera, H. M. Padilla-Nash, C. Sourbier, C. D. Vocke, M. A. Vira, M. S. Abu-Asab, G. Bratslavsky, M. Tsokos, M. J. Merino, P. A. Pinto, R. Srinivasana, T. Ried, L. Neckers, and W. M. Linehan. UOK262 cell line, fumarate hydratase deficient (fh^{-}/fh^{-}) hereditary leiomyomatosis renal cell carcinoma: in vitro and in vivo model of an aberrant energy metabolic pathway in human cancer. *Cancer Genetics and Cytogenetics*, 196(1): 45–55, 2010.

H. N. Yeowell and L. C. Walker. Mutations in the lysyl hydroxylase 1 gene that result in enzyme deficiency and the clinical phenotype of Ehlers–Danlos syndrome type VI. *Molecular Genetics and Metabolism*, 71(1):212–224, 2000.

N. Yosef, A. K. Shalek, J. T. Gaublomme, H. Jin, Y. Lee, A. Awasthi, C. Wu, K. Karwacz, S. Xiao, M. Jorgolli, D. Gennert, R. Satija, A. Shakya, D. Y. Lu, J. J. Trombetta, M. R. Pillai, P. J. Ratcliffe, M. L. Coleman, M. Bix, D. Tantin, H. Park, V. K. Kuchroo, and A. Regev. Dynamic regulatory network controlling TH17 cell differentiation. *Nature*, 496 (7446):461–468, 2013.

M.-Y. Youn, A. Yokoyama, S. Fujiyama-Nakamura, F. Ohtake, K.-i. Minehata, H. Yasuda, T. Suzuki, S. Kato, and Y. Imai. JMJD5, a Jumonji C (JmjC) domain-containing protein, negatively regulates osteoclastogenesis by facilitating NFATc1 protein degradation. *Journal of Biological Chemistry*, 287(16):12994–13004, 2012.

M. Yu, J. Sun, C. Thakur, B. Chen, Y. Lu, H. Zhao, and F. Chen. Paradoxical roles of mineral dust induced gene on cell proliferation and migration/invasion. *PLoS One*, 9(2): e87998, 2014.

Y. Yu, H. Ji, J. A. Doudna, and J. A. Leary. Mass spectrometric analysis of the human 40S ribosomal subunit: native and HCV IRES-bound complexes. *Protein Science*, 14(6): 1438–1446, 2005.

J. Zhang, S.-S. Ni, W.-L. Zhao, X.-C. Dong, and J.-L. Wang. High expression of JMJD6 predicts unfavorable survival in lung adenocarcinoma. *Tumor Biology*, 34(4):2397–2401, 2013.

N. Zhang, Z. Fu, S. Linke, J. Chicher, J. J. Gorman, D. Visk, G. G. Haddad, L. Poellinger, D. J. Peet, F. Powell, and R. S. Johnson. The asparaginyl hydroxylase factor inhibiting HIF-1α is an essential regulator of metabolism. *Cell Metabolism*, 11(5):364–378, 2010.

Y. Zhang and D. Reinberg. Transcription regulation by histone methylation: interplay between different covalent modifications of the core histone tails. *Genes & Development*, 15 (18):2343–2360, 2001.

Y. Zhang, Y. Lu, B.-Z. Yuan, V. Castranova, X. Shi, J. L. Stauffer, L. M. Demers, and F. Chen. The Human mineral dust-induced gene, mdig, is a cell growth regulating gene associated with lung cancer. *Oncogene*, 24(31):4873–4882, 2005.

Z. Zhang, G. T. Kochan, S. S. Ng, K. L. Kavanagh, U. Oppermann, C. J. Schofield, and M. A. McDonough. Crystal structure of PHYHD1A, a 2OG oxygenase related to phytanoyl-CoA hydroxylase. *Biochemical and biophysical research communications*, 408(4):553–558, 2011.

G. Zheng, J. A. Dahl, Y. Niu, P. Fedorcsak, C.-M. Huang, C. J. Li, C. B. Vågbø, Y. Shi, W.-L. Wang, S.-H. Song, Z. Lu, R. P. G. Bosmans, Q. Dai, Y.-J. Hao, X. Yang, W.-M. Zhao, W.-m. Tong, X.-J. Wang, F. Bogdan, K. Furu, Y. Fu, G. Jia, X. Zhao, J. Liu, H. E. Krokan, A. Klungland, Y.-G. Yang, and C. He. ALKBH5 is a mammalian RNA demethylase that impacts RNA metabolism and mouse fertility. *Molecular Cell*, 49(1):18–29, 2013.

X. Zheng, S. Linke, J. M. Dias, X. Zheng, K. Gradin, T. P. Wallis, B. R. Hamilton, M. Gustafsson, J. L. Ruas, S. Wilkins, R. L. Bilton, K. Brismar, M. L. Whitelaw, T. Pereira, J. Gorman, Jeffrey J amd Ericson, D. J. Peet, U. Lendahl, and L. Poellinger. Interaction with factor inhibiting HIF-1 defines an additional mode of cross-coupling between the notch and hypoxia signaling pathways. *Proceedings of the National Academy of Sciences*, 105(9): 3368–3373, 2008.

G. Zhouravleva, L. Frolova, X. Le Goff, R. Le Guellec, S. Inge-Vechtomov, L. Kisselev, and M. Philippe. Termination of translation in eukaryotes is governed by two interacting polypeptide chain release factors, eRF1 and eRF3. *The EMBO Journal*, 14(16):4065, 1995.

H. Zhu, S. Hu, and J. Baker. JMJD5 regulates cell cycle and pluripotency in human embryonic stem cells. *Stem Cells*, (8):2098,Äî2110, 2014.

Z. Zhu, Y. Wang, X. Li, Y. Wang, L. Xu, X. Wang, T. Sun, X. Dong, L. Chen, H. Mao, Y. Yu, J. Li, P. A. Chen, and C. D. Chen. PHF8 is a histone H3K9me2 demethylase regulating rRNA synthesis. *Cell Research*, 20(7):794–801, 2010.